Remodelling of the nuclear envelope during KSHV lytic infection

Alexander John Coleman

Submitted in accordance with the requirements for the degree of

Doctor of Philosophy

The University of Leeds

Faculty of Biological Sciences

School of Molecular and Cellular Biology

September 2018

The candidate confirms that the work submitted is his own and that appropriate credit has been given where reference has been made to the work of others.

This copy has been supplied on the understanding that it is copyright material and that no quotation from the thesis may be published without proper acknowledgement.

This thesis is dedicated to the NHS staff at Leicester Royal Infirmary during my time there from November 1998 till my all clear in 2004. I will be forever grateful for their compassion and professionalism that ensured my chance to perform this work and live a life fulfilled.

Acknowledgements

Abstract

Kaposi's sarcoma associated herpesvirus (KSHV) is a human tumour virus and key aetiological agent for several malignancies including Kaposi's sarcoma. KSHV exhibits a biphasic life cycle split between a persistent latent period with minimal gene expression and a lytic period with an expression cascade that culminates in the release of nascent virions. Crucially, the lytic phase has been shown to be important for tumorigenesis and the spread of Kaposi's sarcoma.

The Nuclear Pore Complex (NPC) is a protein mega-complex that regulates nucleocytoplasmic transport. It is formed by multiple copies of individual nucleoporins that combine into a sophisticated protein gateway. The regulation of nuclear access makes it a target for viruses that subvert the NPC in order to hijack the cell for viral replication. Whilst herpesvirus can induce changes at the NPC, little is known about KSHV NPC remodelling.

This study presents an investigation of how KSHV targets the NPC during its lytic infection highlighting the targeting a specific nucleoporin, Nup98, and an attempt at broader interactomic analysis using proximity dependent biotin identification. Nup98 is specifically downregulated early during lytic infection by the E3 ubiquitin ligase activity of viral protein RTA. This appears to be related to the repression of expression at viral ORF50 promoters when Nup98 is overexpressed in the nucleoplasm. This study also highlights how depletion of Nup98 is detrimental to the virus, leading to failed virion egress.

In summary, this project highlights how KSHV specifically targets one population of Nup98 but requires NPC-bound Nup98 to sequester a cellular mRNA for CHMP7 protein to ensure virion egress. It also provides the first attempt at using interactomic techniques to create a comprehensive, semi-quantitative profile of changes to the NPC during KSHV lytic infection that can pave the way for further interaction studies and the development of targeted antivirals for KSHV.

Contents

Table of Figures

List of tables

Abbreviations

<	less than
=	equals to
>	greater than
2D	2 dimensional
3D-SIM	3D-structured illumination microscopy
Å	angstrom
AAA-ATPase	ATPases Associated with diverse cellular Activities
AAAS	triple A syndrome
ACTH	adrenocorticotropic hormone
AIDS	Acquired Immunodeficiency Syndrome
AMP	adenosine-5'-monophosphate
APEX	ascorbate peroxidase
APS	ammonium persulphate
ATCC	American Type Culture Collection
ATP	adenosine-5'-triphosphate
BAF	barrier to autointegration factor
BCBL-1	body cavity B lymphocytes
BioID	Proximity dependent biotin identification
bp	base pair
BSA	bovine serum albumin
CAS	cellular apoptosis susceptibility gene
CBP	CREB-binding protein
cDNA	complementary deoxyribonucleic acid
ChIP	chromatin immunoprecipitation
CHMP2A	charged multivesicular body protein 2A
CHMP7	charged multivesicular body protein 7
cm	centimetre

CR	cytoplasmic ring
CREB	cAMP response element binding protein
CRM1	chromosomal maintainence protein 1 (or Exportin 1)
Ct	cycle threshold
Da	dalton
DAPI	4', 6-diamidino-2-phenylindole
DDR	DNA damage response
DE	delayed early
dH$_2$O	distilled water
DHX9	DEAD/DEAH box (DExH) -helicase 9
DMEM	Dulbecco's modified eagle medium
DMSO	dimethyl sulfoxide
DNA	deoxyribonucleic acid
DNase	deoxyribonuclease
dox	doxycycline hyclate
E	early
EBV	Epstein-Barr Virus
ECACC	European Collection of Authenticated Cell Cultures
EDTA	ethylenediaminetetraacetic acid
EMDB	Electron Microscopy Data Bank
ERK	extracellular signal–regulated kinase
ES	electrospray ionisation
ESCRT	endosomal sorting complexes required for transport
FBS	foetal bovine serum
FDR	false discovery rate
FG	phenylalanine-glycine
FISH	fluorescence in-situ hybridization
FLIP	(FADD-like IL-1β-converting enzyme)-inhibitory protein
g	gravitational force

g	gram
GAPDH	glyceraldehyde 3-phosphate dehydrogenase
gB	glycoprotein B
GDP	guanosine-5'-diphosphate
GFP	green fluorescent protein
gH	glycoprotein H
gL	glycoprotein L
GTP	guanosine-5'-triphosphate
h	hours
HAART	high active anti-retroviral therapy
HBV	hepatitis B virus
HCMV	Human cytomegalovirus
HDAC	histone deacetylase
HEK	human embryonic kidney
HEPES	4-(2-hydroxyethyl)-1-piperazineethanesulfonic acid
HHV	Human herpesvirus
HIV-1	human immunodeficiency virus type 1
HPI	Human Protein Index
HRP	horseradish peroxidase
HSV-1	Herpes simplex virus 1
HVS	Herpes saimiri virus
ICAT	Isotope-coded affinity tag
ICTV	International Committee on Taxonomy of Viruses
IDD	intrinsically disordered domain
IE	immediate-early
IFN	interferon
Ig	immunoglobulin
IL	interleukin
INM	inner nuclear membrane

IQR	interquartile range
IR	inner ring
IRD	Immune restoration disease
IRES	internal ribosomal entry site
IST1	IST1 homolog
iTRAQ	isobaric tag for relative and absolute quantification
kaps	karyopherin
kbp	kilobase pair
kDa	kilodalton
KS	Kaposi's sarcoma
KS-IRIS	Kaposi's sarcoma-associated immune reconstitution inflammatory syndrome
KSHV	Kaposi's sarcoma associated herpesvirus
L	late
L protein	Leader protein
LANA	Latency associated nuclear antigen
LAT	Latency associated transcript
LB	Luria-Bertani broth
LC	liquid chromatography
LiCl	lithium chloride
LINC	linker of nucleo- and cytoskeleton complex
lncRNA	long non coding ribonucleic acid
m/z	mass to charge ratio
MALDI-TOF	matrix-assisted laser-desorption-ionisation-time-of-flight
MCD	Multicentric castleman's disease
MDa	megadaltons
MDa/s	megadaltons per second
MHV68	Murid herpesvirus 68
min	minutes
miRNA	micro ribonucleic acid

mL	mililitre
Mnase	micrococcal nuclease
mRNA	messenger ribonucleic acid
MS	mass spectrometry
MS/MS	tandem mass spectrometry
MTA	mRNA transcript accumulation protein
MVB	multivesicular bodies
NaCl	sodium chloride
NE	nuclear enevelope
NET	Nuclear envelope transmembrane protein
NF-kB	nuclear factor kappa-light-chain-enhancer of activated B cells
NLS	nuclear localisation sequence
nM	nanomolar
NPC	Nuclear Pore Complex
NR	nucleoplasmic ring
NP-40	Nonidet™ P-40
NTR	nuclear transport receptor
Nup	nucleoporin
Nxf1	nuclear export factor 1
^{o}C	degrees Celsius
ONM	outer nuclear membrane
ORF	Opening reading frame
p	p value
p/s	penicilin/streptomycin
PAGE	polyacrylamide gel electrophoresis
PAN	polyadenylated nuclear RNA
PBS	phosphate buffered saline
PCR	polymerase chain reaction
PEL	primary effusion lymphoma

pgRNA	pre-genomic RNA
polyA	polyadenylated
POMs	integral membrane proteins of the pore membrane domain of the nuclear envelope
PPI	protein-protein interactions
qPCR	quantitative polymerase chain reaction
qRT-PCR	quantitative reverse transcription polymerase chain reaction
Ran	Ras-related nuclear protein
RBP-jk	Recombining binding protein suppressor of hairless kappa
RCC1	regulator of chromosome condensation 1
RNA	ribonucleic acid
RNase	ribonuclease
ROD	reduction of dimensionality
rpm	revolutions per minute
RPMI	Roswell Park Memorial Institute media
RRE	RTA response element
RTA	replication and transcription activator
Scr	scrambled siRNA
SDS	sodium dodecyl sulphate
shRNA	short hairpin ribonucleic acid
SILAC	Stable isotope labelling with amino acids in cell culture
siRNA	short or small interfering ribonucleic acid
SPPLAT	Selective proteomic proximity labelling using tyramide
ssRNA	single stranded RNA
TBS	tris buffered saline
TBS-T	tris buffered saline and Tween® 20
TEMED	tetramethylethylenediamine
TMT	tandem mass tagging
TPA	12-O-tetradecanoylphorbol-13-acetate
TREx	TREx BCBL-1-Rta

USA	United States of America
UTR	untranslated region
v/v	volume per unit volume
VSV	Vesicular stomatitis virus
vFLIP	viral (FADD-like IL-1β-converting enzyme)-inhibitory protein
vIL	viral interleukin
VPS4A	Vacuolar protein sorting-associated protein 4A
w/v	weight per unit volume
μg	microgram
μL	microlitre
μm	micrometre

Bases

A   adenine

C   Cytosine

G   guanine

T   thymine

Amino Acids

Alanine	Ala	A
Arginine	Arg	R
Asparagine	Asn	N
Aspartate	Asp	D
Cysteine	Cys	C
Glutamate	Glu	E
Glutamine	Gln	Q
Glycine	Gly	G
Histidine	His	H
Isoleucine	Ile	I
Leucine	Leu	L
Lysine	Lys	K
Methionine	Met	M
Phenylalanine	Phe	F
Proline	Pro	P
Serine	Ser	S
Threonine	Thr	T
Tryptophan	Trp	W
Tyrosine	Tyr	Y
Valine	Val	V

Chapter 1
~
Introduction

1 Introduction

1.1 Herpesviriales

1.1.1 Classification of Herpesviruses

Viruses are a form of infectious agent that must reproduce within the living cells of a host organism. The origins of viruses are still disputed, but across all domains of life infectious agents that exhibit viral characteristics are observed, with many sharing key genes for viral replication and morphogenesis (Koonin et al., 2006).

Herpesviruses are a morphologically distinct family of DNA virus that belong to the *Herpesviriales* order. The *Herpesvirales* order was established in 2009 by the International Committee on Taxonomy of Viruses (ICTV) in line with recommendations from the *Herpesviridae* study group. The *Herpesvirales* order contains three families of herpesviruses that are related to one another: *Herpesviridae* family, containing viruses that infect mammals, birds and reptiles; *Alloherpesviridae* family, incorporating viruses that infect fish and frogs; and the *Malacoherpesviridae* family, which includes viruses that can infect bivalves (Eberle et al., 2013).

The largest of these families *Herpesviridae* is split into three further sub-families: *alpha-, beta-, gammaherpesvirinae* (Figure 1.1) (Matthews, 1979). Classification of viruses by the ICTV followed the basic principal that "a virus species is a polythetic class of viruses that constitutes a replicating lineage and occupies a particular ecological niche" until the advent of DNA sequencing techniques (Van Regenmortel et al., 1991; Davison, 2010). With the expansion of advanced

2

genomic techniques and metagenomics, the classification of viruses is moving

further away from the polythetic rule as the size of the virome becomes one that

cannot fully establish all the distinct ecological niches that viruses inhabit

(Simmonds et al., 2017).
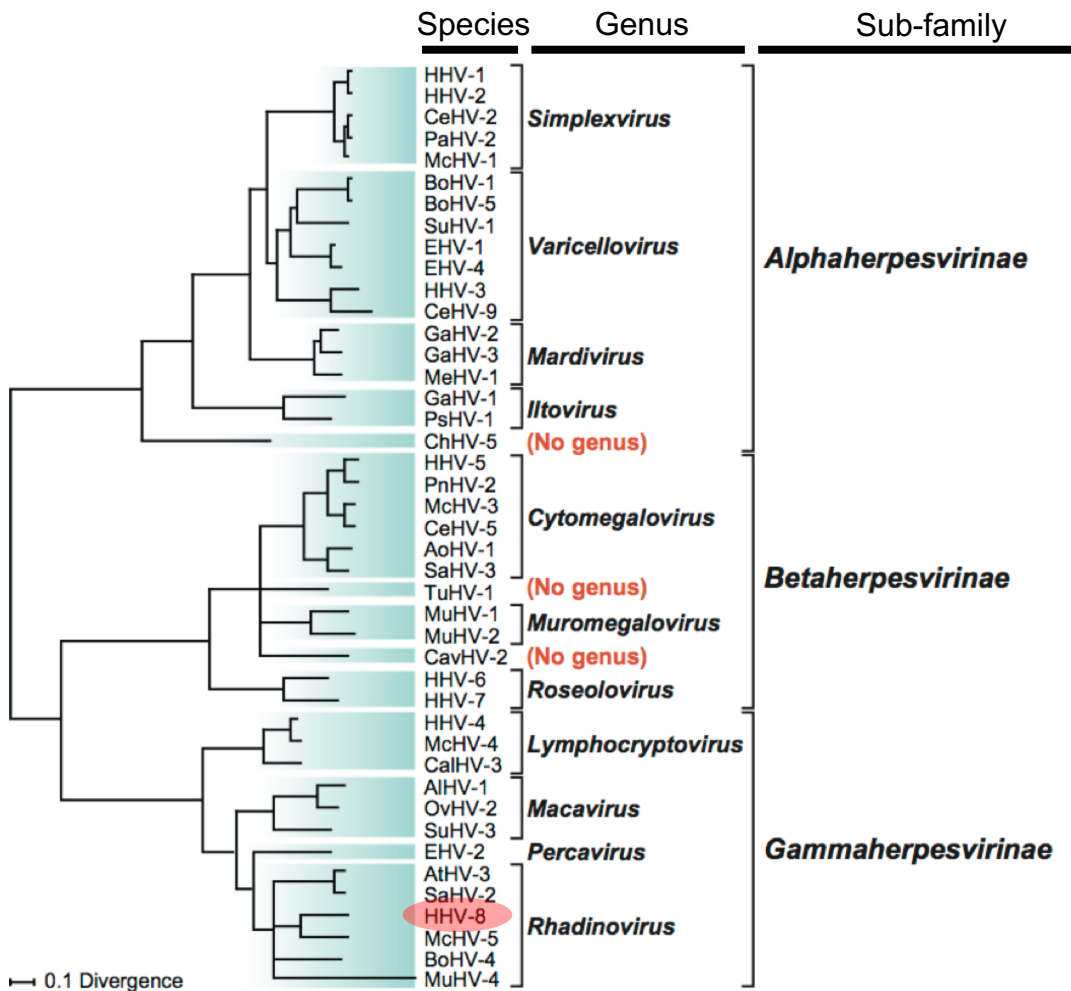
Figure 1.1 The Phylogenetic tree of *Herpesviridae*. An outline of the evolutionary relationship of *Herpesviridae* using amino acid sequence alignment. Human herpesvirus 8 or Kaposi's sarcoma associated herpesvirus is indicated with a red circle. Adapted from (McGeoch et al., 2008a).

1.1.1.1 Alphaherpesvirinae

The three main sub-families of *Herpesviridae* diverged between 180-210 million

years ago (McGeoch et al., 1995). The *Alphaherpesvirinae* subfamily is believed

to have diverged first from the herpesvirus common ancestor. Within the *Alphaberpesvirinae* exist a number of different genuses originally separated by their infectious host. The most clinically relevant of these genuses are the *Simplexvirus* genus containing Herpes simplex 1 and 2 (human herpesviruses (HHV) 1 and 2) and the *Varicellovirus* genus containing Varicella-Zoster Virus (HHV-3). The predominant features of the *Alphaherpesvirinae* sub-family are the ability to infect a wide host cell range, an efficient and rapid reproductive cell cycle and the ability to establish latent infections in sensory ganglia.

Alongside the above-mentioned human pathogens there are several important animal pathogens within the *Alphaherpesvirinae* sub-family. These include: another member of the *Varicellovirus genus* pseudorabies virus (*Suid herpesvirus-1* (SuHV-1)), which primarily infects pigs but has also been shown to infect cattle, dogs, cats and horses; Marek's disease virus also known as Gallid herpesvirus 2, an example of a member of the *Mardivirus* genus, which infects chicken and turkeys; and equine herpesvirus 1 (another member of the *Varicellovirus* genus), which causes encephalomyelitis and respiratory disease in horses (Woźniakowski and Samorek-Salamonowicz, 2015).

1.1.1.2   Betaherpesvirinae

Current approximations suggest the *Betaherpesvirinae* sub-familiy diverged slightly later than the *Alphaherpesvirinae* within the 180-210 million years divergence time frame (Davison, 2002). *Betaherpesvirinae* have a far more restrictive host range compared to *Alphaherpesvirinae*. Their reproductive cycle is also longer, with infected cells often enlarging, referred to as "cytomegaly". These viruses can establish a latent infection in cells of the secretory glands,

reticuloendothelial system and the kidneys (Whitley, 1996). *Betaherpesvirinae* examples include human cytomegalovirus (HCMV, HHV-5) of the *Cytomegalovirus* genus and other human pathogens of the *Roseolovirus* genus (HHV-6A, HHV-6B and HHV-7). The *Betaherpesvirinae* sub-family also includes animal pathogens of the rodent family in the genus *Muromegalovirus* and of the elephant family in the genus *Proboscivirus*.

1.1.1.3 Gammaherpesvirinae

The *Gammaherpesvirinae* sub-family is approximated to follow a similar evolutionary divergence timeline as *Betaherpesvirinae* (Davison, 2002). However, *Gammaherpesvirinae* have the most restricted infectious range primarily infecting lymphocytes although some members can infect endothelial tissues. The most prominent members of the *Gammaherpesvirinae* sub-family are the human pathogens Kaposi's sarcoma-associated herpesvirus (KSHV, HHV-8), a member of the *Rhadinovirus* genus, and Epstein-Barr virus (EBV, HHV-4), of the *Lymphocrytovirus* genus. Another member of the *Rhadinovirus* genus, murid herpesvirus 68 (MHV68), is an important model system for gammaherpesvirus study.

1.1.2 Virion structure

The herpesvirus virion has a distinct morphology that is shared across the order *Herpesvirales* (Figure 1.2). All herpesvirus genomes consist of a single large, linear double-stranded DNA molecule, that is contained within an icosahedral (T=16) capsid. This capsid is formed from 162 capsomers, 150 hexons and 12 pentons, giving an approximate overall diameter of 125-130 nm. One pentameric

5

capsomere is replaced by the portal vertex, the crucial site of genome entry and exit (Chang et al., 2007; Deng et al., 2007). The viral capsid is surrounded by a tegument layer, an amorphous protein coat consisting of both cellular and viral proteins. Proteins within the tegument aid the virus rapidly upon viral entry in a variety of roles such as targeting the capsid to the nucleus, cytoskeletal reassembly, and intiaition of viral and host gene expression (Kelly et al., 2009; Penkert and Kalejta, 2011). Enclosing the tegument is the viral envelope, a lipid bilayer that contains a number of viral glycoproteins that facilitate host cell binding and membrane fusion (Mettenleiter et al., 2009).
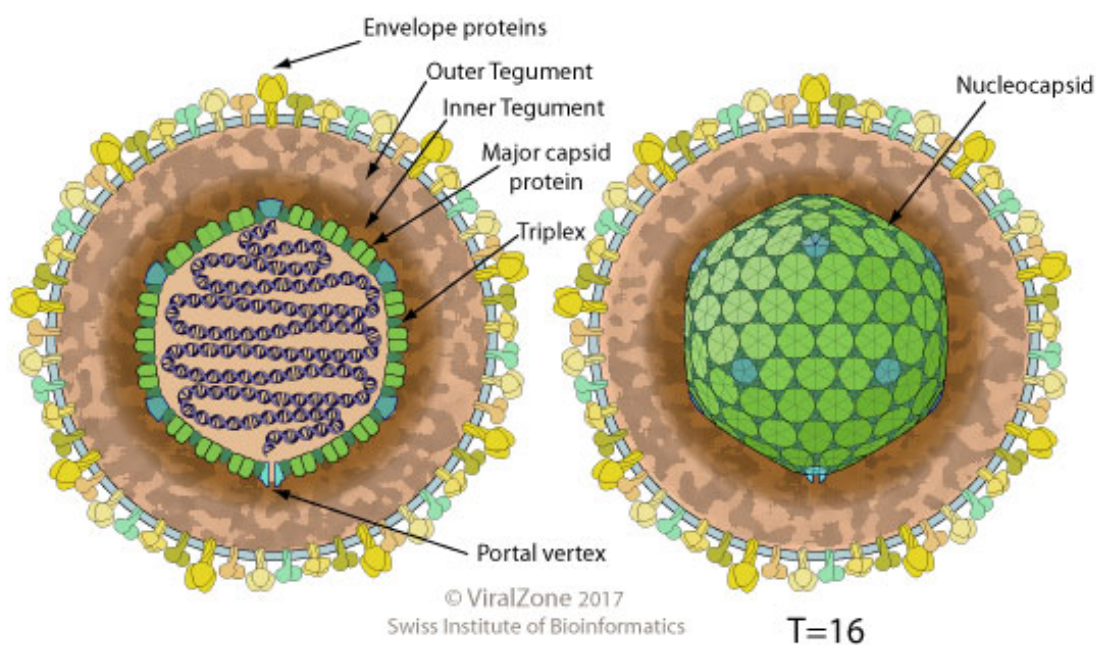
Figure 1.2 Herpesvirus virion structure. Schematic of herpesvirus virion with structural components highlighted. Figure taken from Swiss Institute of Bioinformatics ViralZone.ExPASy.org.

1.1.3 Genomic structure

The herpesvirus genome is a single double-stranded DNA molecule with a size range of 125-250 kbp. Comparative genomic analysis of herpesviruses breaks their genome into sections of unique and repeat regions. These repeat regions

(10^3-10^4 bp in size) are found in many herpesvirus genomes and different patterns of their placement between unique regions has led to the identification of six genome types (Figure 1.3). Genomes of Class A, consist of a unique sequence flanked by a direct repeat region an example of which is HHV-6. Class B genomes, such as KSHV, also exhibit a flanked unique sequence with directly repeated sequences at the genome termini present in multiple copy number. Class C, EBV being the predomiant example, is similar to Class B with its multiple copy number terminal direct repeats, but also contains an internal set of direct repeats. Class D genomes contain two unique regions each flanked by a set of inverted repeat sequences, an example of which is VZV. HSV-1 and 2 have class E genomes which exhibit two unique regions with larger repeat regions around the large unique sequence. Class E genomes also contain a sequence that contains a small section of repeats at the end of genome termini and at the junction between the large and small repeat region. Finally, Class F represents all herpesvirus genomes that do not include repeats characterised in the other classes. Crucially, the genome structure does not correspond to evolutionary relatedness and all genome types occur within *Alpha-*, *Beta-*, and *Gammaherpesvirinae*.
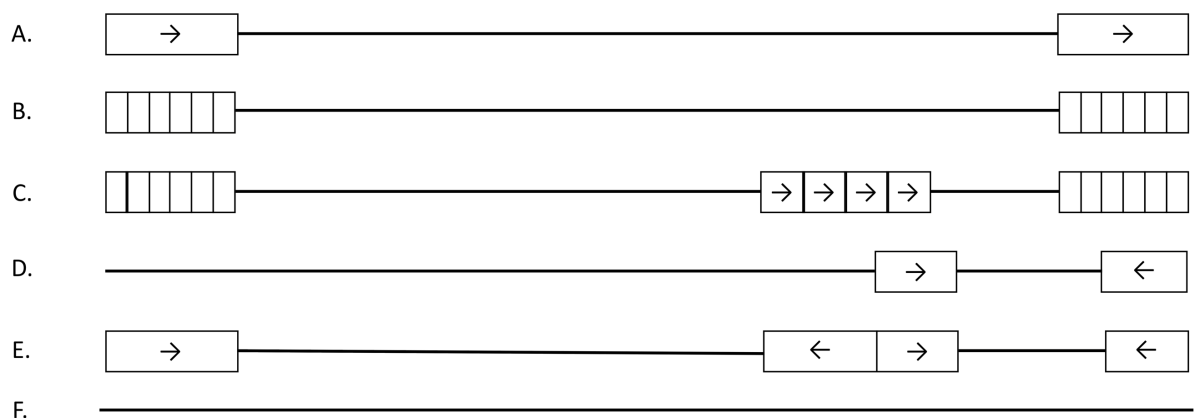
Figure 1.3 The Arrangement of Herpesvirus Genomes. Layouts of forms of herpesvirus genomes with unique (single lines) and repeat (boxes with relative directionality) sequences. For types B and C the numbers of repeats are variable. Adapted from (McGeoch et al., 2008b).

1.1.4 Life cycle

The first moment where a virus moves from an inanimate structural arrangement of lipids, nucleic acids, polysaccharides and proteins to an operational "living" entity is virion binding at the cell surface. Viral surface glycoproteins are essential for viral binding and entry, and in *Herpesvirales* are designated gL, gH and gB. The first contact interaction between herpesvirus and a cell is often via a host cell glycosaminoglycan, such as heparan sulphate (with the exception of EBV) (Shukla and Spear, 2001). This is a reversible reaction that is not essential to viral entry but has been shown to improve the efficiency of viral entry. This interaction with heparan sulphate anchors the virus onto the cell membrane, increasing its probability of interacting with additional cell surface receptors that will initiate viral fusion (Figure 1.4). Once a viral glycoprotein binds to the fusion receptor, the interaction is irreversible and the virus begins to fuse with the cell membrane (Spear and Longnecker, 2003). In KSHV, the viral glycoprotein K8.1A is responsible for the initial binding of the virus to cells via heparan sulphate (Luna et al., 2004). After fusion the capsid and viral tegument proteins are released into the cytoplasm. The capsid is trafficked to the nucleus via the microtubule network, which is stabilised by the action of tegument proteins (Sodeik et al., 1997; Naranatt et al., 2005). The capsid disassembles when it reaches the nuclear pore complex releasing the viral genome in linear form. This enters the nucleus and is circularised by covalent linkage at the head and tail of the DNA molecule (Poffenberger and Roizman, 1985; Garber et al., 1993; McVoy and Adler, 1994).

8
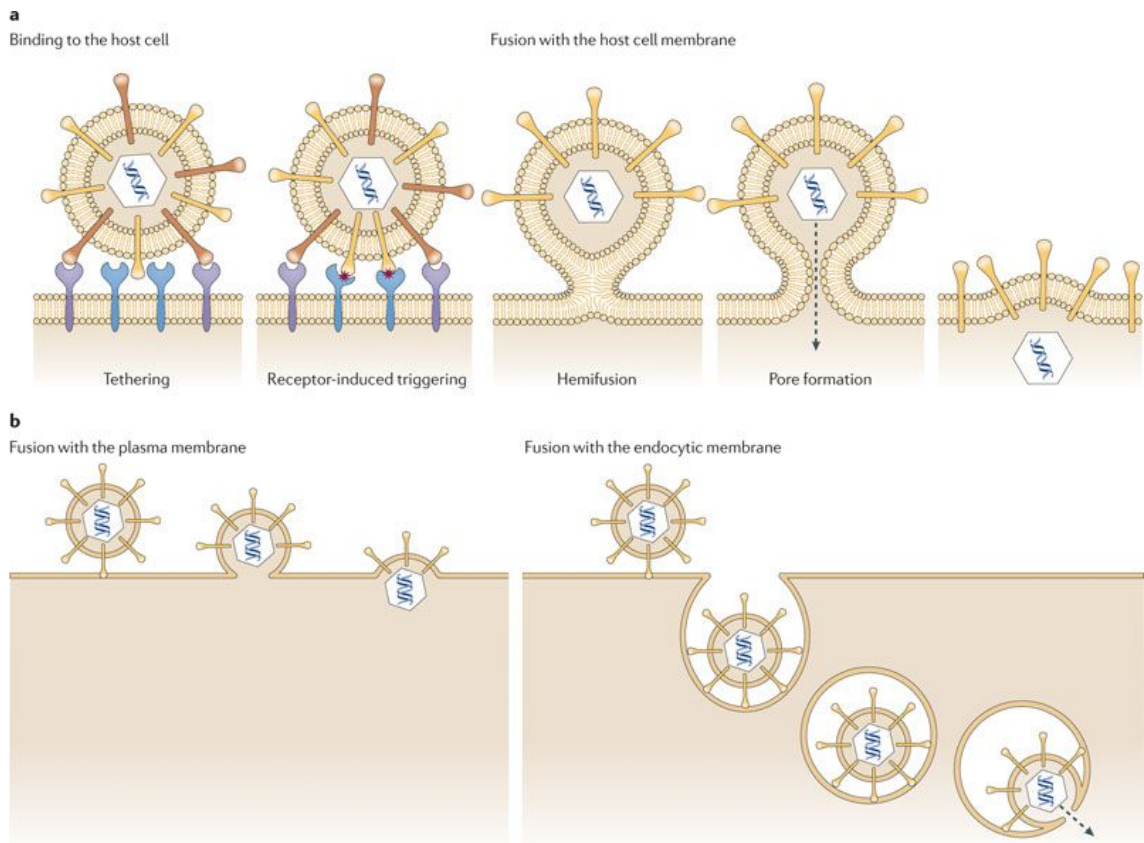
Figure 1.4 Viral entry mechanisms. a) Binding and fusion steps at the plasma membrane. Initial interactions between envelope glycoproteins (brown) and membrane receptors (purple) tether the virus to the plasma membrane, whilst other interactions trigger conformational changes that mediate membrane fusion (blue receptors and yellow glycoproteins). The fusion of viral and cellular membranes creates a hemifusion intermediate followed by full fusion. b) Alternate routes of entry, some herpesviruses are able to enter the cell via either fusion with the plasma membrane or fusion with the endocytic membrane after endocytosis. Taken from (Connolly et al., 2011).

1.1.4.1   Latency

The key characteristic of herpesviruses is their ability to establish a quiescent latent infection in order to maintain a long-term persistent infection. During this latent state the virus remains dormant and does not produce new virions. The sites of latency differ between the subfamilies of *Herpesviridae* with *Alphaherpesvirinae* such as HSV and VSV establishing a latent reservoir in neuronal cells, *Betaherpesvirinae* such as HCMV establish their latency in myeloid cells whilst *Gammaherpesvirinae* such as KSHV do so in B lymphocytes. How herpesviruses establish latency is poorly understood, however within the model herpesvirus system of HSV-1 it has been demonstrated that the

9

establishment of latency is a direct result of a failure to initiate immediate-early genes expression (Conn and Schang, 2013; Lee et al., 2016). This leads to histone deposition on the viral genome which establishes the latent transcriptional state (Deshmane and Fraser, 1989). During latency, herpesviruses transcribe a subset of genes called latency associated transcripts (LATs) that maintain the viral episome with minimal disruption to cell survival (Stevens et al., 1987). This ability to exist in a latent form is a key aspect of herpesvirus biology and the etymology of herpesviruses. Where the prefix herpes- is derived from the ancient greek verb *hérpein,* meaning to creep, this reflects the trait of establishing a dormant, creeping latent infection.

1.1.4.2 Lytic

The reactivation of a latent virus commits it to the second phase of the herpesvirus lifecycle, lytic replication (Figure 1.5). During lytic replication, an expression cascade is triggered leading to the full expression of the viral gene complement. This occurs in three different temporal stages of expression: immediate-early, delayed-early and late gene expression. Immediate-early genes are produced rapidly after the trigger of reactivation, their protein products initiate the transcription of delayed-early genes and begin to subvert host cell processes. Before DNA synthesis can begin, delayed-early genes are translated, helping concert efforts to drive the cell to produce nascent virions over regular cellular processes and begin viral DNA synthesis. The viral genome that was circularised when it entered the nucleus is replicated via a rolling circle style mechanism. This involves large-scale nuclear reorganization to form replication compartments,

where concatamers are produced from a single viral episome and then cleaved off to begin the packaging process (Reviewed in (Weller and Coen, 2012)).

The packaging process is completed in the nucleus prior to virion maturation, which occurs through a series of envelopment and de-envelopment stages. This begins with capsids in the nucleus budding into the perinuclear space through the inner nuclear membrane (INM). For primary envelope-mediated nuclear egress to occur all herpesviruses encode two proteins that make up the nuclear egress complex (NEC) (Mettenleiter et al., 2013). In HSV-1, these are the proteins pUL34 and pUL31 which form a heterodimer which is essential for successful viral egress (Sam et al., 2009). The NEC recruit conserved herpesviral protein kinases (CHPKs) such as UL13, UL97 and BGLF4 (from HSV-1, HCMV and EBV respectively) to disassemble the nuclear lamina (Lee et al., 2008; Hamirally et al., 2009). This gives capsids access the the INM where the NEC hijacks cellular endosomal sorting complex required for transport-III (ESCRT-III) proteins (Arii et al., 2018). The ESCRT-III complex is responsible for a diverse number of cellular membrane-related functions including multivesicular body (MVB) formation, cytokinesis, and viral budding (Alonso Y Adell and Teis, 2011; Morita et al., 2011; Vita and Broadie, 2017). The HSV-1 NEC appears able to recruit ESCRT-III during nuclear egress through an interaction with ESCRT-III adaptor ALIX which is then able to recruit CHMP4 proteins to the INM at sites of HSV-1 virion envelopment (Arii et al., 2018). This envelope includes several viral glycoproteins such as gB and gH that promote de-envelopment of the perinuclear capsid by fusion with the ONM (Farnsworth et al., 2007). After de-envelopment, the capsid is released into the cytoplasm where tegument proteins are acquired by the capsid through a variety of processes including during capsid transport by

11

microtubules and within the *trans*-Golgi network (TGN) where the second envelopement step occurs (Luxton et al., 2006; Loomis et al., 2006). Viral glycoproteins are essential for secondary envelopement at the TGN along with the ESCRT-III complex which leads to a final enveloped virion within a TGN vesicle (Brack et al., 2000; Farnsworth et al., 2003; Pawliczek and Crump, 2009). Herpesviruses disrupt the TGN transport network during lytic replication which has been suggested to prevent recycling of TGN-derived vesicles, promoting forward transport to the plasma membrane (Wisner and Johnson, 2004). Capsid-containing vesicles are then able to exocytose at the plasma membrane releasing newly produced virions.
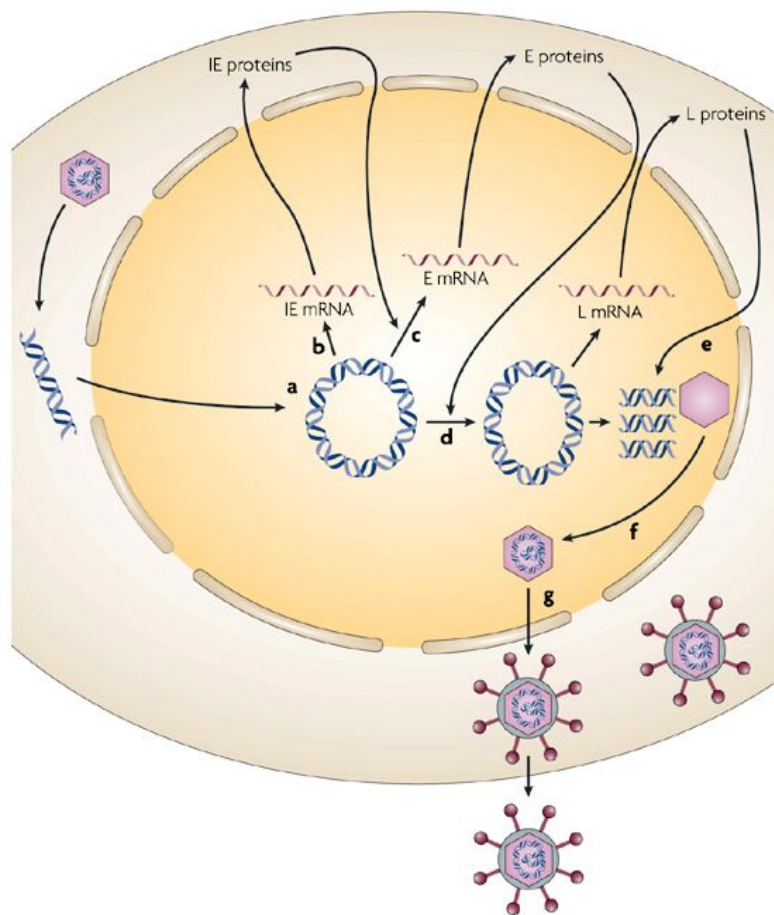
Figure 1.5 Herpesvirus lytic replication. a) After infection the virion releases the viral DNA which enters the nucleus and is rapidly circularised. b) Reactivation of the virus causes the expression of immediate-early (IE) genes. c) IE proteins move back into the nucleus and initiate the production of early (E) genes. d) DNA replication stimulates the production of late (L) genes, which encode key virion proteins. e,f) Late proteins

are reimported into the nucleus and assemble into nascent virions with newly replicated viral genomes. g) Virion egress via a multistep process, obtaining tegument proteins in the cytoplasm before final egress as the plasma membrane. Taken from (Knipe and Cliffe, 2008).

1.2   Gammaherpesvirinae

The *Gammaherpesvirinae* sub-family consists of four genera: Lymphocryptovirus, Macavirus, Percavirus, Rhadinovirus (Davison, 2010). The latent infection of *Gammaherpesvirinae* occurs in either B- or T-lymphocytes; however, their lytic infection occurs in fibroblasts or epithelial cells. These viruses all have a linear double-stranded DNA genome, the structure of which contains a large central region containing most of the viral genes. The ends of the genome are capped by variable numbers of direct repeat sequences required for genome circularisation during latency.

The propensity to establish a latent infection in dividing lymphocytes means *Gammaherpesvirinae* have evolved a variety of mechanisms to ensure genome propagation without cell lysis. These include driving cell cycle progression, repressing antiviral signals and production of anti-apoptotic factors (Li et al., 1997; Li et al., 1998; Sun et al., 2003). This manipulation of cell cycle and apoptotic signalling is linked to the ability of many gamma-herpesviruses to induce neoplasia and transform cells in culture. EBV and KSHV are two such human gamma-herpesviruses that are capable of causing multiple cancers and lymphoproliferative disorders.

1.2.1 Epstein-Barr Virus

Epstein-Barr virus (EBV) or human herpesvirus 4 is a gammaherpesvirus of the Lymphocryptovirus genus. The virus was first identified in 1964, after Michael

13

Epstein and Yvonne Barr visualised a section of lymphoblasts derived from Burkitt's Lymphoma. This had been prompted after Epstein attended a lecture in 1961 given by Denis Burkitt on the epidemiology surrounding the eponymous lymphoma in Africa. Epstein and Barr noted in their paper the "overall appearance of the virus resembles herpes simplex" and, after further collaboration with Werner and Gertrude Henle in Philadelphia, they observed viruses from "EB" (the name denoting the Burkitts lymphoma derived cell lines) and were confirmed as a new human herpesvirus (Epstein et al., 1964; Epstein et al., 1965). The virus was first described as Epstein-Barr Virus (after the cell lines from which it was first identified) and linked to the more common infection infectious mononucleosis by the Henle laboratory in 1968 (Henle et al., 1968).

Structurally, EBV is a typical gammaherpesvirus with a linear double stranded DNA genome of 184 kbp. It encodes 85 genes that are expressed dependent on the lifecycle stage of the virus (Baer et al., 1984; de Jesus et al., 2003). Like other herpesviruses, the EBV lifecycle is split between a quiescent latent phase and a productive lytic phase. Whilst our understanding of EBV has improved significantly since its discovery in the 1960s, it remains a serious human pathogen due to its aetiological relationship with a number of malignancies such as Burkitt's lymphoma, nasopharyngeal carcinoma, post-transplant lymphoproliferative disease, Hodgkin's lymphoma and gastric carcinoma. Estimates in 2010 suggested that EBV-related cancers led to the deaths of around 143,00 people worldwide per year (a figure described as an underestimate), highlighting the continued relevance in understanding EBV and how it leads to cancer (Khan et al., 2014).

1.2.1.1 EBV Life cycle

EBV forms a highly persistent infection (~95% global seroprevalence) due to its ability to infect the B-cell reservoir. It infects B-cells via the CD21 B-cell surface molecule but can also infect other cell types such as epithelial cells, mesenchymal cells and T-cells. Upon the initial infection of a naïve B-cell, EBV initiates the latency III programme with the full complement of latent viral proteins and RNAs expressed. This induces B-cells to transform into proliferating blast cells, establishing an infection-mediated lymphoblastoid cell line (Thorley-Lawson, 2001). Within the proliferating blast cell the virus restricts its protein expression to latency II, which stimulates the formation of germinal centres by inducing infected B cell differentiation into latent B memory cells (which can be attributed to the viruses high persistence) (Casola et al., 2004). In B memory cells, EBV restricts its latent programme even further to latency I where a minimal number of viral proteins and RNAs are produced. Finally, these resting EBV positive, B cells can enter latency 0, a state with no viral protein production at all (Young and Rickinson, 2004).

All EBV-induced malignancies are driven by viral latency however the alternate expression programmes described above are responsible for different pathologies (Figure 1.6). After latency 0, where no viral proteins are produced, latency I is the most restricted of EBV latency programmes. During latency I EBNA1 is the only viral protein produced, along with viral miRNAs and virally encoded small RNAs (EBERs) (Rowe et al., 1987; Yajima et al., 2005). Latency I is observed in all cases of endemic Burkitt's lymphoma, the exact mechanism by which EBV induces Burkitt's lymphoma is not well understood with some

studies showing EBNA1 can promote cell survival and others showing the contrary and it simply maintains the viral genome (Kang et al., 2001; Kennedy et al., 2003). Latency II, which is found in tumours in Hodgkin's lymphoma, T cell and Natural Killer (NK) cell carcinomas, is characterised by the expression of EBNA1, latent membrane protein (LMP) 1, 2A, 2B along with EBERs and viral miRNAs. LMP1 is a viral oncogene capable of promoting cellular proliferation and survival (Pratt et al., 2012). LMP2A and 2B act together to elicit a B cell receptor (BCR)-like signalling cascade that promotes cell survival and proliferation (Fruehling and Longnecker, 1997; Lynch et al., 2002). Latency III, has the largest expression complement with all viral nuclear antigens produced (EBNA- 1, 2, 3, 3A, 3B, 3C, leader protein), along with the LMPs, EBERs and viral miRNAs. These additional EBNAs have roles in promoting cell growth and survival (Tomkinson et al., 1993; Hsieh and Hayward, 1995). Latency III is observed in lymphomas in immunodeficient individuals whether post-transplant or in AIDS patients (Kutok and Wang, 2006).
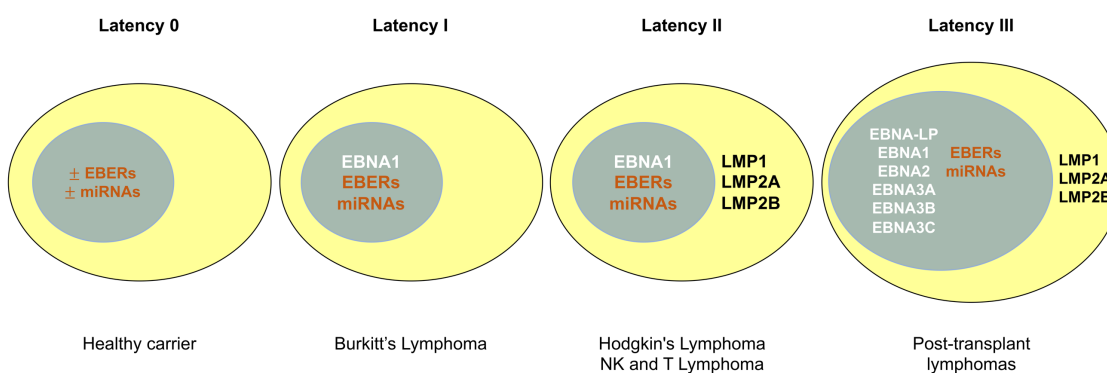
Figure 1.6 EBV latency programmes and associated disorders. Key viral proteins and non-coding RNAs for each latency programme along with associated disorders are highlighted.

1.2.2 Kaposi's sarcoma-associated herpesvirus

16

Human herpesvirus 8 (HHV-8) was initially discovered as Kaposi's sarcoma-associated herpesvirus (KSHV). Kaposi's sarcoma (KS) was first described by Hungarian physician and dermatologist Moritz Kaposi in 1872 as "idiopathic multiple pigmented sarcoma of the skin" (Kaposi, 1872). Until the 1980s, the incidence of KS was very rare (at between 0.02 and 0.06 per 100,000 people), with greater prevalence in middle-aged to elderly men of Mediterranean European or Jewish origin (Safai and Good, 1981). However, with the onset of the AIDS epidemic in the early 1980s, when unprecedented numbers of AIDS patients began to present with KS, careful epidemiological research at this time identified that KS may be caused by a sexually transmitted infectious agent (Beral et al., 1990). It was not until 1994 that DNA fragments of a herpesvirus were isolated from a KS tumour using representational difference analysis of a patient's genomic DNA in both unaffected tissue and tumour tissue (Chang et al., 1994). Subsequently, KSHV was linked to multicentric Castleman's disease (MCD), an atypical lymphoproliferative disorder, and primary effusion lymphoma (PEL), a B-cell lymphoma (Soulier et al., 1995; Cesarman et al., 1995). The viral genome was fully sequenced in 1996, yielding a ~165 kb viral genome, with 81 open reading frames (ORF), many of which were functional homologues of herpesvirus saimiri (HVS), an old world monkey gammaherpesvirus (Russo et al., 1996) (Figure 1.7). Furthermore, KSHV also encodes 25 mature miRNAs, long non-coding RNAs (lncRNAs) and, recently, a number of upstream and small ORFs have been identified (Sun et al., 1996; Cai et al., 2005; Arias et al., 2014).
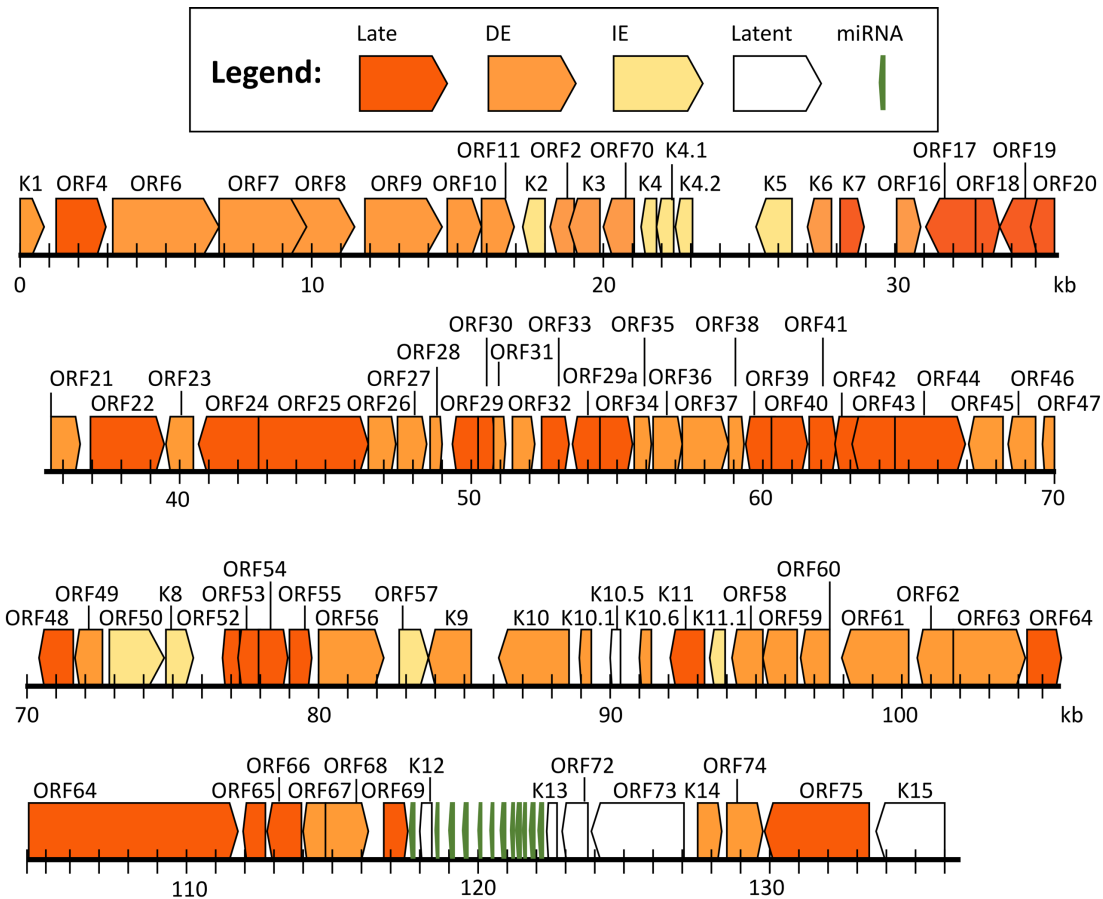
Figure 1.7 KSHV genome map. With ORF locations highlighted for each temporal phase of KSHV lifecycle. KSHV miRNA cluster also included. Adapted from (Coscoy, 2007) after data in (Arias et al., 2014) and (Paulose-Murphy et al., 2001).

With the formalisation of KSHV as the key aetiological agent responsible for KS, PEL and MCD efforts began to understand the epidemiology of the virus. KSHV does not ubiquitously infect the world's population as seen with EBV. A compilation of seroprevalence data in 2010 showed highest seroprevalence in sub-saharan Africa (>50%) (Figure 1.8). However, in Northern Europe and the USA seroprevalence is much lower at <10% and in the Mediterranean and South America seroprevalence is at 10-30% (Mesri et al., 2010). Interestingly, recent studies of the KSHV and KS incidence in Asia has found a marked variation in the seroprevalence of the virus across the continent with high levels of

seroprevalence in the Chinese autonomous region of Xinjiang, once a staging post on the ancient Silk Road between Europe and China, as well as high levels in Taiwan and Cambodia of between 10-30%. This is compared with very low levels of seroprevalence in Japan and Thailand of <10% (Zhang and Wang, 2017).
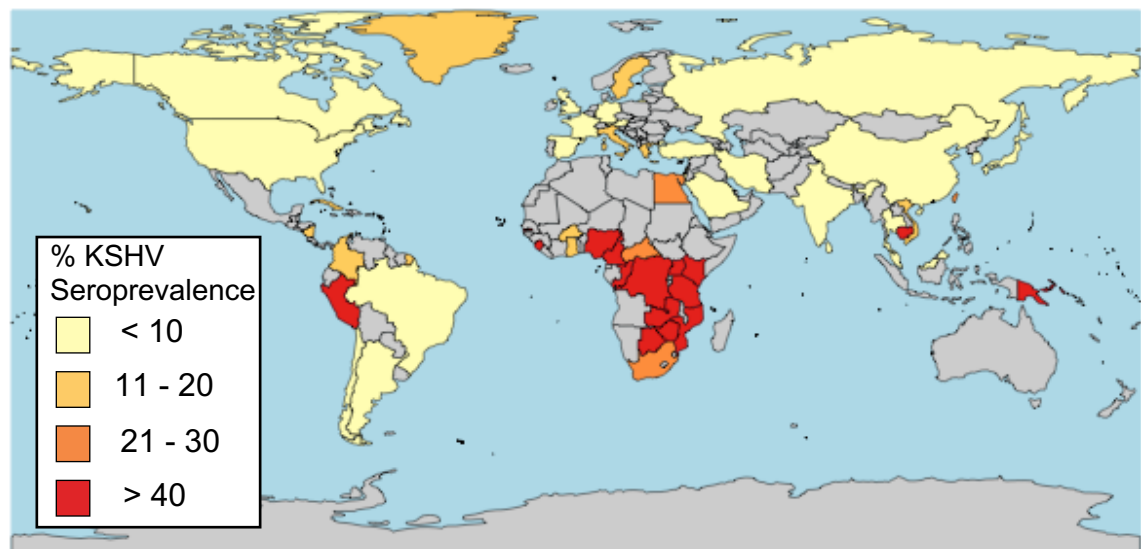
Figure 1.8 KSHV global seroprevalence data. % KSHV seroprevalence mapped per country with countries lacking data coloured grey. Adapted from (Mesri et al., 2010) with additional data from (Zhang and Wang, 2017).

1.2.2.1   KSHV associated diseases

KSHV has been identified as the aetiological agent in three malignancies: Kaposi's sarcoma (KS), multicentric Castleman's disease (MCD) and primary effusion lymphoma (PEL) (Chang et al., 1994; Soulier et al., 1995; Cesarman et al., 1995).

1.2.2.1.1   Kaposi's Sarcoma

Kaposi's sarcoma presents as red-brown macules on the skin that range in size from several millimetres to centimetres. KS is categorised into 4 forms: classic

19

KS, AIDS-associated KS, Endemic KS and Iatrogenic KS (Dezube, 1996). Classic KS is a rare presentation of the disease in elderly Mediterranean men, with lesions predominantly forming on the lower extremities. Patients often live with the disease for 10 years or more and typically do not die of KS (Hengge et al., 2002). AIDS-associated KS is an extremely aggressive form of the disease with lesions developing multifocally on the upper body, head and neck (Hengge et al., 2002). It quickly develops from lesions to tumours with tumour dissemination to organs rapidly leading to high mortality. KS is now the most common neoplasm in homosexual and bisexual men with AIDS. The frequency of this form of KSHV exploded during the AIDS epidemic in the early 1980s with incidence rates in homosexual men in San Francisco USA at 40% (Martin et al., 1998; Goedert, 2000). HIV-1 infection appears to exacerbate KSHV pathogenesis through the HIV-1 tat protein that drives IL-8 expression promoting angiogenesis that contribute to KS tumour formation (Vogel et al., 1988; Lane et al., 2002). Endemic KS or African KS is predominantly observed in young men and young children, with a high prevalence across equatorial Africa. This was proposed to relate to the barefoot exposure to volcanic soils and subsequent uptake of aluminosilicates inducing a level of immunosuppression (Ziegler et al., 1984; Wabinga et al., 1993). However, with the outbreak of the AIDS epidemic, KS also reached epidemic proportions in Africa rendering it difficult to study African KS as an independent disease. Iatrogenic KS is an unusual clinical presentation of KS that occurs on the induction of immunosuppressive therapy. It can occur chronically or rapidly onset and is an emerging clinical concern for those who have received organ transplants (Hengge et al., 2002). Intriguingly, studies have shown that iatrogenic KS is reversible on the removal of

immunosuppression (Hengge et al., 2002). Whilst high active anti-retroviral therapy (HAART) has proven to be highly effective at reversing the effects of AIDS and thus KS, seroprevalence rates are still high among certain demographics, especially in Africa. Furthermore, the emergence of iatrogenic KS in combination with an ageing population in many Western countries highlights the critical importance of continuing research into KS and KSHV to reduce mortality (Figure 1.9).

KS age standardized incidence in males per 100,000: ☐ <1 ☐ 1–4 ☐ 4–22 ☐ >22
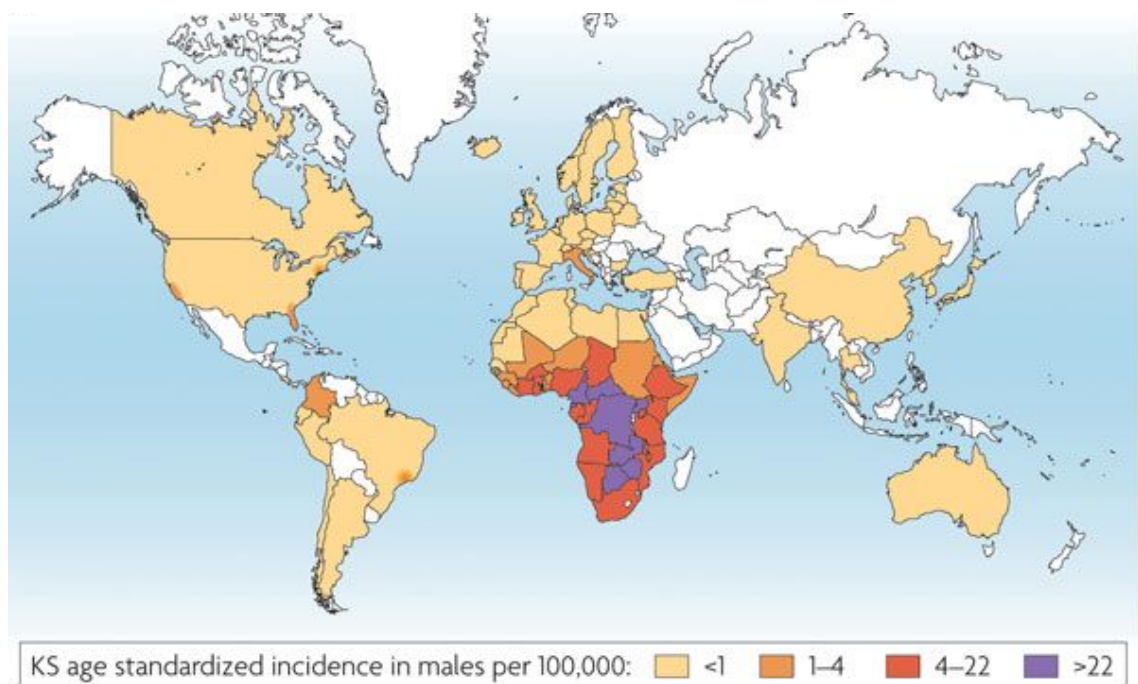
Figure 1.9 Kaposi's sarcoma incidience rates worldwide. Follows the levels of KSHV seroprevalence shown above with highest KS rates in central Africa. No data available for countries in white. Taken from (Mesri et al., 2010).

1.2.2.1.2 Kaposi's sarcoma-associated immune reconstitution inflammatory syndrome (KS-IRIS)

Kaposi's sarcoma-associated immune reconstitution inflammatory syndrome (KS-IRIS) is a form of immune restoration disease (IRD) that occurs in patients treated with HAART. IRDs are rare disorders that develop when the HAART

restored immune system stimulates an immunopathological reaction leading to disease. Whilst IRDs are more commonly seen with bacteria such as Cryptococci and mycobacteria, they have also been observed in patients with latent HSV-1 infection and hepatitis B (French et al., 2004). The establishment of KS as an IRIS-associated disease comes from observations in Africa where a proportion of patients who successfully responded to HAART treatment for HIV went on to develop KS (Bower et al., 2005). Whilst KS-IRIS is not always fatal, it can complicate a patient's recovery. Furthermore, the increasing use of HAART to treat HIV-1 in Africa makes KS-IRIS an emerging clinical problem (Martin et al., 2009).

1.2.2.1.3 Multicentric Castleman's Disease

Multicentric Castleman's Disease (MCD) is a subtype of Castleman's Disease, a group of lymphoproliferative disorders characterised by lymph node enlargement. Whilst there are 3 main subtypes of Castleman's disease, KSHV has only been shown to cause MCD (Soulier et al., 1995). KSHV-MCD saw a resurgence during the AIDS epidemic with a strong correlation of MCD cases in a HIV context being KSHV-associated. The pathophysiology of KSHV inducing MCD is proposed to involve inflammatory dysregulation stimulated by lytic gene product viral homolog of interleukin-6 (vIL-6) (Polizzotto et al., 2012). Whilst the exact mechanism by which vIL-6 drives MCD development is unknown overexpression of IL-6 leads to MCD-like symptoms in mice (Brandt et al., 1990).

1.2.2.1.4 Primary Effusion Lymphoma

Primary effusion lymphoma (PEL) is a B-cell lymphoma that leads to the overproduction of malignant B-cells that invade body cavities such as the pleural

22

space. KSHV is required for PEL to develop and is often found as a complication of HIV-1 induced immune dysfunction (Cesarman and Knowles, 1999; Chen et al., 2007). PEL is highly aggressive and often found at a late stage of lymphoma progression, leading to very poor clinical outcomes for those diagnosed, with only a 52% 1-year survival rate in those diagnosed at an early stage (El-Fattah, 2017).

1.2.2.2 Life cycle

The KSHV life cycle follows the typical herpesvirus pattern as described above. KSHV encodes five conserved glycoproteins gB, gL, gH, gM, and gN. Furthermore, KSHV encodes several unique lytic cycle associated glycoproteins K8.1A, K8.1B, K1, K14, K15 KSHV glycoprotein gB binds heparan sulphate, but also contains the RDG motif which binds specifically to integrin α3β1, unlike other herpesvirus gBs (Akula et al., 2002). This targeting of integrin α3β1 broadly correlates with KSHV target cells, although it is not known whether virus binding to integrin facilitates fusion as gH, gL and gB have been shown to be required for KSHV fusion (Pertel, 2002). The attachment of the virus at the cell surface is then followed by entry and internalisation into the cell which is shown to be rapid reaching a peak within 60 minutes post infection (Krishnan et al., 2004). The interaction of viral glycoprotein gB with host receptors induces focal adhesion kinase (FAK) stimulating cellular signalling pathways to aid with actin rearrangements for virus internalization (Sharma-Walia et al., 2004; Veetti et al., 2010) (Reviewed in (Chakraborty et al., 2012)). Once the viral envelope has fused with the cell membrane the internalized capsids are then trafficked via the host microtubule network to the nuclear periphery. The activation of FAK signalling by gB leads to downstream activation of Rho and Rac, via intermediate signalling

23

steps by Src and phosphoinositide 3-kinase (PI3K), which lead to the stabilization of microtubules for the passage of capsids to the nucleus (Naranatt et al., 2005). Upon reaching the nuclear periphery, the capsid will release its genome cargo into the nucleus. The exact mechanism of KSHV genome delivery at the nuclear pore is not yet fully understood; however, the HSV-1 capsid (which is of a comparable size and diameter to KSHV) has been shown to dock to the nuclear pore via nucleoporins Nup214 and Nup358 (Copeland et al., 2009; Pasdeloup et al., 2009). A currently unidentified triggering event induces the uncoating of the capsid and the viral genome translocates through the nuclear pore complex. It is theorized that the efficiency and speed of the translocation process is driven by either pressurization of the viral genome during packaging, with electrostatic forces between the DNA and capsid proteins maintaining pressurization, or by immediate transcription of the genome providing a mechanical force to pull the viral genome into the nucleus (Reviewed in (Liashkovich et al., 2011)). Upon entry into the nucleus, the KSHV genome is in a linear double-stranded conformation. A crucial step before the establishment of latency is genome circularisation, the exact mechanism by which KSHV circularises its genome is poorly understood but may relate to the initiation of a DNA damage response (DDR) (Lieberman, 2013). This occurs quickly after nuclear entry by the viral genome through the activation of ataxia-telangiectasia mutated kinase (ATM) and an increase in phosphorylation and protein level of histone 2AX (H2AX). This culminates in the formation of phosphorylated H2AX (γH2AX) foci which colocalise with the viral genome and has been hypothesised to assist in the recruitment of chromatin modifier proteins that are required for the establishment of viral latency (Singh et al., 2014).

24

1.2.2.2.1 Latency

Following *de novo* infection it has been shown that the viral transactivator RTA is expressed immediately activating the Latency-associated-nuclear antigen (LANA). LANA expression downregulates RTA and represses its expression, a critical step in the establishment of latency (Lan et al., 2005). During a latent infection, KSHV is maintained as high copy number, circular episomes (~50 per cell) within the nucleus with minimal protein expression. Latently expressed genes predominantly feature around the latency locus which encodes ORF73/LANA, ORF72/v-Cyclin, ORF71/v-Fas-associated death domain-like interleukin-1β-converting enzyme-inhibitory protein (vFLIP) and K12 along with 12 virally encoded microRNAs (Rainbow et al., 1997; Kedes et al., 1997; Dittmer et al., 1998; Sadler et al., 1999; Burýsek and Pitha, 2001). As well as repressing RTA, LANA acts to tether the viral episome to host chromosomes during mitosis, ensuring proper segregation and partition into daughter cells (Ballestas et al., 1999). LANA has also been shown to maintain latency by inhibiting expression of the viral transactivator protein RTA (ORF50) (Lu et al., 2006). v-Cyclin is a viral cyclin homologue that forms a complex with cyclin-dependent kinase 6 and phosphorylates retinoblastoma protein (pRB) in order to dysregulate the cell cycle and promote the expansion of KSHV-infected cells (Godden-Kent et al., 1997; Verschuren et al., 2004). vFLIP is a viral homolog of cFLIP that inhibits Fas ligand induced apoptosis by preventing procaspase-8 activation (Thome et al., 1997). vFLIP also activates NF-kB pathways promoting cell survival (Matta and Chaudhary, 2004). As such these genes contribute to the primary aims of latency:

to maintain the viral genome and ensure transmission to host daughter cells during cell division in order to maintain viral copy number.

1.2.2.2.2 Lytic Replication

Latently infected cells transition to lytic replication can be triggered by a range of stimuli, including hypoxia, co-infection with HIV-1, oxidative stress and inflammatory cytokines (Mercader et al., 2000; Davis et al., 2001; Merat et al., 2002; Ye et al., 2011). All latent-lytic switch events promote the expression of the viral transactivator protein RTA that initiates a temporally regulated sequence of gene expression which culminates in the assembly and egress of nascent virions and cell death. The induction of lytic replication leads to a cascade of changes within the cell, initiated by the virus, to subvert cellular machinery to achieve its key evolutionary goal: replication. In KSHV, lytic replication is marked by three distinct temporal stages of gene expression: immediate-early, delayed-early and late. At the apex of this transcriptional cascade is RTA (ORF50), an immediate-early transcript that is sufficient and necessary for successful viral lytic replication (Lukac et al., 1998; Sun et al., 1998). *In vitro* phorbol esters are commonly used to induce lytic replication of KSHV-infected cell lines via a proposed activation of ERK activation leading to the production of the transcription factor c-Fos and c-Jun which come together to form the AP-1 complex that promotes RTA expression (Cohen et al., 2006).

Reactivation of KSHV from latency is a critical pathogenic step during the progression of KS (Moore et al., 1996). Furthermore, the transition to lytic replication *in vivo* appears inversely related to immunocompetency with tumour development observed in KSHV-positive transplant recipients using

26

immunosuppressants. Tumour development has been shown to successfully regress after the cessation of immunosuppressant treatment in some cases (Farge et al., 1999; Hengge et al., 2002).

Expression of the viral gene *ORF50* leads to the production of the RTA protein, which contains an N-terminal basic domain and a C-terminal acidic domain similar to the transactivating domains in the EBV Zta transactivator protein (Lukac et al., 1998). RTA is expressed as a 110 kDa protein with a 90 kDa minor protein also observed. These two forms differ in their phosphorylation patterns with experiments demonstrating that RTA is phosphorylated by cyclin-dependent kinase 9 (CDK9) in order to maximise its transactivational function (Lukac et al., 2001a; Tsai et al., 2012). Initial studies of how RTA induces the transcription of KSHV genes were focused on two immediate-early transcripts: (MTA) mRNA transcript accumulation protein and polyadenylated nuclear (PAN) RNA. This highlighted two alternate methods of transcriptional activation by RTA. PAN RNA is an abundant non-coding poly-adenylated RNA that is expressed during KSHV lytic replication and appears to be critical for the expression of late viral transcripts (Sun et al., 1996; Borah et al., 2011). RTA was shown to directly bind to the PAN promoter which, in conjugation with the C-terminal activator domain, is sufficient for PAN RNA production. A consensus sequence within the PAN promoter is also found in other immediate-early genes such as Kaposin and is described as an RTA-responsive element (RRE) (Song et al., 2004; Chang et al., 2005). At RREs, RTA directly regulates the expression of certain immediate-early transcripts inducing their expression (Figure 1.10a).

27

However, RTA also activates transcription via an alternative pathway highlighted through studies on the regulation of expression of MTA protein at the *ORF57* promoter. MTA, also referred to as the ORF57 protein, is a viral immediate-early protein that subverts normal nucleocytoplasmic transport to preferentially export intronless viral mRNAs via the cellular TREx complex (Reviewed in (Schumann et al., 2013)). Through experiments characterising the role of RTA at the *ORF57* promoter, RTA was shown to bind to Recombination Signal Binding Protein (RBP)-Jk (Lukac et al., 2001b). This interaction between RBP-Jk and RTA appears crucial for the transcription of certain viral genes via the activation of the Notch signalling pathway (Liang et al., 2002; Swaminathan, 2005) (Figure 1.10b).

RTA also appears to regulate expression through inducing degradation of transcriptional repressors (Yang et al., 2008). This is attributed to an intrinsic ubiquitin E3-ligase activity within RTA that targets cellular repressor proteins for degradation during lytic infection. Specifically, RTA has been shown to induce the degradation of the transcriptional repressor Hey1, allowing for RTA upregulation during lytic replication (Gould et al., 2009) (Figure 1.10c).
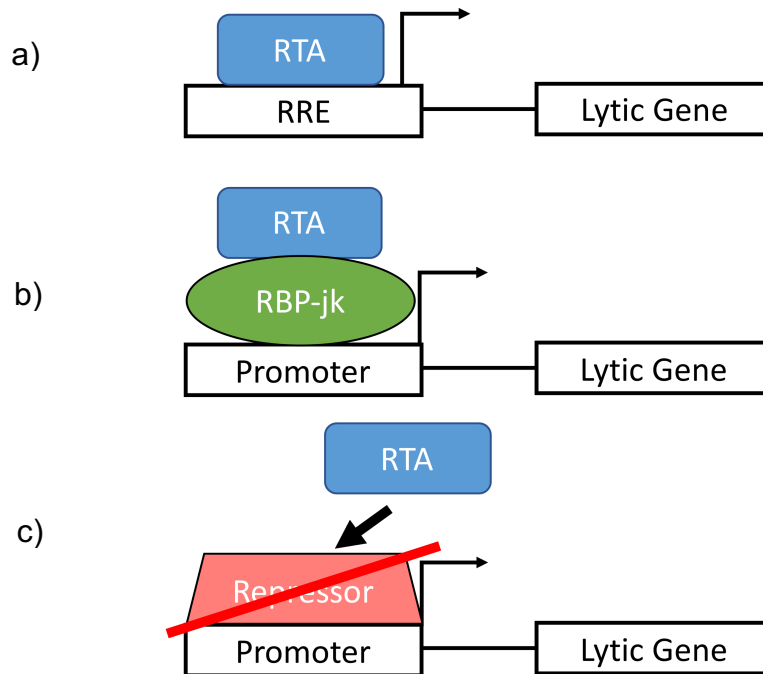
Figure 1.10 Outline of RTA mechanisms for gene transactivation. a) RTA binds directly to the RTA-response element (RRE) initiating transcription. b) RTA recruits cellular transcription factors such as RBP-jk to initiate transcription. c) RTA degrades a transcriptional repressor allowing for transcription.

Through this variety of mechanisms, RTA is able to orchestrate the expression of a variety of immediate-early viral factors that begin to bring the cell under the control of the viral replication programme. K8, modulates cellular transcription via the recruitment of CREB-binding protein (CBP) (Zhu et al., 1999; Hwang et al., 2001). Whilst, viral G-protein coupled receptor (vGCPR) acts as a constitutively active CXC chemokine receptor activating mitogen-activated protein kinase (MAPK), Akt, and phospholipase C (PLC)-mediated pathways in order to promote proliferation (Sun et al., 1999; Chiou et al., 2002; Smit et al., 2002; Cannon, 2007). These immediate-early genes rapidly subvert normal host cell processes and allow for efficient expression of the delayed-early genes prior to viral genome replication.

29

The delayed early genes continue subverting host cell processes via the action of viral proteins like ORF37, which reduces cellular gene expression via increasing global mRNA turnover (Glaunsinger and Ganem, 2004; Glaunsinger et al., 2005), and prepares for the replication of viral genomes via genes such as ORF59, which translocates the viral polymerase ORF9 to the nucleus to initiate viral DNA replication (McDowell et al., 2013). After viral DNA replication the last temporal cohort of genes are expressed, which include components of the virion such as ORF65 and viral glycoproteins like gB (Lin et al., 1997; Pertel et al., 1998).

Nascent virions assemble in the nucleus and undergo a multi-step egress process. This begins at the nuclear membrane where KSHV virions bud into the perinuclear space through the action of the KSHV nuclear egress complex (NEC). This is composed of two proteins ORF67 and ORF69, which share strong similarity with HSV-1 NEC proteins UL34 and UL31(Santarelli et al., 2008). Whilst the HSV-1 NEC proteins have been shown to interact with ESCRT complex proteins to aid with nuclear egress how KSHV subverts ESCRT-III during its own egress is less well characterised. However, experiments in EBV have shown that EBV NEC components also recruit ESCRT-III to aid with nuclear egress suggesting this process may be shared between herpesvirus sub-families. Overexpression of EBV NEC proteins is able to form nuclear membrane-derived vesicles suggesting they are involved in the initial envelopment step at the nuclear membrane during viral egress (Klupp et al., 2007). The enveloped virion then fuses via interactions with ONM proteins and viral glycoproteins with the ONM losing its envelope and releasing the virion into the cytoplasm. Within the cytoplasm the KSHV virion acquires tegument proteins such as ORF45 which

30

interacts with kinesin-2 and is responsible for capsid-tegument transport along microtubules and has been shown to help direct viral particles to the Golgi for final maturation (Sathish et al., 2009; Wang et al., 2015). Within the Golgi viral particles acquire their final envelope containing viral glycoproteins and are transported within a Golgi-derived vesicle to the cell membrane where the vesicle fuses with the cell membrane and releases the virion (Mettenleiter et al., 2009).

1.3 The Nuclear Envelope

The defining separation between prokaryotes and eukaryotes is the presence of a membrane separating the DNA genome from other cytoplasmic compartments. The nuclear envelope (NE) is the specific subcellular compartment that gives rise to this separation and is typically split into three components: the nuclear lamina, the nuclear membrane and the nuclear pore complex (NPC) (Figure 1.11). The nuclear membrane is split into the outer nuclear membrane (ONM) which is continuous with the endoplasmic reticulum and is orientated towards the cytoplasm, while the inner nuclear membrane (INM) is orientated towards the nucleoplasm. The nuclear lamina is a proteinaceous meshwork of class V intermediate filament proteins that act as a scaffold for the nuclear membrane interacting at the INM (Prokocimer et al., 2009). NPCs exist within pores of the nuclear membrane and regulate nuclear cytoplasmic transport. Traditionally, the nuclear envelope was viewed as a static structure that only underwent significant change during mitosis; however, a large body of emerging evidence shows the nuclear envelope compartment is a highly dynamic and responsive part of the cell.

31
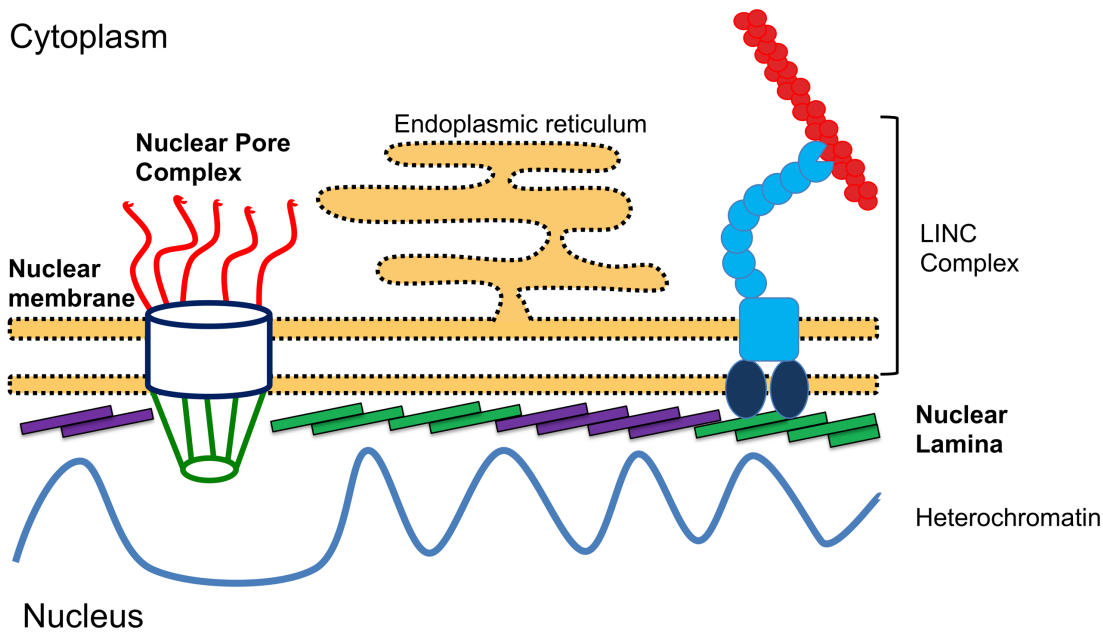
Figure 1.11 Overview of the Nuclear Envelope compartment. Heterochromatin loops close to the nuclear lamina which is attached to the nuclear membrane made up of two lipid bilayers. Nuclear pore complexes reside within natural pores in this double membrane which also houses trans-nuclear membrane proteins that interact with the cytoskeleton through the LINC complex.

1.3.1   The Nuclear Lamina

The lamina is composed of type A or B lamin proteins, lamin B1 and B2 are the most common B lamins and are encoded by distinct genes *LNMB1* or *LNMB2.* B-type lamins have an acidic isoelectric point, at least one form is expressed in all cells, and are permanently found to be isoprenylated (which helps tether the protein to the INM) (Nigg et al., 1992; Gruenbaum et al., 2003). A-type lamins are formed from two splice variants of the *LNMA* gene that give rise to lamin A and lamin C. These proteins have a neutral isoelectric point, are expressed in a tissue-specific manner and may not always be isoprenylated (Gruenbaum et al., 2003). Both types consist of a N-terminal head domain, a coiled-coil central rod

domain and a C-terminal tail domain, and include a nuclear localisation sequence, an immunoglobulin (Ig) fold and a CaaX motif (Gruenbaum and Aebi, 2014). Experiments using 3D-structured illumination microscopy (3D-SIM) showed that lamin filaments form separate continuous meshworks in mammalian nuclei with A-type lamins playing a crucial role in regulating the distribution of NPCs (Shimi et al., 2015; Xie et al., 2016).

The lamin meshwork not only acts as a simple scaffold but also has a multitude of binding partners. These include nuclear envelope transmembrane proteins (NETs) which allow the nuclear lamina to transmit mechanical signals to cellular actin filaments via the linker of nucleo- and cytoskeleton (LINC) complex (Padmakumar et al., 2005; Crisp et al., 2006). Lamins also play a role in binding heterochromatin to the nuclear periphery through interaction of LEM domain proteins and barrier to autointegration factor (BAF). Experimental studies have demonstrated how relocating actively transcribed genes to the nuclear lamina leads to gene silencing, demonstrating the regulatory role of the lamina (Reddy et al., 2008). This highlights how the nuclear lamina contributes to the physical organisation of nuclear contents (especially the genome) in order to regulate gene expression. Localisation to the nuclear periphery and the lamina is associated with an increased level of repression, whilst localisation of genes to the nuclear interior leads to their expression. In developmental contexts this has been shown to be especially important in defining stages of differentiation (Peric-Hupkes et al., 2010).

1.3.2 The Nuclear Membrane

33

The nuclear membrane is composed of two lipid bilayer membranes that are connected via membrane-bound proteins and at NPCs (Figure 1.12). The outer nuclear membrane (ONM) is contiguous with the endoplasmic reticulum and features a number of membrane-bound proteins, such as the Nuclear envelope spectrin repeat proteins (Nesprin) family. These proteins act to help transmit mechanosensory signals between nuclear filaments and the cytoskeleton through the functioning of the LINC complex (Burke and Roux, 2009; Uzer et al., 2015).

The inner nuclear membrane (INM) interacts with the nuclear lamina, giving the nucleus its overall shape, and is also the surface for many membrane-bound proteins. These include proteins that act within the LINC complex to transmit mechanosensory information, such as Sun2. Sun2 binds lamins and other nucleoplasmic factors but also has a lumenal domain targeted to the perinuclear space (the lumenal space between the ONM and INM). There Sun2 interacts with Nesprin proteins, forming a crucial bridge between the nucleus and the cytoplasm for the LINC complex (Hodzic et al., 2004; Crisp et al., 2006; Burke and Roux, 2009).
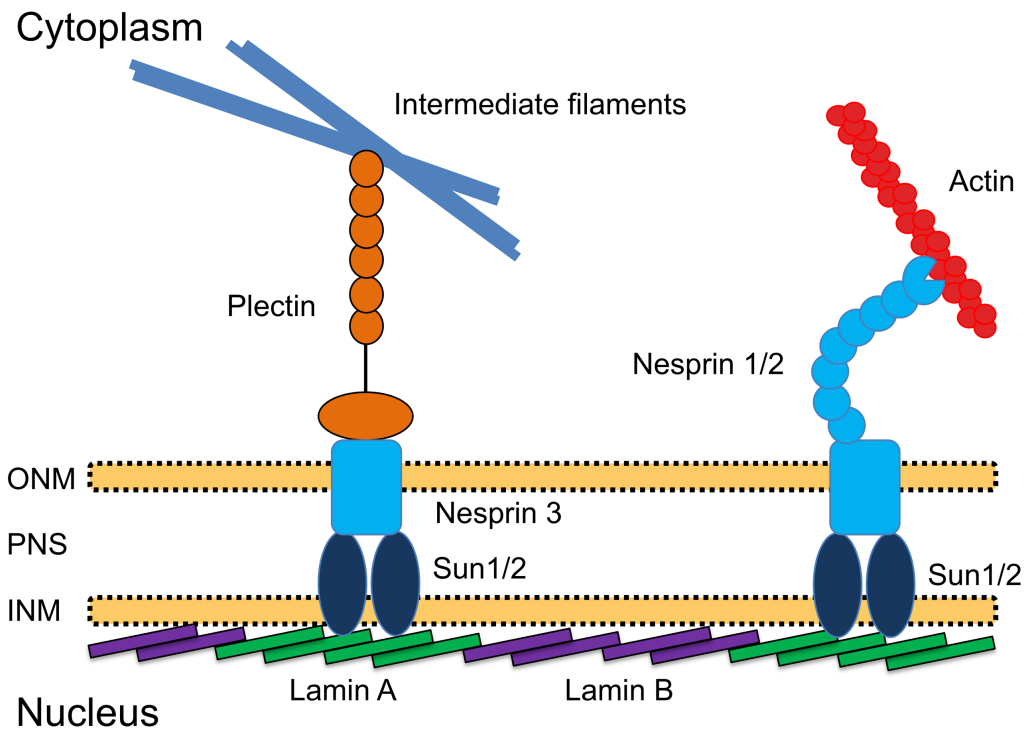
Figure 1.12 Overview of the nuclear membrane. The lamina represented by alternating filaments of lamin A and B attached to the inner nuclear membrane (INM) via Sun1/2 proteins. These proteins bind to Nesprin proteins in the perinuclear space (PNS) which exists as a transmembrane protein between the PNS and the outer nuclear membrane (ONM) attaching to either plectin and then intermediate filaments (Nesprin 3) or actin via Nesprin 1/2.

1.3.3 The Nuclear Pore Complex

The Nuclear Pore Complex (NPC) is a highly conserved protein mega-complex that sits within pores formed within the nuclear membrane. Present in all forms of eukaryotic life, the NPC is the most significant conduit of information in the cell, giving rise to a selective bidirectional transport system. In humans, the complex is approximately 125 MDa in mass and is composed of ~500-1000 copies of 30 different nucleoporins (Nups) (Cronshaw et al., 2002; DeGrasse et al., 2009). These give rise to a protein mega-structure that exhibits eightfold radial symmetry with a series of subcomplexes that perform critical roles in regulating nucleocytoplasmic transport.

35

1.3.3.1 Structure of the NPC

Over the past 50 years significant work has elucidated a highly ordered structure comprising of multiple copies of nucleoporins arranged in eightfold radial symmetry around a pore within the nuclear membrane. Nucleoporins are complexed into different sub-complexes which come together to form substructures that form the overall NPC superstructure. These substructures can be classified into 6 main groups: integral membrane proteins of the pore membrane domain of the nuclear envelope (POMs); membrane apposed coat nucleoporins; adaptor nucleoporins; channel nucleoporins; nuclear basket filaments; and cytoplasmic filament nucleoporins (Hoelz et al., 2011) (Figure 1.13).

The first work on the nuclear pore began in 1950, when H. G. Callan used nuclei from amphibian *Xenopus laevis* to visualise the nuclear membrane using electron microscopy. Through his preparation he observed pores within the nuclear membrane which he described as "evenly space out over its area [outer nuclear membrane]" (Callan and Tomlin, 1950). In 1959, Michael Watson identified discrete densities at these pores with the appearance of a channel and cytoplasmic extrusions. He described these as "sufficiently well differentiated to be classed as an anatomical unit for which we propose the name *pore complex"* (Watson, 1959). Further work showed the pore complex was not circular but exhibited eight-fold radial symmetry and also extended significantly out into the nucleus and the cytoplasm (Abelson and Smith, 1970; Wischnitzer, 1973). As electron microscopy technology improved, the NPC quite literally came into focus with a 90 Å structure in 1982, beginning to highlight the discrete substructures

that make up the NPC (Unwin and Milligan, 1982). In 1986, Günter Blobel's laboratory isolated the first nucleoporin and yielded an antibody for visualising the nuclear pore complex using immunofluorescence (Davis and Blobel, 1986). Increasing improvements have established that the structure of the NPC has two coaxial rings, at both the nuclear and cytoplasmic periphery, which are connected by eight elongated spokes and a central spherical plug region (Jarnik and Aebi, 1991; Stoffler et al., 2003; Beck et al., 2004a). Whilst the core appears like a symmetric doughnut structure, the major structural projections out of the core are not symmetric and form a nuclear basket region and multiple cytoplasmic filaments.
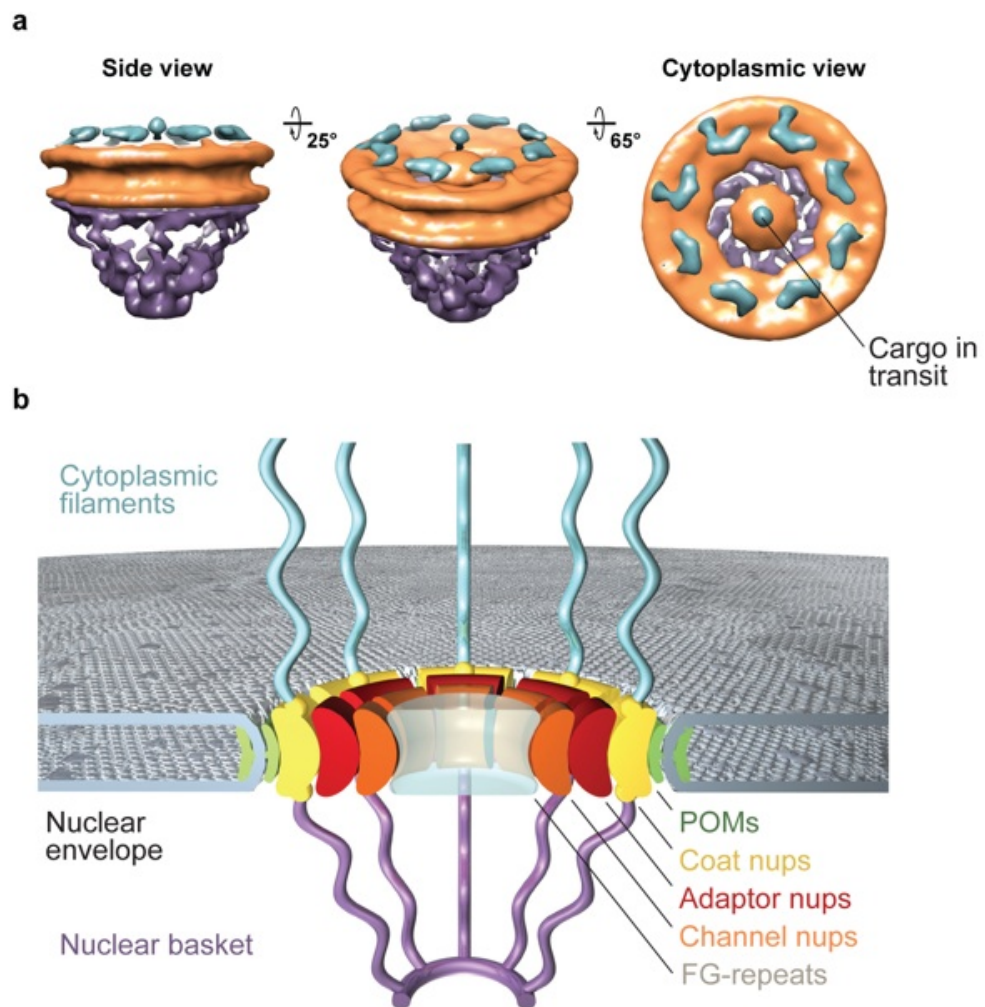
Figure 1.13 The Structure of the Nuclear Pore Complex. a) Cryo-electron tomographic reconstruction of the Dictyostelium discoideum NPC [Electron Microscopy Data Bank (EMDB) code 1097, Beck et al. 2004]. The cytoplasmic filaments, the symmetric core, and the nuclear basket are coloured in cyan, orange, and purple, respectively. b) A schematic model of the NPC. The four concentric cylinders are composed of integral pore membrane proteins (POMs), coat nucleoporins, adaptor nucleoporins, and channel nucleoporins. Natively unfolded phenylalanine-glycine (FG) repeats of a number of nucleoporins make up the transport barrier in the central channel and are indicated by a transparent plug. Taken from (Hoelz et al., 2011).

The nucleoporin composition of these distinct structures has demonstrated how nucleoporins combine into small substructures that exist in multiple copies to give rise to the larger structures. Starting with the non-symmetric structures at the NPC, the cytoplasmic filaments are made up of three nucleoporins Nup358/RanBP2, CAN/Nup214 and Nup88/84 (Kraemer et al., 1994; Wu et al., 1995; Bastos et al., 1997). Nup358 is a nucleoporin specific to vertebrates and is the largest nucleoporin, with purified Nup358 forming ~36 nm long, 5 nm thick filaments (Yokoyama et al., 1995; Delphin et al., 1997). It acts as a key junction during the RanGTP cycle and contains several phenylalanine-glycine (FG) repeats which function as binding sites for transport receptors (Yaseen and Blobel, 1999). Nup88/Nup84 forms a cytoplasmic orientated subcomplex with CAN/Nup214, an apparent component of the cytoplasmic filaments (Kraemer et al., 1994; Panté et al., 1994; Fornerod, van Deursen, et al., 1997; Bastos et al., 1997). Both proteins appear to play a key role in nuclear localisation sequence (NLS)-mediated protein import and bulk mRNA export (van Deursen et al., 1996; Uv et al., 2000).

The other major non-symmetric NPC structure is the nuclear basket. In 1991 the development of high resolution scanning electron microscopy enabled the first visualisation of a basket structure on the nucleoplasmic face of the NPC (Goldberg and Allen, 1992). Starting with the nucleoplasmic coaxial ring at the

38

nuclear pore, eight fibres extend out ~40 nm into the nucleoplasm and attach to a small 'basket' ring of 60 nm in diameter (Goldberg and Allen, 1992). In vertebrates the nuclear basket is composed of three nucleoporins: Nup50, Nup153 and TPR. TPR is the most significant component of the nuclear basket with a molecular mass of 265 kDa forming a coiled-coil structure, although its exact localisation at the nuclear basket is disputed (Cordes et al., 1997; Frosst et al., 2002; Krull et al., 2004). TPR also appears to play a role relating to CRM1-dependent export and mediating a level of RNA export quality control prior to export (Frosst et al., 2002; Coyle et al., 2011). Nup153 is a more peripheral component of the nuclear basket with immunogold staining showing it localises to the nucleoplasmic coaxial ring (Krull et al., 2004). It appears to play a crucial role in nuclear export, and during nuclear pore assembly after cell division (Sukegawa and Blobel, 1993; Ullman et al., 1999; Vollmer et al., 2015). Nup153 also appears to be a mobile nucleoporin, able to diffuse off the NPC, and perform functions within the nucleus (Nakielny et al., 1999; Griffis et al., 2004; Vaquerizas et al., 2010). The final vertebrate nuclear basket nucleoporin is Nup50, a small mobile nucleoporin with a very short residence time at the NPC (Guan et al., 2000; Rabut et al., 2004). Nup50 binding at the nuclear pore is dependent on Nup153 and suggests Nup50 has a role in nuclear import. Furthermore, studies have shown Nup50 binds to importins (Lindsay et al., 2002; Makise et al., 2012). Interestingly, Nup50-depletion is not lethal but does prevent differentiation events in C2C12 myoblasts, suggesting a non-transport based role of this nucleoporin (Buchwalter et al., 2014).

The symmetric core of the NPC is composed of three stacked rings: an inner ring that spans the fused nuclear membranes, and cytoplasmic and nucleoplasmic

39

rings which stack upon the inner ring from each respective side (Unwin and Milligan, 1982). The key scaffold subcomplexes of these rings are the Y-complex and the inner ring complex. The Y-complex is the most well-known and best structurally defined of these subcomplexes with its distinct Y-shape made up of a small arm, a large arm and a stem (Lutzmann et al., 2002; Beck et al., 2004b; Kampmann and Blobel, 2009). The small arm is composed of Nup85, Seh1 and Nup43, whilst the large arm comprises Elys, Nup37, Nup160. These two arms connect to one another via Nup160-Nup85 complex and the stem through Nup96 and Sec13. Nup96-Sec13 connect to a highly flexible stem tip containing Nup133 and Nup107 (Bui et al., 2013; Kelley et al., 2015). Multiple copies of the Y-complex oligomerise into two head-to-stem rings at both the cytoplasmic and nucleoplasmic side. These two rings form an inter-complex crosslink between the inner and the outer ring (Figure 1.14). These rings act as the crucial scaffold on which the asymmetric structures already described connect to the NPC itself.

The inner ring complex is composed of five nucleoporins: Nup205, Nup88, Nup93, Nup155 and Nup53. Nup53 has been shown to bind to the integral membrane protein component of the nuclear pore NDC1 that spans the nuclear membrane, anchoring the NPC (Eisenhardt et al., 2014). Nup155 has also been shown to make contact points with the nuclear membrane and surrounds the membrane in multiple copies as a first layer between the membrane and the remaining inner ring complex proteins (Bui et al., 2013). The second layer of the inner ring complex is comprised of Nup205 and Nup188; however, due to the small size of Nup93 current methods struggle to identify its exact position in the inner ring complex (Andersen et al., 2013) (Figure 1.14). Other subcomplexes have also been shown to interact with the inner ring complex, with both Nup188

40

and Nup93 binding to Nup214-Nup84-Nup62-Nup98-Rae1 complex (Von Appen et al., 2015). Importantly, this highlights that the understanding of the NPC architecture is still developing, with areas of the NPC such as the inner ring complex still poorly understood.
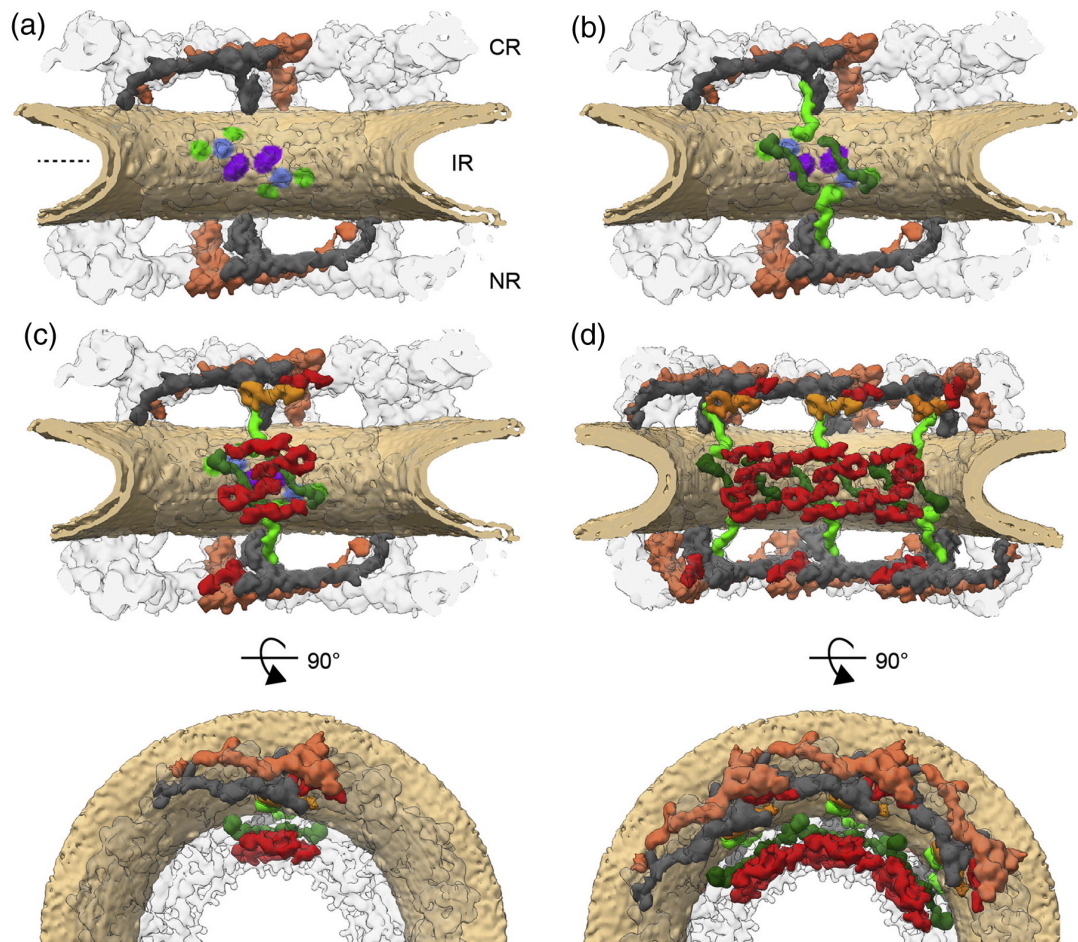
Figure 1.14 The architecture of the NPC scaffold. a) One symmetric unit of the NPC with four copies of the Y-complex that form the scaffold of the cytoplasmic ring (CR) and the nucleoplasmic ring (NR). The outer copy is shown in orange; the inner copy is shown in gray. Multiple membrane contacts of the inner ring complex: region of outer bilipid layer where contacts made are shown in green and purple; apparent transmembrane domains are shown in blue. b) Nup155 (green) appears to interact with the membrane at the points indicated in a). c) Nup205 and Nup188 densities (red) per asymmetric unit localise to the CR, IR and NR. Another copy might reside only on the cytoplasmic site and is shown in orange. d) Proteins of neighbouring asymmetric units are shown as well. Taken from (von Appen and Beck, 2015).

The final symmetric subcomplex is composed of channel nucleoporins Nup62, Nup58 and Nup54. These nucleoporins give rise to the selective barrier of the NPC and many aspects of their protein structure are highly conserved across all

41

eukaryotic life. The Nup62-Nup58-Nup54 complex attaches to the inner ring complex protein Nup93 and extends into the central channel. In the central channel, these subcomplexes oligomerise into a ring structure, able to constrict and dilate dependent on the binding of transport factors (Sharma et al., 2015). These nucleoporins are also rich in FG-repeat regions that extend into the central channel and create the selective barrier. The exact mechanism of nuclear transport that arises from the FG-repeat density in the central channel but is poorly understood although a range of theories have been proposed.

1.3.3.2 Nuclear Transport

The key function of the NPC is to facilitate selective bidirectional transport between the nucleus and cytoplasm. This includes the export of RNAs into the cytoplasm, the import of mature proteins into the nucleus, and the export of enormous ~2.5 MDa pre-ribosomal subunits, to name a select few transport operations. These processes must all occur near simultaneously and in a highly selective manner to prevent damage to the nuclear compartment. Statistical modelling has predicted the scale of nuclear transport to be approximately 1000 translocation events per second of approximately 100 MDa/s (Ribbeck and Görlich, 2001). The NPC achieves this via a highly regulated transport system that combines a permeability barrier and a receptor-based transport system.

1.3.3.2.1 Receptor Transport system

The machinery behind receptor-based transport systems is highly conserved within eukaryotes. This suggests that the development of this system was a critical juncture in the evolution of eukaryotic life, when one of the key constraints of evolving a contained compartment for the genome was overcome. Behind this

42

evolutionary significance is the small GTPase Ras-related nuclear protein (Ran), which is highly conserved and a member of the Ras family of GTPases (Moore and Blobel, 1993).

The Ran cycle describes the process of nucleotide exchange that Ran performs between the cytoplasm and the nucleus. The classical cycle of nuclear transport begins with the formation of a heterotrimer of importin beta, importin alpha and a cargo containing a nuclear localisation sequence (NLS). This complex docks to and is transported through the NPC where the importins facilitate transport through the FG-repeat layer. Once in the nucleus, a high RanGTP environment, importin beta is bound by RanGTP, promoting the disassembly of the heterotrimer. The cargo can now fulfil its role in the nucleus and importin beta and alpha are separately exported after being bound by RanGTP, in the case of importin alpha also binding cellular apoptosis susceptibility gene (CAS) (Kutay et al., 1997). After these factors are transported through the NPC into the cytoplasm, a high RanGDP environment, RanGTP is hydrolysed by RanGAP1 and RanBP1 which causes the dissociation of RanGDP and the importin complex. This releases the importins for any subsequent import events. Meanwhile RanGDP is reimported into the nucleus where the nucleotide exchange factor RCC1 promotes the exchange of GDP for GTP (Figure 1.15).
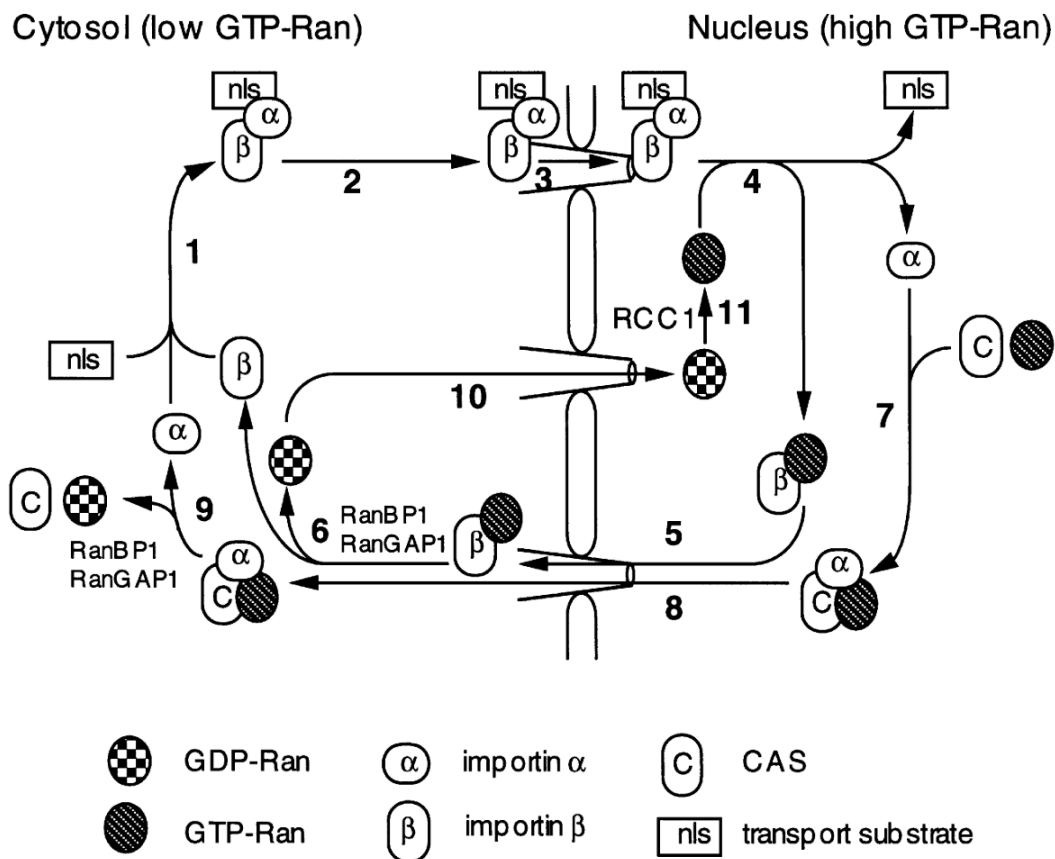
Figure 1.15 The Ran cycle. 1. A heterotrimer of importin alpha, beta and a cargo containing a nuclear localisation sequence (NLS) forms. 2. This complex moves to the NPC. 3. The complex is transported through the NPC with importins interacting with nucleoporins. 4. RanGTP binds causing the dissociation of the heterotrimer binding to importin beta. 5. Importin beta and RanGTP are re-exported out of the nucleus. 6. RanBP1 and RanGAP1 induce the hydrolysis of RanGTP to RanGDP leading to the release of importin beta. 7. Importin alpha interactions with CAS and RanGTP in the nucleus forming a complex. 8. This complex then exits the nucleus. 9. RanBP1 and RanGAP1 induce the hydrolysis of RanGTP to RanGDP inducing the dissociation of importin alpha and CAS in the cytoplasm. 10. RanGDP travels down the concentration gradient into the high RanGTP environment in the nucleus. 11. RanGDP is converted back into RanGTP by RCC1. Taken from (Dasso and Pu, 1998).

Whilst the energetic system powering nuclear transport is well-defined, the exact mechanism of how transport receptors such as importins bind nucleoporins and facilitate transport is less well understood. The hydrophobic environment of the central channel of the NPC has been demonstrated to be critically important for successful transport (Ribbeck and Görlich, 2002). Crystal structure analysis of importin beta bound to the FG-motif complex shows that importin beta has

several hydrophobic pockets that interact with hydrophobic residues in the FG-nucleoporins (Bayliss et al., 2000; Liu and Stewart, 2005; Otsuka et al., 2008). Studies investigating the structure of members of the karyopherin beta superfamily (of both importins and exportins) show a high level of structural similarity between family members even though sequence similarity is very low (Xu et al., 2010; O'Reilly et al., 2011). Structurally, they are composed of a number of HEAT motifs (19-21 repeats), containing two amphiphilic alpha helices connected by a short linker region (Chook and Blobel, 1999; Cingolani et al., 1999). These structures are highly flexible, which is thought to relate to their role binding different cargoes and RanGTP (Conti et al., 2006; Forwood et al., 2010). Many investigators have noted the apparent paradox of strong interactions between karyopherins and FG-nucleoporins and the speed of nuclear transport, questioning how transport complexes do not get trapped within the NPC through these strong hydrophobic interactions. Recently, it has been demonstrated that importin beta undergoes a conformational change during passage through the NPC, mediated by a series of weak hydrophobic interactions with nucleoporins. It is hypothesised that these induced changes lead to highly stochastic transport with a number of outcomes, including a proportion of transport events failing to cross the nuclear pore on a single attempt (Yoshimura et al., 2014).

1.3.3.2.1.1 mRNA Transport

mRNA transport is a crucial example of receptor based transport facilitated by the NPC. mRNA export occurs via a distinct mechanism from nuclear export of proteins, tRNA and miRNAs. The two predominant export adaptor proteins that are loaded onto messenger ribonucleoprotein (mRNP) complexes are Nxf1-Nxt1 and Crm1.

45

Bulk mRNA export occurs through the action of heterodimer of Nxf1/TAP and Nxt1 (Segref et al., 1997; Herold et al., 2000). Nxf1-Nxt1 heterodimer is recruited to mRNP complexes via interactions with ALY a component of the TREX complex. Nxf1-Nxt1 act as a nuclear export receptor that then facilitates passage through the NPC.

A subset of cellular mRNAs are exported via an alternate pathway facilitated by karyopherin Crm1 (Fornerod, et al., 1997). Crm1 is also responsible for mediating export of unspliced and partially spliced HIV mRNA through the action of the HIV Rev protein (Cullen, 2003). The Crm1 pathway requires additional adaptor proteins due to Crm1 lack of an RNA binding function. These appear to vary depending on the transcript being exported, with eukaryotic initiation factor 4E (eIF4e) for cyclin D1 mRNA and HuR reported as an adaptor for Cd83 and Fos mRNA export (Brennan et al., 2000; Culjkovic et al., 2006).

Once these export receptors are recruited to the mRNP it is considered export competent. This targets the mRNP to the NPC where the export receptor is able to directly interact with FG-nups. It has been suggested that the 5' end of the mRNP leads the mRNP into the pore at the nuclear face of the NPC (Visa et al., 1996). How the binding of export receptors to FG-nups facilitates movement of the mRNP in the NPC is unclear and different theories surrounding this are addressed in the next section. However, work has shown that not all FG-nups are required for mRNA export, only specific subcomplexes in the central channel and at the nuclear face hinting that export occurs through a series of thresholds in the pore before final commitment to exit into the cytoplasm (Terry and Wente, 2007).

1.3.3.2.2 Permeability barrier

The permeability barrier acts to prevent the passive diffusion of large molecules into the nucleus; the limits of which are either a mass greater than 40 kDa or a diameter greater than 390 Å (Panté and Kann, 2002). FG-nucleoporins that line the inner channel of the NPC are responsible for the formation of the barrier. Typically, these proteins are composed of a folded domain and an intrinsically disordered domain (IDD) (Wagner et al., 2015). IDD are domains that lack a stable secondary or tertiary protein structure. This often leads to difficulties visualising these proteins through crystallographic techniques and is the predominant research hurdle towards understanding FG-nucleoporin formation at the NPC. FG-nucleoporins also have a low net charge and high mean hydrophobicity, along with repeats of the eponymous FG-motif (Schmidt and Görlich, 2016). The most common of these motifs are: FG, FxFG, GLFG, PxFG, SxFG (Cushman et al., 2006; Denning and Rexach, 2007).

The structure formed by the convergence of FG-nucleoporins in the central channel is a current area of debate and further investigation. A number of models have been proposed, but there is currently no consensus on what structure may exist in the central channel. Some of these models include: the selective phase/hydrogel model, reduction of dimensionality model, the kap-centric model, and the polymer brush model. The selective phase model, also known as the hydrogel model, hypothesises that intra- and intermolecular interactions between FG-nucleoporins create a cohesive, gel-like network (Ribbeck and Görlich, 2002; Frey and Görlich, 2007) (Figure 1.16b). This creates a 3D molecular sieve that occludes large molecules but allows for the diffusion of small molecules, whilst nuclear transport receptors (NTR) are able to pass through the gel via their

47

hydrophobic domains (similar to how lipids pass through a lipid bilayer). To support this theory FG-nucleoporins form a hydrogel *in vitro* and permit the selective transport of importins (Frey and Görlich, 2009; Hülsmann et al., 2012).

The reduction of dimensionality (ROD) model arose from observations that the NPC appeared to be saturated with NTRs at all times and suggested that FG-domains coat the walls of the central channel and are occupied continuously with NTRs (Peters, 2005) (Figure 1.16c). This binding was speculated to cause a collapse of the FG-filaments, creating a small inner lumen at the centre of the pore to allow for small molecule diffusion. FG-bound NTR were then confined to move in only two dimensions, where they would random walk over the FG surface on the sides of the central channel and reach their transport destination (Peters, 2009; Schleicher et al., 2014).

The kap-centric model posits that due to the proportionally greater numbers of karyopherins present in cells compared to nuclear pores, it is karyopherins (kaps) that regulate the speed and selectivity of the NPC (Reviewed in (Lim and Kapinos, 2015)). Proponents of this hypothesis point to evidence that in permeabilised cells where high karyopherin concentrations are added nuclear transport increases, whilst in low karyopherin environments nuclear transport is slower (Timney et al., 2006; Yang and Musser, 2006). They argue that if FG-nucleoporins were predominantly responsible for managing nuclear transport speeds, a high kap environment means more FG-NTR saturation at the NPC leading to slower transport (Figure 1.16d). Given the experimental evidence, they suggest that the key regulators of nuclear transport efficiency and speed are the kaps themselves. They also point to experiments performed which advocate the

hydrogel model and claim these observations support the idea that karyopherins are able to regulate the permeability of FG-nucleoporins with *in vitro* FG-nucleoporin hydrogels able to 'heal' after the diffusion of NTRs through the hydrogel (Frey and Görlich, 2009).

The virtual gate or polymer brush model contrasts with many of the other hypothesises by proposing a mechanism based on thermodynamic considerations rather than elucidating the role of FG-FG interactions (Rout et al., 2003) (Figure 1.16a). This suggests that the movement of a molecule from the cytoplasm to the nucleus involves a loss of entropy, due to few movement possibilities in the smaller nucleus. The energy price of this loss of entropy would be increased by non-cohesive FG-domains that were posited to act as repulsive or entropic bristles which moved randomly (Lim et al., 2006). This would create an entropic gate, preventing the random diffusion of molecules into the nucleus. For transport to occur it was hypothesised that interactions with FG-domains would release enthalpy and, if the binding energy generated was high enough to overcome the loss of entropy, transport would occur.

a) **Virtual gating/polymer brush**

b) **Selective phase/hydrogel**

c) **Reduction of dimensionality**

d) **Kap-centric**
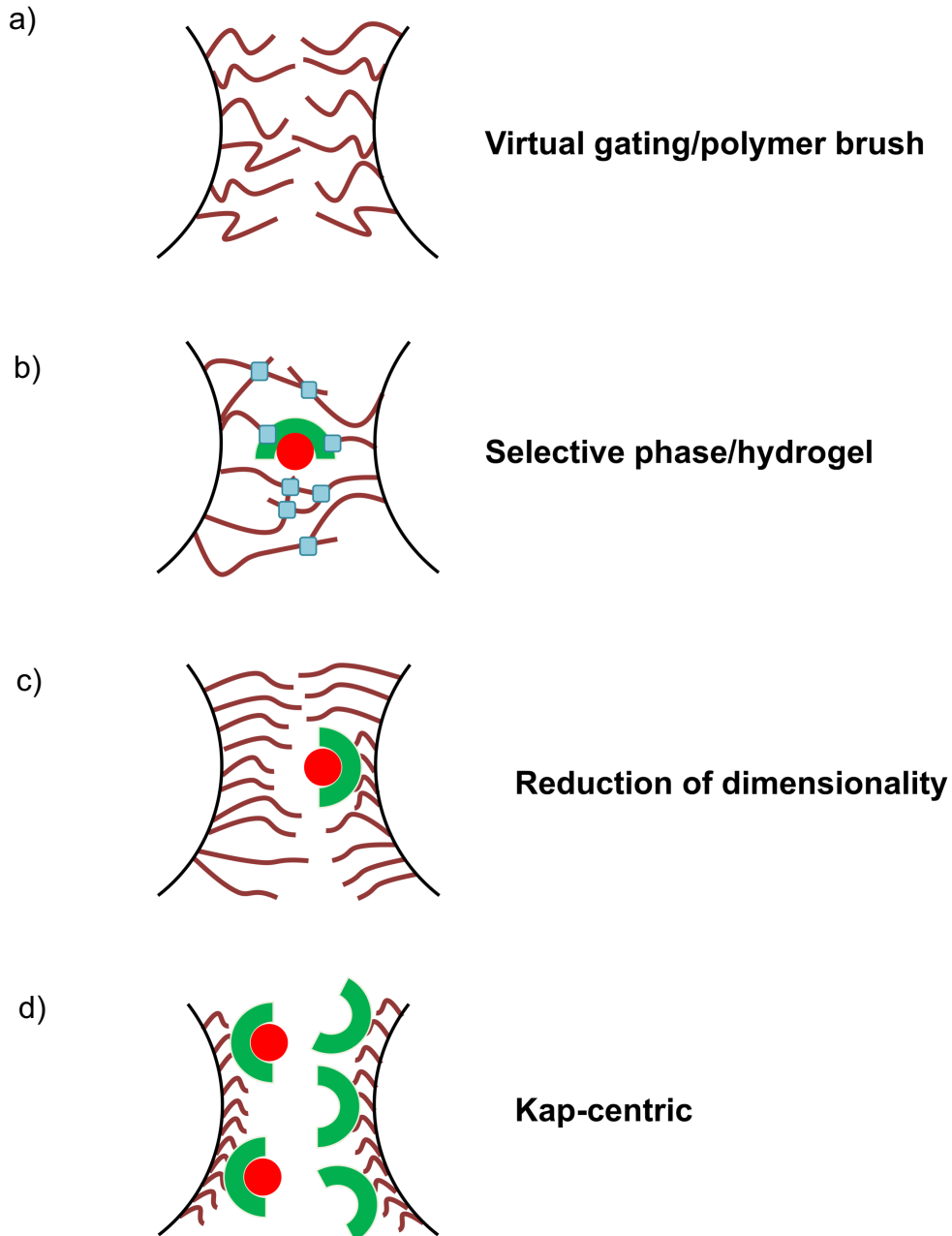
Figure 1.16 Models of the central NPC channel. a) Virtual gating/polymer brush model, characterised by non-cohesive FG-domains acting as entropic barriers. b) Selective phase/hydrogel model, characterised by cohesive FG-domain interactions (blue) between other FG-domains and the NTR (green) this allows for the movement of cargo (red) through the NPC. c) The reduction of dimensionality, FG-nups bind to the NTR allowing for transport along a 2D axis at the sides of the channel, binding of the NTR facilitates collapse of the FG-filaments. d) Kap-centric, the binding of karyopherins occurs continuously and regulates the speed and permeability of the NPC barrier.

50

1.3.4 The Dynamic NPC

With the expansion in understanding of the structure and function of the NPC evidence has begun to emerge suggesting the NPC is a much more dynamic structure than initially thought. The residency time of almost a third of NPC components, typically central channel and nuclear/cytoplasmic facing nucleoporins, has been shown to be short (ranging from a few seconds to a few hours) (Rabut et al., 2004). Scaffold nucleoporins exhibit a far longer residency time often greater than a cell cycle. How these dynamic movements on and off the pore are implicated in the function of the NPC is a developing knowledge domain that has also begun to highlight the many non-transport related roles of nucleoporins.

1.3.4.1 The NPC during development

A number of nucleoporins have been shown to be necessary for the differentiation of different cell types. Nup210 or GP210 is required for both myogenesis and neuronal differentiation in mice. Its expression is induced during differentiation; however its incorporation into the NPC does not appear to alter nuclear transport but rather the expression of myogenesis genes (Capelson et al., 2010; Kalverda et al., 2010; D'Angelo et al., 2012).

Similar to GP210, Nup358 has also been attributed to myoblast differentiation. Increased Nup358 expression is required for correct myoblast differentiation, although, as above, this does not alter nuclear transport pathways. It has been observed that myoblasts and myotubes exhibit different Nup358 copy number at their NPC, suggesting these differentiation changes are structurally-related;

51

however, how this change is important for differentiation is not yet understood (Asally et al., 2011).

Nup133 and ELYS, both components of the Y-complex, are required for successful differentiation of certain cell types. In Zebrafish, the absence of the ELYS homologue results in abnormal neuronal differentiation affecting development of the retina (Cerveny et al., 2010). In mice, a mutation that generates a null allele of Nup133 also leads to neuronal development defects and is lethal (Lupu et al., 2008). The mechanism behind this role is not well understood, but the structural nature of these nucleoporins suggests they function away from the pore during differentiation.

1.3.4.2   Cell type specific NPCs

A number of nucleoporins have been identified that exhibit tissue specific expression patterns. These include Nup210, Nup45, Nup50, Nup133, Nup155 and ALADIN (Hu and Gerace, 1998; Zhang et al., 1999; Guan et al., 2000; Olsson et al., 2004; Cho et al., 2009). Furthermore, mutations in several nucleoporins lead to tissue-specific pathologies. A mutation in Nup155 (found highly expressed in heart, placenta, liver and skeletal muscle) preventing it binding at the NPC leads to heart malfunction and cardiac disease (Zhang et al., 1999; Zhang et al., 2008). Missense mutations in Nup62, a key FG-nucleoporin in the central channel, lead to autosomal recessive infantile bilateral striatal necrosis, a severe brain disorder with degeneration of the basal ganglia (Basel-Vanagaite et al., 2006). Mutations in the nucleoporin ALADIN cause triple A syndrome (AAAS) which causes adrenocorticotropic hormone (ACTH)-resistant adrenal failure (Cho

et al., 2009). These findings developed into a hypothesis that NPCs exists as much more specialised structures across different cell types (Figure 1.17).
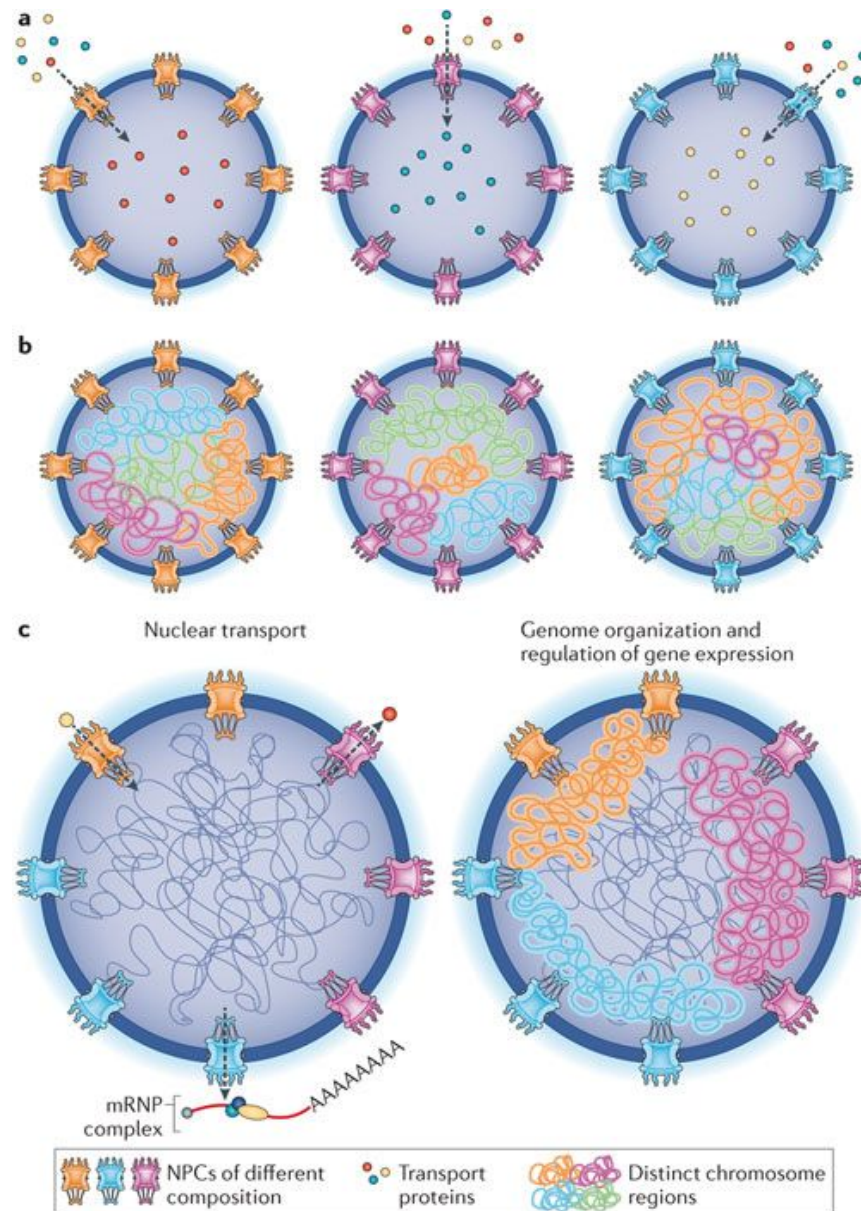
Figure 1.17 Overview of specialised nuclear pore complexes. a) Specialised NPCs with alternate transport pathways. b) Specialised NPCs able to interact with different chromatin sections. c) A model of specialised NPCs within a single cell. Taken from (Raices and D'Angelo, 2012).

1.3.4.3   Nup98

Nup98 is a well-characterised example of a dynamic nucleoporin. Nup98 is expressed predominantly as a bicistronic peptide comprising of Nup96-Nup98.

53

This polypeptide undergoes autoproteolytic cleavage that allows both nucleoporins to localise at the NPC. At the NPC, Nup96 and Nup98 have unrelated roles, with Nup96 acting a component of the structural Y-complex with a residency time of several months, whilst Nup98 cycles on and off the pore and is turned over rapidly (Toyama et al., 2013). This cycling leads to the existence of two pools of Nup98 within the cell, one at the NPC and one within the nucleoplasm (Griffis et al., 2002; Oka et al., 2010). At the NPC, Nup98 is involved in mRNA export through its interaction with mRNA export factors Rae1 and Nxf1 (TAP) (Powers et al., 1997; Bachi et al., 2000; Blevins et al., 2003). Nup98 also interacts with members of the importin beta family and the exportin CRM1 (Allen et al., 2001; Oka et al., 2010).

The nucleoplasmic fraction of Nup98 is a remarkable case study of the dynamic nature of the NPC (Figure 1.18). Extensive work in *Drosophila* has shown that nucleoplasmic Nup98 binds at the promoters of genes responsible for development, and that depletion of Nup98 leads to robust suppression of these promoters (Kalverda et al., 2010; Capelson et al., 2010). Furthermore, Nup98 directly interacts with histone modifying enzymes such as CBP/p300 and histone deacetylases (HDACs) through its unique form of FG repeat, GLFG (Lawryn H. Kasper et al., 1999; Bai et al., 2006). Nup98 translocation mutants are also key promoters of the onset of acute myeloid leukaemia (AML) through the ability of Nup98 to recruit histone deacetylases to promote oncogenic expression (Bai et al., 2006). The GLFG domain is also responsible for the formation of discrete Nup98 foci within the nucleus called GLFG-bodies (Griffis et al., 2002; Griffis et al., 2004). The exact function of these discrete bodies is unclear, and they are not observed across all cell types. RNA polymerase II does not localise at GLFG

54

foci, leading to the suggestion that GLFG-bodies act as dynamic storage centres of nucleoplasmic Nup98 that can rapidly cycle to transcriptional start sites when needed (Griffis et al., 2002; Franks et al., 2017). Nup98 also regulates the expression of antiviral response genes and has been attributed to a phenomenon called 'epigenetic transcriptional memory'. This is predominantly linked to the interferon gamma (IFN-γ) response with IFN-γ-inducible genes able to be induced faster after an initial IFN-γ treatment due to the presence of a histone modification and Nup98 (Light et al., 2013; Panda et al., 2014).
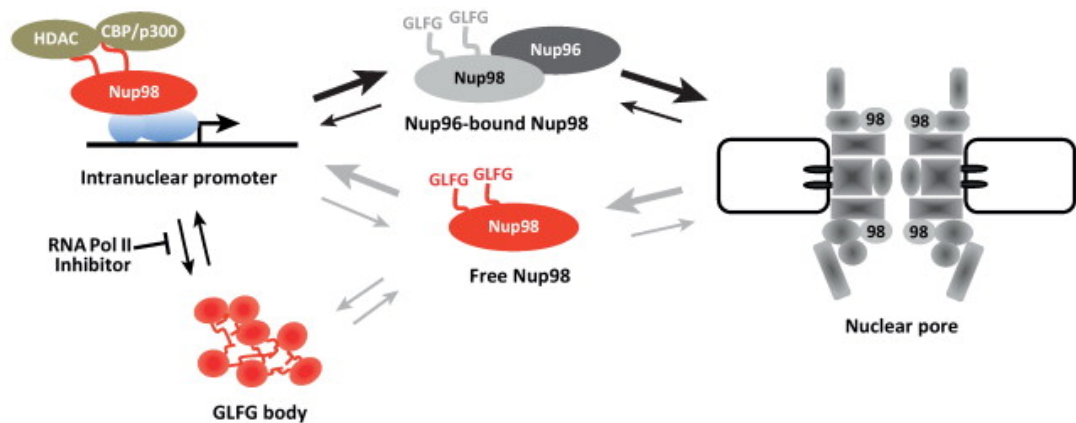
Figure 1.18 Model of the alternate cellular pools of Nup98. The NPC-bound Nup98 is shown in grey. Nup96-bound Nup98 promotes the localisation of Nup98 at the nuclear pore. Free Nup98 (shown in red) is able to diffuse off the NPC and form GLFG bodies or bind at promoters and recruit histone remodelling complexes. Adapted from (Franks et al., 2017).

1.3.5 Viral remodelling of the Nuclear Pore Complex

The position of the NPC as the primary conduit between the nucleus and the cytoplasm makes it a key target for certain viruses. For viruses that replicate relatively quickly access to the nucleus provides an effective way of utilising host DNA replication machinery. If a virus has a relatively longer replication cycle, access to the nucleus provides a safer environment to protect the viral genome

55

and coordinate slow subversion of other cellular processes. Due to the complexity of the NPC, viruses have developed an incredible variety of strategies for subverting its selective barrier function. These include brute force demolition of the central channel, or viral factors binding to nucleoporins or manipulating nuclear transport.

1.3.5.1 Capsid remodelling Events

A common form of NPC remodelling occurs during *de novo* infections where the viral capsid is transported to the nuclear pore. At this stage the goal of the virus is to deliver its genome into the nucleus through capsid interactions with nucleoporins.

Adenovirus is one such virus that utilises capsid-based remodelling to deliver its genome. After internalisation at the plasma membrane, the adenovirus virion is transported along cellular microtubules to the nucleus. The capsid is then able to bind to Nup214 targeting it to the NPC and kinesin-1 light-chain Klc1/2 (Trotman et al., 2001). Nup358, which is a component of the cytoplasmic filaments that includes Nup214, is then bound by kinesin-1 heavy-chain Kif5C (Strunze et al., 2011). This seems to exert a force upon the capsid that causes disassembly and the release of the viral genome along with relocalising Nup358, Nup214 and Nup62 from the NPC. This increases the permeability of the NPC and appears to aid with the import of the viral genome into the nucleus (Strunze et al., 2011).

HSV-1 also exhibits capsid-NPC interactions during initial viral genome delivery. Viral tegument proteins pUL36 and pUL25 mediate docking of the virion to the NPC through interactions with Nup358 and Nup214 at the cytoplasmic filaments

(Copeland et al., 2009; Pasdeloup et al., 2009). These tegument proteins are also involved in the uncoating of the virion once docked to the NPC, triggering the release of the viral DNA.

Hepatitis B virus (HBV), a hepadnavirus that has a double-stranded DNA genome but replicates through an RNA intermediate step, transports its DNA genome into the nucleus on initial infection. Within the nucleus HBV produces pre-genomic RNAs which it uses as a template to produce genomic DNA for new virions. The process of the nuclear entry by HBV is poorly understood, leading to two main theories of HBV genome delivery: the capsid disassembles in the cytoplasm and the DNA-viral polymerase complex is imported into the nucleus via karyopherins; or the virion is imported into the nucleus and disassembles on binding to Nup153, releasing the DNA-viral polymerase complex (Reviewed in (Gallucci and Kann, 2017)).

1.3.5.2 Non-capsid remodelling Events

The alternate form of viral remodelling events is coordinated by non-capsid viral proteins. The overwhelming aim of these remodelling events is to aid viral replication by breaking down normal nucleocytoplasmic transport and inducing preferential transport of viral factors. These strategies range from more subtle hijacking of nucleoporins to the destruction of the NPC central channel.

The *Picornaviridae* family have a single stranded, positive sense RNA genome and replicate exclusively in the cytoplasm. They achieve this by inducing the relocalisation of numerous nuclear factors through a dramatic remodelling of the NPC. Poliovirus, or Enterovirus C, is a form of Enterovirus from the larger

57

Picornaviridae family. Poliovirus encodes 2A^{pro}, a viral protease that causes the proteolysis of a number of key nucleoporins responsible for nucleocytoplasmic trafficking (Gustin and Sarnow, 2001; Gustin and Sarnow, 2002; Park et al., 2008). Nup98 is cleaved first early post infection, followed by Nup62 and then Nup153 at later periods (Gustin and Sarnow, 2002; Park et al., 2008). Electron microscopy appears to show the actions of the cleavage remove a large density at the centre of the NPC attributed to the relocalisation of nuclear factors (Belov et al., 2004). Intriguingly, Cardiovirus, another genus of *Picornaviridae*, increases permeability of the NPC via a different mechanism. The Cardiovirus L protein induces hyperphosphorylation of nucleoporins dependent on the presence of its zinc-finger domain (Bardina et al., 2009; Porter et al., 2010). Nup62, Nup98, Nup153 and Nup214 are all hyperphosphorylated through the action of the L protein, mediated by mitogen activated kinases (Porter and Palmenberg, 2009). These changes inhibit nuclear import and cause nuclear efflux, allowing the virus to utilise nuclear factors for its replication (Porter and Palmenberg, 2009).

Herpesviruses have also been shown to act on the NPC after the capsid remodelling events described above. HSV-1 decreases the expression of Nup153 by greater than 3-fold and Nup153 is relocalised to the cytoplasm during early stages of infection (Ray and Enquist, 2004; Leuzinger et al., 2005). The HSV-1 protein ICP27 interacts directly at the NPC via Nup62 and inhibits several forms of nucleocytoplasmic transport (Malik et al., 2012). This is similar to another herpesvirus, EBV, which encodes a protein kinase BGLF4 that binds Nup62 and Nup153 and induces a reorganisation of the NPC (Chang et al., 2012). The action of BGLF4 on these nucleoporins attenuates importin beta trafficking and promotes the nuclear import of large molecules. BGLF4 appears to enhance the

58

import of several non-NLS containing EBV proteins that are crucial to viral DNA replication (Chang et al., 2015).

HIV-1, a retrovirus, initially utilises the NPC to target the delivery of its genome to the nucleus. HIV-1 appears to undergo uncoating upon entry into the cytoplasm; however, observations suggest this process is not a key delineating step before transport to the nucleus. A number of studies have also shown that HIV-1 capsid proteins are an important determinant of nuclear import and that by interacting with Nup358 HIV-1 are able to attach to pores for genome delivery (Yamashita and Emerman, 2004; Ocwieja et al., 2011). After docking at the NPC via Nup358, the capsid delivers the pre-integration complex (PIC), a complex of the HIV-1 genome and viral and cellular factors that reverse transcribes the HIV-1 ssRNA genome into cDNA (Reviewed in (Jayappa et al., 2012)). The PIC translocates through the NPC and interacts with Nup153, which mediates its exit from the NPC. Nup153 and Nup98 appear to aid in the process of PIC targeting to host chromatin for successful genome integration (König et al., 2008; Woodward et al., 2009; Di Nunzio et al., 2012). However, these interactions don't constitute a formal remodelling of the NPC, rather a hijacking of their normal cellular roles. Nevertheless, over the course of HIV-1 infection, the NPC does appear to be remodelled with significant decreases in the abundance of 18 nucleoporins (Monette et al., 2011a). Furthermore, microarray data of HIV-1 infected T lymphocytes have shown that Nup62 is upregulated 24 h post infection, whilst Nup50 is downregulated (Imbeault et al., 2009). The exact purpose of these changes is poorly understood, although high-throughput screens show many of these nucleoporins are necessary host cofactors for HIV-1 infection (König et al., 2008; Zhou et al., 2008). One proposed downstream effect of these remodelling

59

events is the induced cytoplasmic retention of hnRNP A1, allowing the virus to positively regulate HIV-1 transcripts with an internal ribosome entry site (IRES) (Monette et al., 2009).

1.4   Proteomic approaches

With the advent of mass DNA sequencing technologies in the 1990s, investigators began to look at methods for analysing the global complement of proteins that corresponded to the genome. In 1995, the word 'proteome' was first used to describe the protein complement to the genome and hence the field of proteomics (the study of the global protein network) was born (Wasinger et al., 1995). The idea of the proteome was later described as "the idea of a finite totality, comprising of the functional (protein) molecular specifications of a genome" (Anderson and Anderson, 1998). The large scale study of proteins actually began much earlier in the 1970s with the development of two-dimensional electrophoresis (O'Farrell, 1975). The development of these technologies briefly focused scientific attention on a project to construct the Human Protein Index (HPI); however, major political changes in the early 1980s, and the failure to attract large-scale support, stifled the expansion of this project (Anderson and Anderson, 1982). With the advent of restriction enzyme technology, the genomic revolution quickly overtook much of the previous focus on the HPI, given the feasibility and ease of genomic techniques (Reviewed in (Anderson and Anderson, 1998)). The identification of many of the proteins visualised by 2D gel electrophoresis proved a serious bottleneck until the advent of highly sensitive mass spectrometry (MS)-based techniques combined with protein sequence databases.

60

Mass spectrometry allowed for the identification and quantification of protein samples with greater speed and in a high-throughput work flow. When combined with polyacrylamide gel electrophoresis (PAGE) or liquid chromatography (LC) highly complex protein mixtures could be resolved into more manageable samples, allowing for the potential to resolve proteins from whole-cell lysates (Reviewed in (Owen et al., 2014)). The work flow of MS-based analysis of protein samples begins with a separation step through either LC or PAGE. Samples are then digested into peptides, typically using trypsin, before further separation by LC. Peptides are then ionised through approaches such as matrix-assisted laser-desorption-ionisation-time-of-flight (MALDI-TOF) and electrospray ionisation (ES) and analysed through tandem mass spectrometry (MS/MS) (El-Aneed et al., 2009). In the first round of MS (MS[1]) the mass to charge ratio (m/z) of peptides is determined, generating a spectrum of m/z. These initial peptide spectra are then taken forward for an additional fragmentation step using an approach such as collision induced dissociation (CID), where ions are crashed into inert gas molecules, and fragments are again separated in another round of mass spectrometry. The m/z of these new fragments are then compared to a theoretical database of fragment m/z *in silico* using peak intensities to determine quantities of these peptides (Figure 1.19) (Yates et al., 1995; Washburn et al., 2001; Han et al., 2008).
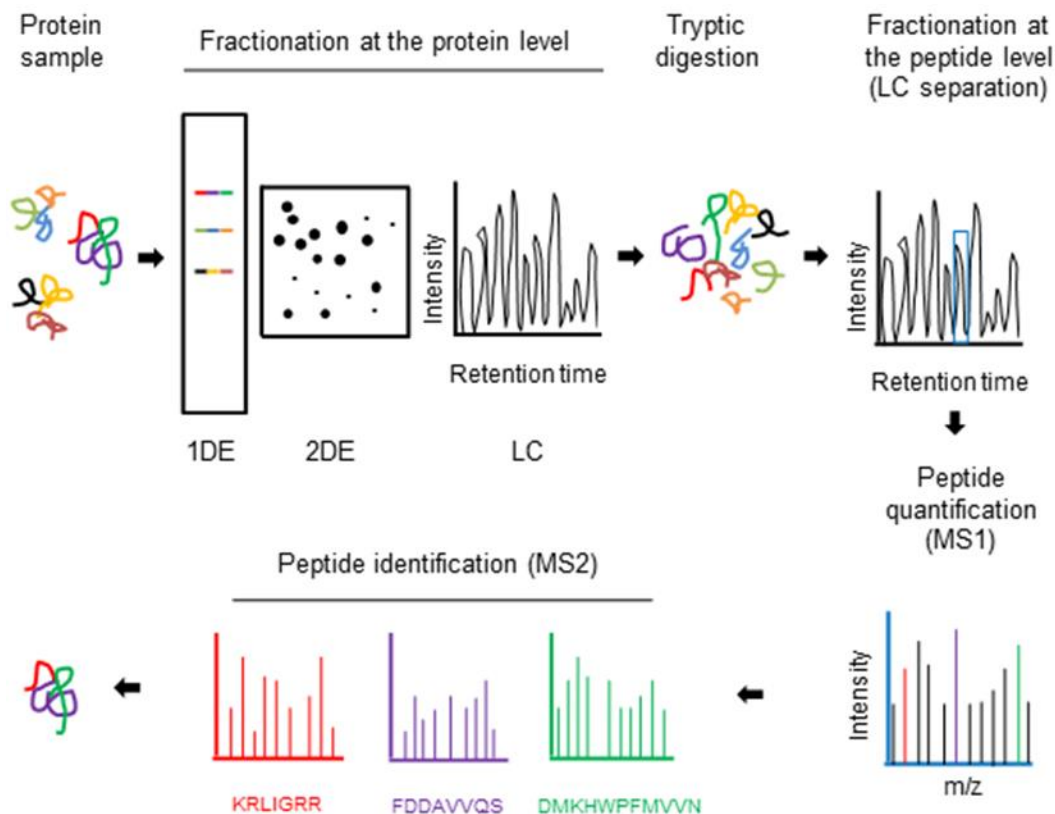
Figure 1.19 Work flow of protein identification and quantification by LC tandem mass spectrometry. The protein sample is separated through electrophoresis (1DE, 2DE) or liquid chromatography (LC), it is then digested into peptides with trypsin and separated again by LC. The first round of mass spectrometry is then performed (MS1) followed by peak identification and further mass spectrometry (MS2) to identify peptides. Taken from (Owen et al., 2014).

1.4.1 Quantitative techniques

Since the advent of 2D gel electrophoresis technologies investigators have also asked how changes in the quantities of these proteins relate to cellular conditions. Initially, computer algorithms were developed to create standard maps of healthy versus pathological cell proteomes. These worked by comparing the intensity of a stain for a given protein on the 2D gel based on the assumption that the staining density corresponded to the protein concentration (Arora et al., 2005). With the application of mass spectrometry technologies, it was possible for the first time to dramatically increase the throughput of quantitative studies. Whilst the intensities of ions observed in MS are theoretically proportional to peptide

62

abundance in a sample, absolute signal intensities can vary from run to run. Differences in sample complexity, chromatographic separation and peptide ionisation efficiency can all contribute to variability when comparing ion ratios (Dijkstra et al., 2007). The application of stable isotopes to proteomic studies provided a crucial answer to these variability problems. Isotopes such as ^{13}C, ^{15}N, ^{18}O and ^{2}H could be incorporated into proteomic samples that allowed for MS traces to highlight 'light' and 'heavy' peptide ions. These signals can be directly compared to give a relative ratio of protein levels between labelled conditions.

1.4.1.1 Isotope-coded affinity tag (ICAT)

An early approach that incorporated stable isotopes was isotope-coded affinity tagging (ICAT). This approach utilises a biotin affinity tag coupled to a stable isotope labelled linker (initial deuterium) and a thiol-reactive group (Gygi et al., 1999). Differences between two cell states were compared by treating cells with isotopically light and heavy ICAT reagents. These are then combined and treated with a protease before affinity isolation of ICAT-labelled peptides, which are then analysed by LC-MS/MS. The ratio of the peptide pairs then provide a relative quantification of the labelled protein (Gygi et al., 1999). This approach suffers from the drawback of relying on cysteine-containing peptides to ensure attachment of the label via the thiol linker, leading to the under-representation of peptides lacking a cysteine, resulting in the development of alternative techniques (Hsu et al., 2003).

1.4.1.2 SILAC

Another commonly raised drawback of ICAT approaches was whether the differences observed only related to differences in sample preparation during the labelling step. Stable isotope labelling with amino acids in cell culture (SILAC) was a metabolic approach that attempted to resolve this problem (Oda et al., 1999; Ong et al., 2002). SILAC involves the addition of isotopically labelled amino acids to cell culture media, ensuring that as cells grow and express protein they incorporate these 'heavy' or 'light' amino acids(Ong et al., 2002). These samples can then be harvested, treated with a protease and analysed by LC-MS/MS. The differences observed between the samples are again calculated into a ratio of the peptide pair and expressed as a relative quantitation (Figure 1.20). This approach alleviated some of the drawbacks of ICAT; however, SILAC is an expensive and time-consuming approach for quantitation that suffers from limitations when attempting to multiplex multiple conditions.
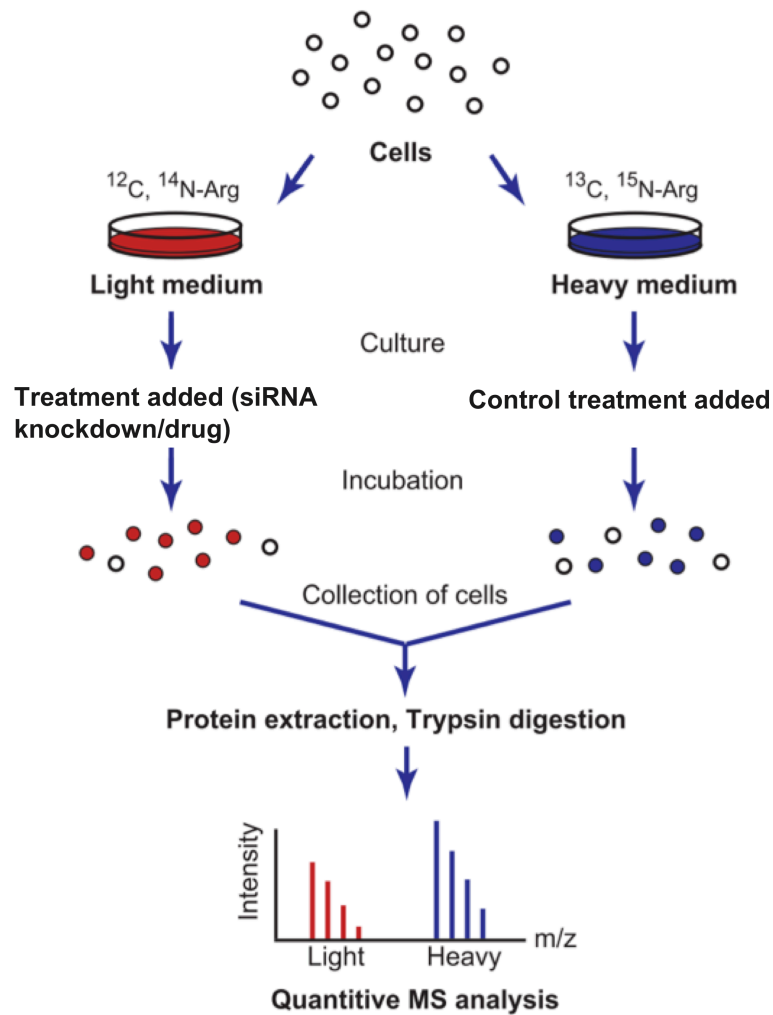
Figure 1.20 Overview of SILAC. Cells are cultured in media containing synthetic arginine with either heavy or light nitrogen isotope. Treatment is then added and incubated onto the cells. These are then collected and analysed via LC-MS/MS. This yields a trace with measurable abundance differences between light and heavy versions of the same peptide. Adapted from (Watanabe and Kanai, 2011).

1.4.1.3 Isobaric labelling approaches: iTRAQ and TMT

The development of iTRAQ (isobaric tag for relative and absolute quantification) arose from the limitations of both ICAT and SILAC approaches (Ross et al., 2004). During iTRAQ, samples from each treatment are harvested and digested with trypsin. The fragments are then treated with the iTRAQ tag to label fragments from each treatment with a specific mass tag. These are then mixed and separated via LC where, due to the isobaric nature of the tags, peptides from

65

differing treatments with alternate tags migrate at the same rate. Peptides analysed by MS/MS and iTRAQ tags are identified after MS2, when the fragmentation stage induces the dissociation of the specific mass tag. This allows for the generation of peptide ratios and relative quantitation data for a given peptide across several treatments (Figure 1.21). Initially, iTRAQ was demonstrated for multiplexing across four different conditions, but has since been developed for eight condition experiments (Ross et al., 2004; Choe et al., 2007). The nature of iTRAQ has alleviated previous drawbacks of quantitative techniques like poor label uptake, multiplexing and detection of post-translation modifications (Zieske, 2006).

Tandem mass tagging (TMT) is another isobaric reporter approach that utilises different structured tags to iTRAQ, but operates on the same experimental basis (Thompson et al., 2003). TMT tags utilise a m/z range from 126 to 131 allowing for a six-plex experiment, although recent advances have enabled TMT to label up to ten different samples through high-resolution instrumentation (McAlister et al., 2012; Werner et al., 2012). TMT has also been used in conjunction with SILAC to create 'hyperplexing', with up to eighteen different experimental conditions analysed through six tag TMT combined with three different SILAC media conditions (Dephoure and Gygi, 2012). This approach could be further combined with the previously described ten-plex TMT approach with the possibility of analysing relative protein changes across up to thirty different conditions.
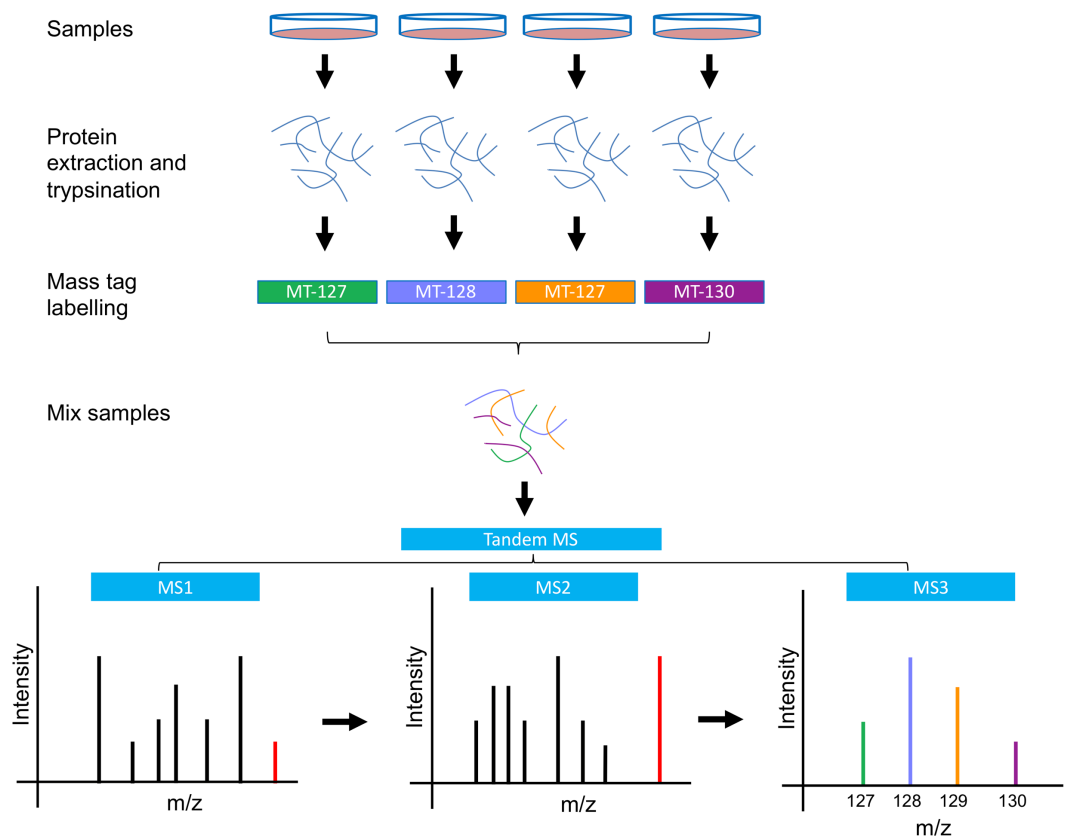
Figure 1.21 Schema of isobaric mass tagging techniques. Protein is extracted from sample conditions and protein digested. Mass tag labels (MT) are added and samples and mixed. These are then separated by liquid chromatography (LC) and analysed by tandem mass spectrometry (MS/MS). In MS1 precursor ions are produced by ionisation, these are then selected and fragmented further before separation into product ions in MS2. MS2 peaks can then be selected and further fragmented before separation in MS3 where mass tags form distinct peaks highlighting relative levels of that peptide between each sample.

1.4.2 Interactome techniques

Whilst advances in proteomics helped identify and quantify changes in proteins across different environmental conditions, these approaches do not, in isolation, elucidate the specific interaction networks of proteins. However, through the combination of modern proteomic techniques and *in situ* labelling techniques major advances have been made in understanding a variety of protein-protein interactions (PPI). This has expanded into the field of interactomics, or the study of both indirect and direct protein interactions (Sanchez et al., 1999). These

67

approaches allow for the development of a more coherent understanding of how proteins accomplish the myriad of cellular processes. With the advent of tools for quantitative proteomics the potential now exists to investigate PPI in a quantitative high-resolution manner, providing new insights into how many of the multiprotein complexes that exist within the cell change over the course of drug treatment, cancer progression or development.

1.4.2.1 Selective proteomic proximity labelling using tyramide

Through investigations into the interaction of the B cell receptor (BCR), a IgM class immunoglobulin, the interactomic technique of selective proteomic proximity labelling using tyramide (SPPLAT) was developed (Figure 1.22) (Li et al., 2014). SPPLAT utilises an unreactive tyramide-biotin molecule and a horseradish peroxidase conjugated antibody that is complementary for a target protein. This anti-target antibody is added to live cells along with tyramide-biotin and hydrogen peroxide. The anti-target antibody binds to the target cell surface molecule and catalyses hydrogen peroxide to water, and in the process adds a free radical to tyramide-biotin allowing it to react rapidly with adjacent molecules. This process labels proximal proteins to the target protein with biotin, allowing them to be specifically purified using streptavidin and analysed using LC-MS/MS (Johanna Susan Rees et al., 2015). Investigators have also combined this approach with quantitative proteomic techniques such as SILAC in order to identify the relative transience of interactions (Li et al., 2014). However, this approach is limited to cell surface proteins and the labelling efficiency of tyramide-biotin is strongly determined by the efficacy of the antibody used.
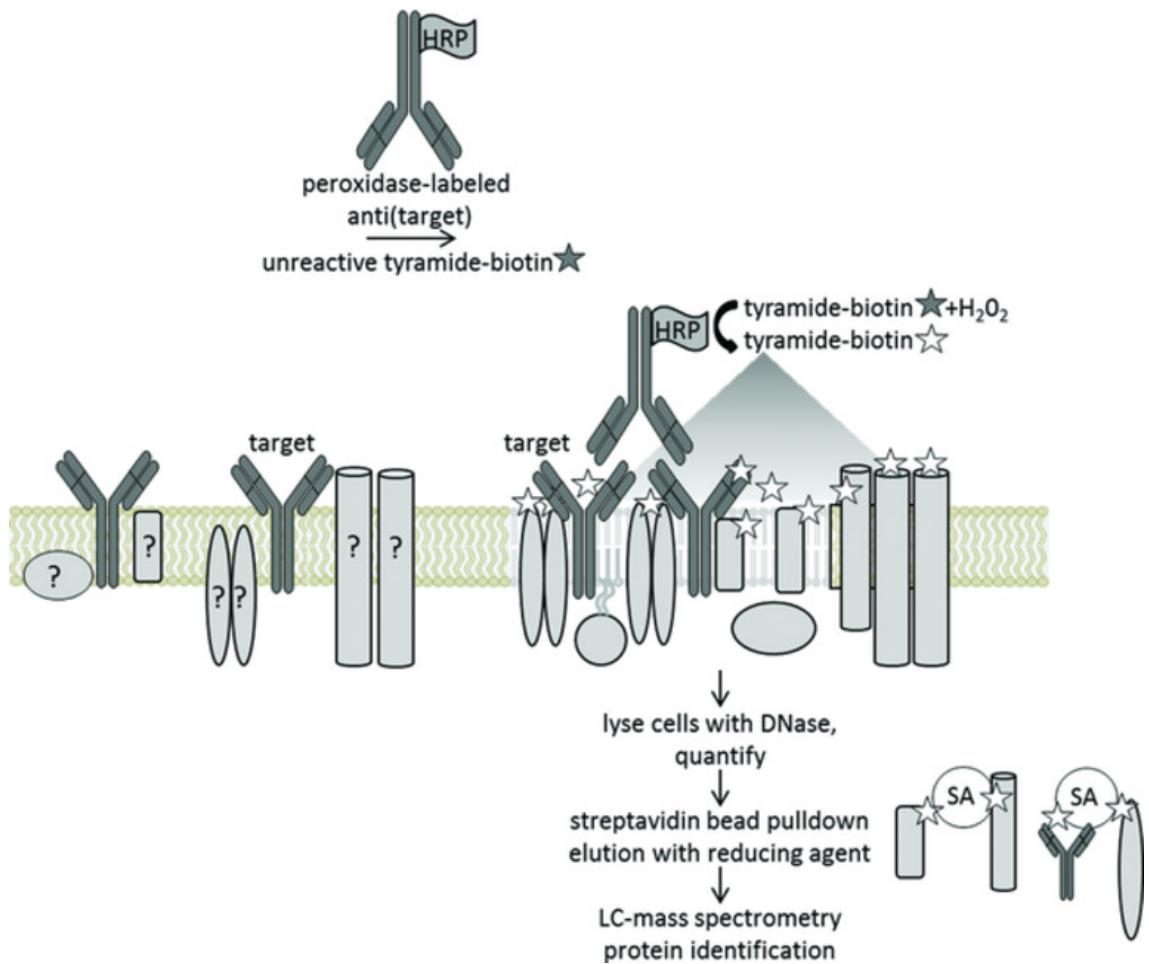
Figure 1.22 Overview of SPPLAT. Anti-target peroxidase conjugated antibody is added along with tyramide-biotin. Anti-target antibody binds and hydrogen peroxide is added leading to activation of tyramide-biotin which reacts with nearby proteins. Cells are then lysed and streptavidin beads are used to pull down biotinylated proteins which are analysed by LC-MS/MS. Taken from (Johanna Susan Rees et al., 2015).

1.4.2.2 APEX tagging

Another independently developed labelling method utilises engineered ascorbate peroxidase (APEX). This technique was developed for *in vivo* labelling that occurs rapidly, within a small radius, and is performed via a genetically targetable enzyme (Rhee et al., 2013). The first demonstrated use of APEX was targeting the enzyme to the mitochondrial matrix. The targeted protein, Mito-APEX, was expressed and, on the addition of biotin-phenol, catalysed the reaction of phenol to phenoxyl-radicals which exist for a short half-life and react with adjacent

69

proteins labelling them with biotin (Rhee et al., 2013). Cells can be lysed, and protein extracted before biotinylated proteins are purified with streptavidin beads and analysed by mass spectrometry (Figure 1.23). Whilst SPPLAT allows for biotin labelling at the cell surface, APEX can be expressed within the cell allowing for specific and temporally regulated labelling. This control of the time of labelling is often contrasted to the final interactomic approach described, namely BioID, where the labelling process can take several hours (Hwang and Espenshade, 2016). APEX can again be adapted to combine quantitative proteomic approaches to include relative quantitation of the specific interactome under investigation (Hung et al., 2016). An important consideration of this approach is whether the diffusion of the enzyme-labelling complex will introduce false-positively labelled proteins. It has been argued that even with a biotinylation speed of 1 min this would give sufficient time for the complex to diffuse around half the size of a typical cell (10 µm) (Johanna S. Rees et al., 2015).
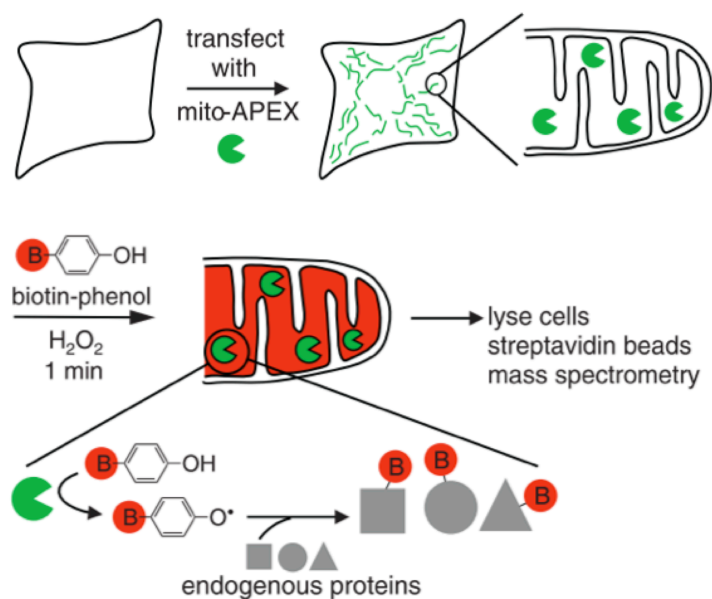
Figure 1.23 Outline of APEX in mitochrondria. Mito-APEX is transfected into cells with targeting to the mitochrondrial matrix. Biotin-phenol is then added with hydrogen peroxide, mito-APEX catalyses the

conversion of phenol to phenoxyl which rapidly reacts with local proteins labelling them with biotin. Cells are then lysed and biotinylated protein captured with streptavidin beads and identified via mass spectrometry. Taken from (Rhee et al., 2013).

1.4.2.3 Proximity dependent biotin identification

Proximity dependent biotin identification (BioID) was developed in 2012 as a method for understanding protein interactions *in vivo*. BioID utilises a mutant form of *Escherichia coli* biotin ligase (BirA*) to promiscuously biotinylate proximal proteins on the addition of biotin (Roux et al., 2012). In *E.coli* this biotin ligase is responsible for post-translationally modifying a subunit of acetyl-Coenzyme A (acetyl-CoA) carboxylase. The process of biotinylation is ATP dependent, with the ligase using biotin and ATP to produce a biotinyl-5'-AMP (adenosine monophosphate) intermediate, which is able to react with the target protein forming an amide bond between biotin and a lysine functional group, releasing AMP (Lane et al., 1964; Chapman-Smith and Cronan, 1999). The wild type form of BirA has a high affinity for biotinyl-5'-AMP, which is retained in its active site until binding to the acetyl-CoA carboxylase subunit. A mutant form of BirA* was also discovered that carries the R118G mutation at the active site leading to reduced affinity for biotinyl-5'-AMP leading to premature release (Kwon and Beckett, 2000; Choi-Rhee et al., 2004). The development of BirA* allowed for the cloning of a fusion gene of a target protein of interest and BirA* at either the C or N terminus. These fusion proteins can then be expressed in cells and biotinylation induced by the addition of biotin to cell culture media. Cells are then harvested, proteins extracted and biotinylated proteins purified using streptavidin. Mass spectrometry can then be used to identify the biotinylated proteins (Figure 1.24).

71
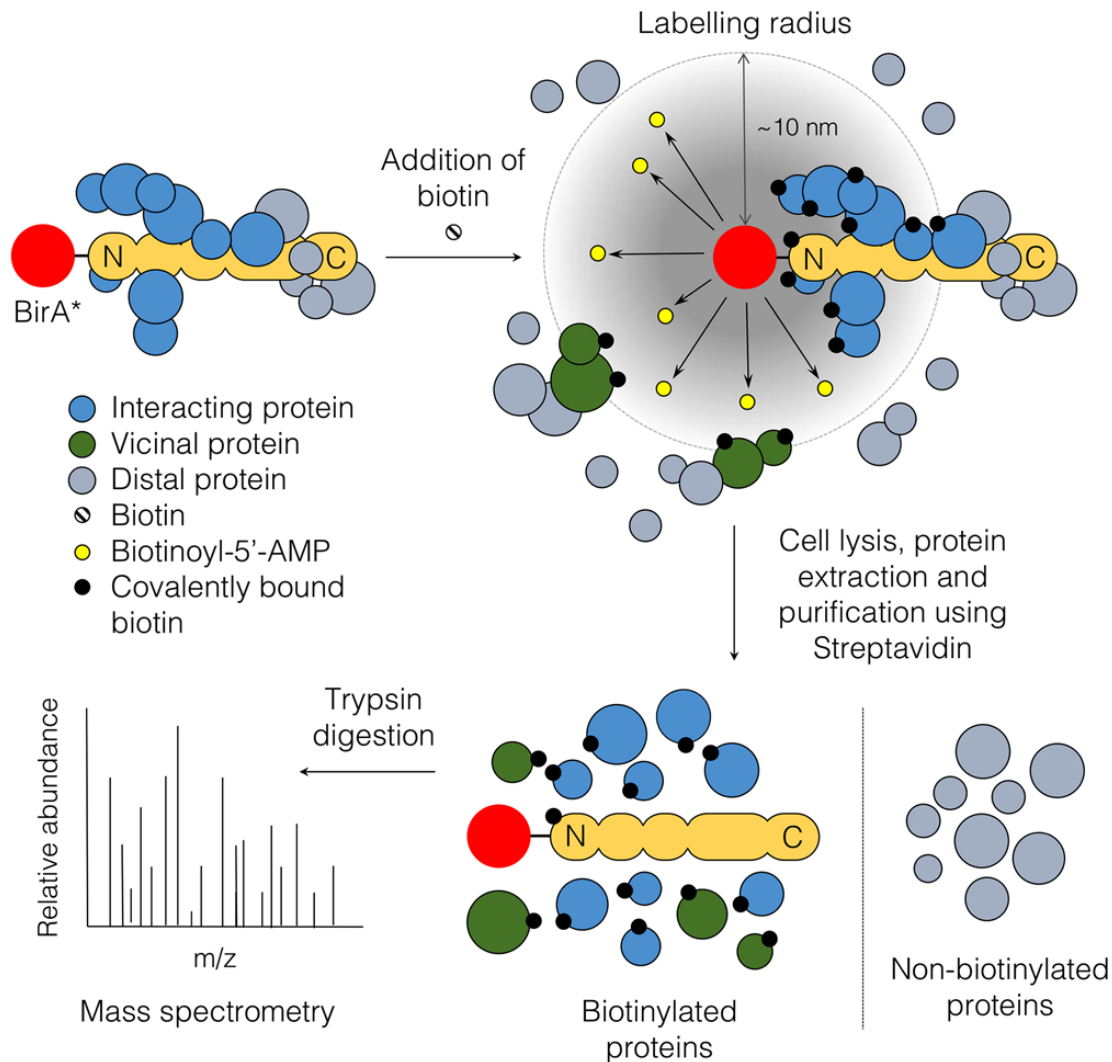
Figure 1.24 Outline of proximity dependent biotin identification. A fusion protein of BirA* and the target protein is expressed, biotin is added to the media leading to biotinylation of adjacent proteins within a ~10 nm radius. Cells are then lysed, proteins extracted and streptavidin is used to purify biotinylated protein before analysis by mass spectrometry. Taken from (Varnaitė and MacNeill, 2016).

The labelling process is proximity dependent on the area reachable by biotinyl-5'-AMP and was initially described as within a radius of 20 to 30 nm from the ligase (Roux et al., 2012). Further experiments demonstrated a small range of 10 nm when using the construct to label components of the nuclear pore complex, based on the known structural dimensions of the NPC (Kim et al., 2014). Through this radius of biotinylation, BioID is able to label not only proximal protein-protein interactions at the target molecule, but also indirect and dynamic interactions.

This makes BioID a key tool in understanding the adaptive landscape of protein interactomes over time with successful implementation of BioID investigating the nuclear lamina, centrosome components, c-Myc interacting partners in tumour cells and chromatin-associated proteins (Roux et al., 2012; Firat-Karalar et al., 2014; Dingar et al., 2015; Lambert et al., 2015). Nevertheless, the accuracy of the BioID approach is also constrained by the radius of labelling and the duration of biotinylation. Even with a labelling radius of 10 nm it has been suggested that, due to the crowded nature of the cell, there is still a large risk of biotinylating unrelated proteins (Phillips et al., 2009). This potential for false-positives is exacerbated by the long duration of labelling (18-24 h) which increases the potential of labelling false-positives. Overall, these constraints are common across all forms of *in vivo* proximity-based labelling systems and require crucial consideration when interpreting data. Often it has been shown that combining these techniques with quantitative proteomics aids in determining degrees of association (Rhee et al., 2013).

1.5 Thesis Aims

The aim of this thesis is to build upon previous work from the Whitehouse Laboratory, which highlighted through quantitative proteomic analysis changes in the protein levels of nucleoporins after the induction of KSHV lytic infection. Little is known about how KSHV alters the NPC during the lytic infection and this work aimed to address this lack of knowledge through two approaches. First, using traditional biochemical techniques identify and characterise specific changes at the NPC during KSHV lytic infection. Second, utilise new interactomic techniques to capture a more holistic understanding of changes at the NPC during KSHV lytic infection.

Chapter 3 aimed to validate and characterise observations from quantitiative proteomic work previously performed by the Whitehouse laboratory. This identified Nup98 as a nucleoporin specifically downregulated early after the induction of KSHV lytic infection (8 h post induction). Interestingly, this nucleoporin appears to have a restrictive effect on the expression at the viral ORF50 promoter, which appears related to the role of Nup98 within the nucleus rather than at the NPC. The targeting of Nup98 by KSHV is linked to the E3 ubiquitin ligase activity of viral immediate-early protein RTA and appears important for the transcription of viral genes containing an RTA-response element.

Chapter 4 expands on a series of investigations that also aimed to characterise KSHV targeting of Nup98 using siRNAs to depleted Nup98 before lytic replication was induced. Contrary to expectations, results show Nup98-depletion was

detrimental to the virus, leading to failed virion egress at the late stage of KSHV lytic replication. Results suggested this was related to the role of Nup98 at the nuclear pore as a component of the Nup98-Rae1 complex, which is targeted by KSHV to induce nuclear retention of a subset of host RNAs. One such RNA encodes the ESCRT-III component CHMP7, which has a crucial role recruiting the ESCRT-III complex to membranes, to induce repair and abscission. Results suggested that overexpression of CHMP7 induced a phenotype in lytic replicating cells similar to that of Nup98-depletion, corroborating the hypothesis that nuclear pore-bound Nup98 is crucial for successful viral replication due to its anchor role at the NPC for Rae1.

Finally, chapter 5 aimed to implement proximity dependent biotinylation (BioID) and tandem mass tagging at the NPC during KSHV lytic infection to identify stochiometric changes at the pore. This involved attempts to develop cell lines that stably expressed BioID nucleoporin fusion proteins ensuring proper targeting at the nuclear pore complex. However, difficulties establishing stable cell lines led to the use of transient transfection procedures to incorporate correctly localised fusion nucleoporins. A pilot experiment was then performed to confirm successful streptavidin immunoprecipitation of biotinylated proteins, before a large scale ten-plex experiment was performed to attempt to characterise changes at the NPC during lytic infection. The results of these experiments were then analysed using automated data analysis scripts written in R and interactome maps generated using STRING-db.

Overall, this work highlights the specific targeting of a nucleoporin and the NPC during KSHV lytic infection. It highlights the alternate roles of Nup98 with KSHV

appearing to target a specific subcellular population of the protein, whilst requiring the presence of Nup98 at the NPC. In the longer term, the characterisation of this interaction and further elucidating of mechanisms by which the virus targets cellular proteins early during lytic infection may highlight potential targets for future antiviral therapies. Furthermore, the datasets acquired from the BioID analysis may offer a unique insight into KSHV-interactomic approaches.

Chapter 2
~
Materials and Methods

2 Materials and Methods

2.1 Materials

2.1.1 Antibodies

All antibodies, their species, working dilutions and suppliers are outlined in Table 2.1 Horseradish peroxidase (HRP)-conjugated anti-mouse, anti-rabbit and anti-rat secondary IgG, used for Western Blotting at a 1:5000 dilution, were obtained from Dako (a brand subsidiary of Agilent). For confocal immunofluorescence (IF) Alexa Fluor® 594-, 488-, 546-, and 633- conjugated anti-rabbit, anti-mouse and anti-rat were used at a dilution of 1:500 and obtained from Life Technologies (Thermo Fisher Scientific).

Table 2.1 List of antibodies, their species, working dilution for western blotting (WB) and immunofluoresence (IF) and suppliers.

Antibody	Species	Working dilution		Supplier
		WB	IF	
Anti-GAPDH	Mouse	1:5000	-	Abcam®
Anti-Mab414	Mouse	1:1000	1:200	Abcam®
Anti-Lamin B1	Rabbit	1:1000	1:500	Abcam®
Anti-Nup98	Rat	1:1000	1:100	Abcam®
Anti-Nup98	Rabbit	For ChIP		Abcam®

(ab45584)				
Anti-ORF57	Mouse	1:1000	1:200	Santa Cruz Biotech®
Anti-ORF65	Mouse	1:500	1:200	S J Gao, University of Southern California
Anti-RTA	Rabbit	1:500	1:500	David Blackburn, University of Birmingham

2.1.2 Cell culture reagents

All cell culture reagents, media and selection antibiotics used were supplied as shown in Table 2.2.

Table 2.2 List of cell culture reagents and their suppliers.

Reagent	Supplier
Doxycycline hyclate	Sigma-Aldrich®
Lipofectamine 2000	Thermo Fisher

Hygromycin B	
Puromycin dihydrochloride	
Nucleofector Reagent V	Lonza
Phosphate buffered saline (PBS)	
Dulbecco's Modified Eagle Medium (DMEM)	
Roswell Park Memorial Institute medium (RPMI1640)	Gibco™
Opti-MEM®	
Foetal Bovine Serum (FBS)	
Penicillin/Streptomycin (P/S)	
Trypsin-EDTA	

2.1.3 Chemicals

Unless otherwise stated, chemicals were obtained from Sigma-Aldrich®, Thermo Fisher Scientific brands (including Invitrogen™ and Gibco™), Melford, VWR International, Merck Millipore. Sterilisation was achieved by sterile filtering (0.22 µm filters, Millipore) or by autoclaving (121 °C, 30 min, 15 psi).

2.1.4 Enzymes

All enzymes and their suppliers are listed in Table 2.3.

Table 2.3 List of enzymes and their suppliers.

Enzyme	Supplier
DNA-*free* DNA removal kit (DNase I treatment)	Ambion
DNase I	Invitrogen™
ProtoScript II Reverse transcriptase	
RNase inhibitor, Murine	New England Biolabs

2.1.5 Oligonucleotides

Oligonucleotide primers used in quantitative PCR (qPCR), as well as oligo(dT)$_{15}$ were obtained from Sigma-Aldrich®.

Table 2.4 List of oligonucleotides used and their sequences (forward and reverse, 5'-3').

Gene name	Sequence (5'-3')
ORF57	F – GCCATAATCTAAGCGTACTGG

	R - GCAGACAAATATTGCGGTGT
ORF47	F - CGCGGTCGTTCGAAGATTGGG
	R - CGAGTCTGACTTCCGCTAACA
GAPDH	F - TGTGGTCATGAGTCCTTCCACGAT
	R – AGGGTCATCATCTCTGCCCCCTC
CHMP7	F – TCCCAGACAGATCAGATGGTT
	R - TTCATCCTGGGTGTCACAGA
Nup98	F - TGGGTGAAGGGCTAAATAG
	R - GGCGATCTGGGCTCTTTATT
Myc (ChIP) -475 to -396	F - TTTGTCAAACAGTACTGCTACGG
	R - CTCCCTCTCAAACCCTCTCC
ORF50	F - ATGACAAGGGTAAGAAGCTTCGG
	R - ACTGGTAGAGTTGGGCCTTCAGTT

2.1.6 DNA constructs

All DNA plasmid constructs were either present in the Whitehouse Laboratory, purchased from commercial sources or kindly donated by collaborators, as shown in Table 2.5.

Table 2.5 List of all DNA constructs used, their donors and references.

Plasmid	Kindly provided by	Reference
pLX_TRC317 CHMP7	Mission TRC3 Sigma TRCN0000478910	
pLX_TRC317 IST1	Mission TRC3 Sigma TRCN0000471238	Purchased from the MISSION® TRC3 Human LentiORF collection
pLX_TRC317	Mission TRC3 Sigma TRCN0000472187	
pLX_TC317 VPS4A	Mission TRC3 Sigma TRCN0000480591	
pVSV.G	Dr. Edwin Chen	-
psPAX2		
pLKO.1 DHX9 shRNA		Purchased from Dharmacon

	TRCN0000001208	TRC Lentiviral Human shRNA
pLKO.1 DHX9 shRNA	TRCN0000001209	RHS4533-EG1660
pLKO.1 DHX9 shRNA	TRCN0000001210	
pLKO.1 DHX9 shRNA	TRCN0000001211	
pLKO.1 DHX9 shRNA	TRCN0000001212	
Nup85-GFP		
Nup133-GFP		
Nup160-GFP		
Nup53-GFP		
pcDNA3.1 mycBioID-Nup53	Dr. Kyle Roux	(Roux et al., 2012)
pcDNA3.1 mycBioID-Nup160		
pcDNA3.1 mycBioID-Nup133		

pcDNA3.1 mycBioID-Nup85		
pcDNA3.1 mycBioID		
pcDNA3.1 mycBioID-R118G		
GFP-Nup98	Professor Richard Wozniak	(Capitanio et al., 2017)
pGL3-RTA-luc	Professor Adrian Whitehouse	(Gould et al., 2009)
pRTA	Gary Hayward	(Yu et al., 2005)
pEGFP-N1	Clontech	Catalogue No. 6085-1
pRTLK Renilla	Promega	Catalogue No. E2261

2.2   Methods

2.2.1   Cell culture

2.2.1.1   Cell lines

BCBL-1 are a cell line derived from B lymphocytes latently infected with KSHV originally from a patient with body cavity-based lymphoma. These cells were obtained from the American Type Culture Collection (ATCC). TREx BCBL1-Rta, a cell line derived from BCBL-1 cells containing an inducible myc-tagged RTA

85

plasmid, were a kind gift of Jae Jung, University of Southern California (Nakamura et al., 2003). Both BCBL-1 and TREX BCBL-1-Rta cells (referred to as TREx cells) were used for KSHV lytic replication experiments, unless otherwise stated. Human embryonic kidney (HEK) 293T cells (referred to as 293T cells) were obtained from the European Collection of Authenticated Cell Cultures (ECACC). These cells were used for all plasmid transfection experiments.

2.2.1.2 Cell maintenance

BCBL-1 and TREx cells were grown in RPMI medium 1640 (Gibco) with glutamine, supplemented with 10 % (v/v) foetal bovine serum (FBS, Invitrogen) and 1 % (v/v) penicillin-streptomycin (Invitrogen) (referred to hereafter as complete RPMI). This cell line was maintained under hygromycin B (Life technologies) selection (100 µg/ml). 293T cells (ATCC) were grown in DMEM (Life technologies) and supplemented with 10 % (v/v) foetal bovine serum (FBS, Invitrogen) and 1 % (v/v) penicillin-streptomycin (Invitrogen) (referred to hereafter as complete DMEM). TREx cells were maintained under hygromycin B selection (100 µg/ml). All cells were grown at 37 ^{o}C in a humidified incubator with 5 % CO_2.

2.2.1.3 Cell viability assay

Cell viability was determined using the MTS-based CellTiter 96® AQ$_{ueous}$ One Solution Cell Proliferation Assay (Promega). For this 1 ml of 1 x 10^6 TREx cells were seeded into a 12-well plate with fresh complete RPMI containing drug or selection agent (G418). After 24 h, 100 µL of treated cells were transferred into a 96-well plate and 20 µL of CellTiter 96® AQ$_{ueous}$ One Solution Reagent was added. The 12-well plate was then incubated at 37 ^{o}C for 1 h before the

absorbance was measured at 490 nm using the Infinite® F50 Robotic microplate reader (Tecan).

2.2.1.4 siRNA knockdown

8×10^6 TREx cells were transfected once with 100 µL of Nucleofector solution V (Lonza) to which 100 nM Allstars negative control siRNA (Qiagen) or Nup98 Silencer Select siRNA (ID s9782, Life Technologies) was added. Cells were transfected using the T-01 programme of an Amaxa nucleofector I (Lonza). Immediately after nucleofection, 300 µL fresh RPMI 1640 media was added and cells incubated for 10 min at room temperature. Cells were then added to 8 mL of fresh complete RPMI 1640 media and maintained in 6-well plates. Cells were then reactivated 48h post transfection and incubated for the desired time.

2.2.1.5 Transient transfection

3×10^6 293T cells were seeded out per well into 6-well plates and grown to approximately 60 % confluence before transfection. Cells were transfected using Lipofectamine® 2000 following the manufacturer's instructions. Briefly, per well, 100 µL of Opti-MEM was mixed with 3 µL Lipofectamine® 2000 and in a different mix 100 µL of Opti-MEM was combined with 1 µg of plasmid DNA for 10 min at room temperature with gentle agitation. Mixtures were then combined and incubated at room temperature for a further 10 min. Fresh media was added to cells during this time and finally the combined 200 µL Opti-MEM lipofectamine:plasmid mix was added dropwise to the cells. Experiments were conducted 24 h post transfection unless otherwise stated.

2.2.1.6 Lentiviral transduction

3×10^6 293T cells were seeded into a volume of 1 mL complete DMEM per well of a 6-well plates and grown until reaching >80 % confluence. Cells were then transfected with 0.65 µg of psPAX and pVSV and 1.2 µg of lentiviral plasmid of interest (Table 2.5) using Lipofectamine® 2000. Cells were then incubated for 48 h after which the lentivirus-containing supernatant was collected and filtered with 0.45 µm filter. 1 mL of lentivirus-containing supernatant was added to 0.5 mL fresh RPMI 1640 media containing 0.5×10^6 TREx cells supplemented with 8 µg/mL polybrene and spin-inoculated by centrifuging for 1 h at 800 x g at room temperature. Media-lentiviral supernatant was then left on the cells till the end of the day before being removed and replaced with fresh RPMI 1640 medium. 2 µg/mL of puromycin was added 48 h after viral spin-inoculation to select for successfully transduced TREx cells (Figure 2.1) (Balistreri et al., 2016). Cells were selected alongside a non-transduced control in 6-well plates for 12 days before being transferred into T75 flasks for expansion for experiments. Complete RPMI medium supplemented with 2 µg/mL of puromycin was used for all subsequent passaging.
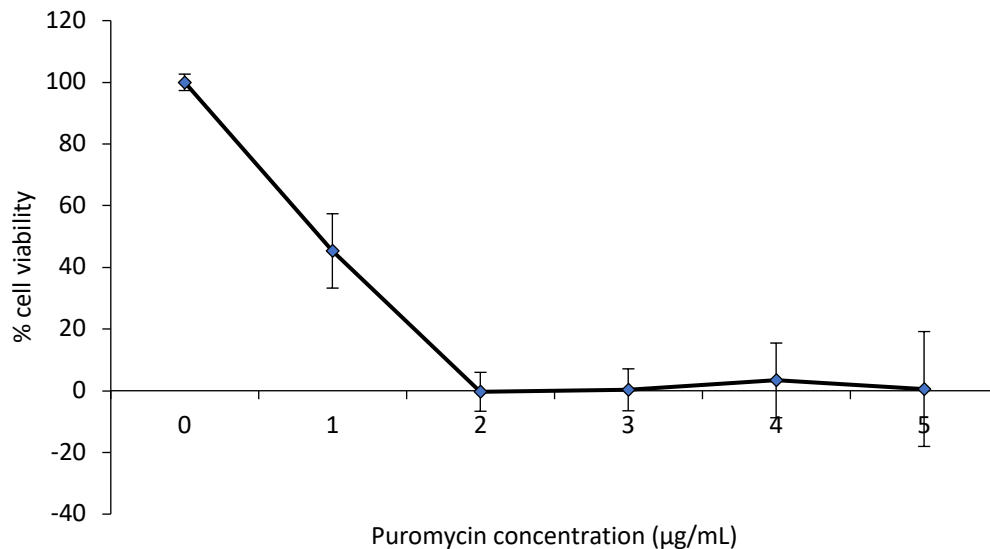
Figure 2.1 Puromycin kill curve for TREx cells. Different dilutions of puromycin were mixed with fresh media and incubated with TREx cells for 24 h before an MTS assay was performed to determine cell viability. n=4, standard deviation shown. Experiment from (Baquero et al. unpublished data).

2.2.2 Virus based assays

2.2.2.1 Induction of KSHV lytic replication

To induce KSHV lytic replication, 0.8×10^6 TREx cells were treated with 2 μg/ml doxycycline (Sigma). Unless stated otherwise, viral mRNA export assays, protein expression studies, immunoprecipitation and immunofluorescence experiments were performed at 24 h post-induction of KSHV lytic replication. BCBL-1 cells were induced by the addition of 3 mM sodium butyrate and 20 ng/mL 12-*O*-tetradecanoylphorbol-13-acetate (TPA).

2.2.2.2 Viral re-infection assay

Lytic replication was induced for 72 h in 2.0×10^6 TREx cells. Cells were then spun down at 500 x *g* for 5 min at room temperature and 2 mL of cell supernatant was mixed 1:1 with 2 mL of DMEM and added to confluent 293T cells seeded in

89

6-well plates. After 24 h, the 293T cells were washed with PBS and total RNA was extracted using 1 mL TRIzol (Invitrogen™) as described below and were subsequently used for quantitative reverse transcriptase PCR (qRT-PCR) as described below.

2.2.2.3 Viral replication assay

To assess changes to the level of KSHV DNA production within cells after siRNA treatment, 1×10^6 TREx cells per well were seeded onto 6-well plates and nucleofected with either scrambled or Nup98 siRNAs, as described in section 2.2.1.4, and then induced 48 h post-nucleofection. 72 h post-doxycycline induction cells were spun down at 500 x g for 5 min at 4 °C. Viral and cellular DNA was purified using the QIAamp DNA Mini kit (QIAGEN) following the manufacturer's instructions. Initially the cell pellet was resuspended in 200 µL PBS and cells were lysed by addition of proteinase K (QIAGEN) and buffer AL followed by 15 s pulse vortexing and 10 min incubation at 56 °C. 100 % ethanol was then added, and the solution was applied to a QIAquick spin column. Columns were centrifuged at 6,000 x g for 1 min at room temperature and flow-through was discarded. Wash buffer AW1 was then added to the column and the above centrifugation step was repeated. Wash buffer AW2 was then added and the column was centrifuged at 8,000 x g for 3 min at room temperature. Flow-through was discarded and DNA was eluted by the addition of 50 µL dH$_2$O. The column was then incubated at room temperature for 1 min and centrifuged at 6,000 x g for 1 min. Eluted DNA was stored at -20 °C. Viral and cellular DNA levels were quantified by qPCR as described below (Section 2.2.5.4).

2.2.2.4 Cytoplasmic fractionation

1×10^6 TREx cells were induced as described in section 2.2.2.1 and 24 h later cells were collected by 500 x g 5 min spin followed by a wash in 1 mL of PBS. Cells were then lysed in 600 µL of 1 % (v/v) Triton X-100 in PBS for 10 min on ice. 350 µL of the lysate were then transferred to fresh microcentrifuge tubes and spun for 5 min at 2000 x g at 4 °C and the supernatant was transferred to fresh microcentrifuge tubes as the cytoplasmic fraction. The remaining 250 µL was divided into 200 µL for extraction of RNA with the use of TRIzol as described in section 2.2.5.1 and the remaining 50 µL were kept for protein analysis via western blotting. The supernatant of the cytoplasmic fraction was also divided for total RNA extraction and protein analysis into volumes of 300 µL and 50 µL.

2.2.3 Analysis of proteins

2.2.3.1 Quantification of protein samples

Protein sample concentrations were determined using the Bio-Rad DC^{TM} protein assay following the manufacturer's instructions. In a 96-well plate, 5 µL of protein lysate or pre-diluted bovine serum albumin (BSA) standards, obtained by serial dilution of a 5 mg/ml BSA stock, were incubated with 25 µL Reagent A' (25 µL of reagent S in 1 mL of reagent A) and 200 µL reagent B. After 15 min of incubation at room temperature with constant agitation absorbance was measured at 620 nm using the Infinite® F50 Robotic microplate reader (Tecan). Protein concentration was determined through calculation of a standard curve of known protein concentrations using BSA in the specific lysis buffer used for the experiment. The absorbance of the known concentrations was determined as described above and Microsoft Excel was used to determine the function of the

standard curve. The function was then applied to all experimental samples to determine protein concentration.

2.2.3.2 SDS-PAGE Electrophoresis

Protein samples were mixed 1:1 with 2 x SDS loading buffer [100 mM Tris/HCl, pH 6.8, 4 % (w/v) SDS, 20 % (w/v) glycerol, 10 mM DTT, 0.25 % (w/v) bromophenol blue], and subsequently boiled for 5 min at 95 °C. Samples were then separated via molecular weight using sodium dodecyl sulphate (SDS)-polyacrylamide gel electrophoresis (PAGE). After boiling samples, these were loaded alongside Precision Plus Protein™ Dual Colour Standards (Bio-Rad®) onto a 10 % polyacrylamide gel (unless otherwise stated) composed of a stacking gel [5 % (v/v) acrylamide/bis-acrylamide 37.5.1 (Severn Biotech Ltd.), 375 mM Tris/HCl, pH 8.8, 0.1 % (w/v) SDS, 0.12 % (v/v) APS, 0.012% TEMED (v/v)] and a resolving gel [10% (v/v) acrylamide/bis-acrylamide 37.5.1 (Severn Biotech Ltd.), 125 mM Tris/HCl, pH 6.8, 0.1 % (w/v) SDS, 0.08 % (v/v) APS, 0.008 % TEMED (v/v)]. Gels were run at 180 V for 60 min or until the dye front reached the bottom of the resolving gel. The running buffer used was 25 mM Tris, 192 mM Glycine, and 0.1 % (w/v) SDS.

2.2.3.3 Western Blotting

Protein samples separated by SDS-PAGE (Section 2.2.3.2) were transferred to an Amersham™ Protran™ NC Nitrocellulose Membrane (Thermo Fisher Scientific). Proteins were electrophoretically transferred onto the nitrocellulose membrane via a wet transfer system. The nitrocellulose membrane was assembled into a "blotting sandwich" composed of a blotting pad, two pieces of

Whatman filter paper, gel, nitrocellulose membrane, two pieces of Whatman filter paper and a blotting pad. Prior to use the membrane was pre-soaked alongside all other blotting components in transfer buffer [20 % (v/v) methanol, 25 mM Tris, 192 mM glycine]. The "blotting sandwich" was then transferred into a blotting rig and run at 100 V for 1 h. The transfer of the ladder onto the nitrocellulose membrane was used to evaluate the efficiency of the transfer. Non-specific protein binding was then blocked for 1 h incubating the membrane in 5 % (w/v) non-fat milk (Marvel) in Tris buffered saline and Tween-20 (TBS-T) [150 mM NaCl, 50 mM Tris/HCl, pH 7.5, 1 % (v/v) Tween-20] on a rocking platform. The membrane was then incubated with primary antibody in 2.5 % (w/v) non-fat milk in TBS-T for 60 min at room temperature, followed by three 5 min washes in TBS-T. Secondary antibody (HRP-conjugated IgG) was applied in 2.5 % (w/v) non-fat milk in TBS-T for 60 min at room temperature, followed by five 5 min washes in TBS-T. Chemiluminescence was developed by adding enhanced chemiluminescence (ECL) system (Geneflow) to the membrane for 1 min. A photographic Hyperfilm™ ECL (Thermo Fisher Scientific) was then exposed to the membrane for the desired amount of time. The film was developed with a Konica SRX-101A developer.

2.2.4 Analysis of protein interactions

2.2.4.1 Immunofluorescence

293T cells or TREx cells were grown on 24-well plates containing sterile glass coverslips, which had been coated in poly-l-lysine (Sigma-Aldrich®) for 5 min and washed three times in PBS. Once 293T cells had reached at least 50 % confluence they were transfected as described in section 2.2.1.5. TREx cells

were nucleofected as described in section 2.2.1.4 and seeded onto coverslips immediately. TREx cells were then induced either 48 h post-transfection as described in section 2.2.2.1. At the required experimental time point coverslips were washed in PBS and fixed with 4 % (v/v) formaldehyde for 15 min at room temperature. Formaldehyde was then removed, and coverslips washed three times with PBS. Cells were then permeabilised using 1 % (v/v) Triton X-100 in PBS for 15 min at room temperature. To prevent non-specific binding cells were incubated with 1 % (w/v) BSA in PBS for 1 h at 37 ^{o}C in a humidity chamber. After blocking, cells were incubated with primary antibodies in 1 % (w/v) BSA in PBS for 1 h at 37 ^{o}C in a humidity chamber. After three washes with PBS, Alexa Fluor®-conjugated secondary antibodies were incubated under the same primary antibody conditions. For the analysis of biotinylation, Alexa Fluor®-conjugated to streptavidin was used. Following secondary antibody treatment, coverslips were washed a further five times with PBS and mounted onto microscope slides with DAPI containing mounting medium (VECTASHIELD®, Vector Laboratories) for nuclei labelling. Slides were stored at 4 ^{o}C until visualisation on an inverted LSM 880 confocal microscope (Ziess) using Zen 2011 software (Ziess).

2.2.4.2   Co-immunoprecipitation of proteins

For co-immunoprecipitation assays, TREx cells were prepared and induced as described in section 2.2.2.1. At different time points post induction of lytic replication (0, 8, 16, 24 h), cells were harvested at 500 x g for 5 min at 4 ^{o}C, washed once with PBS and lysed for 10 min using 1 mL of modified RIPA buffer [150 mM NaCl, 50 mM Tris/HCl; pH 7.6, 1 % (v/v) Nonidet™ P-40 (NP-40)]. The insoluble fraction was pelleted at 10,000 x g for 10 min and the supernatant was

kept on ice. The supernatant was then incubated by rotation with 5 µg of Nup98 antibody (Abcam®) overnight at 4 °C. The following day, protein A agarose beads (Roche) were pelleted at 500 x g for 5 min and washed 3 times with modified RIPA buffer to remove residual storage buffer. 30 µL of beads were then incubated by rotation with the antibody-supernatant mix for 1 h at 4 °C. The beads were then pelleted by centrifugation at 500 x g for 5 min at 4 °C and washed in ice cold modified RIPA buffer 3 times further before the agarose-antibody-antigen complex was mixed with 60 µL 2 x SDS loading buffer (Section 2.2.3.2) and proteins eluted by heating at 95 °C for 5 min before analysis by SDS-gel and Western blotting.

2.2.4.3   Chromatin immunoprecipitation (ChIP)

1×10^7 TREx cells were prepared per ChIP in a six-well plate and induced as described in section 2.2.2.1. Cells were fixed for 10 min with 1 % (v/v) formaldehyde at room temperature. Fixation was then quenched by the addition of 10X Glycine solution to a final concentration of 1X and incubated for 5 min at room temperature. Formaldehyde crosslinked chromatin was then obtained using the Pierce Chromatin Prep Module (Thermo Scientific) according to the manufacturer's protocol to obtain formaldehyde crosslinked chromatin. Chromatin was digested incubating six units of micrococcal nuclease (MNase) per 100 µL of MNase digestion buffer in a 37 °C water bath for 15 min. These conditions resulted in optimal digestion of chromatin with most fragments ranging between 150-300 nucleotides in length which was confirmed via running for 40 min at 100 V on a 1 % (w/v) TAE-agarose gel and staining with 0.2 µg/mL ethidium bromide. Immunoprecipitations were carried out using EZ-ChIP kit

(Millipore) according to the manufacturer's instructions. Immunoprecipitations were performed overnight at 4 °C and contained 50 µL of digested chromatin (1 x 10^7 cells), 450 µL ChIP dilution buffer and 1.5 µg Nup98 antibody (ab45584) or 1.5 µg of normal mouse IgG (Millipore) which was used as negative control antibody. Prior to qPCR analysis, DNA was subjected to a DNA clean up step using DNA spin columns provided in the EZ-ChIP kit (Millipore). qPCR reactions were performed as described in section 2.2.5.4. using either 4 µL ChIP DNA or 4 µL of 1 % input DNA as template.

2.2.5 Quantification of mRNA levels

2.2.5.1 Total RNA isolation

Total RNA was extracted from cells using the TRIzol reagent (Life Technologies) according to the manufacturer's protocol. 1 mL of TRIzol was added to 2 x 10^6 TREx, BCBL-1 or confluent 293T cells from one well of a 6-well plate. Cells were resuspended in TRIzol for 5 min at room temperature after which 200 µL of chloroform was added and samples were vigorously shaken for 15 s. Samples were then incubated for a further 3 min at room temperature and then centrifuged at 12,000 x g for 15 min at 4°C. 500 µL of the upper phase layer, containing RNA, was transferred to a fresh microcentrifuge tube containing 500 µL of isopropanol. Samples were mixed and incubated for 10 minutes at room temperature before a further centrifugation step to precipitate the RNA at 10,000 x g for 10 minutes at 4°C. The supernatant was then discarded, and the RNA pellet was washed in 70% ethanol and centrifuged at 7,500 x g for 5 minutes at 4°C. After this centrifugation the supernatant was discarded, and the RNA pellet was air-dried

at room temperature for approximately 5 minutes. The pellet was then resuspended in 16 μL of DNase and RNase free H_2O.

2.2.5.2   DNase I treatment

To remove any contaminating DNA from the total RNA isolate, samples were treated with DNA-free™ DNA removal kit (Ambion®) following the manufacturer's instructions. Briefly, 0.1 volumes of 10x DNase I buffer and 1 μL of DNase I were added per sample and incubated for 30 min at 37 °C. Next, samples were treated with 0.1 volumes of DNase inactivating reagent and gently mixed for 2 min at room temperature. The DNase inactivating agent was pelleted from the RNA solution by centrifugation at 10,000 x g for 2 min at 4 °C. The supernatant was transferred to a new microcentrifuge tube and stored at -80 °C.

2.2.5.3   Reverse transcription (RT)

Total RNA concentrations were measured using a NanoDrop ND-1000 spectrophotometer (NanoDrop Technologies, a Thermo Fisher Scientific Company). 1 μg of total RNA was added to the following reaction to synthesise complementary DNA (cDNA). Initially, 1 μL Oligo(dT)$_{15}$ (500μg/mL) and 1 μL dNTP mix (2.5 mM/dNTP) were added per sample and incubated at 65 °C for 5 min and then immediately cooled on ice. The following master mix was then added per sample: 4 μL 5x ProtoScript® II Reverse Transcriptase Reaction Buffer (NEB), 2 μL 0.1 M DTT (NEB), 1 μL RNase Inhibitor, Murine (NEB), 1 μL ProtoScript® Reverse Transcriptase (NEB). Samples were also prepared with the same master mix but omitting the reverse transcriptase, as a negative RT

control. Samples were then incubated at 42 °C for 50 min, followed by inactivation of the reverse transcriptase at 65 °C for 20 min. The cDNA was stored at -20 °C.

2.2.5.4   Quantitative PCR (qPCR)

Quantification of cDNA or genomic DNA was carried out using a Rotor-Gene 6000 Real-Time PCR machine (QIAGEN) and sequence-specific primers. The amplification efficiency of primers was determined prior to primer use for qPCR by the following procedure: serial dilutions of cell lysate cDNA were prepared from neat to 1:128 and qPCR was performed using the primer set. Cycle threshold (Ct) values were then determined using the method outlined below. These were plotted on a logarithmic scale and a linear function was determined. The slope coefficient of the function was then used to calculate the % amplification efficiency using the formula $E=-1+10^{\left(-\frac{1}{slope}\right)}$. Primers with efficiencies between 90 % and 110 % were selected for subsequent use. For each sample 4 µL of cDNA, as well as RT negative samples and no-template control samples were added to a master mix [10 µL 2x SensiMix™*Plus* SYBR (Bioline), 5 µL dH$_2$O, 1 µL primer mix (10 µM forward and reverse primers)]. These were prepared in 0.1 mL strip tubes (QIAGEN). The qPCR programme used was: initial denaturation step 95 °C for 10 min, 35 cycles of denaturation 95 °C for 15 s, annealing at 60 °C for 30 s, and elongation at 72 °C for 20 s. Ct values were acquired at the elongation step of each cycle and analysed using the Rotor-Gene 6000 Series Software Version 1.7. After the completion of 35 cycles, a melt curve analysis was performed to confirm single-product amplification. Samples were normalised against the housekeeping gene *GAPDH* (unless otherwise stated) and quantified using the comparative C_T method. This involves calculating the

difference in Ct values (ΔCt) between the gene of interest and reference housekeeping gene. The difference between the ΔCt values between the experimental condition versus control condition are then calculated giving a $\Delta\Delta$Ct value. The fold change between these conditions was then calculated using the formula $2^{(-\Delta\Delta Ct)}$.

2.2.6 Molecular cloning

2.2.6.1 Transformation of *E.coli* DH5α

All constructs contained a kanamycin or ampicillin resistance gene. Initially competent *E. coli* DH5α cells were thawed on ice. 1 ng of plasmid DNA was mixed with 50 µL of competent cells and incubated on ice for 30 min. Cells then underwent heat shock at 42 ^{o}C for 30 s before immediately cooling on ice for 5 min. SOC medium [0.5 (w/v) yeast extract, 2 % (w/v) tryptone, 10 mM NaCl, 2.5 mM KCl, 10 mM MgCl$_2$, 10 mM MgSO$_4$, 20 mM Glucose] was then added and the mixture was incubated at 37 ^{o}C for 1 h while shaking at 140 rpm. After 1 h cells were then spread onto Luria-Bertaini (LB) broth-agar plates [1.5 % (w/v) microagar in LB medium] containing 100 µg/mL ampicillin or kanamycin. Plates were then incubated at 37 ^{o}C overnight.

Transformed DH5α cells were saved as glycerol stocks for long term storage. This was obtained by picking a single bacterial colony from an agar plate and grown in 3 mL LB medium containing 100 µg/mL ampicillin or kanamycin overnight at 37 ^{o}C with shaking at 140 rpm. This starter culture was then mixed with LB-medium containing 40 % glycerol at 1:1 ratio and stored at -80 ^{o}C.

2.2.6.2 Plasmid purification

For isolation of large amounts of plasmid DNA the Plasmid Maxi Kit (QIAGEN) was used following the manufacturer's guidelines. For each plasmid, a single bacterial colony of DH5α cells were picked from agar plates and grown in 3 mL LB medium containing 100 µg/mL ampicillin or kanamycin overnight at 37 °C with shaking. Of these starter cultures, 200 µL were then used to inoculate 100 mL LB media containing 50 µg/mL of the relevant antibiotic and was grown overnight at 37 °C with shaking. The bacterial cultures were harvested at 5,000 x g for 15 min at 4 °C and then resuspended in 10 mL buffer P1. 10 mL of lysis buffer P2 was then added and the solution incubated for 5 minutes at room temperature. 10 mL of neutralisation buffer P3 was then added and incubated on ice for 10 min. Insoluble debris was then spun down at 5,000 x g for 1 h at 4 °C and the clear supernatant was added to a pre-equilibrated QIAGEN-tip 500. After the supernatant had passed through the column by gravity flow, two rounds of resin washing were performed with 30 mL of wash buffer QC. The plasmid DNA was then eluted into 10.5 mL of 100 % isopropanol by addition of 15 mL elution buffer QF. The eluted DNA:isopropanol solution was then spun at 5,000 x g for 1 h at 4 °C to produce a precipitated DNA pellet. This was then washed in 1 mL of 70 % ethanol and spun down at 16,000 x g for 10 min. The supernatant was removed, and the DNA pellet was then air-dried at room temperature for 5 min and resuspended in 200 µL dH$_2$O. DNA content and purity were determined using a NanoDrop ND-1000 spectrophotometer (NanoDrop Technologies, a Thermo Fisher Scientific Company).

2.2.7 Biotin affinity identification (BioID)

2.2.7.1   Transfection of BioID constructs

8×10^6 TREx cells were nucleofected once with 100 µL of Nucleofector solution V (Lonza) to which 2 µg of plasmid DNA was added. Cells were nucleofected using the protocol described in section 2.2.1.4.

1×10^6 293T cells were transfected with the same amount of BioID plasmid DNA using the previously described technique in section 2.2.1.5.

2.2.7.2   Biotin affinity purification

Two independent nucleofections for each BioID plasmid in TREx cells were performed as described in section 2.2.1.4 and then pooled to give a final cell number of 1.6×10^7. Cells were either induced to KSHV lytic replication as described in section 2.2.2.1 or maintained as unreactivated. 24 h prior to harvesting, cells were incubated with 100 µM biotin (Sigma)-containing media. Cells were lysed following the protocol described in (Roux et al., 2012) which is briefly outlined below. Cells were harvested by a 5 min spin at 500 x g in PBS and then lysed in Roux lysis buffer [50 mM Tris, pH 7.4, 500 mM NaCl, 0.4 % (w/v) SDS, 5 mM EDTA, 1 mM DTT and 1x Complete Protease Inhibitor (Roche)] for 10 min at room temperature and then sonicated. Triton X-100 was then added to 2 % (v/v) final concentration. An equal volume of chilled 50 mM Tris, pH 7.4 was added before another round of sonication and centrifugation at 4 °C 16,000 x g. Supernatants were then incubated by rotation with 200 µL of Dynabeads (MyOne Streptavidin C1, Invitrogen) overnight. Beads were collected by spinning at 500 x g for 5 min and washed twice for 8 min at room temperature in wash buffer 1 [2 % (v/v) SDS in dH$_2$O], then washed at room temperature in wash buffer

2 (0.1 % deoxycholate (w/v), 1 % triton-X100 (v/v), 500 mM NaCl, 1 mM EDTA and 50 mM HEPES, pH 7.5), once with wash buffer 3, (250 mM LiCl, 0.5 % NP-40 (v/v), 0.5 % deoxycholate (w/v), 1 mM EDTA, and 10 mM Tris, pH 8.1) and twice with wash buffer 4 (50 mM Tris, pH 7.4, and 50 mM NaCl). Bound proteins were eluted from the beads with 50 µL 2 x SDS loading buffer (Section 2.2.3.2) saturated with 100 mM biotin by incubating beads at 95 °C for 5 min. Protein samples were then stored at -80 °C before being shipped to the University of Bristol Proteomic Facility in dry ice.

2.2.8 Data analysis

2.2.8.1 Experimental design and null-hypothesis significance testing

Experiments were performed as experimental replicates by the n number specified in the figure legends (unless otherwise stated) and data analysis for bar plots was performed exclusively in Microsoft® Excel. Data was averaged using the built in AVERAGE function and standard deviations calculated using the STDEV.S function. Standard error of the mean was then calculated using the standard deviation and number of samples and 95 % confidence intervals were calculated for error bar parameters. All error bars shown are the 95 % confidence intervals around the mean of the data and all p-values shown were calculated using the T.TEST function set for a two-tailed, two-sample with equal variance test.

All box and whisker plots were plotted using R package ggplot2 utilising the geom_boxplot setting. In ggplot2 a box and whisker plot shows the median, the 25th and 75th percentiles (interquartile range, IQR) as the upper and lower hinges, and whiskers extending 1.5*IQR. The box plots are notched to highlight the 95 %

102

confidence intervals around the median calculated as $1.58*IQR/\sqrt{n}$. More documentation can be found at https://ggplot2.tidyverse.org/reference/geom_boxplot.html.

2.2.8.2 Densitometry analysis

Densitometry analysis was performed using ImageStudioLite® from Li-COR Biosciences. Scanned .tiff images were imported into ImageStudioLite® and converted to grayscale. Using the draw rectangle function a box was drawn around a band and then using the copy and paste function the identical shape was produced for each band to be analysed. This was performed for both GAPDH and the protein band of interest producing a data table that was copied into Excel. The signal column was then used to calculate the relative intensity of the band versus the control band, this relative intensity was then normalised by protein of interest relative intensity divided by loading control (GAPDH) relative intensity. These were plotted as a standard Excel bar plot.

2.2.8.3 ImageJ analysis

For the counting of BioID-expressing cells to calculate biotinylation rates:

Nucleofected TREx cells were prepared as described in section 2.2.4.1. Tile scans were performed using the LSM 880 confocal microscope (Ziess) creating an RGB 3000 x 3000 pixel image of approximately 1.5 cm^2 of a tile. This was exported as a .tiff from Zen 2011 using the Save As function and then opened in Fiji (Schindelin et al., 2012). The image was then split into three separate images for each channel. The following was performed on both the blue channel for DAPI, and the red channel for Biotin: Remove background, threshold was adjusted with

a maxima of approximately 40. Images were then converted to mask, the fill holes command was used and watershed was performed. Particles were then analysed using a size threshold of 25 pixels-infinity, no circularity threshold was set, and outlines were selected as the preferred output. The data from this count was then exported as a .csv file and analysed using Excel.

For cell membrane analysis using phalloidin:

Transduced TREx cells were prepared as described in section 2.2.4.1. Tile scans were performed using the LSM 880 confocal microscope (Ziess) creating an RGB 3000x3000 pixel image of approximately 1.5 cm^2 of a tile. This was exported as a .tiff from Zen 2011 using the Save As function and then opened in Fiji (Schindelin et al., 2012). The image was then split into three separate images for each channel. The red channel (phalloidin) was kept, background was removed, and threshold set to 25-255. Images were converted to mask, holes filled and watershed set. Global measurement settings had been set to mm and particles were analysed for perimeter and area using a size threshold of 10 mm-infinity, no circularity threshold was set, and outlines were selected as the output. Data was then exported as a .csv and analysed in Rstudio (R version 3.4.0 (2017-04-21) -- "You Stupid Darkness") using the script in section 2.2.8.4.2.1.

2.2.8.4 Bioinformatics analysis:

Tandem mass tagging (TMT) mass spectrometry data was provided as an excel spreadsheet that was converted to a .csv file using the Excel Save As function. Rstudio (R version 3.4.0 (2017-04-21) -- "You Stupid Darkness") was then used to filter data to provide a new enriched hits datasheet using the ratio of protein

104

between IP and R118G, the non-biotinylating control, (induced or uninduced depending on the IP sample) was greater than 1.5, code available in section 2.2.8.4.1. This list of proteins was further refined using an additional R script (Section 2.2.8.4.1.3) which also included proteins that were significantly downregulated or upregulated using the protein ratio between reactivated and unreactivated conditions (BioID-nup+/BioID-nup-). This produced a new list including enriched proteins compared to beads-only, and proteins upregulated during lytic replication by >2.0 or downregulated during lytic replication <0.33. This list was then outputted as a .csv and protein accession codes were converted to gene names using Uniprot mapper (https://www.uniprot.org/mapping/, Options: UniProtKB AC/ID to Gene name). All successfully mapped identifiers were copied and used in a multiple protein search on STRING (https://string-db.org/). The STRING network map was rendered and filtered to exclude edges derived from text mining data. Using the Analysis tab nodes were coloured by selecting the Gene Ontology cellular component categories cytoplasm and nuclear part.

2.2.8.4.1 R language scripts for BioID data analysis

2.2.8.4.1.1 BioID script workflow

Import and initial filter script

V

Combinatorial refinement script

V

Protein names then converted from accession to gene names

105

STRING-db analysis

2.2.8.4.1.2 Import script and initial filter versus background

Below example for unreactivated samples:

```
library(dplyr)
library(ggplot2)
# Set working directory for import of mass spec csv files
setwd("C:/Users/bsac/OneDrive for Business/PhD/PhD s- drive/Omic
data/BioID/TMT/Total with Human and KSHV prot/CSV Human and KSHV
prot")
# create a dataframe containing .csv data from reactivated BioID
sample
BioIDun <- data.frame(read.csv("211116 Total Human Plus KSHV v BioID -
.csv", header = TRUE))
# create a dataframe containing .csv data from unreactivated
R118G (beads only) sample
R118Gun <- data.frame(read.csv("211116 Total Human Plus KSHV v R116G-
.csv", header = TRUE))
# filter a refined table with only columns of accession, description,
R118G/nup- and nup+/nup-
# produce a table of nup+/nup-
nup_ratio <- BioIDun[,c("Accession","Description","X128C.131")]
# filter for induced nup hits
BioIDun_hits <- filter(R118Gun, R118Gun[,"X128_C.129_N"] > 1.5)
# BioIDind_hits has a list of enriched hits compared to beads only
# for validation purposes we will save this data to confirm these hits
# are nuclear versus bioid
setwd("/Users/alexcoleman/OneDrive - University of Leeds/Code/R
scripts/Bioid analysis/Enriched hits scripts/Enriched lists")
write.csv(BioIDun_hits, file = "BioIDind_hits.csv")
```
Below example for reactivated samples:

```
library(dplyr)
library(ggplot2)
# Set working directory for import of mass spec csv files
```

```
setwd("C:/Users/bsac/OneDrive for Business/PhD/PhD s- drive/Omic
data/BioID/TMT/Total with Human and KSHV prot/CSV Human and KSHV
prot")
```

```
# create a dataframe containing .csv data from reactivated BioID
sample
```

```
BioIDun <- data.frame(read.csv("211116 Total Human Plus KSHV v BioID -
.csv", header = TRUE))
```

```
# create a dataframe containing .csv data from reactivated
```

```
R118G (beads only) sample
```

```
R118Gind <- data.frame(read.csv("211116 Total Human Plus KSHV v
R116G+.csv", header = TRUE))
```

```
# filter a refined table with only columns of accession, description,
R118G/nup- and nup+/nup-
```

```
# produce a table of nup+/nup-
```

```
nup_ratio <- BioIDun[,c("Accession","Description","X128C.131")]
```

```
# filter for induced nup hits
```

```
BioIDind_hits <- filter(R118Gind, R118Gind[,"X128_C.129_N"] > 1.5)
```

```
# BioIDind_hits has a list of enriched hits compared to beads only
```

```
# for validation purposes we will save this data to confirm these hits
```

```
# are nuclear versus bioid
```

```
setwd("/Users/alexcoleman/OneDrive - University of Leeds/Code/R
scripts/Bioid analysis/Enriched hits scripts/Enriched lists")
```

```
write.csv(BioIDind_hits, file = "BioIDind_hits.csv")
```

2.2.8.4.1.3 Combinatorial refinement script

```
# this is the working library for allocating final key hits
```

```
# it takes from previous enriched hits versus beads only
```

```
# then creates final list of hits that are present in both OR
```

```
# present in uninduced list but ratio is less than <0.33 OR
```

```
# present in induced list but ratio is greater than 2
```

```
library(dplyr)
```

```
# set working dir
```

```
setwd("/Users/alexcoleman/OneDrive - University of Leeds/Code/R
scripts/Bioid analysis/Enriched hits scripts/Enriched lists")
```

```
# imports Nup85 hits datasets (enriched over R118G)
```

```
Nup85in <- data.frame(read.csv("Nup85ind_hits.csv", header = TRUE))
```

```
Nup85un <- data.frame(read.csv("Nup85un_hits.csv", header = TRUE))
```

```
# Imports original Nup85 unreactivated dataset containing the
Nup85+/Nup85- ratios
```

```
Nup85un_origin <- data.frame(read.csv("/Users/alexcoleman/OneDrive -
University of Leeds/PhD/PhD s- drive/Omic data/BioID/TMT/Total with
Human and KSHV prot/CSV Human and KSHV prot/211116 Total Human Plus
KSHV v Nup85-.csv", header = TRUE))
```

107

```r
# create a list of shared proteins in both Nup85+ hit list and Nup85-
hit list

shared_85 <- Nup85in[Nup85in$Accession %in% Nup85un$Accession,]

# Create a long list of all hits identified but not all necessarily
shared between +/-

prot_names <- bind_rows(Nup85un, Nup85in)

# removes duplicates

prot_names <- unique(prot_names)

# creates new dataframe to calculate relative abundance differences
from

# original dataframe versus Nup85- by selecting out proteins by
Accession from long list of all hits

prot_names1 <- Nup85un_origin[Nup85un_origin$Accession %in%
prot_names$Accession,]

# reduce columns to relevant columns

prot_names1 <-
prot_names1[,c("Accession","Description","X..Unique.Peptides","X129_C.
127_N")]

# filter the list for proteins in the shared list defined above, or
proteins with a Nup85+/Nup85- ratio greater than 2 or proteins with a
Nup85+/Nup85- ratio less than 0.33.

prot_names1 <- prot_names1[prot_names1$Accession %in%
shared_85$Accession | prot_names1$X129_C.127_N > 2.0 |
prot_names1$X129_C.127_N <= 0.33,]

# create a new column to highlight if this protein was present in the
Nup85+ hit list

prot_names1$In <- prot_names1$Accession %in% Nup85in$Accession

# create a new column to highlight if this protein was present in the
Nup85- hit list

prot_names1$Un <- prot_names1$Accession %in% Nup85un$Accession

# set working directory for saving

setwd("/Users/alexcoleman/OneDrive - University of Leeds/Code/R
scripts/Bioid analysis/Enriched hits scripts/Enriched lists")

write.csv(prot_names1, file = "Nup85_hits_combo2.csv")
```

2.2.8.4.2 R language scripts for perimeter data analysis

2.2.8.4.2.1 Boxplot analysis of perimeter data

```r
library(ggplot2)
# quick analysis of ImageJ features

rx1_scr <-data.frame(cbind(read.csv('dir/to/csv
/reactivated_tile1.csv'),treatment='Mock'))[,c(2,3,4)]

rx2_scr <- data.frame(cbind(read.csv('/Users/alexcoleman/OneDrive -
University of Leeds/Images for
classification/Phalloidin/Scr/Analysis/Rx
only/reactivated_tile2.csv'),treatment='Mock'))[,c(2,3,4)]
```

108

```r
rx1_ist1 <- data.frame(cbind(read.csv('/Users/alexcoleman/OneDrive -
University of Leeds/Images for
classification/Phalloidin/ist1/Analysis/Rx_only/reactivated_tile1.csv'
),treatment='IST1'))[,c(2,3,4)]

rx2_ist1 <- data.frame(cbind(read.csv('/Users/alexcoleman/OneDrive -
University of Leeds/Images for
classification/Phalloidin/ist1/Analysis/Rx_only/reactivated_tile2_outl
i.csv'),treatment='IST1'))[,c(2,3,4)]

rx1_7 <- data.frame(cbind(read.csv('/Users/alexcoleman/OneDrive -
University of Leeds/Images for
classification/Phalloidin/chmp7/Analysis/Rx_only/reactivated_tile1.csv
'),treatment='CHMP7'))[,c(2,3,4)]

rx2_7 <- data.frame(cbind(read.csv('/Users/alexcoleman/OneDrive -
University of Leeds/Images for
classification/Phalloidin/chmp7/Analysis/Rx_only/reactivated_tile1_2.c
sv'),treatment='CHMP7'))[,c(2,3,4)]

main_df <- rbind(rx1_scr,rx2_7,rx2_ist1,rx2_scr,
row.names=c('Perim.','Area','Label'))

main_df$Area <- sapply(sapply(main_df$Area, as.character), as.numeric)

main_df$Perim. <- sapply(sapply(main_df$Perim., as.character),
as.numeric)

main_df$Perim.Area <- main_df$Perim./main_df$Area

# set up saving at 300dpi

tiff('test.tiff',units = 'px', width = 1500, height = 1200,res= 300)

ggplot(main_df, aes(x=treatment, y=Perim.Area))+
  stat_boxplot(geom='errorbars')+
  geom_boxplot(notch=TRUE,
               lwd = 0.7) +
  scale_x_discrete(limits=c('Mock','IST1','CHMP7'),
                   name = 'LentiORF')+
  scale_y_continuous(expand=c(0,0),
                     limits=c(0,2.6),
                     breaks=seq(0,2.6,0.2),
                     name = 'Perimeter/Area')+
  theme_classic()
# confirm saving of tiff file
dev.off()
```

109

Chapter 3
~
Nup98 is remodelled by KSHV during lytic infection

3   Nup98 is remodelled by KSHV during lytic infection

3.1   Introduction

KSHV is a member of the *Gammaherpesvirinae* sub-family. Its lifecycle is divided into two distinct replication stages: latency with minimal gene expression and a focus on episome maintenance; and lytic replication, where the full complement of viral open reading frames (ORFs) are expressed and nascent virions are produced and released. Lytic replication itself is split into three temporal stages based on the kinetics of ORF expression: immediate-early, delayed-early and late. At each of these stages different viral proteins are expressed that remodel endogenous cellular processes from mRNA export through immediate-early ORF57 protein to global mRNA turnover via delayed-early ORF37 protein (Glaunsinger and Ganem, 2004; Majerciak and Zheng, 2009).

The nuclear pore complex (NPC) is a protein mega-complex that sits at the nuclear envelope and regulates nucleocytoplasmic transport. It is formed from multiple copies of 30 different proteins called nucleoporins, giving rise to a mega-complex of approximately 125 MDa (Hoelz et al., 2011). It acts as both a barrier and a sophisticated conduit permitting regulated transport of protein and RNA (Moore, 1998; Cautain et al., 2014). Nup98 is a nucleoporin crucial for various RNA export pathways, as well as playing a variety of off-pore regulatory roles within the nucleus (Powers et al., 1997; Light et al., 2013). Viral remodelling of nucleoporins is an established strategy of cellular subversion during viral infection and alterations in nucleoporin levels had been identified from whole cell lysate

proteomic data from lytically induced KSHV-infected B cells (Sophie Schumann, Unpublished data). Therefore, it was speculated that KSHV may specifically remodel components of the NPC during lytic infection to aid its replication.

In this chapter, Nup98 is identified as a nucleoporin that is remodelled during early KSHV lytic infection via a large quantitative proteomic screen. A range of techniques are then employed to confirm and characterise the importance of Nup98 targeting during KSHV lytic replication.

3.2 Nup98 is specifically downregulated early during KSHV lytic infection

SILAC-based quantitative proteomics is a mass spectrometry technique that detects changes in protein abundance between samples using non-radioactive isotope labelling (Oda et al., 1999; Ong et al., 2002). Previously, members of the Whitehouse laboratory had prepared BCBL-1-Rta cells (subsequently referred to as TREx cells) grown in either heavy, light or medium isotopic conditions. Cells in the heavy and medium conditions were treated with doxycycline to induce KSHV lytic replication through an inducible mycRTA construct and lysed at 24 h and 8 h post doxycycline treatment, respectively. Lysed samples were then sent to Dr Kate Heesom at the University of Bristol Proteomic Facility for analysis and the SEQUEST data was obtained with relative protein levels expressed as ratios between the three conditions. Whole cell lysate quantitative proteomic data with a 1% false discovery rate (FDR) showed Nup98 levels were reduced by approximately half when comparing the SILAC ratio of protein levels between 0 h and 8 h post induction of lytic replication (Figure 3.1a). Nup98 is a nucleoplasmic-orientated nucleoporin containing GLFG repeats that has a key

role in nuclear export but has also been shown to diffuse off the pore into the nucleus (Powers et al., 1997; Griffis et al., 2002). Nup98 therefore, exists as two populations within the cell, a pore-bound population facilitating export with the adaptor protein Rae1 (Blevins et al., 2003), and a nucleoplasmic population playing roles in transcription (Capelson et al., 2010; Kalverda et al., 2010). Similar decreases in other nucleoporin levels were not observed for other nucleoporins including Nup160, Nup133, Nup107, key structural nucleoporins that form the Nup160-Nup107 complex (Walther et al., 2003), and Nup153, another nucleoplasmic-oriented nucleoporin involved in nuclear import (Sukegawa and Blobel, 1993; Ullman et al., 1999). From the quantitative proteomic data corresponding to Nup160-Nup107 complex nucleoporins it could be inferred that the overall number of nuclear pores did not decreased within 8 h of lytic infection.

To validate the observed downregulation of Nup98, western blot analysis was performed on TREx cells at different time points post induction of KSHV lytic replication via doxycycline-inducible mycRTA (Figure 3.1b). The decrease in Nup98 protein levels was confirmed at 8 h and shown to be specific when compared to Nup153, similar to the quantitative proteomic data. Densitometry analysis confirmed this decrease in Nup98 protein levels was significant compared to Nup98 levels at 0 h and was comparable in magnitude to the observation in the quantitative proteomic data (Figure 3.1c). Intriguingly, qPCR analysis of Nup98 mRNA levels over the course of KSHV lytic infection did not show a decrease in Nup98 mRNA, in fact at 8 h post induction of lytic replication Nup98 mRNA levels rose significantly to 2.5 fold when compared to 0 h post doxycycline treated TREx cells (Figure 3.1d). These results suggest that Nup98

was specifically targeted by the virus rather than the NPC as a whole and that

Nup98 protein was specifically targeted rather than Nup98 mRNA.
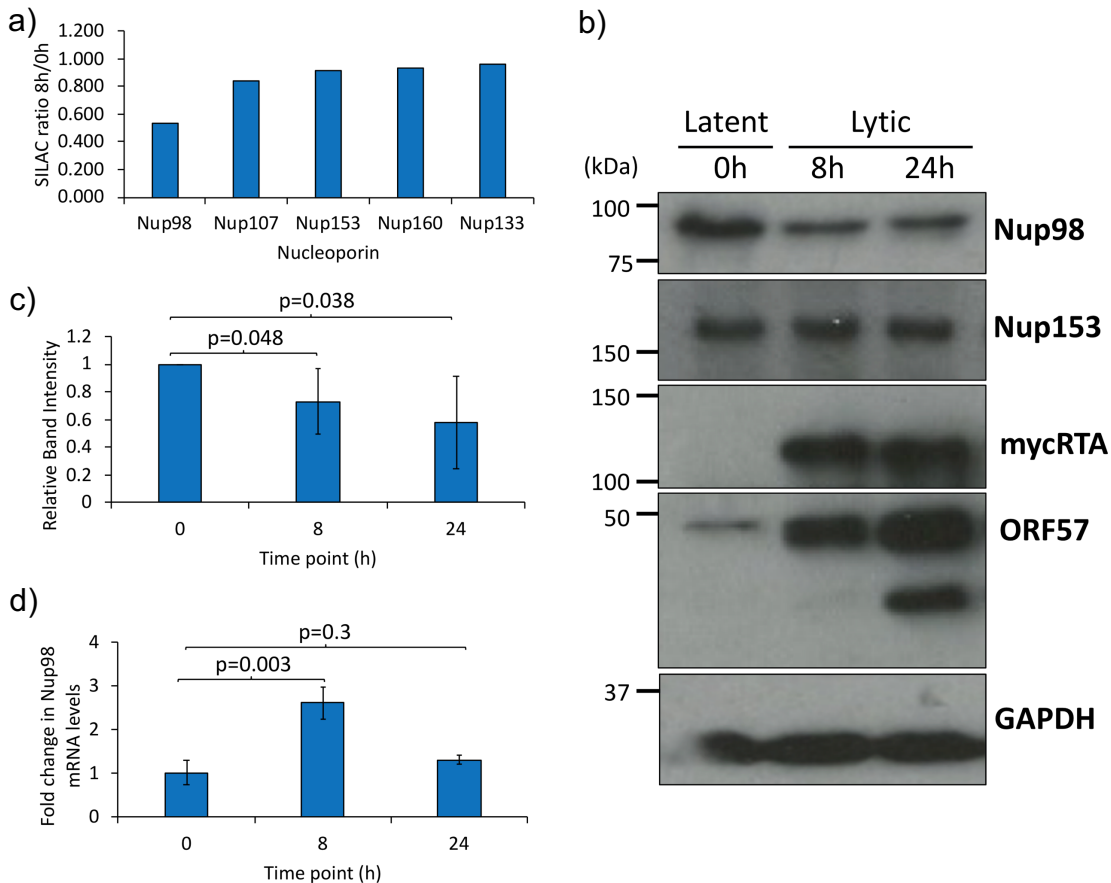
Figure 3.1 Nup98 is specifically downregulated at 8 h post induction of KSHV lytic replication in TREx cells. a) 1% FDR quantitative proteomic ratio of nucleoporin protein levels at 8 h post induction of lytic replication compared with protein levels at 0 h post induction of lytic replication (Sophie Schumann, unpublished data). n=1. b) A representative Western blot of nucleoporin levels at 0 h, 8 h and 24 h post induction of lytic replication in TREx cells. mycRTA represents a control for induction of lytic replication via the doxycycline-inducible mycRTA construct, ORF57 shows mycRTA is able to activate the viral lytic cascade and GAPDH represents a loading control. c) Quantified densitometry of Nup98 band intensity normalised to GAPDH for reactivation time course experiments shown in b). n=3, 95% confidence intervals shown, T-test p-value shown between indicated conditions. d) qPCR analysis of Nup98 mRNA levels relative to GAPDH mRNA from TREx cells at times shown post induction of lytic replication. n=3, confidence intervals shown, T-test p-value shown between indicated conditions.

3.3 The localisation of Nup98 is not altered during KSHV lytic infection

In order to understand the above changes, it was important to first determine the proportion of TREx cells that undergo KSHV lytic replication after treatment with doxycycline to promote mycRTA expression. Using confocal microscopy, it was possible to determine the percentage of lytically replicating TREx cells at each time point (Figure 3.2). This shows that in TREx at 0 h there were <5 % of cells that expressed RTA in line with expectations surrounding rates of spontaneous reactivation (Lukac et al., 1998). At 8 h, the time point where we observe a decrease in Nup98 protein levels, 23.8 % of cells were expressing RTA. This suggests that the level of Nup98 protein decrease may be greater than that observed through western blot analysis given the low proportion of cells that were expressing RTA at 8 h post induction of lytic replication. These data help inform subsequent analyses given that the virus is reactivated only within a proportion of TREx cells at each time point with a majority of cells expressing RTA by 24 h (57.2 %).
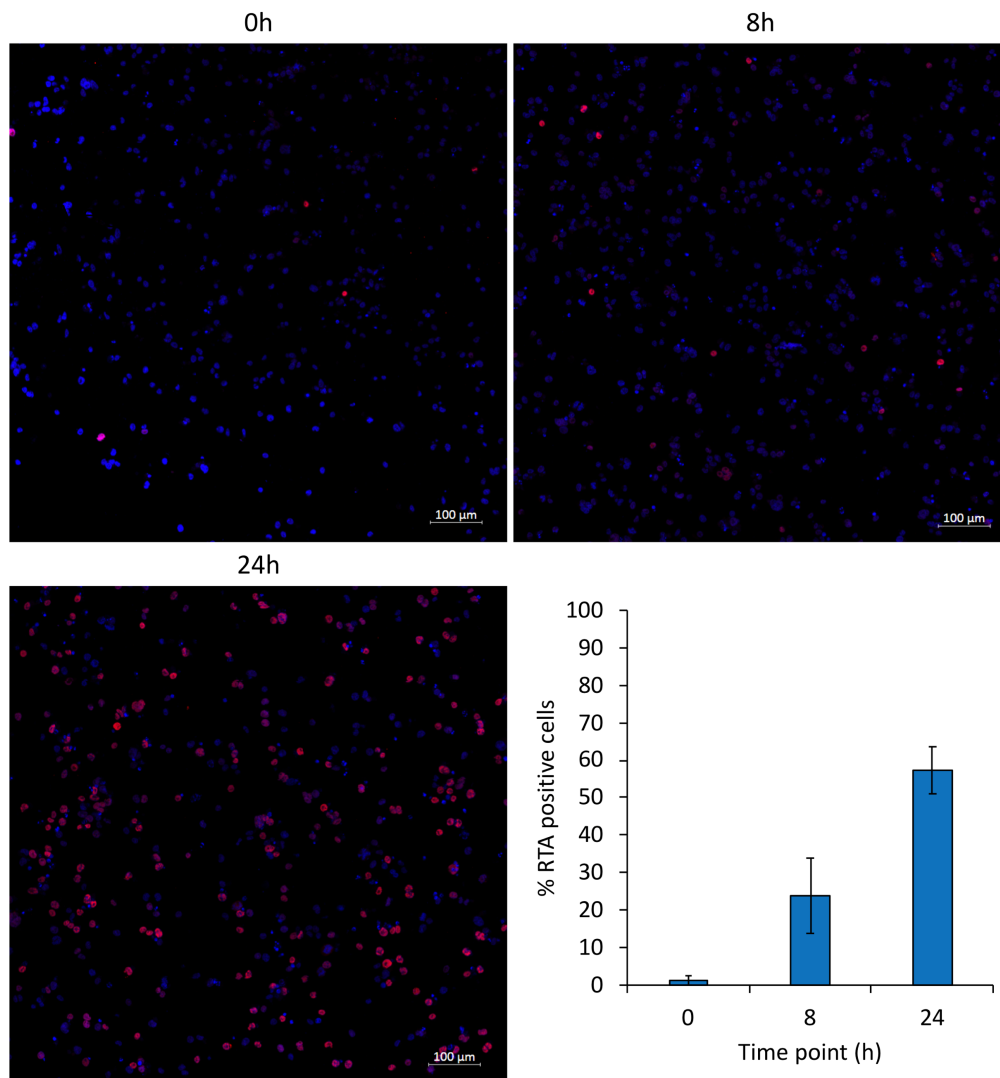
Figure 3.2. Confocal microscopy-based quantification of the proportion of TREx cells that undergo KSHV lytic replication. Representative tilescan confocal images of TREx cells at either 0, 8 or 24 h after the induction of lytic infection. DAPI in blue, RTA in red. ImageJ quantification of the % of RTA positive cells shown. n=3, 95% confidence intervals shown.

Following on from these observations, confocal immunofluorescence was performed to determine whether a decrease in Nup98 protein levels could be visualised in RTA expressing TREx cells. Confocal immunofluorescence analysis of the localisation of Nup98 in TREx at different time points after the induction of KSHV lytic replication showed that there was no obvious decrease of Nup98 signal at the nuclear pore or relocalisation of Nup98 as KSHV lytic replication

progressed (Figure 3.3). Nup98 can be observed through confocal immunofluorescence predominantly at the nuclear pore as strong, discrete signals indicating NPCs, there is also a faint diffuse signal in the nucleoplasm although no discrete GLFG-bodies are visible as has been observed in some cell types (Griffis et al., 2002). At 0 h, differences in Nup98 levels can be observed in cells lacking RTA expression suggesting a level of baseline variability. At 8 h, there are some cells that have begun to express RTA however there is no consistent Nup98 phenotype when these cells are compared to cells lacking RTA expression. At 24 h, replication compartments have begun to form in RTA expressing cells but again there is no observable decrease in Nup98 signal or localisation. These results suggest that decreases in Nup98 protein levels during KSHV lytic replication may not occur at the NPC. The approach taken for confocal microscopy here aimed to minimise background signal and therefore involved focusing upon the NPC Nup98 signal at the expense of the more diffuse signal within the nucleoplasm. Technically this made visualising nucleoplasmic Nup98 difficult in TREx cells however the observation of no consistent NPC Nup98 phenotype suggested that the nucleoplasmic fraction of Nup98 may be being targeted.
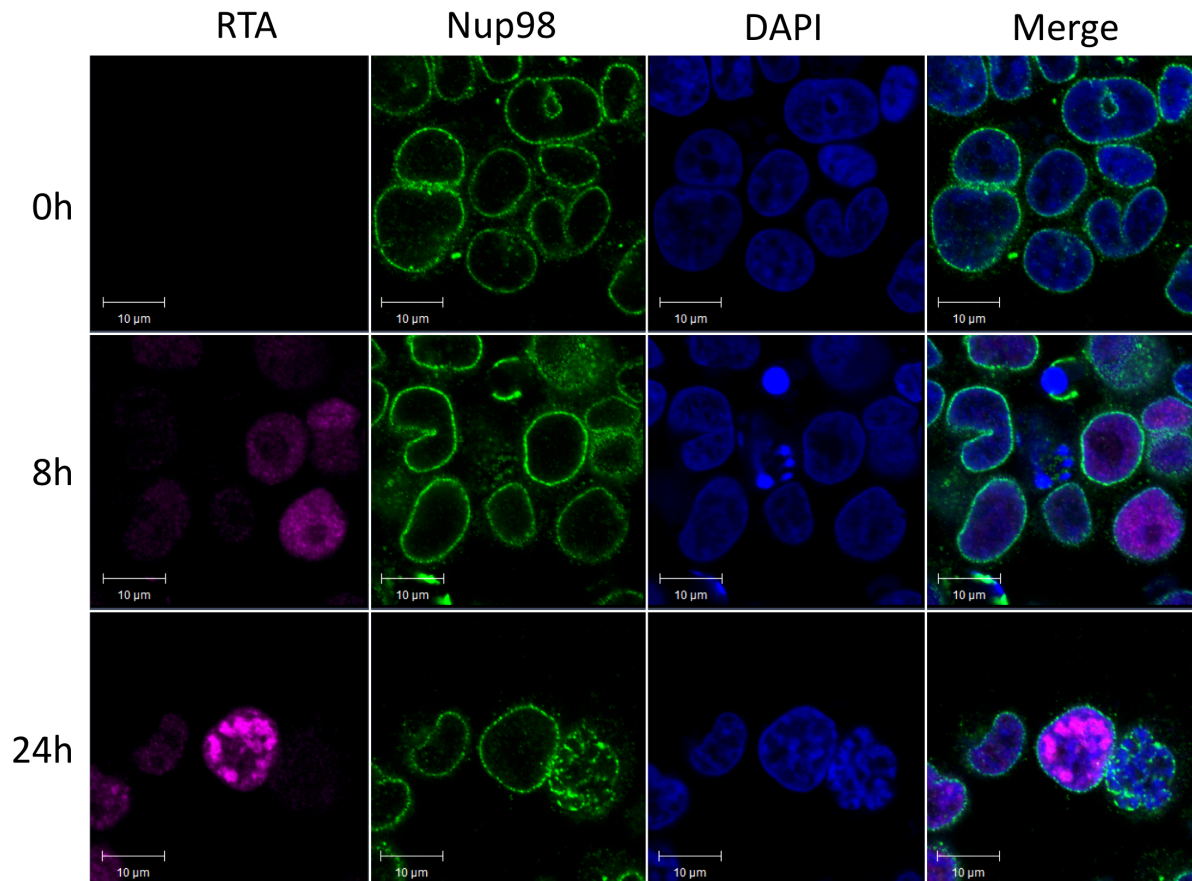
Figure 3.3 Nup98 localisation in TREx cells is not altered on the reactivated of KSHV. Confocal immunofluorescence analysis of Nup98 in TREx cells at 0 h, 8 h and 24 h post induction of KSHV lytic replication with doxycycline, endogenous RTA staining present to confirm induction to lytic replication, DAPI to identify cell nucleus.

3.4 Increased Nup98 degradation in the presence of KSHV RTA is dependent on the ubiquitin-proteasome pathway

The decrease of Nup98 protein during KSHV lytic infection appeared to occur within 8 h of reactivation of TREx cells without a concurrent downregulation of Nup98 mRNA levels. Therefore, it was hypothesised that Nup98 could be being targeted for degradation through the ubiquitin-proteasome pathway. Furthermore, KSHV immediate-early protein RTA, the viral transactivator responsible for initiating the transition from latency to lytic replication (Lukac et

118

al., 1998), has previously been shown to specifically target other cellular proteins via a ubiquitin E3 ligase-like domain (Yu et al., 2005; Gould et al., 2009). Therefore, the targeted degradation of Nup98 during KSHV lytic infection could be linked to RTA-induced proteasomal degradation.

In order to test this hypothesis a series of experiments were performed in RTA-transfected 293T cells. Initially, these experiments simply involved transfecting a construct that constitutively expressed RTA into 239T cells, incubating the cells for 24 h before western blot analysis of Nup98 protein levels. This showed that 24 h after transfection with an RTA expression plasmid Nup98 protein levels decreased significantly compared to an untransfected control (Figure 3.4a). This was further quantified using densitometry confirming a significant decrease when compared to Nup98 protein levels in untransfected control 293T cells (Figure 3.4b). To confirm that the transfection of RTA did not lead to a decrease in Nup98 mRNA levels, RNA was also extracted from transfected cells and analysed by qPCR. A modest decrease in Nup98 mRNA levels after RTA transfection was observed however the scale of the decrease did not account for the decrease in protein levels observed (Figure 3.4c). This suggested that expression of RTA could lead to a decrease in Nup98 protein levels in 293T cells in the absence of all other KSHV lytic factors.
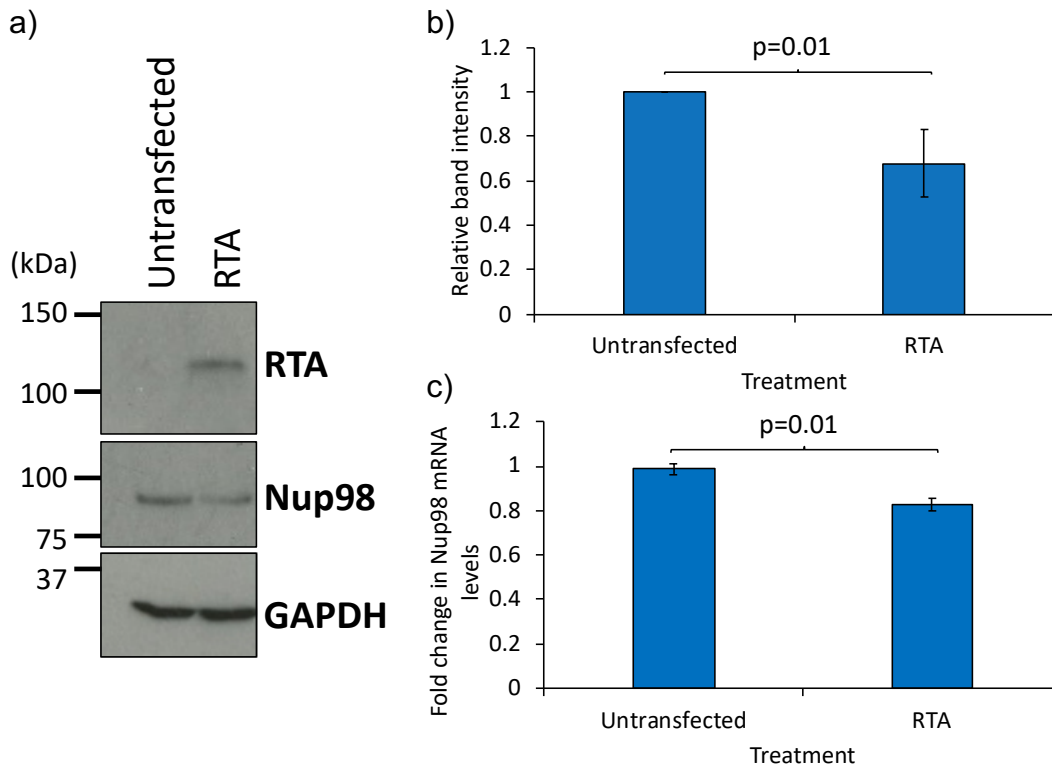
Figure 3.4 Nup98 protein levels decrease in 293T cells after transfection with KSHV RTA protein. a) A representative western blot of Nup98 levels in 293T cells 24 h post transfection with RTA expression plasmid and untransfected cells. RTA levels also shown along with GAPDH as a loading control. b) Densitometry of the Nup98 band intensity from western blot analysis normalised to GAPDH for experiments where RTA was transfected into 293T cells with protein extracted 24 h post transfection. n=3, 95% confidence intervals shown, T-test p-value shown between indicated conditions. c) qPCR analysis of Nup98 mRNA levels normalised to GAPDH mRNA in untransfected and RTA transfected 293T. n=3, confidence intervals shown, T-test p-value shown between indicated conditions.

Having demonstrated that transfection of RTA led to a decrease in Nup98 protein levels but did not reduce Nup98 mRNA levels to the same extent the next step was to identify whether the downregulation was via the ubiquitin-proteasome pathway. Therefore, a series of experiments were performed with MG132, a peptide aldehyde that binds to the chymotrypsin-like active site of the β subunit of the proteasome inhibiting protein degradation (Rock et al., 1994), to determine whether Nup98 degradation upon transfection of RTA could be prevented.

Initially, 293T cells were transfected with an untagged RTA expression construct and incubated for 24 h before cells were treated with DMSO or 20 µM MG132. 6 h after treatment with MG132 or DMSO cells were harvested and lysed for western blot analysis. Western blots were performed to confirm RTA expression and to compare Nup98 protein levels in each treatment (Figure 3.5a). A significant downregulation of Nup98 was observed in RTA-transfected 293T cells compared with untransfected cells treated with DMSO however, this significant decrease is not detectable between untransfected and RTA-transfected cells that were treated with 20 µM MG132 (Figure 3.5b). Similar experiments were performed on reactivated TREx cells, with TREx cells treated with doxycycline to induce KSHV lytic replication and 2 h post doxycycline treatment DMSO or 20 µM MG132 was added. 6 h after DMSO or MG132 treatment cells were harvested and lysed. This allowed for the comparison of Nup98 levels at 8 h post induction of lytic replication, the timepoint where the downregulation of Nup98 is observed in lytically replicating cells. Western blot analysis of these samples showed that doxycycline treated cells were able to induce mycRTA expression and that Nup98 levels decreased in reactivated cells treated with DMSO, however in MG132 treated cells Nup98 levels did not decrease between 0 h and 8 h (Figure 3.5c). Densitometry analysis of Nup98 relative band intensity normalised to GAPDH showed a significant decrease in Nup98 in DMSO treated TREx cells at 8 h post doxycycline treatment when compared to Nup98 at 0 h (Figure 3.5d). This decrease was not observed in reactivated MG132 treated TREx between 8 h and 0 h, with an apparent increase in Nup98 at 8 h compared to 0 h although this was not significant (Figure 3.5d). These observations showed that the RTA-induced decrease of Nup98 in 293T was sensitive to inhibition of the proteasome and that

the Nup98 decrease observed in TREx cells at 8 h post reactivation with doxycycline was also dependent on the proteasome. Overall, these data suggested that RTA was responsible for decreasing Nup98 protein levels via the ubiquitin-proteasome pathway.
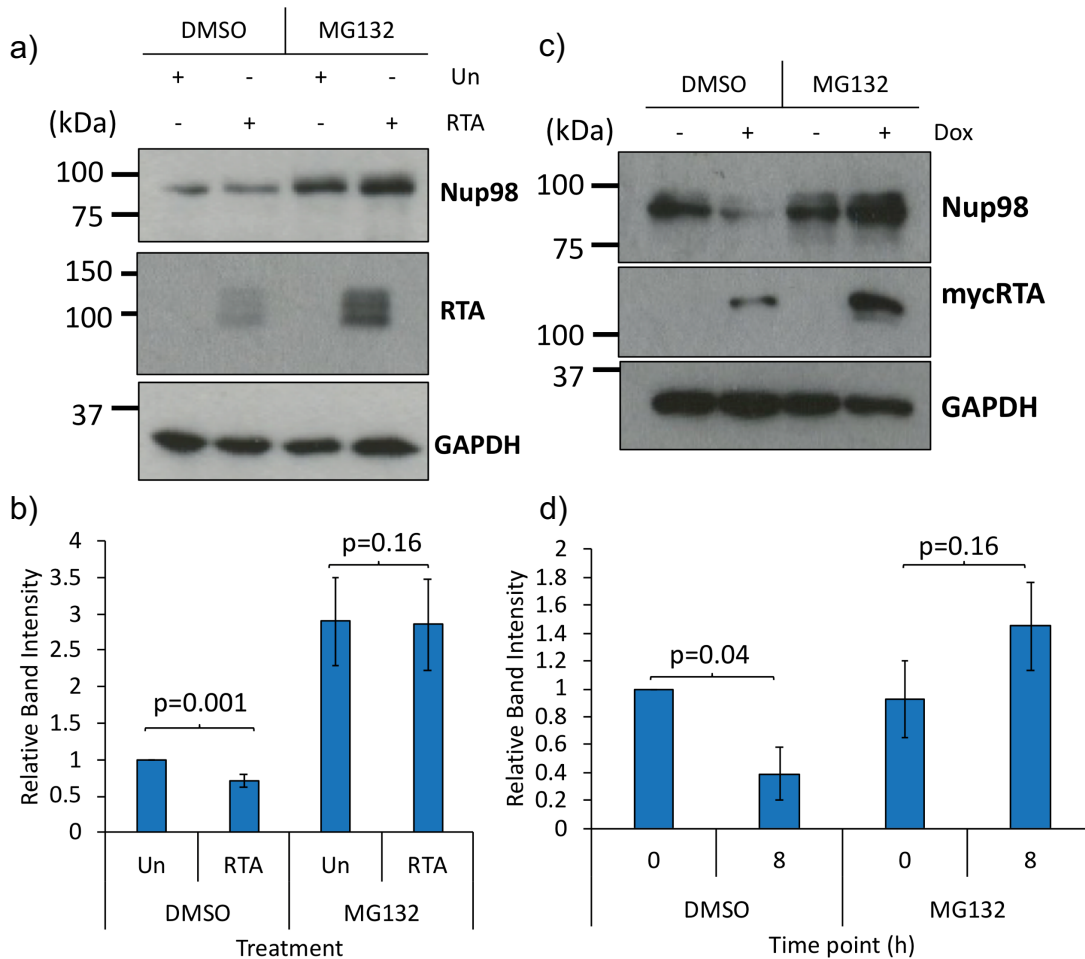
Figure 3.5 Nup98 degradation is prevented on treatment with proteasome inhibitor MG132. a) A representative western blot of Nup98, RTA and GAPDH (loading control) from 293T cells that were either untransfected or transfected with RTA for 24 h before treatment with either DMSO or 20 µM MG132 for 6 h before protein was collected. b) Densitometry analysis of Nup98 band relative intensity normalised to GAPDH from western blots of protein extracted from 293T cells (untransfected or RTA transfected 24 h post transfection) treated for 6 h with either DMSO or 20 µM MG132. n=3, 95% confidence intervals shown, T-test p-value shown between indicated conditions. c) A representative western blot of Nup98, mycRTA and GAPDH (loading control) from TREx cells treated with doxycycline and 2 h subsequently treated with DMSO or 20 µM MG132 before protein extracted 8 h post doxycycline treatment. d) Densitometry analysis of Nup98 band relative intensity normalised to GAPDH from western blots of protein extracted from TREx cells treated with doxycycline and 2 h later either DMSO or 20 µM MG132 with protein extracted at 8 h post doxycycline treatment. n=3, 95% confidence intervals shown, T-test p-value shown between indicated conditions.

Next, attempts were made to use co-immunoprecipitation techniques to pull down Nup98 protein and determine whether RTA binding could be detected. This involved inducing lytic replication in TREx cells and performing Nup98 immunoprecipitations on protein lysates at different time points post induction of lytic infection. RTA was not identified when immunoprecipitation samples were analysed via western blotting (Figure 3.6). However, this did not exclude the hypothesis that RTA is targeting Nup98 for degradation via its E3 ubiquitin ligase as interactions between E3 ligases and their substrates can be highly transient and therefore not always identifiable via co-immunoprecipitation experiments (Pierce et al., 2009).
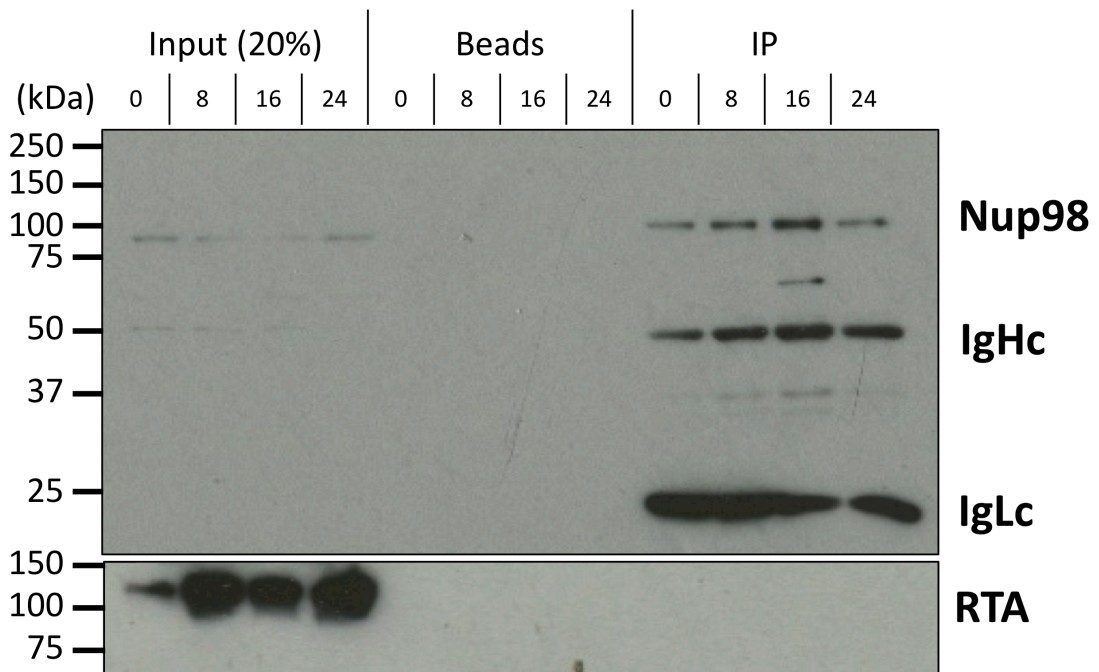
Figure 3.6 RTA could not be shown to co-immunoprecipitate with Nup98 in TREx. Immunoprecipitations using anti-Nup98 antibodies were performed at different time points post the induction of lytic replication in TREx cells with doxycycline. Endogenous RTA was probed at each time point and no co-immunoprecipitation was observed. n=2.

3.5 Nucleoplasmic Nup98 binding partner DHX9 does not play a role during early KSHV lytic replication

Thus far experiments had indicated that Nup98 protein was downregulated early during KSHV lytic infection via enhanced degradation through the proteasome-ubiquitin pathway. This decrease did not appear to occur at the NPC and therefore was speculated to be specific to the nucleoplasmic Nup98 fraction. The next steps of this work involved determining why KSHV targeted Nup98 and the mechanism behind its hypothesised restrictive role of viral replication. The function of Nup98 within the nucleoplasm is not fully understood but has been suggested to involve transcription regulation via its interaction with a range of nucleoplasmic binding partners (Light et al., 2013; Panda et al., 2014; Capitanio et al., 2017). One of its main binding partners is DExH-helicase 9 or DHX9 (also referred to as RNA Helicase A) (Capitanio et al., 2017). It was therefore speculated that the targeting of nucleoplasmic Nup98 by KSHV could be related to DHX9 due to its interactions with CREB-binding protein (CBP) and RNA Polymerase 2 (Nakajima et al., 1997). This is a critical pathway for KSHV during early lytic infection because RTA, the viral transactivator, also recruits CBP to stimulate transcription of early viral genes (Gwack et al., 2001). It was hypothesised therefore that the nucleoplasmic Nup98-DHX9 interaction maybe disrupted by RTA early during lytic infection to allow DHX9 to be recruited as part of the CBP complex with RTA to KSHV early lytic gene promoters.

To investigate this hypothesis, shRNAs against DHX9 were transduced with Lentivirus into BCBL-1 cells to deplete DHX9. It was hypothesised that upon the reactivation of lytic replication in DHX9-depleted cells RTA expression would

124

have a less efficient induction of lytic replication due to the potential role of DHX9. BCBL-1 cells were chosen for these experiments rather than TREx cells to eliminate the potential for doxycycline induced mycRTA expression to mask the proposed effect of DHX9 at early lytic promoters. Many of these early lytic promoters rely on RTA to stimulate expression through ORF50 response elements, therefore the doxycycline inducible mycRTA system was inappropriate for these experiments. DHX9 protein levels were successfully depleted using targeted shRNAs and subsequent analysis of BCBL-1 cells induced into lytic replication with 12-*O*-tetradecanoylphorbol-13-acetate (TPA) and sodium butyrate showed a modest decrease in RTA levels at 48 h in DHX9-depleted cells compared to scrambled treated cells (Figure 3.7a). However, there were minimal observable differences in ORF57 expression levels at both 24 h and 48 h time points post induction of the lytic replication. qPCR analysis of ORF57 and ORF50 RNA levels further confirmed there was no significant difference in expression levels at 24 h post induction of lytic replication (Figure 3.7b). At 48 h there was an increase in ORF50 levels observed in DHX9-depleted cells but this was not significant when compared to scrambled treated cells, ORF57 levels were observed to be significantly different however the difference was only a slight increase (0.56 fold in scrambled treated cells, 0.75 fold in DHX9-depleted cells, Figure 3.7b). This data suggests no significant role of DHX9 specifically in KSHV lytic infection although it is possible that redundancy within the dead-box helicase family means the effects of DHX9-depletion were obscured.

125
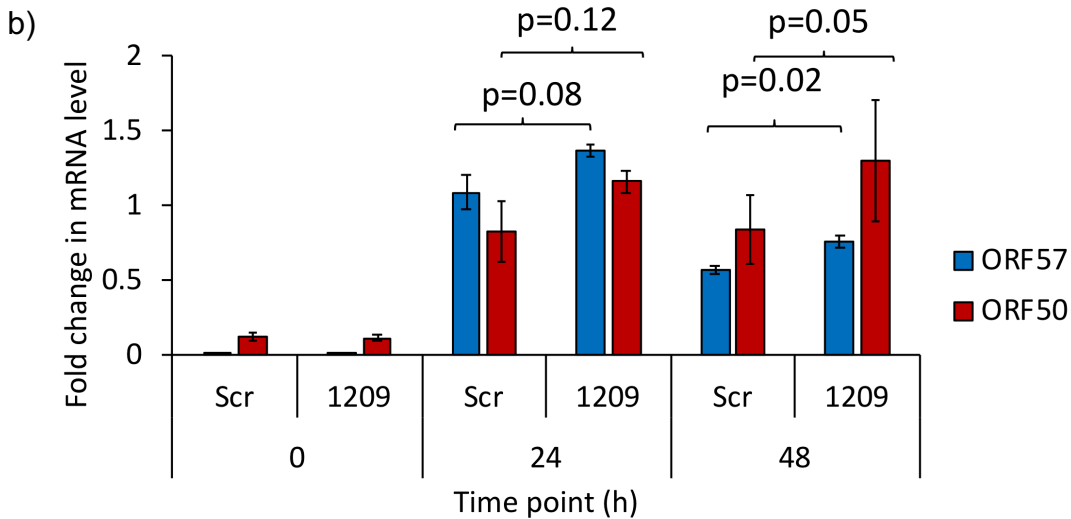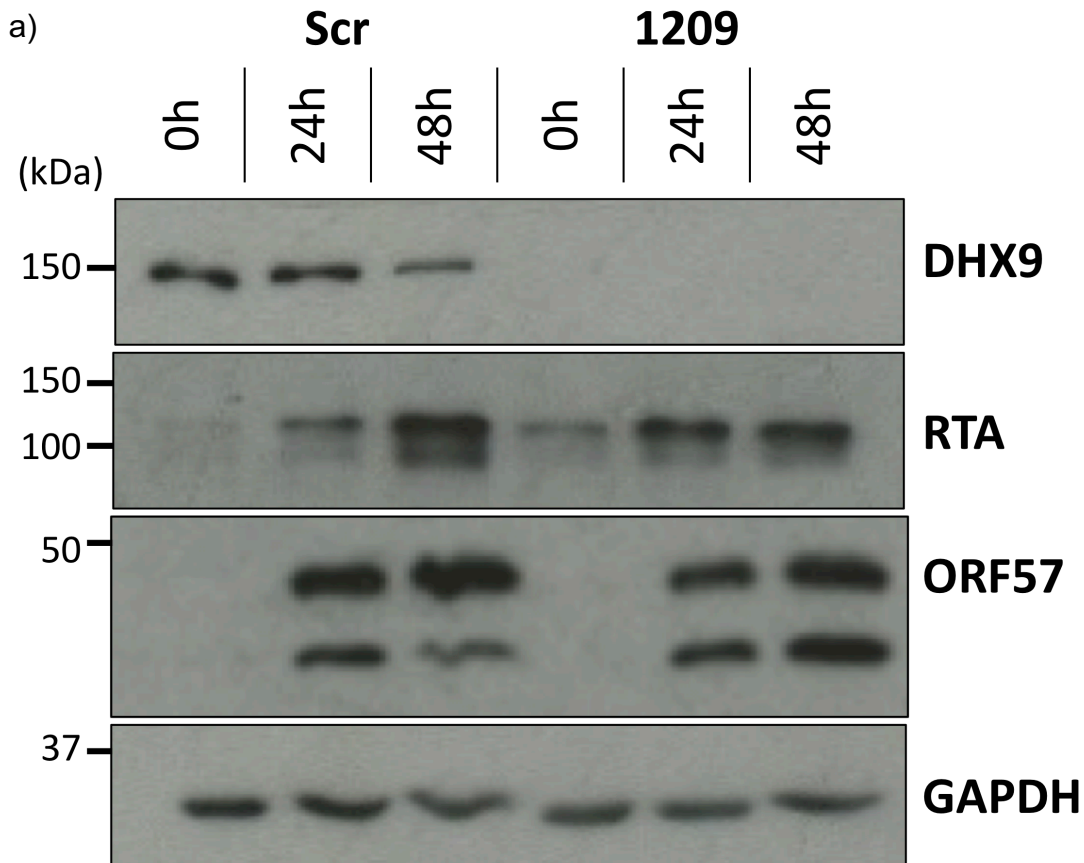
Figure 3.7 The depletion of Nup98 nucleoplasmic binding partner DHX9 did not impact KSHV lytic replication. a) A representative western blot of viral immediate-early proteins (ORF57 and RTA) in BCBL-1 cells expressing either scrambled or 1209 shRNA against DHX9, lytic replication induced with TPA and sodium butyrate. GAPDH shown as a loading control. b) qPCR analysis of KSHV immediate-early transcripts in BCBL-1 cells expressing either scrambled or 1209 shRNA targeting DHX9 at time points post induction of lytic replication with TPA and sodium butyrate. n=3. 95% confidence intervals shown, T-test p-value shown between indicated conditions.

3.6 Nucleoplasmic Nup98 acts to prevent transcription of KSHV lytic ORFs at ORF50-promoters

The observations thus far led to the speculation that KSHV was targeting the nucleoplasmic fraction of Nup98 due to no observable changes of Nup98 localisation. To test whether nucleoplasmic Nup98 had a restrictive effect on early KSHV lytic processes, 293T cells were transfected with a series of plasmid combinations to test the effect of overexpressing GFP-Nup98, a donation from collaborators from the Wozniak Laboratory, on a viral ORF50-promoter-luciferase construct. Overexpression of Nup98 has been shown to saturate the nucleoplasmic fraction which could highlight the more transient impacts of Nup98 on KSHV (Griffis et al., 2002). Cells were transfected in triplicate and incubated for 24 h before lysis and luciferase substrate addition. Luminescence readings were then obtained using an automated plate reader and results analysed. Interestingly, overexpression of GFP-Nup98 along with an FLAG-RTA overexpression construct led to a significant decrease in the luminescence produced from ORF50-promoter luciferase construct compared to luminescence in FLAG-RTA and GFP transfected cells (Figure 3.8a). An empty FLAG vector was used to control for RTA overexpression showing the baseline level of luminescence from the ORF50-promoter luciferase construct (Figure 3.8a). This suggested that when cells were oversaturated with GFP-Nup98, RTA was unable to induce transcription at the ORF50 promoter. To test the kinetics of GFP-Nup98 repression of RTA-induced transcription at the ORF50 promoter, the above luciferase experiments were extended using sequentially increased doses of GFP-Nup98 and GFP. Results showed that the negative transcriptional effect of GFP-Nup98 was dose-dependent with luminescence from ORF50-driven

luciferase decreasing as the amount of GFP-Nup98 transfected increased (Figure 3.8b). This suggests that nucleoplasmic Nup98 negatively regulates RTA-induced transcription at the ORF50 promoter and furthermore, suggests that this negative effect is implicitly linked to the level of Nup98 present within the cell. Therefore, the targeting of Nup98 protein levels by KSHV early during lytic replication is essential to ensure transcriptional activation of immediate-early KSHV genes.
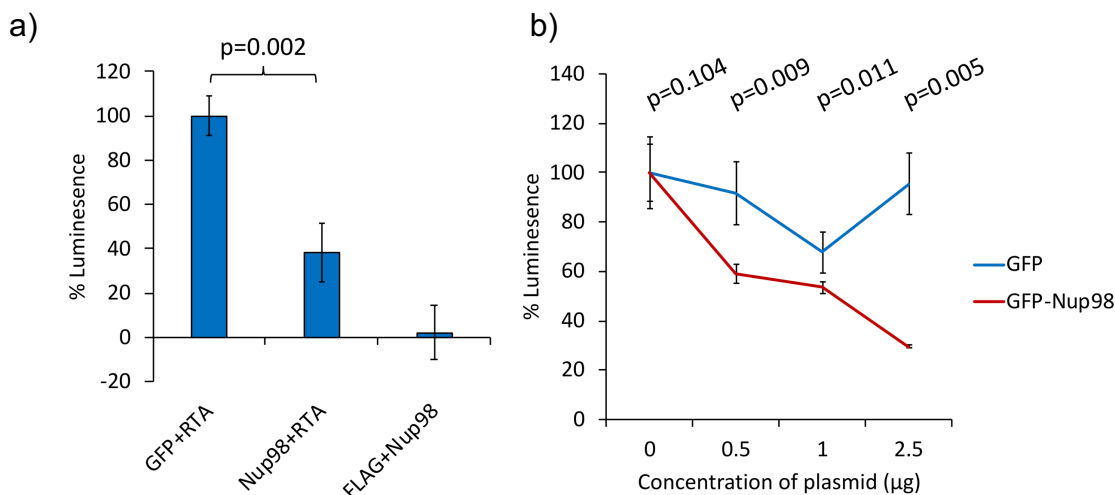
Figure 3.8. Overexpressing Nup98 alongside RTA and an ORF50 luciferase construct in 293T cells significantly reduces luminesence. a) Luminesence analysis of ORF50 luciferase construct when treated with FLAG-RTA and GFP, FLAG-RTA and GFP-Nup98 or an empty FLAG-vector and GFP-Nup98 in 293T cells. Luminescence standardized to Renilla control. n=4, 95% confidence intervals shown, T-test p-value shown between indicated conditions. b) Dose dependent experiment transfecting ORF50 luciferase promoter, FLAG-RTA and GFP or GFP-Nup98 at various concentrations. Luminescence standardized to Renilla control. n=3, 95% confidence intervals shown, T-test p-value shown between indicated conditions.

3.7 Chromatin Immunoprecipitation of Nup98

To identify whether the downregulation of expression at the RTA promoter was mediated by binding of Nup98 at the ORF50 promoter, chromatin immunoprecipitations were attempted. Initial work to optimise the protocol was

performed on unreactivated TREx cells to confirm that Nup98 immunoprecipitation could be accomplished. Anti-RNA polymerase II antibody was utilised as a positive control, as it had been previously used for ChIP experiments in the Whitehouse Laboratory, anti-rabbit IgG was utilised as a negative control. Cells were harvested using the Pierce Chromatin Prep Module to obtain formaldehyde fixed chromatin. Chromatin was then digested into fragments for ChIP using micrococcal nuclease. Successful fragmentation was visualised on an agarose gel and samples were carried forward for immunoprecipitation (Figure 3.9a). The EZ-ChIP kit from Millipore was utilised for the immunoprecipitation alongside a rabbit anti-Nup98 antibody previously used for Nup98 ChIP (Light et al., 2013). Immunoprecipitations were performed overnight, and DNA was obtained for both sample inputs and immunoprecipitations via a DNA spin clean column from the EZ-ChIP kit. qPCR was then performed to quantify the % of input obtained from the immunoprecipitations for the DNA at the MYC promoter, a site Nup98 has previously been shown to bind (Capitanio et al., 2017). Disappointingly, there was very poor fold enrichment of the MYC promoter from the anti-Nup98 immunoprecipitation when compared to the IgG control. Further to this, when compared to anti-RNA polymerase II where 23.6 fold enrichment was observed it was apparent that immunoprecipitation with anti-Nup98 had been unsuccessful (Figure 3.9b). This result was consistent across two experiments and led to the prioritisation of alternative experiments to look for the interaction between Nup98 and the KSHV genome.
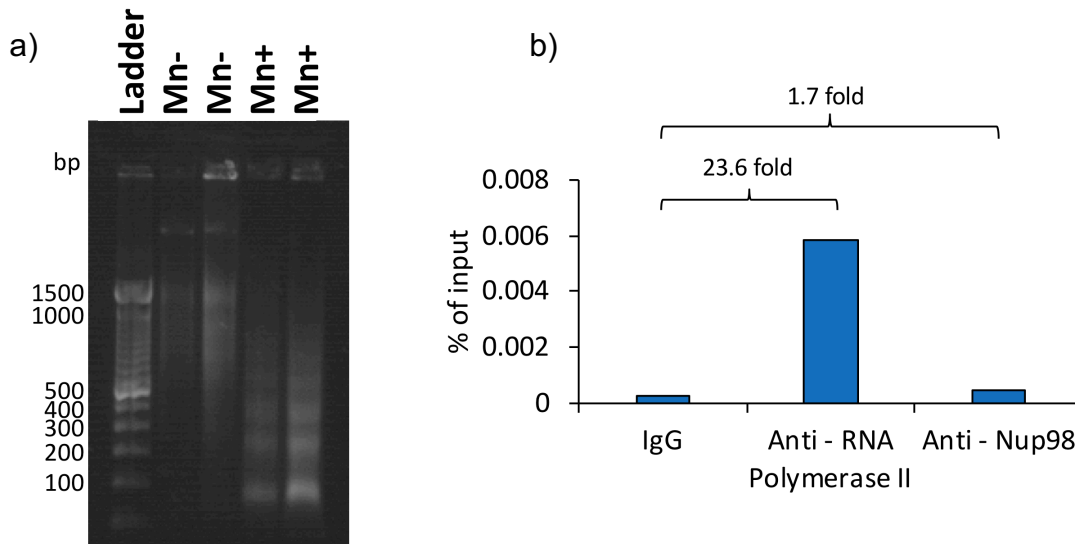
Figure 3.9 Chromatin Immunoprecipitation in TREx cells using Nup98 was unsuccessful. a) DNA gel showing the efficiency of micrococcal nuclease shearing of genomic DNA for ChIP. 100kbp ladder used, between each treatment lane volumes have been doubled for better resolution. b) Comparison of the fold enrichment between IgG, anti-RNA polymerase II and anti-Nup98 antibodies for ChIP of MYC promoter. n=2.

3.8   Overexpression of GFP-Nup98 in TREx does not prevent the progression of KSHV lytic infection when induced with sodium butyrate

Utilising the GFP-Nup98 expression described above, a Lentiviral transfer vector was developed to allow for the generation of stably expressing GFP-Nup98 cell lines. Lentiviral transduction was performed with this transfer vector and an empty GFP vector on TREx cells and puromycin at 2 µg/mL was used select stably expressing cells (Balistreri et al., 2016). Untransduced cells were used as a control to confirm puromycin induced cell death and after 12 days of selection no control cells were alive. At this stage a hypothesis had been developed that speculated nucleoplasmic Nup98 was targeted early during KSHV lytic infection in order to prevent Nup98 negatively regulating ORF50 responsive KSHV genes.

This negative regulation was speculated to revolve around the ability of nucleoplasmic Nup98 to bind at promoters and recruit histone remodelling complexes (Liang et al., 2013; Franks et al., 2017). Therefore, it was hypothesised that the inclusion of overexpressed GFP-Nup98 may act to prevent expression at ORF50 responsive viral genes on the induction of KSHV lytic replication.

Due to the proposed action of RTA downregulating Nup98 protein levels induction of TREx cells via doxycycline to induce lytic replication with mycRTA was not possible. This is due to the potential for doxycycline-induced mycRTA expression to counter-act the action of GFP-Nup98 due to previously demonstrated RTA-induced Nup98 degradation and mycRTA ability to activate endogenous RTA expression via the ORF50 promoter. This high level of cross talk could potentially mask any real protective effects offered by GFP-Nup98. Therefore, TREx cells were induced to KSHV lytic replication via treatment with sodium butyrate, a well-established alternative (Lu et al., 2003). Cells were induced with sodium butyrate and left for 24 h before they were harvested and lysed for RNA isolation and protein isolation. Western blot analysis was performed and showed poor expression of GFP and GFP-Nup98, in fact, levels were so low that blotting for GFP resulted in a blank blot (Figure 3.10a). GFP-Nup98 could only be detected in lytically replicating cells when probing for Nup98 but the signal was minimal suggesting poor transduction efficiency or a loss of the GFP expression cassette. Western blots for endogenous RTA and ORF57 protein showed higher levels of RTA in GFP-Nup98 cells in both NaBut treated and untreated cells however ORF57 levels appeared slightly reduced in treated GFP-Nup98 cells compared to GFP cells (Figure 3.10b). Nevertheless, the low detection of GFP-Nup98

131

means these differences may results largely from variations in reactivation efficiency than any effect of GFP-Nup98. qPCR was also performed RNA levels for viral immediate-early transcripts ORF50 and ORF57 with no significant difference in ORF57 transcript levels (Figure 3.10a) However, there was a slight but significant increase in ORF50 levels observed (1 fold in GFP lytic cells, 1.16 fold in GFP-Nup98 lytic cells, Figure 3.10), but again this difference cannot be attributed to any effect of GFP-Nup98 given its low level of expression.
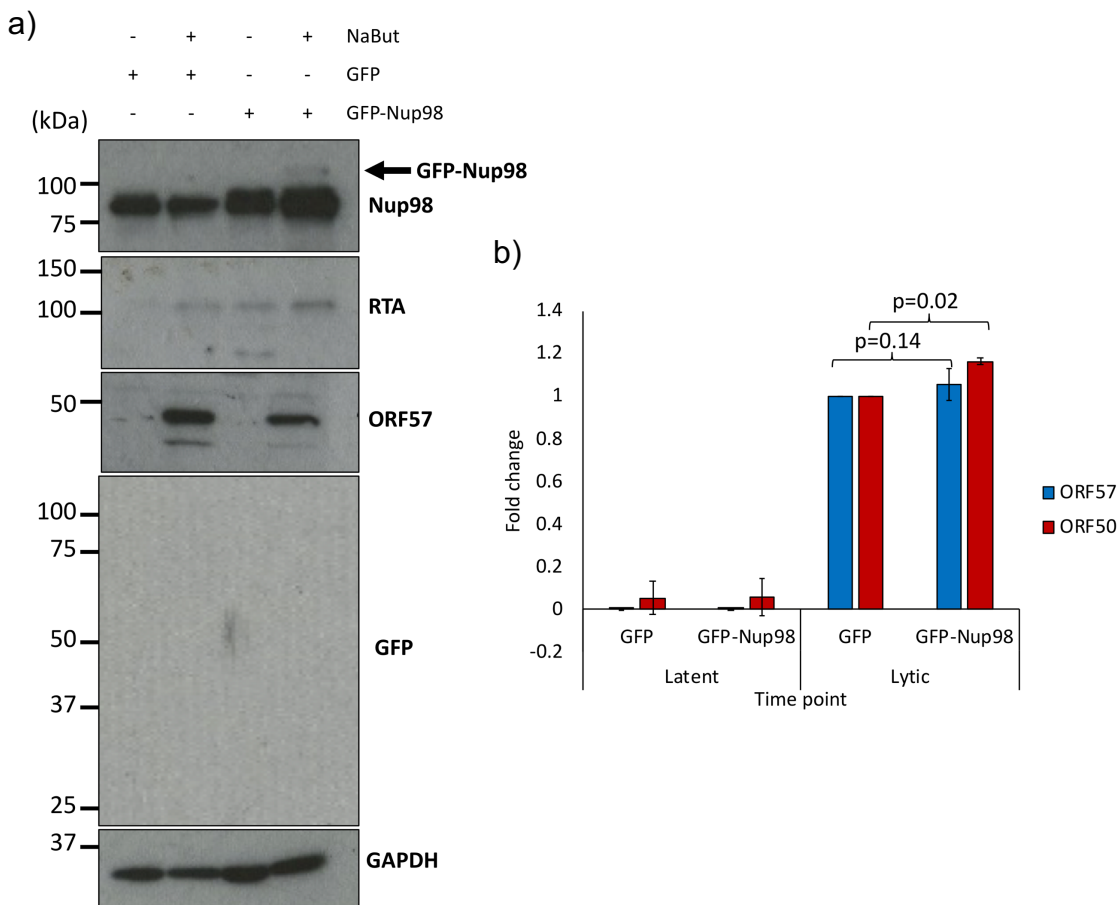
Figure 3.10 Overexpression of GFP-Nup98 in TREx cells could not be detected by western blot and no significant changes to KSHV early lytic infection mRNA or protein was observed. a) A representative western blot of KSHV immediate-early lytic genes (endogenous RTA and ORF57) after stably expressing GFP and GFP-Nup98 cells were treated with sodium butyrate (NaBut), GFP shown to probe GFP constructs, GAPDH is a loading control. b) qPCR analysis of immediate-early KSHV lytic genes ORF57 and ORF50 after stably expressing GFP and GFP-Nup98 cells were treated with sodium butyrate. n=3, 95% confidence intervals shown, T-test p-value shown between indicated conditions.

Concomitant with these experiments, immunofluorescence was performed on GFP and GFP-Nup98 expressing cells induced to KSHV lytic replication with sodium butyrate. Given the indication from western blot analysis that GFP/GFP-Nup98 expression had been lost or transduction efficiency low it was hoped that confocal immunofluorescence would allow for the identification of a phenotype within the small number of GFP-Nup98 expressing cells. GFP and GFP-Nup98 TREx cells were seeded onto poly-l-lysine coated coverslips and incubated for 24 h before sodium butyrate was added to stimulate reactivation of KSHV lytic replication. Cells were fixed 24 h post sodium butyrate treatment and stained for anti-RTA, to confirm successful induction of KSHV lytic replication, before washing and staining with secondary antibodies conjugated to Alexa Fluor™ before finally being mounted onto coverslips with DAPI. Coverslips were then visualised on a Ziess LSM 880 confocal microscope and both GFP and GFP-Nup98 cells were observed although at a very low rate as suggested by western blotting (Figure 3.11).

Nevertheless, GFP-Nup98 was seen to localise at the NPC and in the nucleoplasm as expected. Interestingly, the nucleoplasmic signal of GFP-Nup98 occurred as both a diffuse stain and also as discrete, intense foci (Figure 3.11). These were not previously observed when staining for endogenous Nup98 in TREx cells (Figure 3.3a) and appear to be a common artefact of Nup98 overexpression refered to as GLFG-bodies (Griffis et al., 2002). Nevertheless, the induction of KSHV lytic replication does not appear ablated in GFP-Nup98 overexpressing cells with a strong RTA stain present alongside good GFP-Nup98 staining (Figure 3.11). There was observed a level of colocalization between GFP-Nup98 particularly with several GLFG-foci although this was not

133

consistently seen with some GLFG-bodies occurring in the nucleolar regions of the nucleus which have minimal RTA signal. These data suggested that even amoungst the low level of successfully overexpressing GFP-Nup98 TREx cells that increased cellular saturation of Nup98 at both the NPC and in the nucleoplasm did not affect the induction of KSHV lytic replication when cells are treated with sodium butyrate.
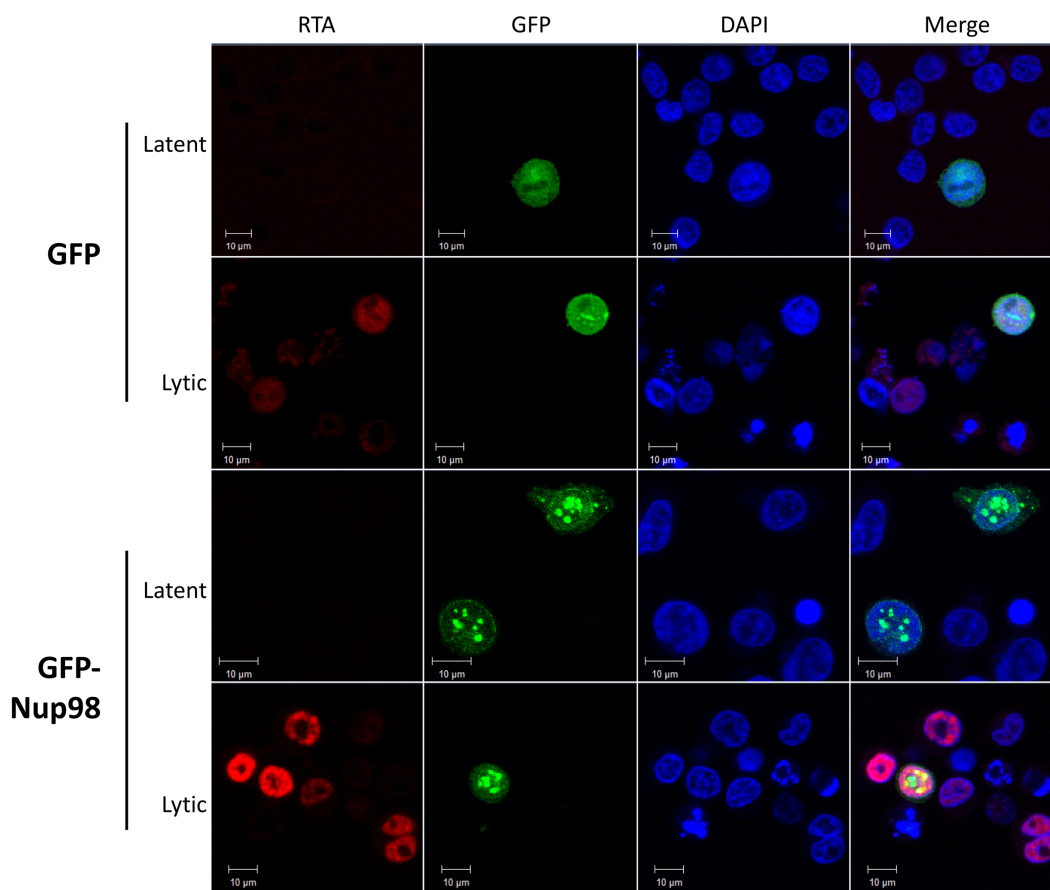
Figure 3.11 Immunofluorescence analysis of stably expressing GFP and GFP-Nup98 TREx cells shows no difference RTA levels or localisation in reactivated cells. Cells were treated with sodium butyrate to induce KSHV lytic replication and fixed 24 h post induction of KSHV lytic replication. Cells were then permeabilized, blocked with BSA and stained with anti-RTA before mounting with DAPI and visualisation on a Zeiss LSM 880 upright confocal microscope.

3.9 Discussion

In this chapter the nucleoporin Nup98 protein has been shown to be specifically targeted early during KSHV lytic infection (Figure 3.1). The decrease in Nup98 can be achieved through the overexpression of RTA and Nup98 degradation can be ablated by inhibiting the ubiquitin-proteasome pathway (Figure 3.4 and Figure 3.5). However, attempts to visualise a relocalisation or decrease of Nup98 by confocal microscopy were inconclusive, with levels at the NPC remaining unchanged (Figure 3.2) This led to the hypothesis that KSHV was targeting the nucleoplasmic fraction of Nup98 in order to subvert a transcriptional role of Nup98 rather than a nucleocytoplasmic role. Further experimentation showed that overexpressing Nup98 led to reduced transcription at viral promoters specifically the ORF50-promoter (Figure 3.8). This observation has serious implications for early KSHV lytic infection; with several immediate-early KSHV genes requiring the ORF50 gene product, RTA for their transcription (Song et al., 2001; Lukac et al., 2001b; Deng et al., 2002; Chang et al., 2002). It was hypothesised this restrictive action of Nup98 could be a serious impediment during the latent-lytic switch to the low initial concentrations of RTA.

The next steps of this work aimed to validate this hypothesis by confirming binding of Nup98 to the KSHV genome using ChIP and utilising a GFP-Nup98 overexpression construct in TREx cells to test its effect on KSHV lytic replication. Previous work had shown ChIP of Nup98 was possible and Nup98 binding had previously characterised at a variety of cellular genomic sites (Liang et al., 2013). Nevertheless, attempts at ChIP in TREx cells with this particular Nup98 antibody were unsuccessful although remain a key experiment for future work, in order to

135

confirm whether Nup98 directly binds to the ORF50 promoter (Figure 3.9). To investigate whether overexpressing Nup98 could have a preventative effect on the induction of KSHV lytic replication, a GFP-Nup98 overexpression construct was produced as a lentiviral transfer plasmid to allow for the establishment of stably expressing GFP-Nup98 TREx cells. Experiments were performed reactivating cells to KSHV lytic replication using sodium butyrate rather than the doxycycline inducible mycRTA system to prevent overexpressed mycRTA masking an effect. However, low levels of GFP and GFP-Nup98 expression were achieved after puromycin selection either due to low transduction efficiency or loss of the expression cassette (Figure 3.10). In the small set of GFP/GFP-Nup98 positive cells the overexpression of GFP-Nup98 did not lead to reduce RTA expression (Figure 3.11). This could relate to the role of sodium butyrate as a histone deacetylase inhibitor that induces global changes to the epigenetic landscape (Davie, 2003). It has previously been shown that nucleoplasmic Nup98 is able to alter chromatin structures and affect transcription (Liang et al., 2013; Light et al., 2013; Franks et al., 2017). Therefore, the action of sodium butyrate treatment could disrupt a hypothetical Nup98-induced chromatin remodelling event, masking any potential protective effect. Therefore, it is crucial that for future work efforts are made to test alternative methods of reactivation of KSHV lytic replication, including heat shock or hypoxia to test for a protective effect of Nup98.

Chapter 4

~

CHMP7 is targeted by KSHV via a Nup98-dependent mechanism to enhance virion egress

4 CHMP7 is targeted by KSHV via a Nup98-dependent mechanism to enhance virion egress

4.1 Introduction

In the previous chapter, it was demonstrated that KSHV downregulates a specific nucleoporin, Nup98, early during KSHV lytic replication. Nup98 is a dynamic nucleoporin that exists both at the nuclear pore and within the nucleoplasm playing multiple roles within the cell. At the NPC, Nup98 is orientated towards the nucleoplasm facilitating a range of RNA export pathways via complex formation with host proteins NXF1 and Rae1 (Powers et al., 1997; Blevins et al., 2003). Nup98 has also been shown to be interferon inducible and regulate antiviral gene expression (Enninga et al., 2002; Panda et al., 2014). KSHV has been shown to target factors that prevent the interferon response during early lytic infection (Ma et al., 2015; Ma et al., 2017). Initial experiments therefore looked to investigate whether KSHV downregulated Nup98 as part of a preventative strategy against an antiviral response. This chapter expands upon the unexpected results of those experiments which led to an entirely new line of enquiry regarding the role of Nup98 at the NPC during KSHV lytic infection and the requirement of Nup98 to ensure successful virion egress.

KSHV virion egress is a complex, multistep process as new virions transition from the nucleus to release from the cell (Mettenleiter et al., 2009). The general model for herpesvirus particle assembly is: newly synthesised viral DNA is packaged into the capsid in the nucleus; the capsid leaves the nucleus by primary envelopment at the inner nuclear membrane, the primary envelope then fuses

with the outer nuclear membrane releasing capsids into the cytoplasm; final maturation of the capsid occurs in the cytoplasm where the capsids acquire a tegument layer before the secondary envelopment step via budding at the *trans* Golgi network (TGN); at this stage the virus acquires its glycoproteins and exits the TGN within a cellular vesicle; this capsid-containing-vesicle is transported to the cell surface where the vesicle fuses with the plasma membrane releasing a mature, enveloped virion (Reviewed in (Mettenleiter, 2002; Mettenleiter et al., 2009)). However, much of this work has been performed primarily using alphaherpesviruses and there is much still to be elucidated regarding how the gammaherpesviruses interact with cellular components to ensure successful packaging and eventual egress.

Herein, it is shown that whole-cell Nup98 depletion does not alter early KSHV lytic replication however Nup98-depleted TREx cells exhibit reduced infectious virion egress. This phenotype is attributed to Nup98-depletion disrupting the action of KSHV lytic ORF10, a viral protein that interacts at the NPC with Rae1, a Nup98 binding partner, to inhibit RNA export a certain cellular mRNA. One cellular mRNA targeted in this manner is that of ESCRT-III component charged multivesicular body protein 7 (CHMP7). Through experiments overexpressing CHMP7 it was demonstrated that a similar failed virus egress phenotype could be observed leading to the hypothesis that KSHV targets CHMP7 mRNA during lytic infection to prevent its role in membrane repair. Crucially, this work highlights an interesting juxtaposition to the previous chapter where it was shown Nup98 is reduced during KSHV lytic infection with evidence suggesting this was targeted to nucleoplasmic Nup98. This chapter highlights how KSHV may require Nup98 at the NPC during lytic infection for the action of viral ORF10.

139

4.2   siRNA treatment successfully depleted Nup98 in TREx cells

In the Chapter 3, Nup98 levels were shown to be downregulated early after the induction of KSHV lytic infection (Figure 3.1). Nup98 has previously been shown to be targeted by other viruses to inhibit bulk mRNA export and furthermore, Nup98 expression can be induced by interferon to alleviate a virally-induced export block (Enninga et al., 2002). Therefore, it was hypothesised that KSHV was downregulating Nup98 early during KSHV lytic infection to prevent a Nup98-mediated antiviral pathway. To test this, siRNAs against Nup98 were nucleofected into TREx cells and after 48 h RNA and protein was collected. qPCR analysis showed a significant ~70 % reduction in Nup98 mRNA levels (Figure 4.1a). Western blot and densitometry analysis also showed a significant reduction Nup98 protein levels (Figure 4.1b and Figure 4.1c).
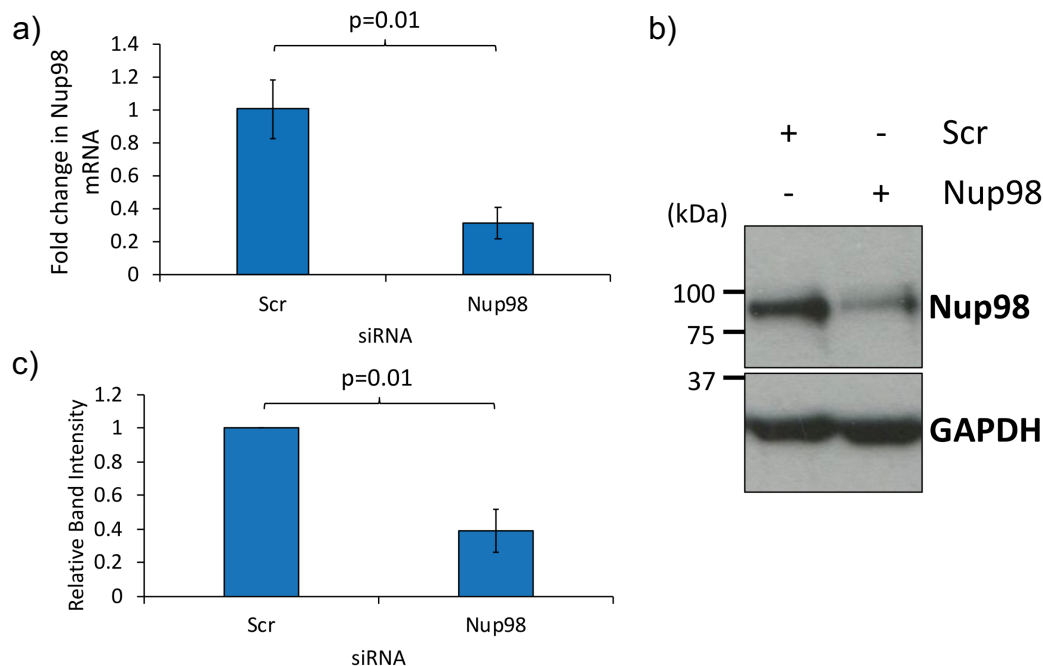
Figure 4.1 Nup98 can be significantly depleted by siRNAs in TREx cells. a) qPCR analysis of Nup98 mRNA levels in TREx cells nucleofected with scrambled (scr) and Nup98 siRNAs 48 h post nucleofection. n=3. 95 % confidence intervals shown, T-test p-value shown between indicated conditions. b) A

representative western blot of Nup98 protein levels 48 h post nucleofection with scrambled and Nup98 siRNA treated TREx cells, loading control GAPDH. c) Quantified densitometry of Nup98 band intensity normalised to GAPDH for siRNA treated TREx cells. n=3, 95 % confidence intervals shown, T-test p-value shown between indicated conditions.

4.3   Normal bulk mRNA export is maintained during Nup98 siRNA treatment

With the establishment of a functional Nup98-depletion system in TREx cells, it was important to initially identify whether depletion of Nup98 led to alterations in mRNA export. Fluorescence *in-situ* hybridization (FISH) was used to identify whether the siRNA depletion of Nup98 arrested bulk mRNA export in TREx cells. TREx cells were nucleofected with scrambled or Nup98 siRNA and incubated for 48 h before treatment with doxycycline to induce KSHV lytic replication. 24 h after doxycycline treatment cells were fixed and cells permeabilised and stained with fluorescently labelled oligo(dT) probe to detect polyadenylated (polyA) RNA. These cells were visualised using an LSM 880 confocal microscopy and showed that in unreactivated TREx cells depletion of Nup98 did not lead to significant differences in bulk mRNA localisation (Figure 4.2a). This was further confirmed using pixel profiling of the confocal images which showed that in unreactivated TREx the strongest fluorescent oligo-dT signal was seen outside the nucleus or in specific low DAPI intensity foci within the nucleus (Figure 4.2b). Nup98 depletion did not affect changes in bulk mRNA localisation caused by KSHV lytic replication (Figure 4.2a). In scrambled treated reactivated cells fluorescent oligo-dT overlaps more with areas of DAPI signal, with less signal in the cytoplasm but high intensity foci still apparent in the nucleus (Figure 4.2b). These changes on reactivation are also observed in Nup98-depleted TREx cells with predominant oligo-dT signal overlapping with the DAPI signal along with high intensity foci in the nucleus. Overall, this work suggests that Nup98-depletion does not alter

141

normal bulk mRNA nucleocytoplasmic transport in TREx cells and does not

prevent mRNA retention observed on TREx reactivation.
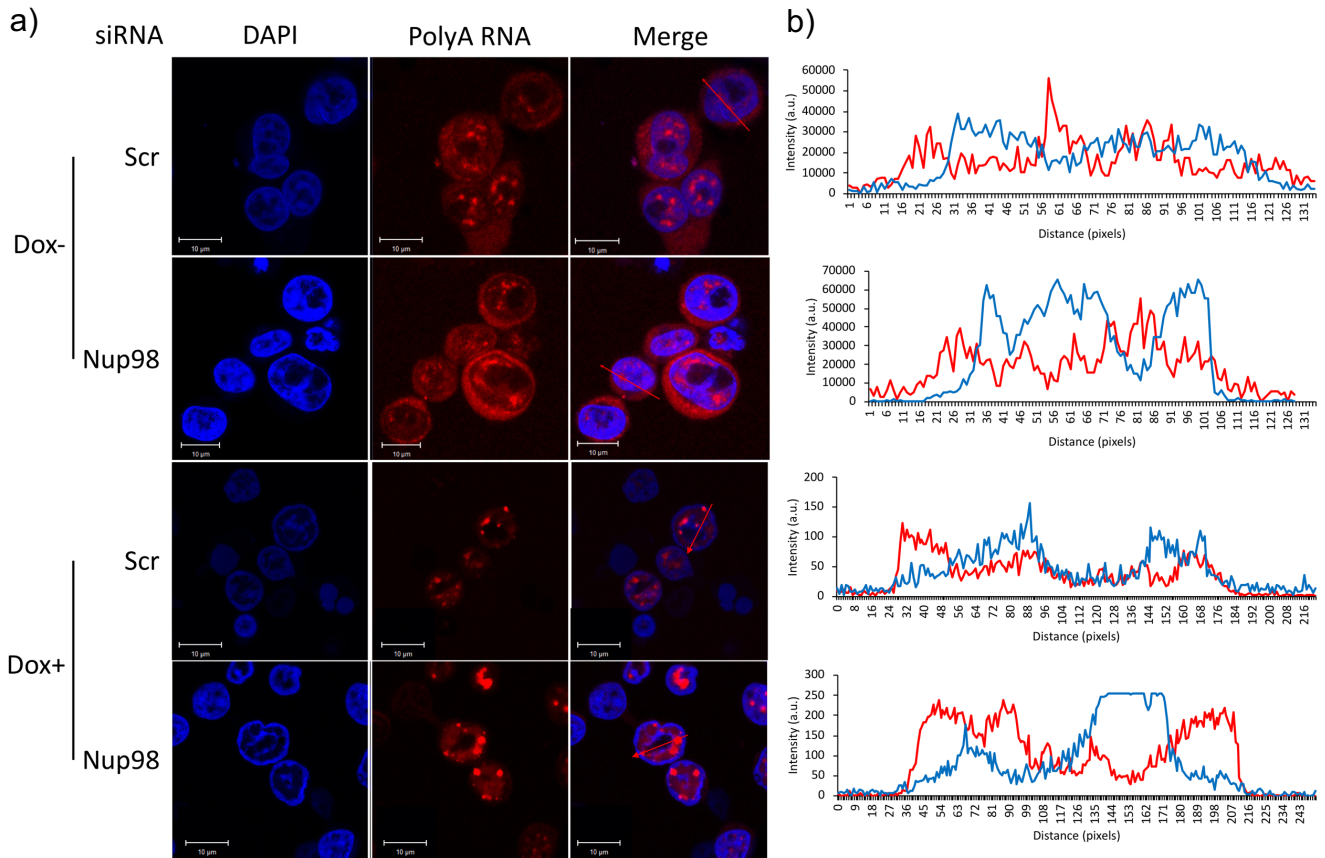
Figure 4.2 SiRNA depletion of Nup98 does not impact bulk mRNA export in unreactivated TREx or prevent the retention of PolyA RNA during KSHV lytic replication. a) Confocal microscope images of FISH analysis between scrambled (scr) and Nup98 siRNA treated cells, 48 h post nucleofection cells were treated with doxycycline to induce KSHV lytic replication. Cells were then fixed 24 h post doxycycline treatment. Cells were permeabilized and stained with fluorescently tagged oligo-dT. b) Confocal pixel profiling of a single cell from each image (shown by red arrow in Merge) showing DAPI intensity (blue) and Poly A signal intensity.

4.4   Nup98-depletion did not impede normal KSHV lytic gene expression

Next, Nup98-depleted TREx cells were reactivated to investigate whether the

depletion of Nup98 would aid the progress of viral lytic replication. qPCR analysis

showed that the depletion of Nup98 did not significantly impact ORF50

expression suggesting that induction via the doxycycline inducible system was not affected (Figure 4.3a). Moreover, analysis of ORF57, an RTA-responsive immediate-early gene, showed that ORF57 transcription was similarly not significantly impacted by Nup98-depletion (Figure 4.3a). Western blot analysis of ORF57 protein levels showed a similar phenotype with ORF57 levels unaffected by Nup98 depletion with no significant difference in ORF57 relative band intensities detected (Figure 4.3b and Figure 4.3). This suggested that the absence of Nup98 did not affect the kinetics of lytic replication progression, nor did it lead to increased levels of spontaneous reactivation in latent cells. These results suggested that depletion of Nup98 did not effect KSHV lytic induction via the doxycycline-mycRTA system and did improve the level of immediate-early gene expression.
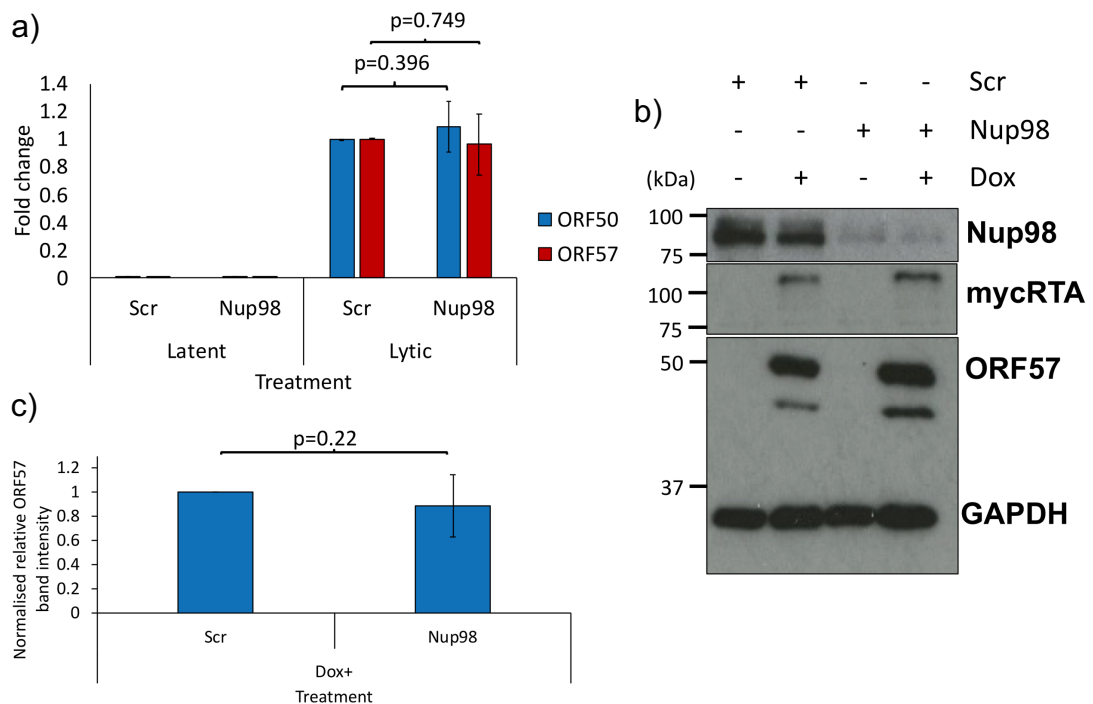
Figure 4.3 SiRNA depletion of Nup98 does not impact the expression of IE KSHV genes during lytic infection in TREx cells. a) qPCR analysis of KSHV immediate-early transcripts ORF50 and ORF57 in TREx cells nucleofected with siRNAs and 48 h treated with doxycycline to induce KSHV lytic replication. RNA

extracted at 24 h post doxycycline treatment. n=3, 95 % confidence intervals shown, T-test p-value shown between indicated conditions. b) A representative western blot analysis ORF57 levels in TREx cells nucleofected with scrambled (scr) and Nup98 siRNAs for 48 h before doxycycline treatment to induce KSHV lytic replication. Lysates taken at 24 h post doxycycline treatment, Nup98 shown to confirm siRNA depletion, mycRTA to confirm doxycycline induction, GAPDH present as loading control. c) Quantified densitometry of ORF57 band intensity normalised to GAPDH at 24 h post doxycycline treatment in TREx cells nucleofected with scr and Nup98 siRNA 48 h prior to doxycycline treatment. n=4, 95 % confidence intervals shown, T-test p-value shown between indicated conditions.

In the previous chapter it was shown that Nup98 decreased early during KSHV lytic infection, but confocal analysis showed no change in localisation or Nup98 levels (Figure 3.4). Therefore, a series of experiments were performed on TREx cells treated with scrambled or Nup98 siRNA and seeded onto poly-l-lysine coverslips. 48 h after nucleofection with siRNAs cells were treated with doxycycline to induce KSHV lytic infection and fixed at either 0 h, 8 h, 24 h post doxycycline treatment. TREx cells were then permabilized, blocked with BSA and stained with anti-RTA and anti-Nup98 before washing and secondary antibody treatment. Cells were then mounted with DAPI and visualised using an LSM 880 confocal microscopy (Ziess). In Nup98-depleted cells, Nup98 levels appear significantly reduced at all time points post doxycycline treatment at both the NPC and the nucleoplasm (Figure 4.4). Nup98-depletion however does not appear to have a negative effect on RTA expression levels with replication compartments occurring in both scrambled and Nup98 siRNA treated cells by 24 h (Figure 4.4). Overall, these results suggest Nup98 depletion with siRNAs achieves a significant reduction in whole-cell Nup98 levels and confirms observations from the previous chapter that Nup98 levels at the NPC do not appear to change within 8 h of the induction of lytic infection with doxycycline.
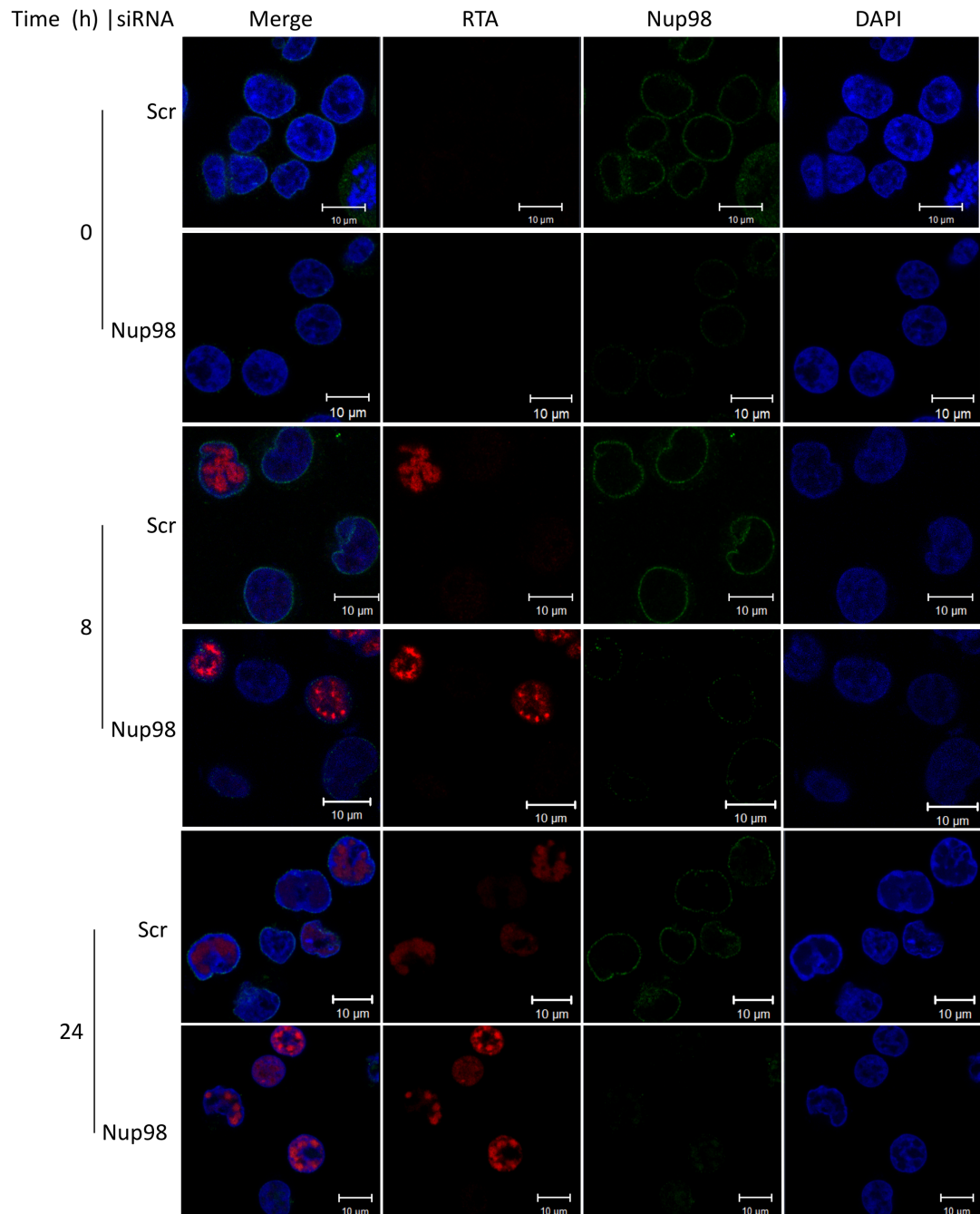
Figure 4.4 Nup98 siRNA treatment significantly decreased Nup98 at the NPC and in the nucleoplasm. TREx cells were nucleofected with either scrambled or Nup98 siRNA and seeded onto poly-l-lysine coverslips, 48 h post nucleofection cells were treated with doxycycline to induce KSHV lytic replication. Cells were then fixed at either 0 h, 8 h or 24 h post doxycycline treatment and stained with anti-RTA and anti-Nup98. Coverslips were mounted with DAPI and visualised using an LSM 880 confocal microscope.

4.5 Nup98-depletion reduced viral infectivity but did not impact KSHV DNA replication

To examine whether Nup98 depletion affected late stages of viral lytic replication, viral DNA load and infectious virion production were assessed. In order to test viral load TREx cells were nucleofected with either scrambled or Nup98 siRNA and incubated for 48 h before cells were treated with doxycycline to induce KSHV lytic replication. Cells were incubated for 72 h after doxycycline treatment before DNA was extracted. qPCR was then performed to determine viral DNA load which showed that the depletion of Nup98 actually increased viral DNA load levels but not significantly when compared to scrambled cells (Figure 4.5a). To determine the effect of Nup98-depletion on viral infectivity, TREx cells were treated as described above and 72 h post doxycycline treatment supernatant was collected from TREx cells and added at a 1:1 ratio with DMEM and incubated for 24 h with naïve 293T cells. RNA was then extracted from these 293T cells and qPCR performed to determine levels of ORF57. A significant reduction in ORF57 levels was observed in 293T cells treated with supernatant from Nup98-depleted TREx cells (Figure 4.5b). Furthermore, western blot analysis of viral capsid protein ORF65 showed an increase within Nup98-depleted cells at 72 h post doxycycline treatment to induce KSHV lytic replication (Figure 4.5c). Due to difficulties consistently detecting ORF65 by western blot this experiment was only performed once. Overall, depletion of Nup98 did not appear to impact viral DNA production, which corroborates the findings in Figure 4.3 that showed no impact on the induction of lytic replication or IE gene expression. However, Nup98-depletion did significantly reduce the rate of infectivity of virions produced from Nup98-depleted cells. This finding, along with the suggestive observation of

146

increased levels of the viral capsid protein ORF65 in Nup98-depleted TREx cells,

led to the hypothesis that Nup98-depletion negatively impacted virion egress at

an unspecified stage.

a)

b)

c)
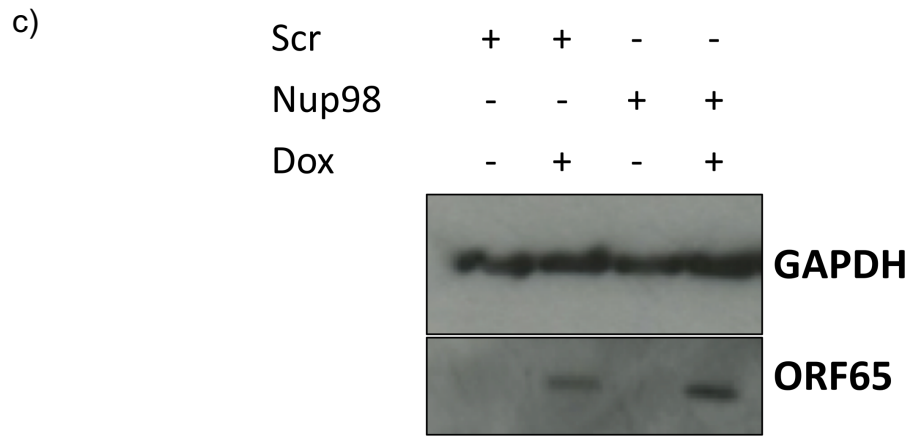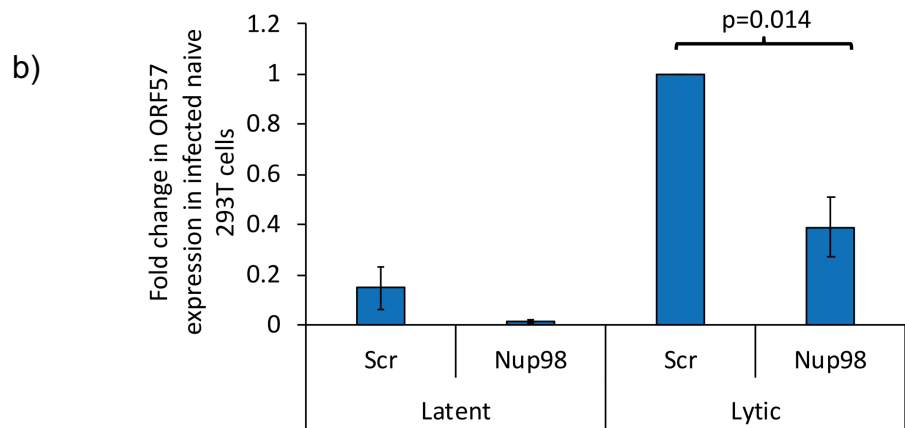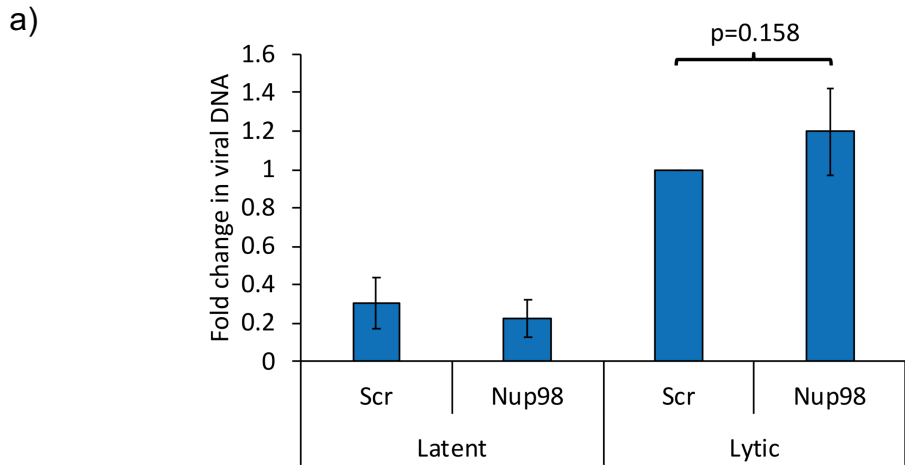
Figure 4.5 SiRNA depletion of Nup98 does not impact KSHV genome replication but reduces viral reinfectivity and leads to an accumulation of viral late protein ORF65. a) qPCR analysis of viral DNA levels in scrambled (scr) and Nup98 siRNA treated TREx cells reactivated for 72 h. n=3, 95 % confidence intervals shown, T-test p-value shown between indicated conditions. b) Viral progeny levels measured as ORF57 expression in infected naïve 293T cells 24 h post addition of supernatant from scrambled (scr) and Nup98 siRNA treated TREx cells 72 h post induction of lytic replication. n=3, 95 % confidence intervals shown, T-test p-value shown between indicated conditions. c) Western blot analysis of ORF65 protein levels in siRNA treated TREx reactivated for 72 h. GAPDH shown as a loading control. n=1.

4.6 Nup98-depletion led to an accumulation of viral capsids at the plasma membrane suggesting impaired virion egress

To determine how Nup98-depletion led to reduced KSHV infectivity confocal immunofluorescence was performed on TREx cells treated with either scrambled or Nup98 siRNA. These experiments looked to confirm the observation by western blot that levels of viral capsid protein ORF65 were increased at 72 h in Nup98-depleted TREx cells. TREx cells were nucleofected with either scrambled or Nup98 siRNAs and after 48 h treated with doxycycline to induce KSHV lytic replication. 72 h post doxycycline treatment cells were fixed, permeabilized and stained with antibodies against the viral capsid protein ORF65. Nup98 depletion was confirmed prior to this experiment via western blotting at 48 h post nucleofection. In Nup98-depleted cells an accumulation of ORF65 was observed at the plasma membrane forming a halo like phenotype when compared to comparable cells treated with the scrambled siRNA (Figure 4.6a). Inspection of Nup98-depleted cells at a higher zoom clearly shows a build-up of ORF65 at a periphery outside the DAPI stain rather than a more dispersed appearance outside the DAPI stain in scrambled treated TREx cells (Figure 4.6c). This suggested that Nup98 depletion was affecting virion egress at the plasma membrane. Utilising the tile scan functionality of the confocal microscope multiple 1.5 mm^2 tiles of images were taken and the observed phenotype was quantified

148

and calculated as a percentage of total ORF65 positive cells (Figure 4.6c). This analysis showed a significant increase in the occurrence of the halo phenotype in Nup98-depleted cells compared to scrambled siRNA treated cells. This supported the hypothesis that Nup98-depletion impaired virion egress, presumably via a mechanism affecting the final step of egress at the plasma membrane.

a)

	DAPI	ORF65	Merge

Scr

1

2

3

Nup98

1

2

3

150
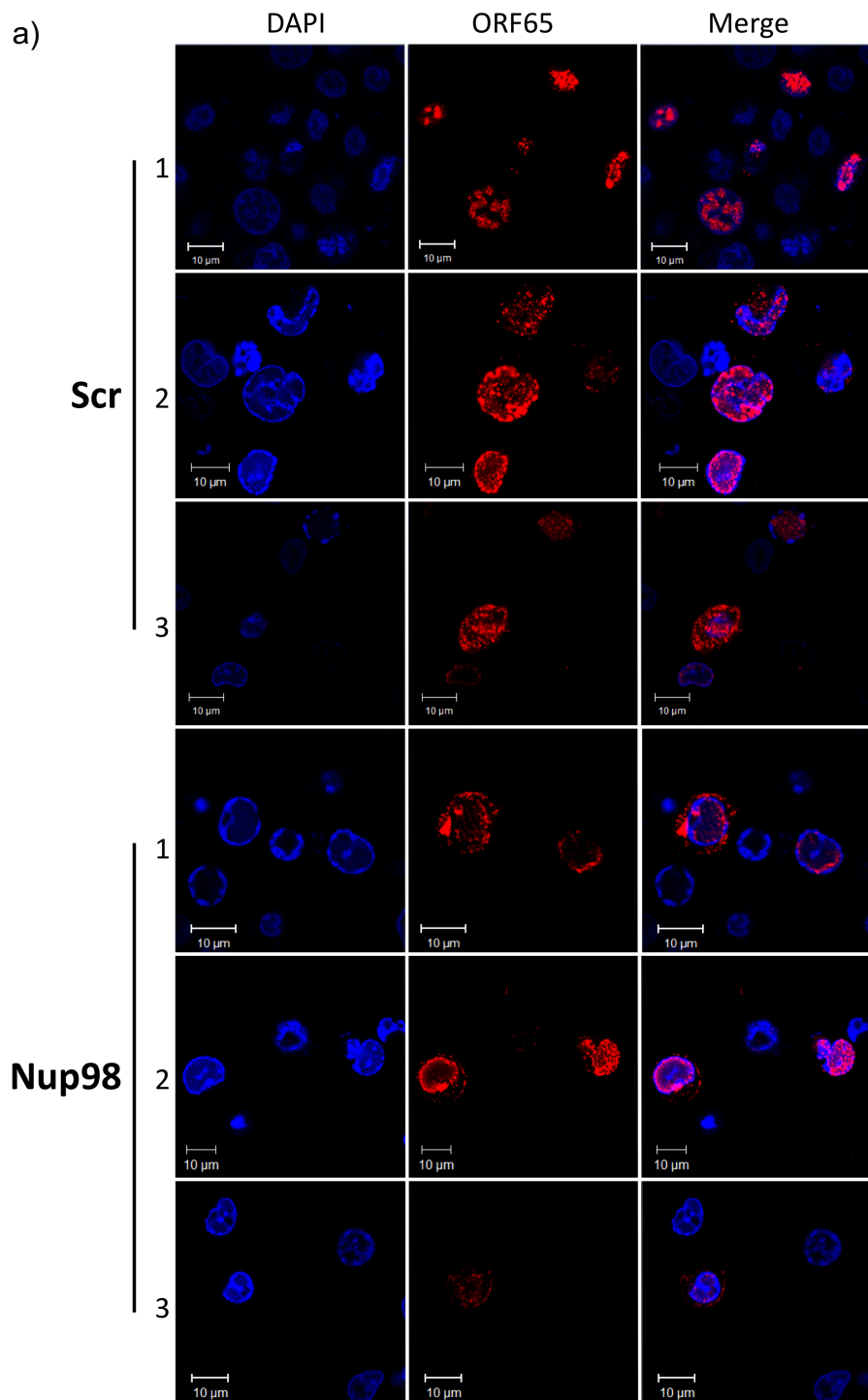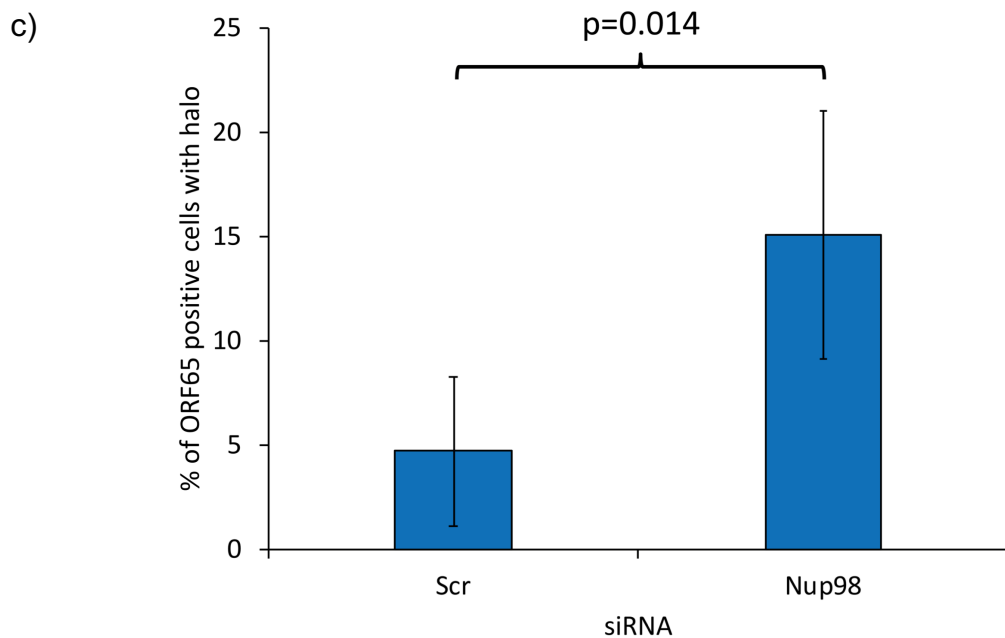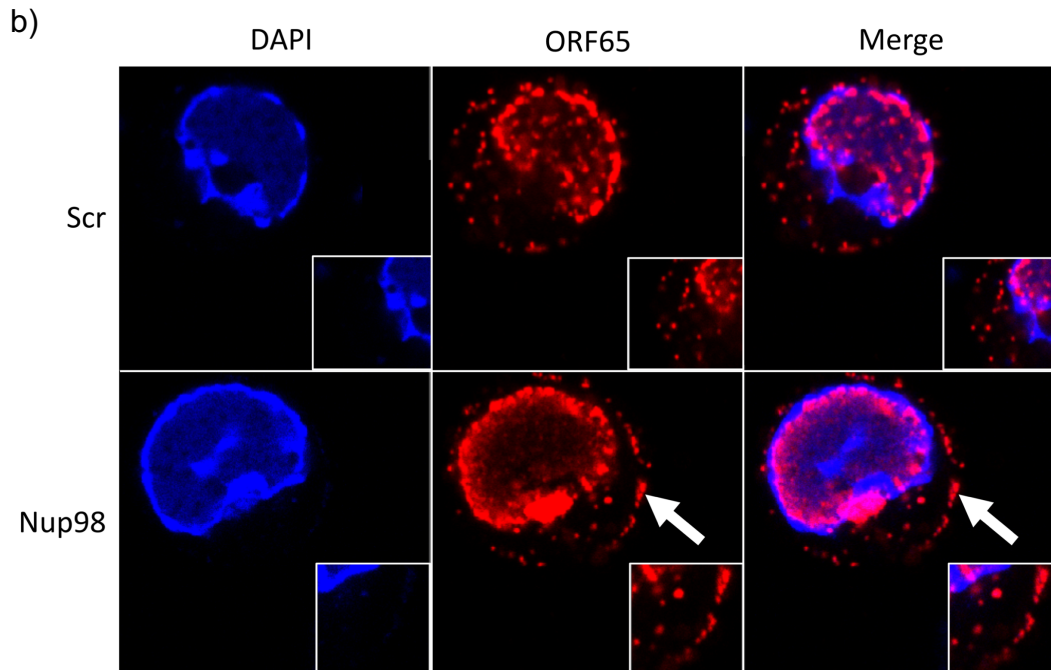
Figure 4.6 Depletion of Nup98 leads to ORF65 accumulation at the cell membrane in a halo pattern when visualised by confocal immunofluorescence microscopy. a) A panel of multiple confocal immunofluorescence microscopy images of siRNA treated TREx cells reactivated for 72 h (Scr or Nup98 siRNA), stained with DAPI and viral capsid protein ORF65. b) A single cell comparison of ORF65 localisation in siRNA treated TREx cells reactivated for 72 h (Scr or Nup98). 5x zoom window inset, white arrow indicates 'halo' phenotype. c) Quantification of halo phenotype (ORF65 stain as a semi-continuous ring outside the DAPI stain) in both Scr and Nup98 siRNA treated cells reactivated for 72 h. n=5, 95 % confidence intervals shown, 95 % confidence intervals shown, T-test p-value shown between indicated conditions.

4.7 Nup98-depletion led to maintained expression of KSHV-targeted cellular protein CHMP7

Previous results raised the interesting question of how a nucleoporin could inhibit virion egress from the plasma membrane. It was hypothesised this effect may be related to the role of Nup98 at the nuclear pore in mRNA export and how KSHV subverts nucleocytoplasmic transport during lytic replication. A recent study had highlighted how the KSHV ORF10 protein interacts with Nup98-binding partner Rae1 to scan the 3'UTRs of a subset of cellular mRNAs preventing them from being exported during KSHV lytic infection (Gong et al., 2016). Crucially, this study showed that mutating ORF10 led to a decrease in viral titre but did not impact viral DNA load, a similar phenotype to the one observed in the Nup98-depletion experiments described previously. Therefore, it was hypothesised that Nup98-depletion disrupted the action of ORF10 during lytic replication and allowing previously retained mRNAs to be transported and translated.

The previous study identified 686 genes that showed a significant 50 % increase in nuclear/cytoplasmic ratio which included CHMP7, a member of the endosomal sorting complexes required for transport (ESCRT) complex (Gong et al., 2016, Table S3). When corroborating this data with an existing whole cell SILAC data set (Schuman et al., unpublished data) components of the ESCRT-III complex including CHMP7 were substantially downregulated by 24 h after the induction of KSHV lytic infection (Figure 4.7a). The downregulation of CHMP7 was subsequently confirmed with western blot analysis and densitometry showing that CHMP7 protein levels significantly decreased (~80 %) between 8 h and 24 h post induction of lytic replication (Figure 4.7b and Figure 4.7c). Overall, this work

characterised the observation from previously published work that KSHV targets CHMP7 and the ESCRT-III complex during lytic infection.
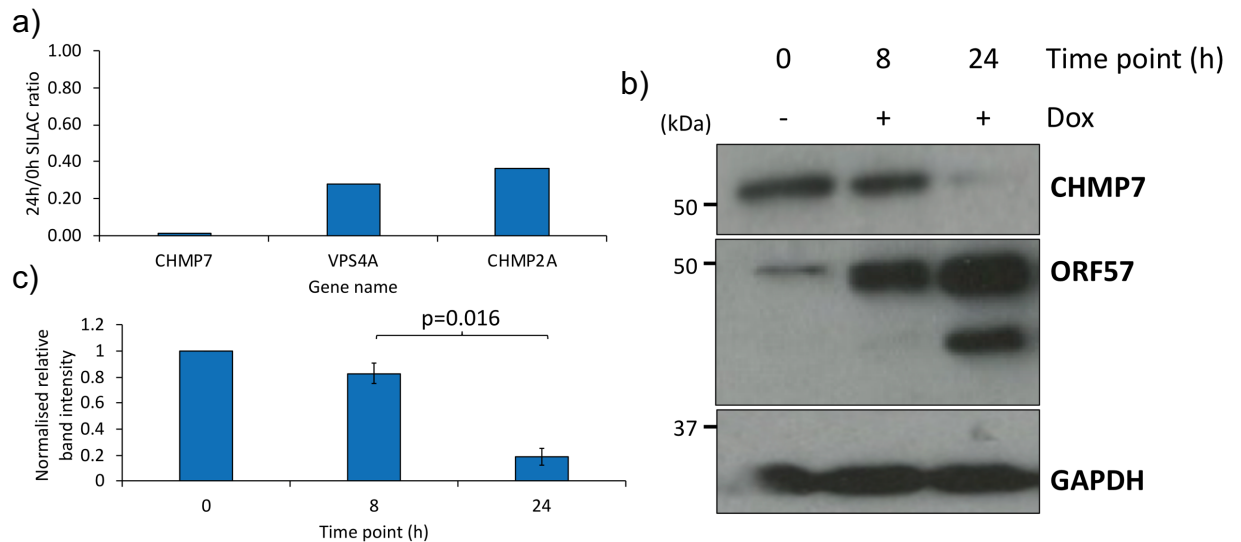
Figure 4.7 CHMP7 is specifically downregulated during KSHV lytic infection in TREx cells. a) SILAC ratios of protein levels at 24h/0h for three ESCRT-III complex proteins. Data from a whole-cell SILAC screen performed on TREx cells reactivated at 0 h, 8 h, 24 h with doxycycline (Schuman et al., unpublished data). n=1. b) A representative western blot of CHMP7 levels in TREx cells treated with doxycycline to induce KSHV lytic replication at 0 h, 8 h, 24 h post doxycycline treatment. c) Quantified densitometry of CHMP7 band intensity normalised to GAPDH at either 0 h, 8 h, 24 h post doxycycline treatment in TREx cells nucleofected with scrambled (scr) and Nup98 siRNA 48 h prior to doxycycline treatment. n=3, 95 % confidence intervals shown, T-test p-value shown between indicated conditions.

To further test the hypothesis that Nup98-depletion disrupted KSHV induced CHMP7 mRNA retention subcellular fractionation was performed on scrambled and Nup98 siRNA treated TREx cells. RNA was isolated from the whole cell and cytoplasmic fractions and CHMP7 mRNA levels compared between latent and lytically replicating cells (Figure 4.8a). Results demonstrated that whole cell CHMP7 mRNA levels decreased 24 h after the induction of KSHV lytic replication by doxycycline (~50 %) and in scrambled treated cells the cytoplasmic fraction of CHMP7 mRNA significantly decreased (Figure 4.8a). However, in Nup98-

153

depleted TREx cells the proportion of CHMP7 mRNA in the cytoplasm was not significantly different to CHMP7 levels in unreactivated Nup98-depleted TREx cells (Figure 4.8a). Furthermore, western blot analysis of CHMP7 protein levels showed that in scrambled siRNA treated cells, CHMP7 protein levels decreased at 24 h post induction of KSHV lytic replication, in contrast a smaller scale reduction was observed in Nup98-depleted cells (Figure 4.8b). These observations were confirmed by densitometry analysis of western blots which showed a significant difference in CHMP7 normalised relative band intensity between reactivated and unreactivated scrambled treated cells but no significant change between Nup98 siRNA treated cells (Figure 4.8c). It is important to note that a complete rescue of CHMP7 levels should not be expected even if Nup98-depletion prevents nuclear sequestration of CHMP7 mRNA. This is because during KSHV lytic infection the virus initiates host cell shut off through the action of the ORF37 protein which accelerates global mRNA turnover (Glaunsinger and Ganem, 2004). Overall, these results further confirm the observations that CHMP7 mRNA is sequestered in the nucleus during KSHV lytic infection and show that this sequestration is dependent on the presence of Nup98. Furthermore, the depletion of Nup98 from the NPC prevents CHMP7 mRNA sequestration in the nucleus leading to maintained CHMP7 protein levels during KSHV lytic infection.
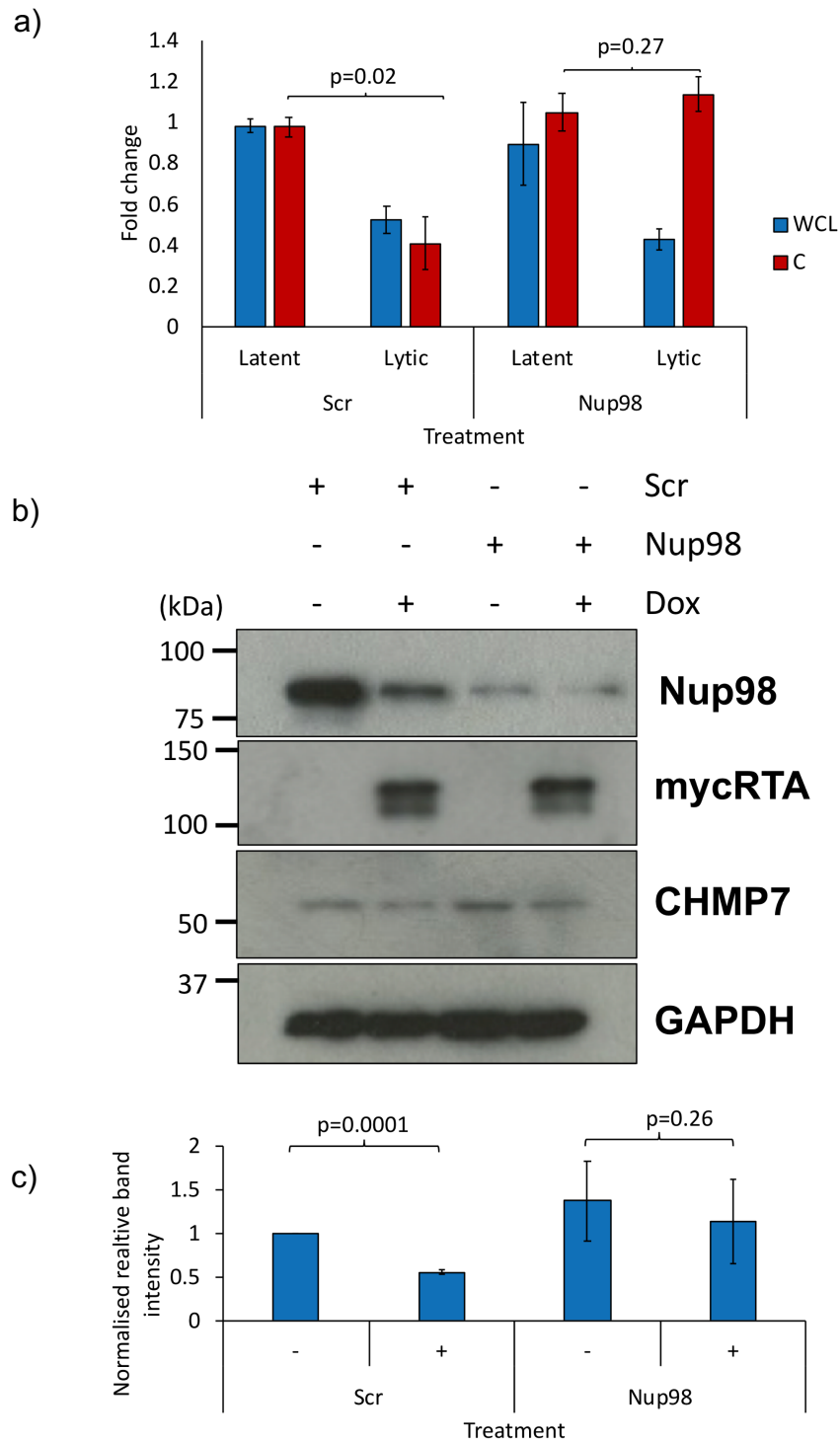
Figure 4.8 Cytoplasmic CHMP7 mRNA reduction during KSHV lytic infection is ablated by Nup98-depletion. a) qPCR analysis of CHMP7 mRNA levels in whole-cell (WCL) and cytoplasmic (C) compartments in scrambled (scr) or Nup98 siRNA treated cells in either a latent (0 h) or lytic state (24 h post doxycycline treatment). n=3, 95 % confidence intervals shown, T-test p-value shown between indicated conditions. b) A representative western blot analysis of CHMP7 levels in either scrambled (scr) or Nup98 siRNA treated cells and treated with doxycycline to induce KSHV lytic replication. Nup98 shown to confirm knock down, mycRTA to confirm induction via doxycycline, GAPDH present as a loading control c) Quantified densitometry of CHMP7 band intensity normalised to GAPDH for scrambled (scr) or Nup98 siRNA treated

4.8 Overexpression of ESCRT-III components has no impact on KSHV lytic gene expression or replication compartment formation

Having established that upon Nup98-depletion KSHV-mediated targeting of CHMP7 was disrupted, work began to confirm that CHMP7 had a protective role within the cell by preventing virion egress. To test this a number of ESCRT-III complex protein overexpression transfer vectors were transduced into TREx cells using a second-generation Lentiviral system. These included CHMP7, IST1 and VPS4A in order determine whether the observation was specifically related to the role of CHMP7 or the ESCRT-III complex more broadly (Horii et al., 2006; Guizetti, Schermelleh, Mäntler, et al., 2011; Mierzwa et al., 2017). All overexpressed proteins were V5-tagged allowing for simple detection via western blot and confocal microscopy, an empty Lentiviral transfer vector was used as a transduction control (referred to as mock). Transduced cells were selected with puromycin alongside untransduced control TREx cells for 12 days to ensure all untransduced cells died before transduced cells were transferred to larger flasks for expansion.

Initially, it was important to establish the transduction efficiency of the ESCRT-III overexpression proteins. Therefore, confocal microscopy was performed to determine the percentage transduction efficiency 28 days post transduction. Multiple tile scans were performed and quantified using ImageJ to determine the percentage of V5 positive cells. These experiments showed a low level of V5 expression within transduced cells (20 %) suggesting that there was either loss of the expression cassette or poor transduction efficiency (Figure 4.9).
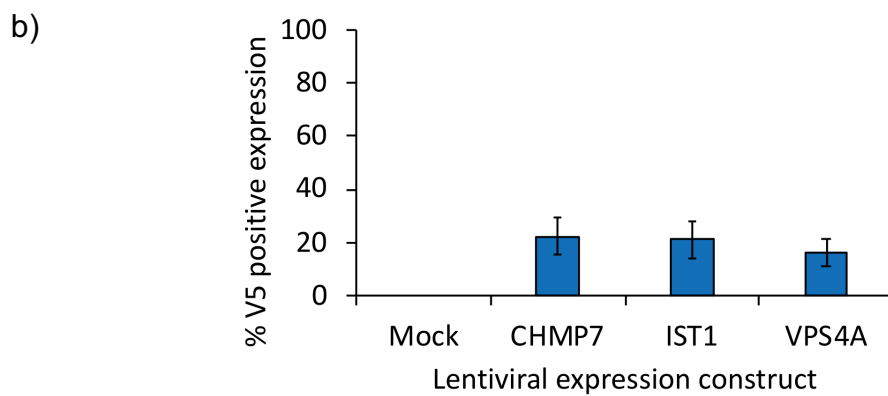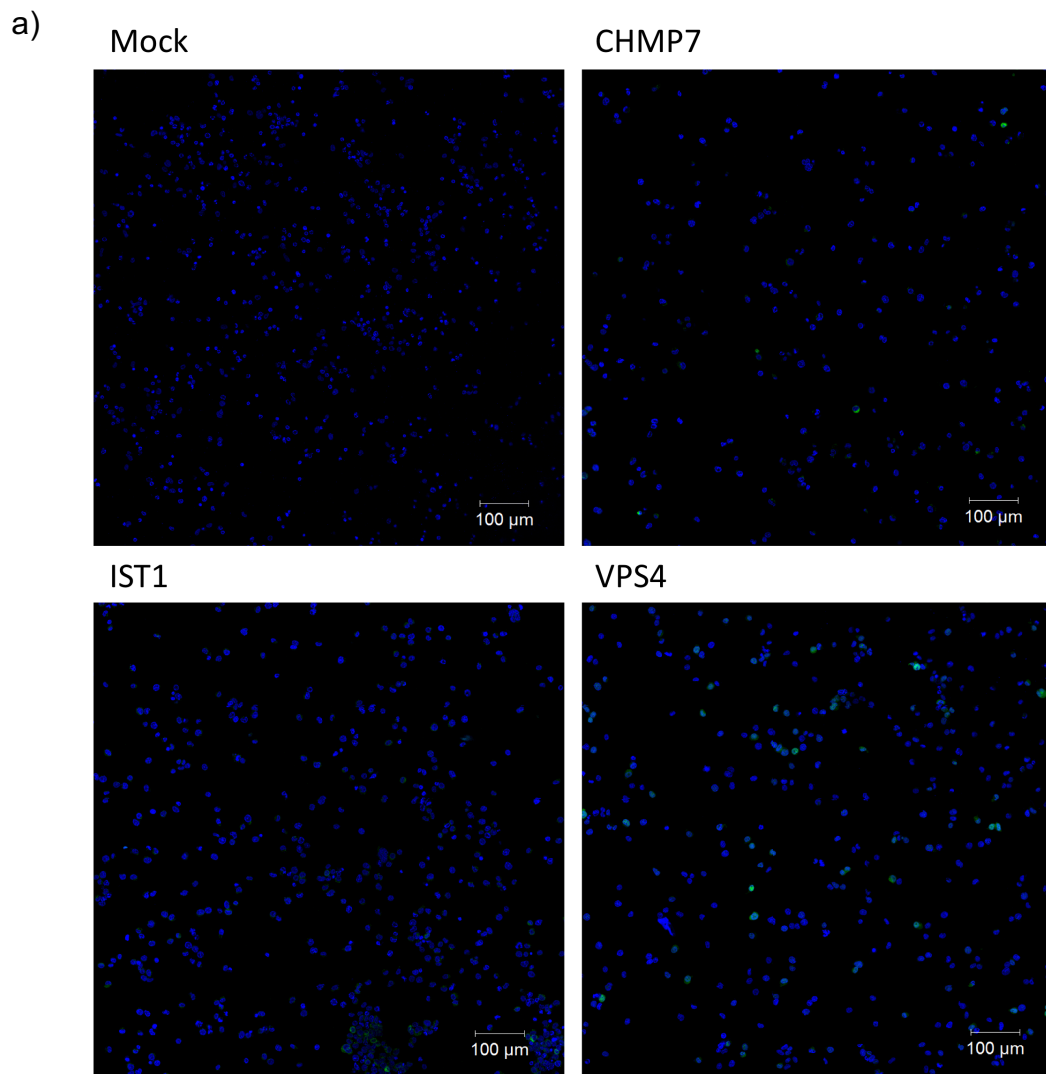
Figure 4.9 Lentiviral transduction of ESCRT-III components in TREx cells produced a low transduction level. a) Representative confocal tile scans of TREx cells transduced with Lentiviral overexpression constructs including an empty puromycin vector (Mock), CHMP7, IST1, VPS4 transfer vectors. b) Quantification of confocal tile scans showing the percentage transduction efficiency (number of V5 positive cells divided by total cells per image). n=3, 95 % confidence intervals shown.

Due to time constraints the decision was taken to pursue experiments with these transduced cells. Furthermore, given the complexity of the ESCRT-III complex it was decided to conduct subsequent experiments comparing IST1 and CHMP7 overexpression alongside a mock transduced control. IST1 was chosen because of similarities in its role recruiting the ESCRT-III complex during multivesicular body trafficking and CHMP7 role recruiting ESCRT-III at the endoplasmic reticulum (Olmos et al., 2016; Frankel et al., 2017). Whilst VPS4A, an AAA-ATPase, is involved in the disassembly of the ESCRT-III complex (Merrill and Hanson, 2010; Takahashi et al., 2018). Having determined there was a level of expression of proteins of it was now important to determine that the doxycycline-inducible system of initiating KSHV lytic replication was not disrupted by the Lentiviral transduction. Transduced TREx cells were treated with doxycycline to induce KSHV lytic replication and protein extracted at 24 h post treatment. Western blot analysis was performed on cell lysates and probes for levels of the V5 tagged ESCRT-III complex proteins, mycRTA and ORF57 (Figure 4.10a). Probing with anti-V5 antibody yielded bands at the expected approximate sizes of IST1 at 39 kDa and CHMP7 at 51 kDa. It also confirmed the low level of expression of both of these proteins with no IST1 detectable in unreactivated cells although it was detectable in reactivated cells. CHMP7 was detectable in both unreactivated and reactivated cells but at a low intensity (Figure 4.10b). Crucially, there was no observable impact on the induction of KSHV lytic replication in these transduced cells in the western blot with ORF57 expression following on from mycRTA expression. However, differences in ESCRT-III overexpressing cells could be masked by the low expression rate therefore confocal microscopy was also performed to ensure that overexpression did not prevent the formation of

158

KSHV replication compartments in the nucleus, a critical step in successful KSHV lytic replication (Figure 4.10b). Both CHMP7 and IST1 staining occurred in the cytoplasm as expected along with the correct formation of viral replication compartments confirmed via RTA staining within discrete nuclear foci at 24 h post induction of KSHV lytic replication (Figure 4.10b). These results confirmed that in transduced cells that successfully expressed ESCRT-III complex proteins the induction and progression of KSHV lytic replication was not disrupted.
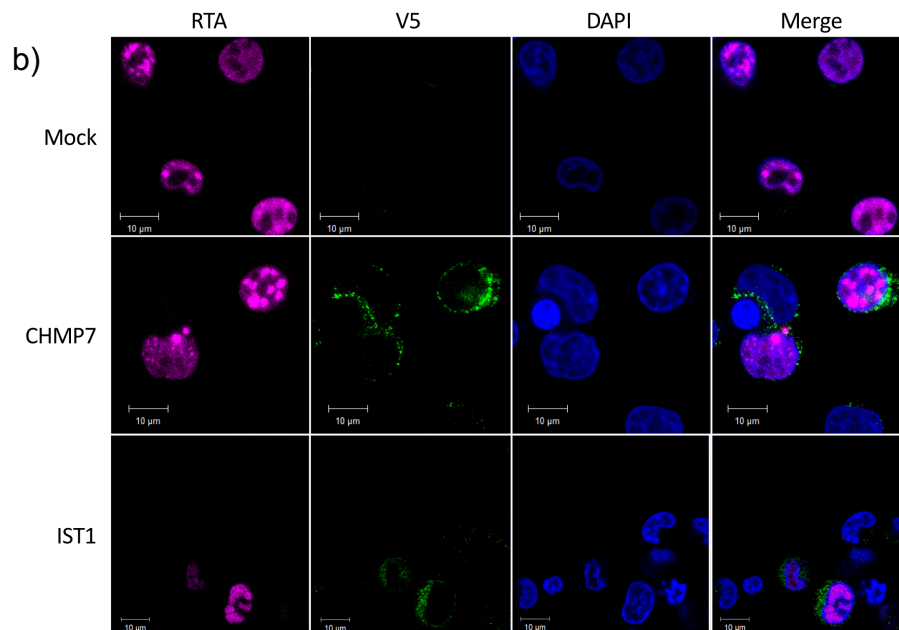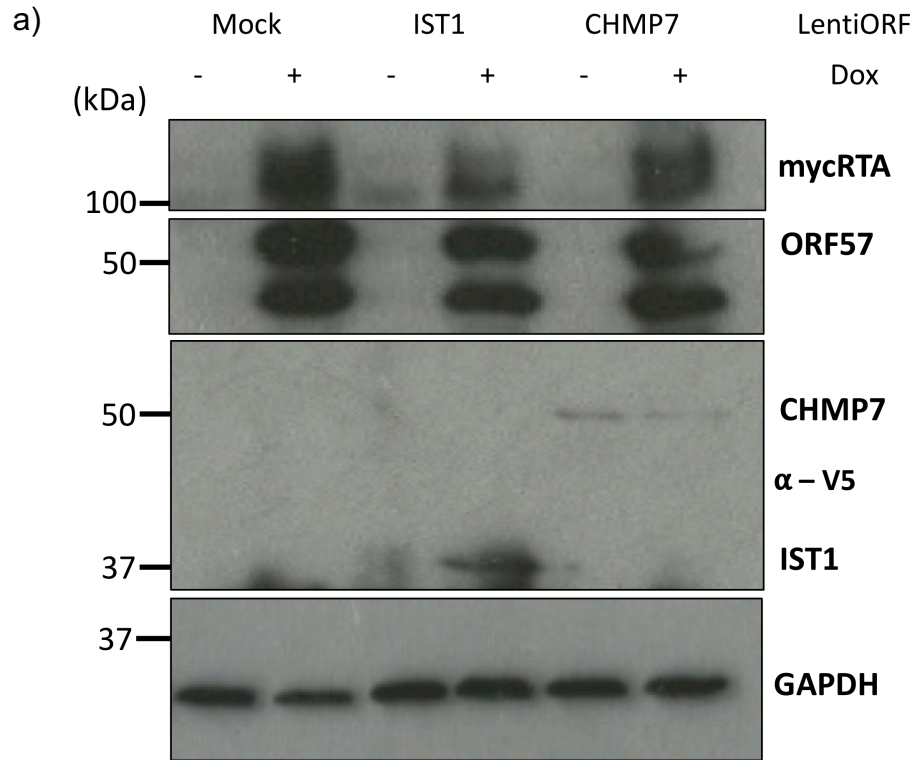
Figure 4.10 Overexpressing CHMP7 and IST1 of the ESCRT-III complex in TREx does not affect the induction of KSHV lytic replication and the formation of replication compartments. a) Western blot analysis of overexpressed ESCRT-III components with V5 tag alongside mycRTA and ORF57 to show induction of KSHV lytic infection at different time points post doxycycline treatment. b) Confocal immunofluorescence of KSHV replication compartments in stably expressing CHMP7 or IST1 or mock transduced cells 24 h post the induction of KSHV lytic replication.

4.9 Overexpression of CHMP7 leads to a decrease in infectious virion release

After demonstrating that the overexpression of ESCRT-III components did not impact on KSHV lytic replication in TREx cells attempts were made to test whether the overexpression of CHMP7 reduced viral infectivity. This was derived from the observation that CHMP7 levels were maintained in Nup98-depleted cells where reduced viral infectivity was also observed. Mock transduced, CHMP7 and IST1 overexpressing cells were reactivated for 72 h and DNA was extracted before quantification of viral DNA levels by qPCR. qPCR showed increases in viral DNA in both ESCRT-III overexpressing cell lines compared to mock transduced cells however neither of these increases can be considered significant (Figure 4.11a). The release of infectious virions from these cell lines was also tested, with cells treated with doxycycline to induce KSHV lytic replication and incubated for 72 h before supernatant taken and mixed 1:1 with DMEM and incubated for 24 h on naïve 293T cells. 293T cells were then lysed and RNA extracted to determine KSHV ORF57 mRNA levels. Interestingly, there was a significant ~65 % decrease in the production of ORF57 mRNA in naïve 293T cells treated with supernatant from CHMP7 overexpressing cells compared to mock transduced cells, implying that either fewer infectious virions had been released or virions released were less able to infect 293T cells (Figure 4.11b). Furthermore, this decrease in infectious virion production appeared specific to CHMP7 and was not observed in IST1-overexpressing cells (Figure 4.11b). Overall, these data suggest that increased levels of CHMP7 during KSHV lytic replication impair virion infectivity. Whether this related to release of virion or the production of defective virions was unclear. Interestingly, this observation

161

mirrored the observation made in Nup98-depleted cells suggesting CHMP7 was the factor responsible in Nup98-depleted cells for reduced viral infectivity.
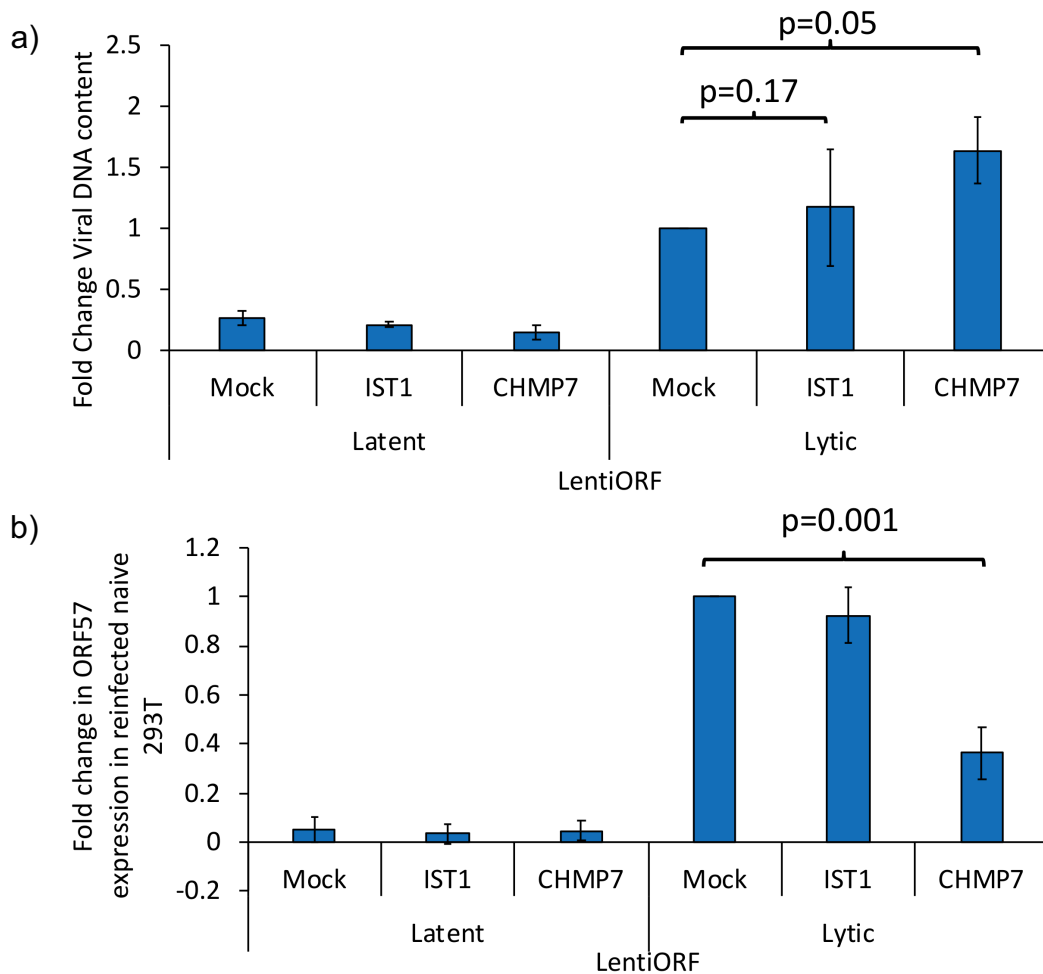
Figure 4.11 Overexpressing CHMP7 reduces the production of infectious virions of KSHV but does not decrease viral DNA production. a) Relative levels of viral DNA in mock transduced, IST1, CHMP7 overexpressing cells compared in latent cells and cells 72 h post the induction of lytic replication. n=3, 95 % confidence intervals shown, T-test p-value shown between indicated conditions. b) Levels of ORF57 expression in naïve 293T cells reinfected with the supernatant of mock transduced, IST1, CHMP7 overexpressing cells that were either latent or had been induced to lytic replication for 72 h. n=3, 95 % confidence intervals shown, T-test p-value shown between indicated conditions.

As previously mentioned, confocal microscopy of Nup98-depleted cells showed the ORF65 capsid protein formed a halo outside of the DAPI stain at the plasma membrane. Identical confocal immunofluorescence experiments were performed

on CHMP7- and IST1-overexpressing cells and the ORF65 halo phenotype was observed in TREx cells that had been transduced with the CHMP7-overexpression construct (Figure 4.12a). Crucially, these experiments were lacking confirmation that the cells visualised are overexpressing CHMP7-V5 due to cross-species reactivity problems with the ORF65 antibody and the anti-V5 tag antibody. Attempts were made to visualise V5 with antibodies from different animal species however none were able to successfully. In order to determine whether the ORF65 halo phenotype was more frequent in cells transduced with the CHMP7 overexpression construct tile scans were performed on multiple coverslips to produce a series of 1.5 mm^2 images that were analysed to quantify the proportion of ORF65 halo cells, as a proportion of all ORF65 positive cells. This quantification showed a significantly greater proportion of ORF65 positive cells had the halo phenotype in cells transduced with the CHMP7-overexpression construct when compared to mock transduced cells (Figure 4.12b). Whilst it was disappointing that overexpression of ESCRT-III components could not be confirmed in ORF65 positive cells the global analyses of tile scans suggested that the transduction of CHMP7 specifically lead to increased ORF65 halos even though overexpression was occurred in a minority of cells.

a)

164
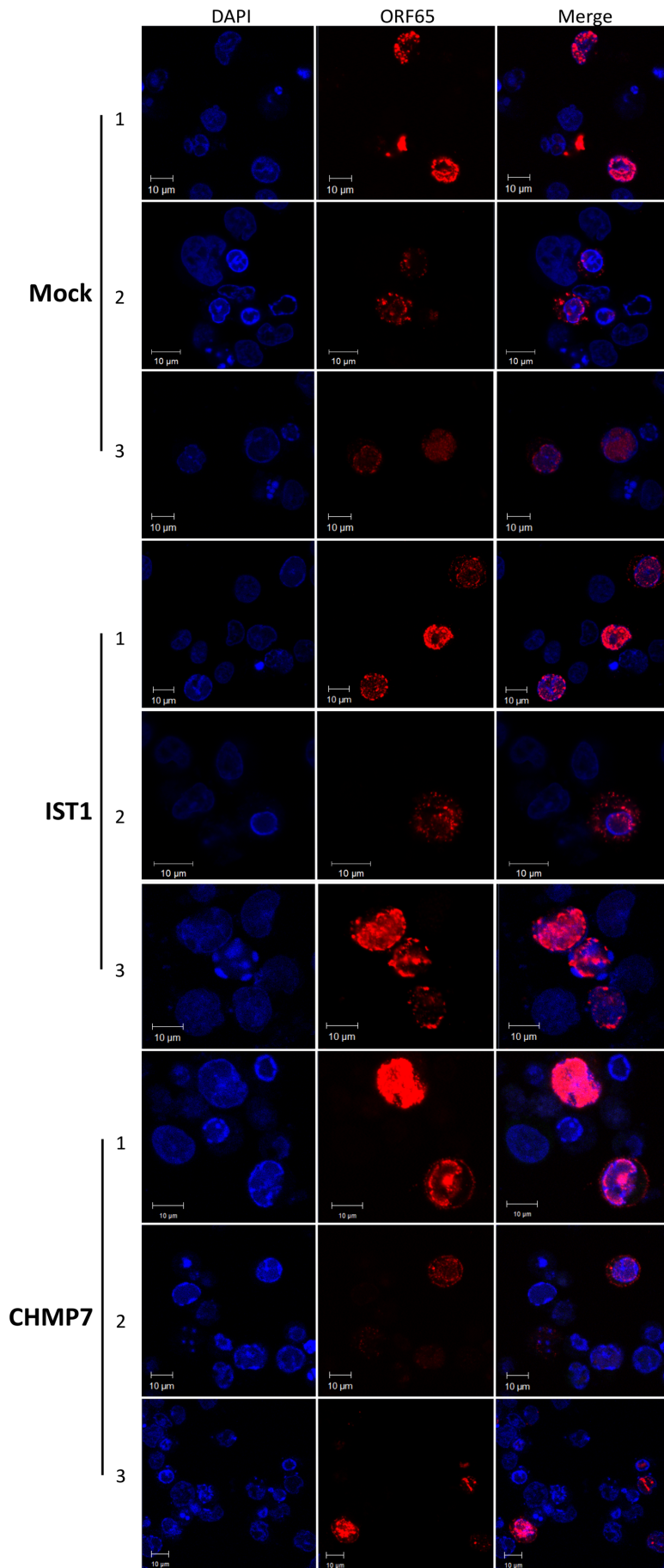
b)
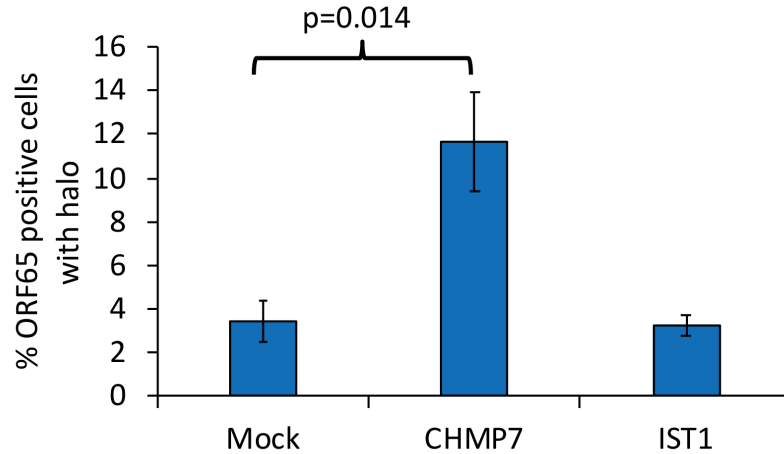
Figure 4.12 Overexpression of CHMP7 leads to an increase in the halo phenotype of ORF65 at the cell membrane during KSHV lytic infection. a) A panel of multiple confocal immunofluorescence images of ORF65 in 72 h reactivated TREx cells either mock transduced, or overexpressing CHMP7 or IST1. V5 is missing due to cross species reactivity between the anti-ORF65 and anti-V5 antibodies b) The percentage of ORF65 halo phenotypes observed as a percentage of total ORF65 positive cells from 3 x 1.5 mm^2 tile scans for reactivated (72 h) mock transduced cells, or overexpressing IST1 or CHMP7. n=5, 95 % confidence intervals shown, T-test p-value shown between indicated conditions.

4.10   Overexpression of CHMP7 led to increased membrane bubbling and maintenance of membrane integrity

Having tentatively demonstrated that the overexpression of CHMP7 led to reduced virion infectivity and a potential reduction in viral egress at the plasma membrane the next step was to test a mechanism by which CHMP7 prevented viral egress. This was crucial in understanding how Nup98-depletion also led to reduced virion infectivity and would highlight, the importance of Nup98 at the NPC during KSHV lytic replication. Given the variety of functions of the ESCRT-III complex within the cell initial attempts to characterise the action of CHMP7 in preventing viral egress focused on the action of ESCRT-III at the plasma membrane given the phenotype of the ORF65 halo. CHMP7 and other ESCRT-III factors have been shown to regulate plasma membrane integrity during necroptosis, a regulated form of cell death. During necroptosis, ESCRT-III

165

components bind at sites of damage to the plasma membrane and excise damaged sections as membrane bubbles (Gong et al., 2017). Therefore, it was hypothesised CHMP7 was targeted by KSHV during the lytic infection to prevent this membrane repair pathway which disrupted viral egress. To test whether cells transduced with a CHMP7 overexpression construct had a greater degree of membrane bubbling at late stages of KSHV lytic replication the perimeter/area ratio of TREx cells transduced with CHMP7, IST1 overexpression constructs or mock transduced was measured. This followed the assumption that cells able to produce membrane bubbles would have a greater perimeter/area ratio given the additional cell membrane perimeter produced by the bubble. In order to quantify the plasma membrane, cells were stained with phalloidin conjugated to rhodamine, which stained F-actin at the cell membrane. In order to stain just the plasma membrane cells were unpermeabilized during this experiment meaning it was not possible to co-stain for V5 to determine which cells were overexpressing ESCRT-III components. Confocal microscopy was then performed to produce tile scans of coverslips for perimeter analysis by ImageJ. Normally, it was observed that phalloidin stained the plasma membrane sufficiently well in all cell lines at 72 h post doxycycline treatment to induce KSHV lytic replication (Figure 4.13a). Subjectively, it was apparent that in cells transduced with CHMP7 overexpression construct there was a greater proportion of cells with small bubbles contiguous with or proximal to the normal cell membrane when compared to mock transduced or cells transduced with IST1 overexpression construct (Figure 4.13b). However, given the inability to visualise whether these cells were overexpressing ESCRT-III components it is impossible to draw strong conclusions from this cell-to-cell analysis. Therefore, to determine whether this

trend was observable across a wider sample of cells confocal tile scans were performed to quantify the perimeter/area ratio of hundreds of cells from each condition. This data was analysed through ImageJ and plotted as a box and whisker plot (Figure 4.13c). Overall the variety of cell shapes and sizes are broadly similar between all three cell lines as seen by the similarity in distribution of the interquartile ranges (Figure 4.13c). However, in cells transduced with the CHMP7 overexpression construct the median perimeter/area ratio is significantly increased when compared to mock transduced and IST1-overexpressing cells. This suggests that whilst overexpressing ESCRT-III components does not change the distribution of cell sizes (as seen with the similarity in interquartile ranges) it does lead to an increase in the typical cell perimeter/area ratio in CHMP7-overexpressing cells. Whilst it was not possible to show CHMP7 overexpression in cells with membrane bubbling these data do suggest there was a positive effect on global cell perimeter/area values within cells that were transduced with a CHMP7 overexpression construct.

a)

DAPI Phalloidin Merge

Mock

IST1

CHMP7

b)

Mock IST1 CHMP7

c)

p=0.04

p=0.26
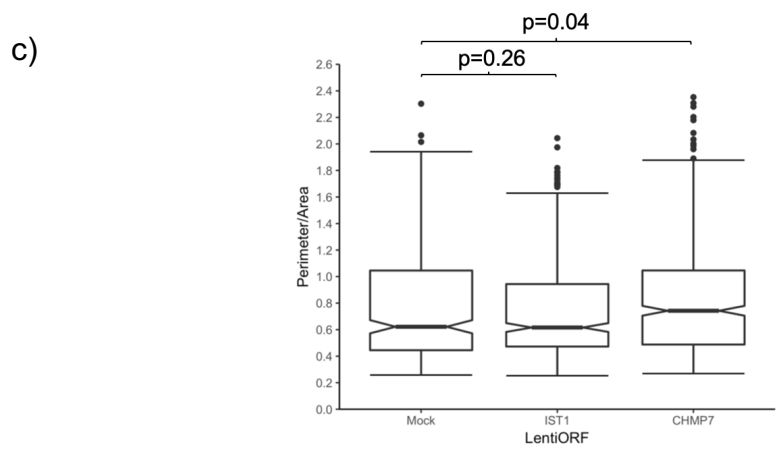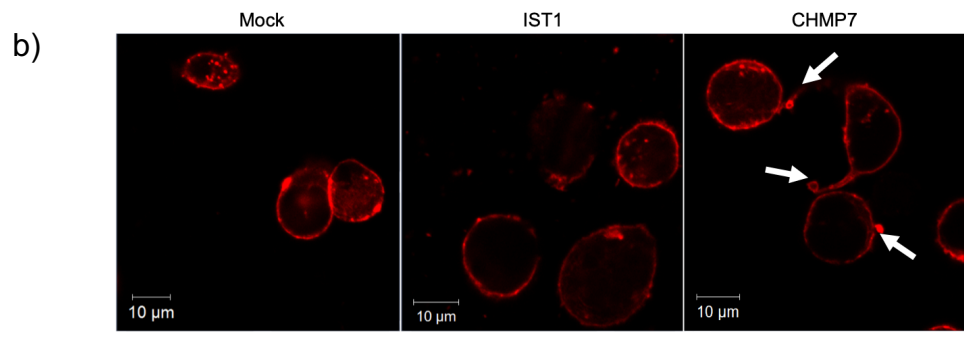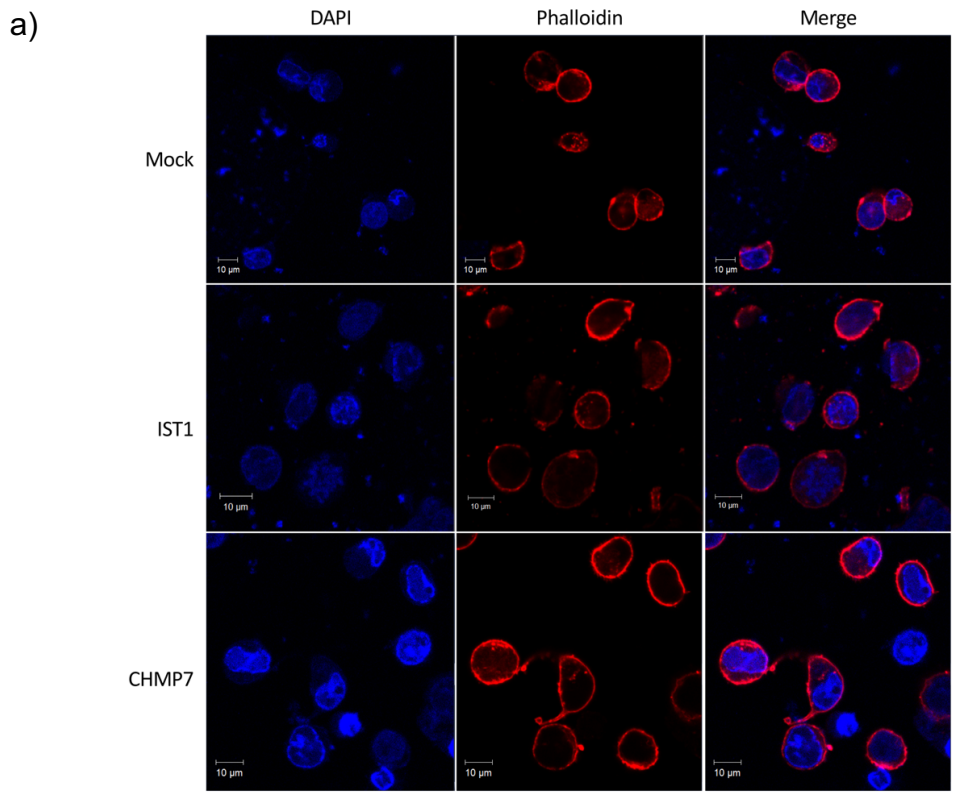
Figure 4.13 Overexpressing CHMP7 leads to bubbles forming at the plasma membrane during KSHV lytic infection. a) Confocal immunofluorescence of transduced cells (mock, IST1, CHMP7) reactivated for 72 h stained with DAPI and phalloidin. b) Phalloidin-only images magnified 5x with white arrows highlighting potential membrane bubbles. c) Box and whisker plot of perimeter/area ratio of cells from each transduced cell line (mock, IST1, CHMP7). Black dots are outliers outside of 1.5*IQR, notches around median line

indicate 95% confidence intervals of the median shown as notches. n=2, with >100 cells counted for each condition in each tile scan, T-test p-value shown between indicated conditions.

4.11   Discussion

Previous work has highlighted how specific herpesviruses have targeted components of the nuclear pore complex to aid their replication (Wild et al., 2009; Chang et al., 2015). However, little is known about how KSHV interacts with nucleoporins during its lytic replication cycle. Whole cell proteomic work previously performed in the Whitehouse laboratory had identified that between latency and the first 8 hours of lytic replication, Nup98 was specifically downregulated when compared to other nucleoporins although levels at the NPC appeared unchanged (Figure 3.3). Initially, it was hypothesised that this may be due to the virus targeting an antiviral role of Nup98, as previous studies had shown it could restrict viral infection and reverse virally induced mRNA export arrest (Enninga et al., 2002; Panda et al., 2014). However, upon Nup98-depletion from the whole-cell it became apparent that the significant Nup98 reduction was detrimental to viral lytic replication, specifically to virion infectivity (Figure 4.4). Further analysis suggested this was due to an accumulation of virions at the plasma membrane suggesting a failure in viral egress (Figure 4.6).

In order to determine how Nup98-depletion could lead to reduce virion infectivity and inhibit viral egress, work focused on previous studies that have shown KSHV utilises the Nup98-binding partner and export adapter protein Rae1 during KSHV lytic infection to retain certain cellular transcripts in the nucleus (Pritchard et al., 1999). This occurs through the action of the viral protein ORF10 that interacts with Rae1 to scan the 3' UTR of transcripts as they prepare to be exported at the

169

nuclear pore (Gong et al., 2016). Nup98 and Rae1 interact at the NPC to help facilitate mRNA export therefore it is not surprising that depletion of Nup98 could disrupt the action of ORF10 protein (Blevins et al., 2003; Ren et al., 2010). Therefore, it was hypothesised that whilst KSHV decreased Nup98 protein levels early during lytic replication it did not decrease them sufficiently at the NPC to disrupt the Rae1-Nup98 interaction that was observed in siRNA depleted cells.

Comparing datasets from previous published work on ORF10 and the existing proteomic work of the Whitehouse laboratory led to a potential link in the ESCRT-III pathway, specifically CHMP7 (Sophie Schuman, unpublished data) (Gong et al., 2016). CHMP7 is a component of the ESCRT-III complex that is responsible for membrane manipulation within the cell, including the formation of multivesicular bodies (MVB), cellular abscission, and viral budding (Alonso Y Adell and Teis, 2011; Morita et al., 2011; Vita and Broadie, 2017). Existing data suggested that CHMP7 was specifically targeted by KSHV during lytic infection by ORF10 sequestering CHMP7 mRNA in the nucleus. Using subcellular fractionation, it was demonstrated that this sequestration of CHMP7 mRNA could be disrupted by siRNA depletion of Nup98, and that this led to maintained CHMP7 protein levels during lytic infection (Figure 4.8). To test whether CHMP7 was responsible for decreasing viral infectivity TREx cells were transduced with a Lentiviral overexpression construct for CHMP7 along with IST1 (another ESCRT-III component) and a mock transduced control. Cells transduced with a CHMP7 overexpression construct exhibited significantly reduced viral infectivity when compared to the other cell lines (Figure 4.11). Furthermore, there was also an observable increase in the proportion of cells exhibiting an accumulation of viral capsid protein at the plasma membrane, although it was not possible to confirm

170

this occurrence was specifically linked to CHMP7 overexpressing cells (Figure 4.12).

Finally, attempts were made to determine the mechanism by which CHMP7 expression was able to reduce viral infectivity. This focused on whether CHMP7 overexpression was able to promote an ESCRT-III plasma membrane repair pathway (Gong et al., 2017). During this process the ESCRT-III complex controls plasma membrane integrity by producing bubbles from the plasma membrane helping sustain cell survival. A greater frequency of membrane bubbles were observed in lytically replicating cells transduced with a CHMP7 overexpression construct and a significantly greater median perimeter/area ratio were observed in these cells compared to mock transduced cells and cells expressing other ESCRT-III proteins (Figure 4.13). However, at a cell-to-cell level it was not possible to establish whether cells with membrane bubbles were overexpressing CHMP7. Therefore, it is difficult to draw meaningful conclusions on whether this is the mechanism of reduced KSHV virion infectivity. More work is required to determine how exactly CHMP7 could act to inhibit late stage viral processes. Given that evidence from other studies that some ESCRT-III components are required for successful herpesvirus replication the observation that CHMP7 is specifically downregulated and negatively affects virion infectivity warrants further exploration (Crump et al., 2007; Pawliczek and Crump, 2009).

Overall, the observations in this chapter open interesting questions regarding how KSHV targets Nup98 during its lytic infection. Observations outlined above demonstrate that a significant depletion in Nup98 across the whole cell is detrimental to KSHV lytic replication. Therefore, it could be hypothesised, given

no observations of a decrease in Nup98 levels at the NPC during lytic infection that the downregulation of Nup98 at 8 h during lytic infection is specifically targeting the nucleoplasmic fraction.

Chapter 5

~

Using proximity dependent biotin identification to probe for nuclear pore remodelling during KSHV lytic infection

5 Using proximity dependent biotin identification to probe for nuclear pore remodelling during KSHV lytic infection

5.1 Introduction

The traditional understanding of the NPC held that the nucleoporin composition of the pore was uniform across cell types and environments. However, recent work has established that NPC specialization can occur in different cell types and cellular circumstances (Ori et al., 2013). The specialization of nuclear pores also opens an interesting question regarding virus-nuclear pore interactions, specifically do viral remodelling events specialise nuclear pores to aid viral replication?

Previous work on viral remodelling of the nuclear pore has demonstrated how viruses target single or subsets of nucleoporins to aid with viral replication. For example, *Picornaviridae* have been shown to target FG-nucleoporins for proteolytic cleavage, whilst HSV-1 has been shown to inhibit host nucleocytoplasmic transport and induce nuclear pore dilation (Gustin and Sarnow, 2001; Wild et al., 2009; Malik et al., 2012). Interestingly, during HIV-1 infection the NPC undergoes a range of extensive compositional changes without affecting overall nuclear envelope integrity. Many of these changes appear critical to HIV-1 replication suggesting that the virus remodels and specialises NPCs to enhance HIV-1 replication (Monette et al., 2011b).

To determine whether KSHV lytic replication induced a stoichiometric remodelling at the nuclear pore a novel technique called proximity dependent biotin identification (BioID) was utilised. BioID is a technique developed by Roux et al. (2012) that adapts a similar technique Dam-ID, for analysing proximal protein-protein interactions. The principal is to fuse a promiscuous biotin ligase to a protein of interest, express this fusion protein *in vivo* where it will biotinylate proximal proteins after biotin is introduced to the media. These biotinylated proteins can then be isolated using streptavidin beads and identified by mass spectrometry. This technique had previously been used to analyse interactions at the nuclear pore and therefore offered an immediate starting point for understanding remodelling events during KSHV lytic infection (Kim et al., 2014).

In this chapter, BioID was applied to TREx cells that were reactivated to the lytic replication cycle to identify protein changes at the NPC. Initial work aimed to optimise the experimental system in both 293T and TREx cells. This was initially performed with GFP-nucleoporin and BioID-nucleoporin plasmids provided by the Roux laboratory. Attempts were made to establish TREx cell lines that stably expressed these plasmids after transfection, however this led to persistent mislocalisation of the target protein. Work then continued using transient transfections, which achieved good target localisation and was optimised to achieve the best biotinylation efficiency. LC-MS/MS analysis showed these transient transfections were able to specifically target a nuclear subset of proteins compared to the free ligase. Finally, work attempted to combine this system with tandem mass tagging-based quantitative proteomics which allowed for relative quantitation of protein levels between KSHV latent and lytic replication phases.

These data were then analysed using bioinformatic tools and clustering analysis to identify potential changes at the nuclear pore.

5.2 Optimisation of BioID-nucleoporin expression and subcellular targeting

The premise of the experiment was to use BioID to specifically biotinylate nucleoporins via a biotin ligase fusion protein with nucleoporin members of the Y-complex (Nup160, Nup85, Nup133, Nup53) (Kim et al., 2014). This would ensure the labelling of the majority of the NPC due to the stability and positioning of the Y-complex within the inner rings of the NPC. Biotin labelled nucleoporins could then be isolated after SDS lysis of transfected cells via biotin affinity capture with streptavidin (Figure 5.1a). The first steps of developing the BioID system to analyse KSHV-mediated NPC remodelling were performed using analogous GFP-nucleoporin plasmids. This allowed for faster analysis via confocal microscopy to confirm successful subcellular targeting of overexpressed nucleoporins.

GFP-nucleoporin plasmids were transfected into 293T cells and visualised via confocal immunofluorescence to confirm that nucleoporin overexpression resulted in subcellular targeting. However, these experiments showed consistent mistargeting of the GFP-nucleoporin constructs in 293T cells (Figure 5.1b). Using Lamin B1 to costain for the nuclear envelope highlighted the level of mistargeting with the GFP signal predominantly in the cytoplasm rather than at the nuclear envelope. In the case of Nup85-GFP, there is observable staining at the nuclear envelope however a strong dense stain is also present in the cytoplasm. It is thought that this localisation is precursor NPCs within the specialised

176

endoplasmic reticulum region of the annulate laemalle which are oversaturated

by the overexpression of Nup85-GFP.

a)
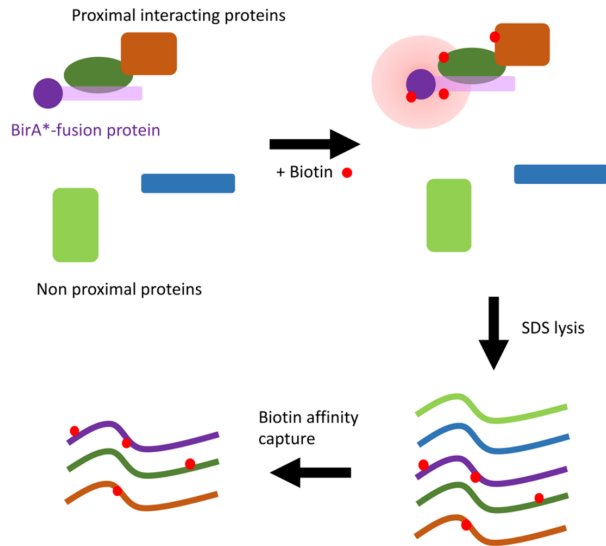
b)
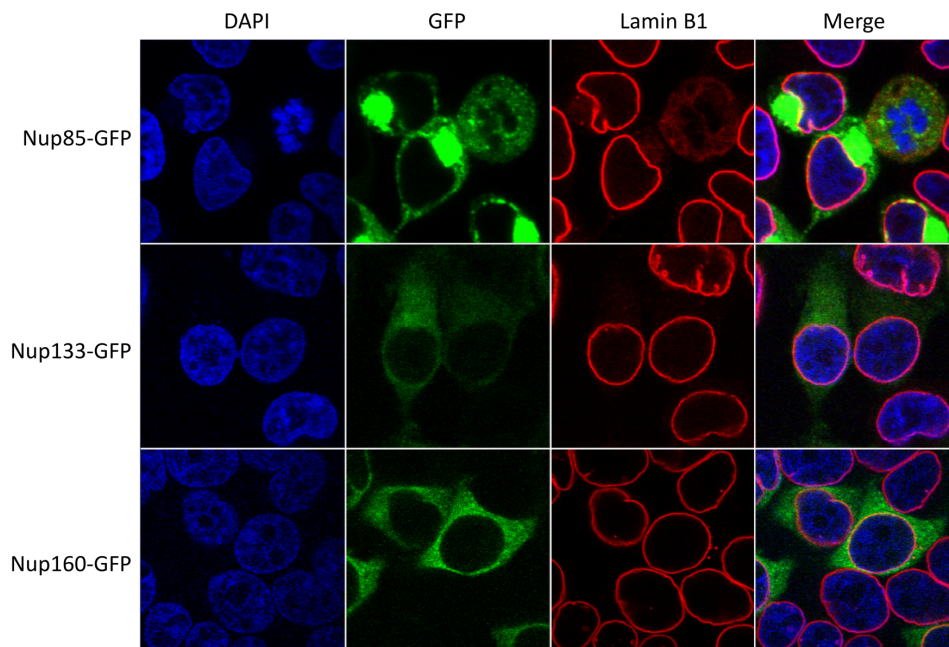
Figure 5.1 Transfection of GFP-nucleoporin constructs in 293T cells led to mistargeting of nucleoporins away from the nuclear envelope. a) Representation of the principal of proximity dependent biotinylation. b) Confocal immunofluorescence of GFP-nucleoporin transfected into 293T cells. Lamin B1 was used as a nuclear envelope stain.

Due to the availability of TREx cells it was decided to move away from optimisation of these constructs in 293T-based cell lines and focus on developing correct targeting in TREx. Using Amaxa nucleofector® technology, TREx cells were nucleofected with GFP-nucleoporin constructs which showed successful localization at the nuclear envelope (Figure 5.2b). Attempts were then made to select these cells to create a stably-expressing cell line. Cells were treated with G418 due to the neomycin resistance marker within the plasmid backbone. A kill curve for G418 in TREx cells was determining by performing a serial dilution of G418 and determining cell viability 24 h after the addition of G418. This showed ~100 % cell death at a concentration of 0.4 mg/ml G418 and so was the concentration taken forward to for selection (Figure 5.2a). However, after four weeks of selection the overexpressed nucleoporin became mistargeted with diffuse staining within the cytoplasm and no specific signal at the nuclear pore (Figure 5.2b). Therefore, it was decided to proceed using transient nucleofections as the biotin affinity identification protocol contained sufficient steps to specifically isolate biotinylated proteins.
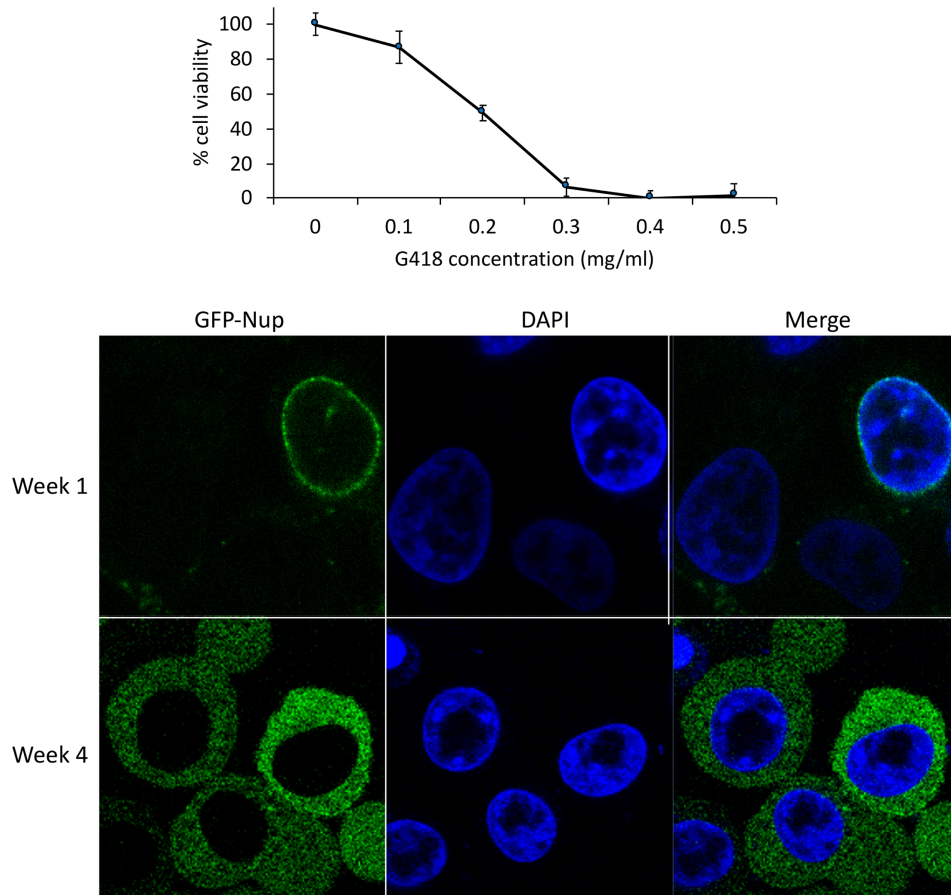
Figure 5.2 Selection of GFP-nucleoporins in TREx after nucleofection led to loss of targeting after 4 weeks. a) A G418 kill curve for TREx cells. Different dilutions of G418 were mixed with fresh media and incubated with TREx cells for 24 h before an MTS assay was performed to determine cell viability. n=5, 95 % confidence intervals shown. b) Confocal immunofluorescence of GFP-nucleoporins nucleofected into TREx cells 1 week after transfection and 4 weeks after selection with G418.

Subsequently, transient nucleofection was performed using BioID-nucleoporin plasmids, along with the free ligase (BioID) and the non-biotinylating mutant (R118G) (Figure 5.3a). Transfections were performed, and cells given at least 24 h recovery time before media was supplemented with biotin. Immunofluorescence and confocal microscopy were used to determine the targeting of biotinylation (Figure 5.3a). This showed good targeting at the nuclear pore complex in BioID-Nup53, still with occasional staining of the annulate

179

laemalle. BioID, or the free ligase, showed staining throughout the cell, with a stronger signal within the nucleus but still diffuse and not specific to the nuclear envelope. R118G showed no signal when probed with Alexa-Fluor conjugated streptavidin indicating that biotinylation detected was specific to the BioID ligase.

One key concern surrounding transient nucleofections was the proportion of successful transfection. Therefore, ImageJ was used to quantify confocal tile scans of coverslips to determine from a large field image the proportion of biotinylation. This was performed as a time course post nucleofection to determine the best time to conduct the biotin affinity pull down. Unfortunately, the level of biotinylation detected was very low (<10 %) and gradually decreased over time (Figure 5.3b). 3 days post nucleofection appeared to most consistently give the highest level of biotinylation for BioID-nup53 and thus it was decided that for experiments this time point would be used. Similar analysis was also performed to determine whether the induction of lytic replication in TREx using doxycycline had any impact on biotinylation efficiency (Figure 5.3c). These cells were induced 48 h post nucleofection and simultaneously induced with doxycycline and biotin added to the media. Whilst there was an observable decrease in biotinylation efficiency in both BioID and BioID-nup53 after induction it was not of a large enough magnitude to suggest that using this technique to identify nuclear pore components would be unfeasible.
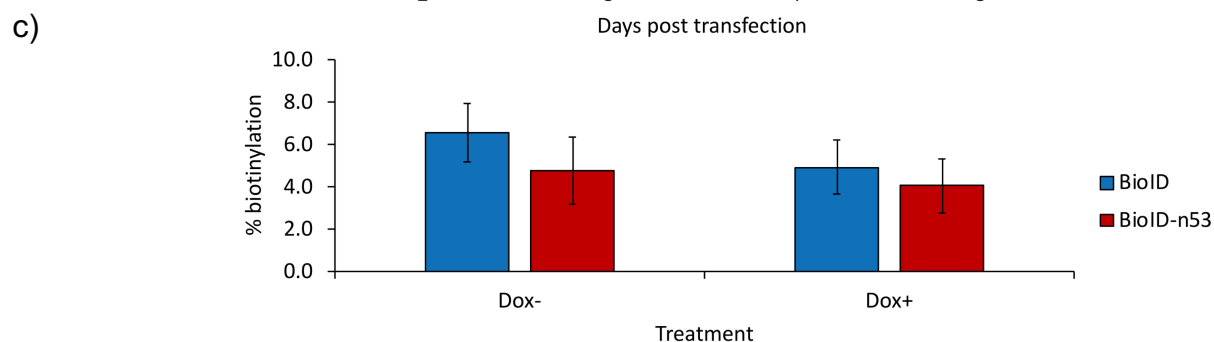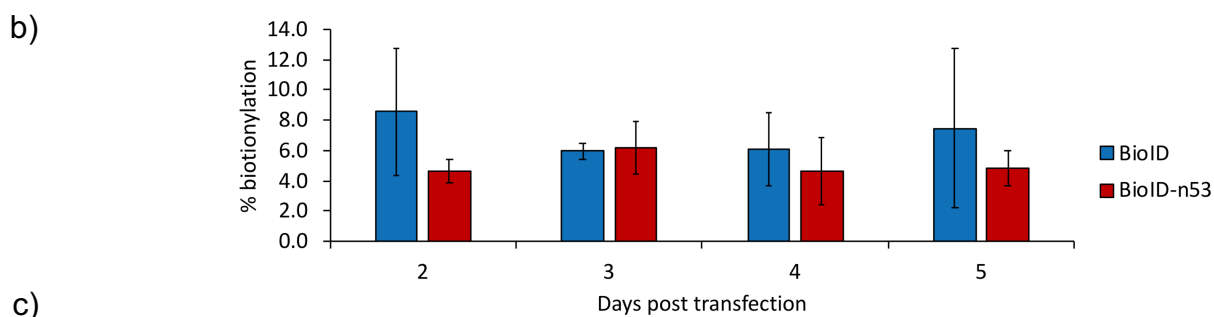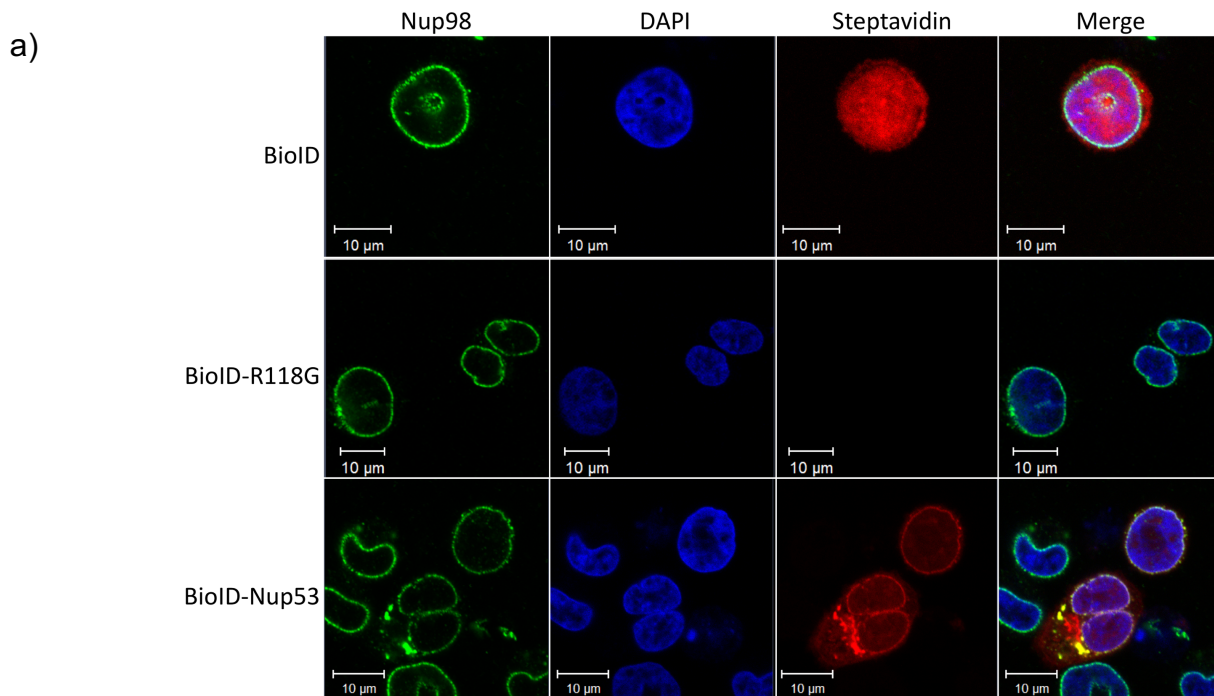
Figure 5.3 Transient nucleofection of BioID-nucleoporins showed efficient biotinylation targeting even after the induction of lytic replication. a) Confocal immunofluorescence of transiently nucleofected TREx after the introduction of biotin to media. Nup98 shown as a control to confirm biotinylation at the nuclear pore. b) ImageJ quantitation of % biotinylation over several days post nucleofection for free ligase (BioID) and nucleoporin-bound ligase (BioID-nup53). n=3, 95 % confidence intervals shown. c) ImageJ quantitation of % biotinylation between induced and uninduced TREx cells when transfected with free ligase (BioID) and nucleoporin-bound ligase (BioID-nup53). n=3, 95 % confidence intervals shown.

5.3 Pilot LC-MS/MS analysis of BioID-nucleoporin pull downs

After initial difficulties the BioID system was demonstrated to work within the TREx cell line and biotinylation was maintained after the induction of lytic replication. The next steps of this project involved biotin affinity capture of biotinylated proteins and analysis via mass spectrometry comparing latent and lytic replicating cells.

Following the biotin affinity capture protocol previously used by the Roux laboratory to investigate structural interactions in the NPC Y-complex (Kim et al., 2014), initial work used LC-MS/MS to identify proteins biotinylated by either the free ligase or BioID-nup53 (Figure 5.4). This approach produced two datasets that were analysed through an automated work flow to produce a list of enriched hits and unique hits (Figure 5.4a). Enrichment was defined by comparing the number of peptide fragments of one protein observed in the BioID condition and BioID-nup53. If 2x as many peptides were observed between those conditions the protein was considered enriched in its respective condition. These enriched hits were combined with unique hits that only occurred in one condition to create a complete hit list from each BioID experiment. These new curated data sets were then further annotated to convert accession codes to gene names using the freely available UniProt tool. These gene names can then be analysed via the free network and cluster analysis tool STRING-db. STRING-db is a web application that predicts protein-protein interactions based on a number of factors including published experimental data, pathway database information, text mining, gene cooccurrence, similar gene evolutionary neighbourhoods, relatedness by gene fusion events (Szklarczyk et al., 2017). STRING network analysis performed here

excluded connections based on text mining data. Pathway analysis of the curated data tables showed that proteins identified from the free ligase BioID fall into a variety of gene ontology groups including a number of cytoplasmic proteins along with components of the nucleus (nuclear part) (Figure 5.4b). Moreover, the network illustrates the predominantly cytoplasmic nodes (red) with fewer nuclear part nodes (blue), there are also few edges between nodes indicating fewer connections (Figure 5.4d). However, when this was compared to pathway analysis for BioID-nup53 a large number of cytoplasmic nodes (red) are still detected however there are more defined clusters of nuclear part nodes (blue) with a greater number of edges between these nuclear part nodes (Figure 5.4e). Furthermore, the false discovery rate calculation for BioID-nup53 pathway analysis is much lower than for BioID, suggesting that STRING-db analysis has a greater confidence that the proteins within the BioID-nup53 curated data set are specifically from these pathways and cellular compartments. Manual analysis of the curated data sets also showed that BioID-nup53 successfully pulled out a number of nucleoporins compared to BioID including Nup62, an expected Nup53 interaction partner, and Nup98, which has been previously identified using BioID-Nup53 (Figure 5.4c) (Kim et al., 2014). It is however, disappointing that the specific bait protein was not itself identified. However, the success of identifying specific subcellular networks of functionally related proteins at and around the NPC led us to proceed with the tandem mass tagging experiment.

a)

b)

BioID
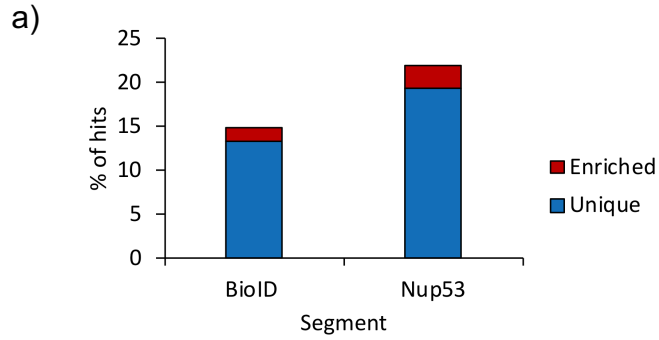
#pathway ID	pathway description	observed gene count	false discovery rate
GO.0005737	cytoplasm	219	1.70E-07
GO.0043233	organelle lumen	115	4.90E-07
GO.0070013	intracellular organelle lumen	113	5.49E-07
GO.0044428	nuclear part	105	5.91E-07
GO.0031981	nuclear lumen	98	9.37E-07
GO.0005654	nucleoplasm	85	3.96E-06
GO.0044444	cytoplasmic part	167	3.96E-06

c)

Nup53

#pathway ID	pathway description	observed gene count	false discovery rate
GO.0031974	membrane-enclosed lumen	183	2.56E-14
GO.0044422	organelle part	281	2.56E-14
GO.0044446	intracellular organelle part	276	2.56E-14
GO.0070013	intracellular organelle lumen	179	2.73E-14
GO.0043233	organelle lumen	180	4.56E-14
GO.0044428	nuclear part	164	4.18E-13
GO.0031981	nuclear lumen	153	1.31E-12

d)

Accession	Description	BioID Peptides	Nup53 Peptides
Q12769	Nup160	1	3
M0QXN5	Nup62	NA	2
P52948	Nup98	NA	3

184

e)

185
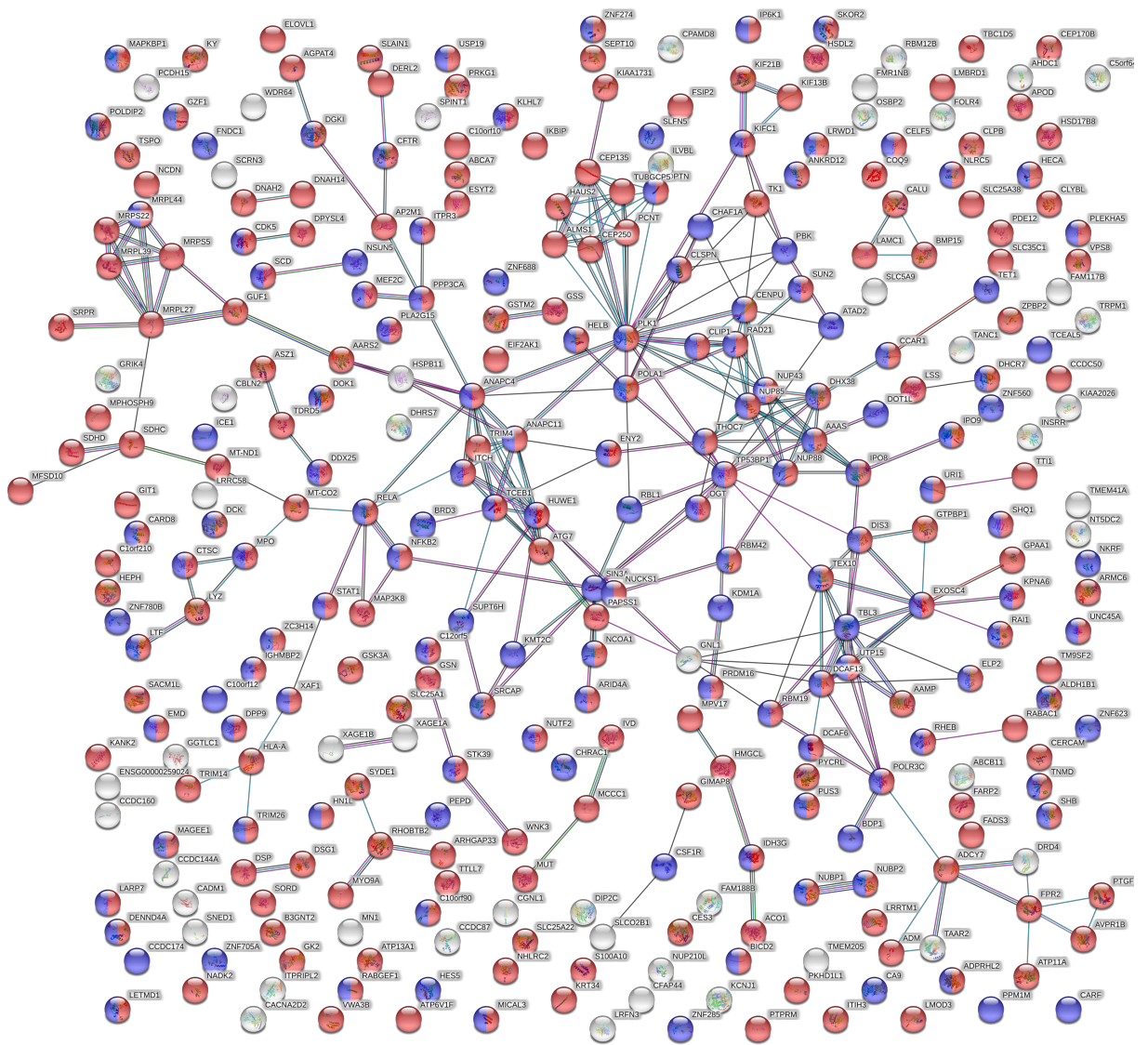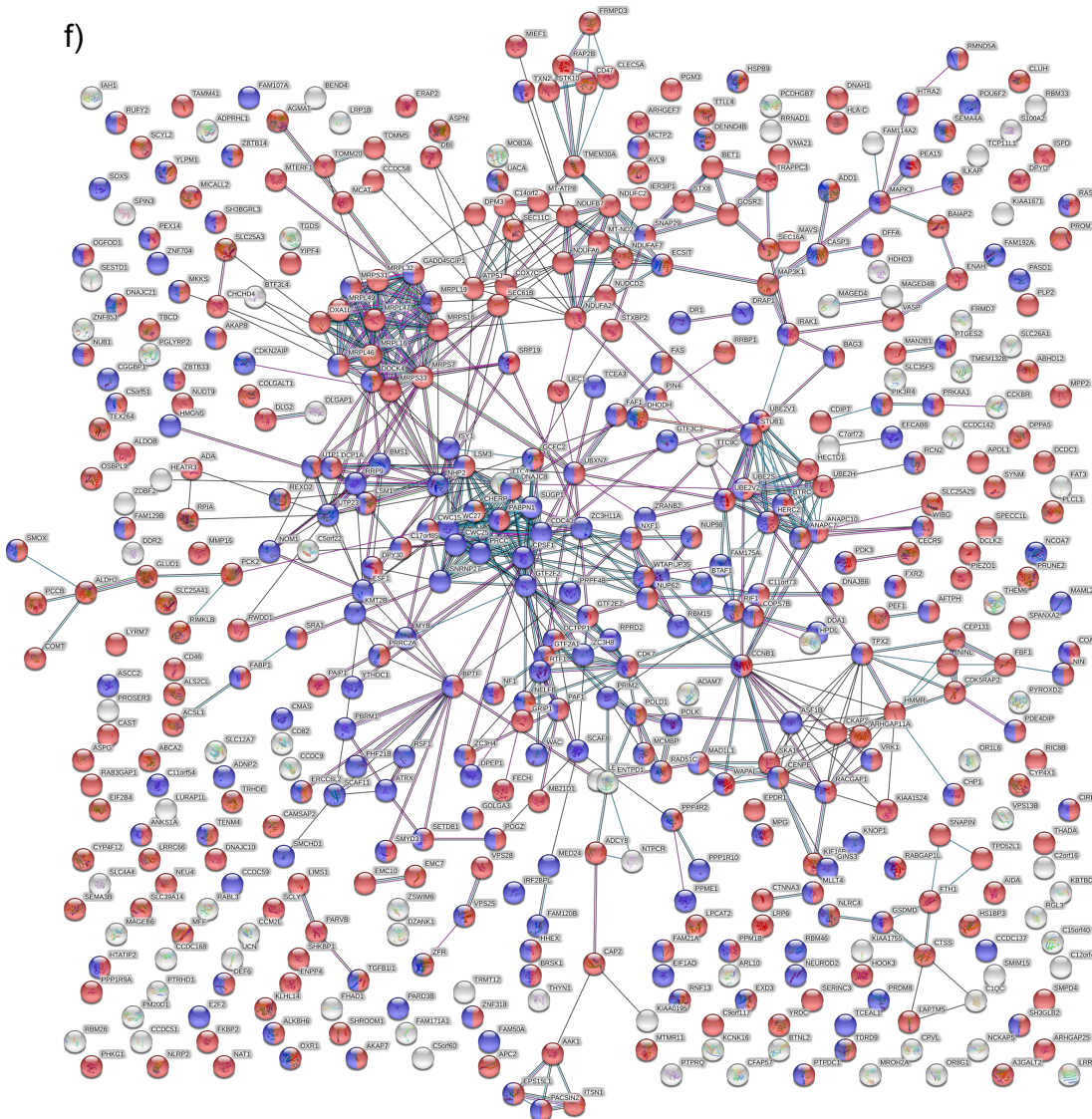
Figure 5.4 LC-MS/MS analysis of biotin affinity immunoprecipitation of BioID and BioID-nup53. a) Percentage comparison of protein hits between BioID and BioID-nup53. Data is expressed as enriched (number of proteins analysed is >2x the opposite condition) or only (where protein is only present in that sample. b) Gene Ontology analysis of the cellular component protein hits from BioID are related to. c) Gene Ontology analysis of the cellular component protein hits from BioID-nup53 are related to. d) Nucleoporin hits identified in BioID-Nup53 hits. e) STRING network map of enriched BioID hits. Nodes coloured red indicated cytoplasmic in gene ontology, nodes in blue indicate nuclear gene ontology. Edge colour indicates a connection between nodes based on of gene fusion evidence (red), gene neighborhood evidence (green), gene cooccurrence evidence (blue), experimental evidence (purple), database evidence (light blue), coexpression evidence (black). f) STRING network map of enriched BioID-nup53 hits. Nodes coloured red indicated cytoplasmic in gene ontology, nodes in blue indicate nuclear gene ontology. Edge colour indicates a connection between nodes based on of gene fusion evidence (red), gene neighborhood evidence (green), gene cooccurrence evidence (blue), experimental evidence (purple), database evidence (light blue), coexpression evidence (black).

5.4 Tandem Mass Tagging LC-MS/MS coupled to BioID

To understand specific stochiometric changes at the NPC during KSHV lytic infection, transient BioID was combined with the quantitative proteomic technique tandem mass tagging prior to LC-MS/MS analysis.

Tandem mass tagging (TMT) is an emerging technique within mass spectrometry for the analysis of relative protein abundance. The concept of TMT is to incorporate a isobaric peptide tag composed of a sensitization (reporter) group, a mass normalization group and a peptide reactive functional region (Thompson et al., 2003). The peptide reactive region attaches the tag to proteins within the sample whilst the mass normalization group acts to ensure that the tag is isobaric after tagging, thus ensuring that proteins tagged from different samples are the same mass and run identically on HPLC. The sensitization or reporter group acts as the internal mass standard and is unique for each sample that is tagged. It is removed from the overall TMT molecule by collision induced dissociation during LC-MS/MS and forms a distinct isotope peak within the MS readout.

Alongside the nucleoporin fusion proteins, the free ligase and ligase mutant R118G were used to provide an internal control to ensure proper targeting and a control for background binding to the streptavidin beads during biotin affinity capture. Samples were labelled with TMT reagents prior to LC-MS/MS to allow for relative abundance measurements (Figure 5.5a). To ensure suitable biotinylation coverage of the NPC these experiments utilised three nucleoporin biotin ligase fusion proteins: Nup53, a nucleoporin that sits centrally within the NPC as part of the Nup93-Nup53 complex helping anchor central plug nucleoporins to the nuclear membrane (Hawryluk-Gara et al., 2005; Mansfeld et

al., 2006); Nup133 and Nup85 are components of the Y-complex, a modular subdomain of the NPC that is critical to nuclear pore assembly and gives rise to central doughnut shaped structure of the NPC (Walther et al., 2003; Harel et al., 2003). These three nucleoporin fusion proteins would provide coverage of both the central plug region and cytoplasmic and nucleoplasmic facing regions as previously demonstrated by the Roux laboratory (Kim et al., 2014).

To analyse the quantitative proteomic data, which was provided as a spreadsheet readout from SEQUEST software set at a 1% False Discovery Rate (FDR), the tables were converted to columns of comma separated values (.csv) and processed through a series of R scripts to clean the data producing lists of proteins that were true hits (i.e. proteins with a greater than 1.5 protein ratio of protein in the experimental condition compared to the corresponding condition ligase mutant R118G). These lists were produced for each nucleoporin fusion protein in the unreactivated and reactivated condition. These were then analysed via STRING-db to identify via Gene Ontology the pathway associated with these proteins and confirm correct biotinylation targeting compared to the free ligase.

Initial network analysis was disappointing (Figure 5.5b). With two key experimental conditions Nup53 and Nup133 not producing significant protein-protein interaction maps based on STRING-db. This was due to a low number of hits being identified and minimal pathway similarity between these proteins. This is potentially a consequence of the transient nucleofection system limiting the initial pool of biotinylated protein alongside the stringent biotin affinity protocol. However, Nup85 did successfully produce a list of hits that produced a significant protein-protein interactions network map. Furthermore, Gene Ontology pathway

188

analysis showed strong identification of nuclear proteins in both unreactivated and reactivated compared to the free ligase (Figure 5.5c).

Having performed network clustering analysis and confirming for each condition enriched nuclear targeting versus the free ligase, these lists were then combined to include peptides that matched one of two criteria: the peptide was present in both unreactivated and reactivated samples; or the peptide was only found in one condition and its relative abundance underwent a significant increase or decrease (for example viral peptides which were significantly increased in abundance during reactivation but not at all present in the unreactivated sample).

a)
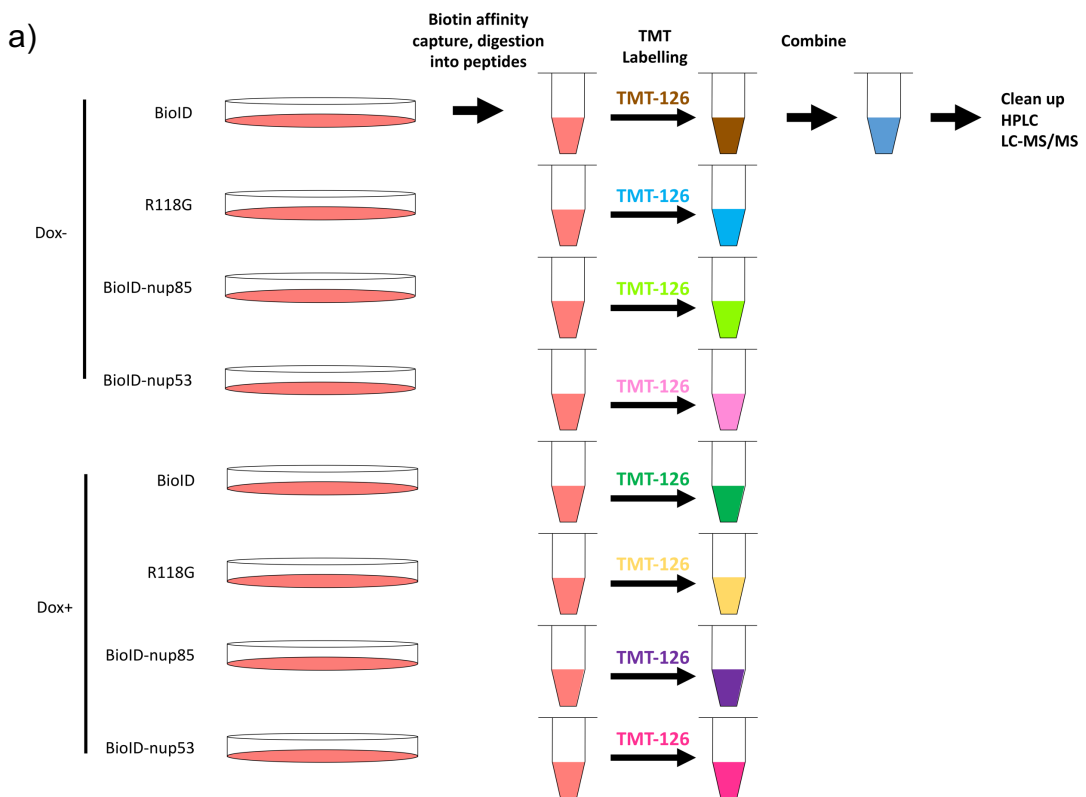
b)

Treatment		Nodes	Edges	Average node degree	Average local clustering coefficient	Expected edges	PPI enrichment p-value
Un	BioID	71	41	1.15	0.34	25	0.00228
	Nup53	31	4	0.258	0.194	5	0.762
	Nup85	90	551	12.2	0.604	135	<1.0e-16
	Nup133	33	7	0.424	0.303	3	0.0585
Ind	BioID	708	16571	46.8	0.452	8526	<1.0e-16
	Nup53	29	5	0.345	0.276	5	0.569
	Nup85	129	238	3.69	0.5	175	3.79E-06
	Nup133	26	2	0.154	0.154	2	0.638

c)

Uninduced

Induced

BioID

Uninduced:

#pathway ID	pathway description	observed gene count	false discovery rate
GO.0070062	extracellular exosome	31	6.44E-08
GO.0044421	extracellular region part	33	2.25E-06
GO.0031988	membrane-bounded vesicle	30	2.78E-05
GO.0005576	extracellular region	32	0.00034
GO.0044422	organelle part	43	0.00146
GO.0044446	intracellular organelle part	41	0.00561
GO.0032991	macromolecular complex	28	0.0285

Induced:

#pathway ID	pathway description	observed gene count	false discovery rate
GO.0030529	ribonucleoprotein complex	161	1.17E-94
GO.0043233	organelle lumen	344	2.10E-72
GO.0031974	membrane-enclosed lumen	345	1.22E-71
GO.0070013	intracellular organelle lumen	339	2.65E-71
GO.0070062	extracellular exosome	278	1.89E-70
GO.0044446	intracellular organelle part	463	4.08E-65
GO.0022626	cytosolic ribosome	60	9.19E-65

Nup53

Uninduced:

#pathway ID	pathway description	observed gene count	false discovery rate
GO.0070062	extracellular exosome	15	0.000719
GO.0044422	organelle part	21	0.0381

Induced:

#pathway ID	pathway description	observed gene count	false discovery rate
GO.0044446	intracellular organelle part	21	0.0327

Nup133

Uninduced:

#pathway ID	pathway description	observed gene count	false discovery rate
GO.0070062	extracellular exosome	15	0.00192

Induced:

#pathway ID	pathway description	observed gene count	false discovery rate
GO.0031974	membrane-enclosed lumen	14	0.042
GO.0044446	intracellular organelle part	19	0.042

Nup85

Uninduced:

#pathway ID	pathway description	observed gene count	false discovery rate
GO.0000786	nucleosome	20	1.08E-26
GO.0000785	chromatin	23	1.64E-17
GO.0005654	nucleoplasm	44	6.66E-14
GO.0000228	nuclear chromosome	20	1.02E-13
GO.0005694	chromosome	24	3.88E-13
GO.0044427	chromosomal part	23	3.97E-13
GO.0070062	extracellular exosome	38	6.61E-10

Induced:

#pathway ID	pathway description	observed gene count	false discovery rate
GO.0044446	intracellular organelle part	88	3.22E-12
GO.0043233	organelle lumen	59	1.13E-09
GO.0070013	intracellular organelle lumen	57	4.76E-09
GO.0044428	nuclear part	50	5.79E-07
GO.0005829	cytosol	45	1.78E-06
GO.0032991	macromolecular complex	55	1.78E-06
GO.0031981	nuclear lumen	46	2.29E-06

Figure 5.5 Overview of Tandem mass tagging of BioID-nucleoporins samples. a) Schematic of process of tandem mass tagging with samples initially prepared, then labelled with different TMT tags (highlighted by colour), then samples are combined before LC-MS/MS analysis. b) STRING overview of node clustering for each experimental condition. c) Gene Ontology analysis of likely Cellular Component that peptide hits (enriched compared to R118G) are associated with for all experimental conditions.

With the combined list of true peptide hits identified from the Nup85 data it was

possible to perform further network analysis to identify clusters of functionally

related peptides and analyse any changes in their relative abundance during lytic replication. This initial network cluster analysis was again performed using STRING-db and showed a good protein-protein interaction p-value (Figure 5.6a), suggesting more interactions than would be typically expected. Gene Ontology pathway analysis then identified a number of pathways which were enriched for a variety of peptides which allowed for further analysis of relative abundance changes of these clusters of functionally related peptides (Figure 5.6b). However, this clustering showed that of proteins identified the majority did not cluster into any highly specific pathways (only the nucleoplasm and cytosol compartments) except a small group involved in the ribonucleoprotein complex. Due to the relative position of Nup85 at the NPC it is plausible for BioID to label proteins that are in the nucleoplasm or the cytosol. When comparing the relative abundance of these identified peptides between latency and lytic replication it was observed that ribonucleoprotein complex proteins identified by BioID were increased by approximately 2.5-fold (Figure 5.6c). However, for nucleoplasmic peptides a much wider range of relative abundance ratios can be seen although the general trend still suggests 2.5-fold increase in relative abundance at the NPC during lytic replication. STRING-db network analysis highlights the areas of functional clustering particularly around proteosomal proteins (PSME1, PSMB1, PSMC4), ribosomal biogenesis-related proteins (RPS21, TBL3, PWP2, RRS1) and regulators of nuclear transcription (UFL1, TCEB2, TCEA1) (Figure 5.6d). However, the experiment failed to identify any nucleoporins other than TPR and failed to pull down the bait protein as would be expected.

a)

Nodes	Edges	Average node degree	average local clustering coefficient	expected no. of edges	PPI enrichment p-value
87	87	2	0.433	70	0.0254

b)

#pathway ID	pathway description	observed gene count	false discovery rate
GO.0044446	intracellular organelle part	52	0.00122
GO.0005829	cytosol	28	0.00761
GO.0016282	eukaryotic 43S preinitiation complex	3	0.00761
GO.0033290	eukaryotic 48S preinitiation complex	3	0.00761
GO.0043232	intracellular non-membrane-bounded organelle	30	0.00761
GO.0070013	intracellular organelle lumen	32	0.00771
GO.0030529	ribonucleoprotein complex	11	0.00859
GO.0044428	nuclear part	29	0.016
GO.0005634	nucleus	43	0.0211

c)
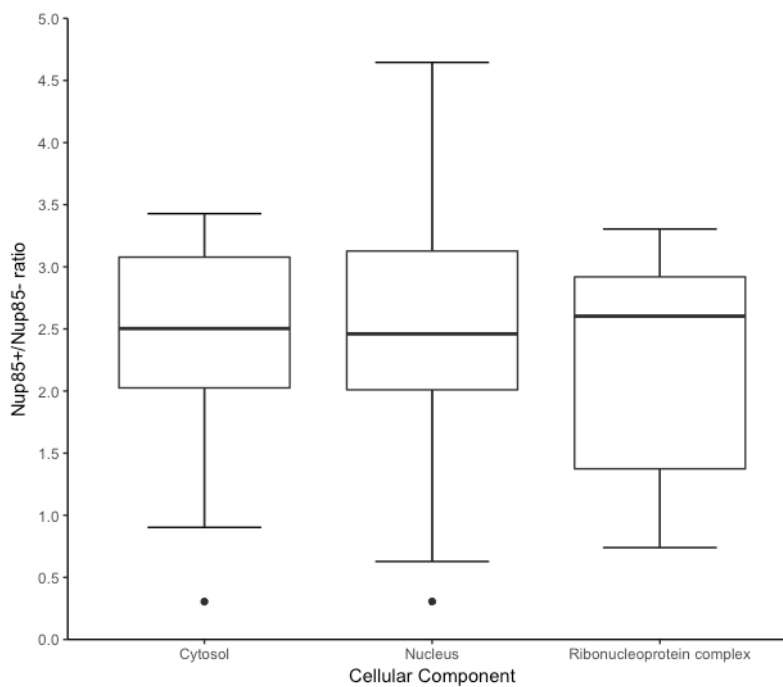
d)
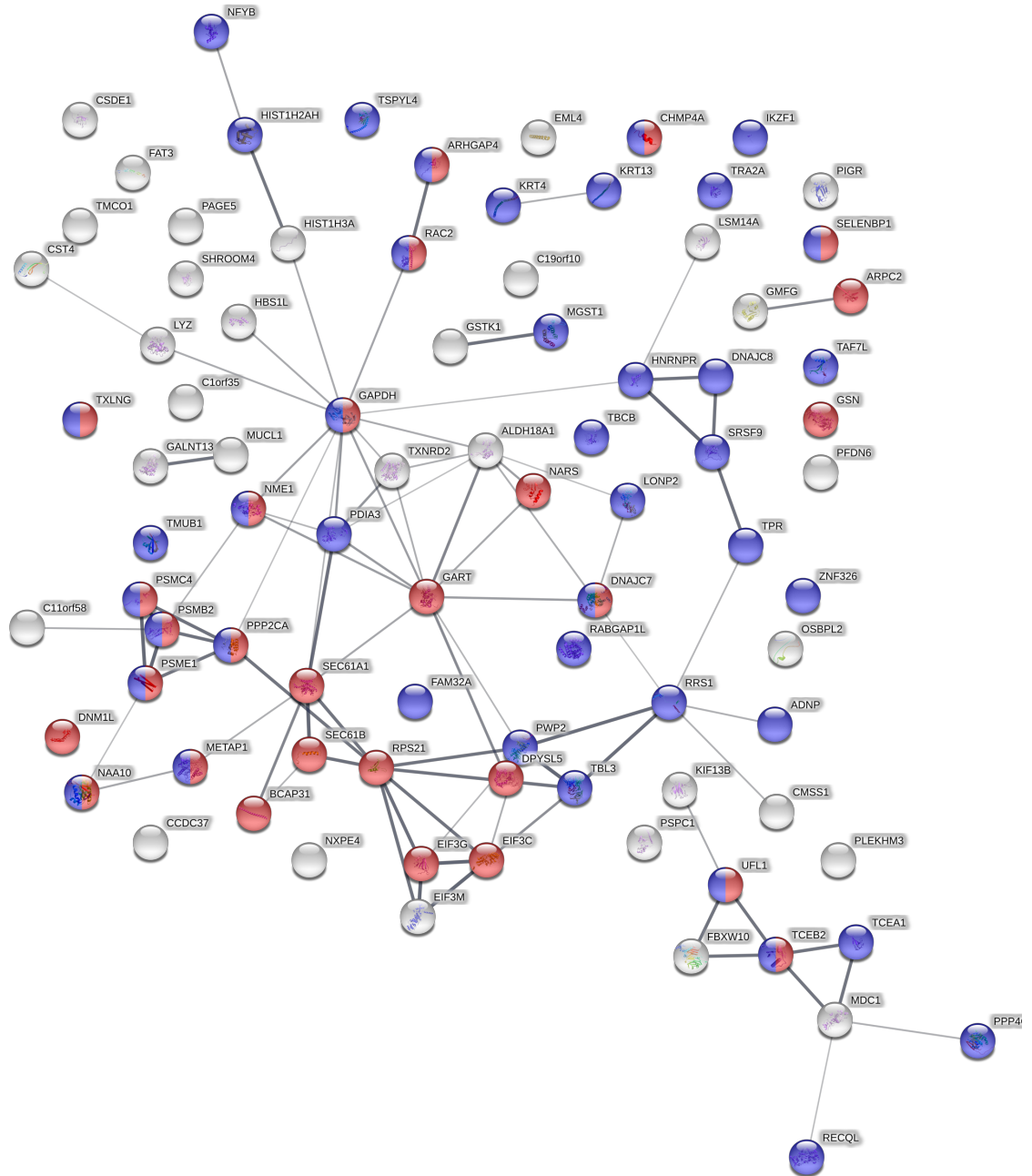
Figure 5.6 TMT of BioID-Nup85 shows that at 24 h post lytic replication specific ribosomal biogenesis pathways are maintained. a) The STRING-db network overview of combined Nup85 peptide hits. b) Gene Ontology analysis of likely Cellular Component that peptide hits (enriched compared to R118G) are associated with for BioID-Nup85. c) Boxplot of reactivated/unreactivated protein ratios for two Cellular component subsets identified from STRING-db. d) STRING-db network of combined Nup85 peptide hits. Nodes coloured red indicated cytoplasmic in gene ontology, nodes in blue indicate nuclear gene ontology. Edge colour indicates a connection between nodes based on of gene fusion evidence (red), gene neighborhood evidence (green), gene cooccurrence evidence (blue), experimental evidence (purple), database evidence (light blue), coexpression evidence (black).

5.5   Discussion

In this chapter the novel technique of proximity dependent biotinylation (BioID) was combined with tandem mass tagging (TMT) in an attempt to identify relative stochiometric changes at the nuclear pore during KSHV lytic replication. This work followed on from previous work using BioID to probe the structure of the nuclear pore, specifically showing new interaction data regarding components of the Y-complex (Kim et al., 2014). This approach was constrained by the difficult-to-transfect cell lines utilised in this study and difficulties establishing stable cell lines (Figure 5.2). Therefore, after work optimising this system through transient nucleofection a series of experiments were performed using three BioID-nucleoporins in tandem with TMT labelling and mass spectrometry to identify changes at the NPC during KSHV lytic infection (Figure 5.3). Through mass spectrometric analysis a series of large, relational datasets were produced. These were analysed via R scripts to identify true hits when compared to a beads-only control and then analysed to identify proteins enriched at the NPC in either latency or lytic replicating cells and proteins present at the NPC during both lifecycle stages. This produced a final list of peptide hits for hierarchical cluster analysis of functions and analysis of relative abundance changes (Figure 5.5). This identified a variety of proteins of interest however time constraints prevented extensive validation in a wet-laboratory setting.

However, only one of the three BioID-nucleoporins, Nup85, successfully pulled down enough peptides to perform network analysis (Figure 5.6). Further analysis of this one successful experiment identified three main groups of labelled proteins: cytosolic, nucleoplasmic and ribonucleoprotein complex. The highly

194

generic nature of these groups suggests no highly specific functional pathways were identified. This is disappointing given it would be expected to identify peptides related to the nuclear pore complex within this experiment. However, the identification of nucleoplasmic and cytosolic proteins is plausible given the approximate position of Nup85 on the NPC (Kelley et al., 2015). Analysis of the relative abundance changes of these peptides between latent and lytic cells showed that across all three groups the levels of these peptides at the NPC increased by approximately 2.5-fold between latent cells to lytic cells. It is important to note that this could be related to the fact that the dataset from lytic replicating Nup85 expressing cells identified the most peptides when compared to beads-only (Figure 5.5b). However, this increase could relate to the virus manipulating export pathways to preferentially boost nucleocytoplasmic transport systems required by the virus. Herpes simplex 1 virus has been shown to inhibit nucleocytoplasmic transport pathways via interaction with nucleoporins (Malik et al., 2012). Research on the impact of KSHV lytic replication on protein export at the NPC is limited but studies with CRM1 inhibitor leptomycin B have shown that viral proteins such as ORF45 require CRM1 to shuttle between the nucleus and the cytoplasm (Li and Zhu, 2009). This would suggest that the CRM1 export pathway is not specifically disabled by the virus during lytic infection, nevertheless future work investigating the impact of KSHV lytic replication on alternate forms of protein import and export would help clarify the increases seen here.

Finally, it is also worth noting the identification of ribonucleoprotein complex proteins from this data. The impact of KSHV on ribosomes during lytic infection is not well characterised but the above data shows a relative increase in

195

ribosomal proteins at the NPC during lytic infection. This suggests that ribosomal proteins are not significantly affected by the virus-induced process of host cell shut off (Glaunsinger and Ganem, 2004). Furthermore, several components of the ribonucleoprotein complex were identified at higher levels during lytic replication suggesting either aspects of the ribosome were upregulated during lytic infection or that components of the ribosome came together more rapidly after pre-ribosomal export at the nuclear pore complex during lytic replication.

Chapter 6
~
Discussion

6   Discussion

The nuclear pore complex (NPC) is a sophisticated barrier that separates the nucleus and the cytoplasm. The protective role of the NPC is challenged by a variety of factors, none more diverse and unrelenting as viruses. Many different families of viruses have co-evolved to target the NPC, leading to a variety of strategies for overcoming the selective barrier.

Little is known about how KSHV targets the NPC therefore this thesis set out to explore how KSHV manipulates the NPC during its lytic infection. It looked to validate observations from previous whole cell quantitative proteomic data obtained by the Whitehouse Laboratory that indicated changes at the NPC during KSHV lytic infection. It also aimed to implement proximity dependent biotin identification (BioID) at the NPC during KSHV lytic replication, in combination with tandem mass tagging (TMT), to develop a semi-quantitative profile of how the NPC is altered over the course of KSHV lytic infection.

Chapters 3 and 4 explored the specific targeting of nucleoporin Nup98 by KSHV early during lytic infection. This began with the observation that 8 h after the induction of KSHV lytic replication whole-cell Nup98 protein levels decreased by approximately half in the proteomic data (Figure 3.1a). This was confirmed by Western blot analysis and pointed to rapid targeting of this nucleoporin by the virus (Figure 3.1b). A number of other viruses have been shown to specifically target Nup98 during their lifecycles: Influenza A has been shown to downregulate Nup98 expression and sequester other components of RNA export machinery to inhibit export of host mRNAs; Vesicular stomatitis virus (VSV) interacts with

Rae1-Nup98 complexes to disrupt nucleocytoplasmic transport (von Kobbe C et al., 2000; Satterly et al., 2007; Chen et al., 2010; Rajani et al., 2012). Furthermore, Nup98 has also been shown to be interferon inducible, specifically in the case of the VSV export block, IFN-γ treatment or ectopic expression of Nup98 reverses virus-mediated disruption (Enninga et al., 2002). However, KSHV has been shown to suppress IFN signalling during lytic replication through the action of caspases (Tabtieng et al., 2018). Notwithstanding, Nup98 has also been shown to regulate antiviral genes in *Drosophila* as part of its off-pore role within the nucleoplasm (Panda et al., 2015). Therefore, it was hypothesised that KSHV targeted nucleoplasmic Nup98 due to its role modulating transcription of antiviral genes. This was supported by observations that the localisation and levels of Nup98 at the NPC did not appear to change during lytic replication (Figure 3.3). This can be compared with a more obvious depletion phenotype seen when TREx cells are treated with Nup98 siRNAs, in these cells a clear decrease in Nup98 levels can be observed at the NPC (Figure 4.4). Therefore, it was hypothesised that KSHV was specifically targeting the nucleoplasmic fraction of Nup98 in TREx cells during lytic replication.

The viral transactivator protein RTA arose as the most likely determinant of Nup98 targeting during early lytic infection. RTA expression occurs rapidly on the switch from KSHV latency to lytic replication, making it highly likely there is sufficient levels of RTA at 8 h post reactivation to negatively impact endogenous Nup98 protein levels (Lukac et al., 1998; Nakamura et al., 2003). This was confirmed by transfecting an RTA overexpression construct into 293T cells which led to a significant decrease in Nup98 levels 24 h post transfection (Figure 3.4). RTA is a multifunctional transcriptional activator and repressor protein. It is able

199

to activate genes through a variety of mechanisms either through direct binding to specific DNA sequences called RTA response elements (RREs) or through interactions with other transcription factors such as RBP-Jk, AP1 and C/EBP (Liang et al., 2002; Wang et al., 2003; Liang and Ganem, 2004; Wang et al., 2004). RTA is also able to suppress transcription through targeting proteins for proteasomal degradation such as Hey1, IRF7 and KSHV-RTA binding protein (K-RBP) through its E3 ubiquitin ligase activity (Yu et al., 2005; Yang et al., 2008; Gould et al., 2009). Therefore, RTA could potentially be downregulating Nup98 through a variety of mechanisms. However, qPCR analysis of both reactivated TREx and transfected 293T showed Nup98 mRNA did not decrease sufficiently to cause a decrease in Nup98 protein levels (Figure 3.1d and Figure 3.4c). This suggested RTA was targeting Nup98 protein levels through its E3 ubiquitin ligase domain. RTA has previously been shown to target transcriptional repressor Hey1 for degradation via its E3 ubiquitin ligase domain in order to prevent Hey1 repressing transcription at the ORF50 promoter (Gould et al., 2009). ICP0, an immediate-early HSV-1 lytic protein, also possesses a RING-finger ubiquitin ligase activity that acts to disrupt ND10 bodies in the nucleus that participate in host cell antiviral responses (Maul et al., 2000; Boutell et al., 2002; Gu and Roizman, 2003). Utilising the proteasome inhibitor MG132, Nup98 degradation was shown to be dependent on proteasome activity both when overexpressing transfected RTA in 293T cells and during lytic replication in KSHV-infected B cells (Figure 3.5). Further efforts were made to co-immunoprecipitate RTA bound to Nup98 to support the hypothesis that RTA directly interacts with Nup98 to induce its degradation. These experiments were not successful but do not exclude the possibility that RTA is inducing the degradation of Nup98 (Figure 3.6). The

interaction between E3 ligases and their targets is highly dynamic through very weak, transient interactions making the determination of E3 ligase substrates technically difficult (Pierce et al., 2009).

Having established that the decrease in Nup98 was dependent on RTA and the activity of the proteasome the crucial question now turned to why KSHV was targeting Nup98. As described above, Nup98 is interferon inducible and responsible for regulating antiviral genes. This suggested Nup98 might play a restrictive role on the virus which was explored in two experiments: the first by comparing immediate-early gene expression in Nup98-depleted TREx cells; the second by looking at the effect of overexpressing Nup98 and RTA in 293T cells along with a luciferase gene controlled by the ORF50 promoter. In Nup98-depleted TREx cells, the absence of Nup98 had no impact on the expression of immediate-early gene ORF57 at both the mRNA and protein level (Figure 4.3). It was hypothesised that the absence of Nup98 might lead to either greater levels of spontaneous reactivation or increased ORF57 expression in the absence of Nup98 as a viral restriction factor. Neither was observed although this could be due to the doxycycline inducible mycRTA system for inducing lytic replication in TREx cells leading to overexpressed mycRTA that obscured an effect in Nup98-depleted cells. However, the second experiment showed that overexpressing Nup98 and RTA led to decreased luciferase luminescence from the ORF50-promoter in a dose-dependent manner suggesting Nup98 had a restrictive effect on the ORF50 promoter (Figure 3.8). ORF50 encodes for the viral transactivator RTA highlighting the importance to the virus of disrupting this restrictive role of Nup98 for successful viral lytic replication. The exact mechanism of how Nup98 would repress expression at the ORF50 promoter is unclear, however,

201

nucleoplasmic Nup98 binds to promoters of developmental and cell cycle genes and when depleted from these sites gene expression is concomitantly downregulated (Kalverda et al., 2010; Capelson et al., 2010). Furthermore, the overexpression of Nup98 enhances the transcription of Nup98-bound genes, pointing to a key transcriptional role of Nup98 in the nucleoplasm (Kalverda et al., 2010). Nup98 also plays a causative but poorly understood role in human leukaemia, with chromosomal translocations in acute myeloid leukaemia resulting in chimeric proteins containing the Nup98 FG-domain and homeobox transcription factors (Lam and Aplan, 2001). Both these domains are required for the transforming ability of these chimeric proteins which appear to potently active Hox genes (L H Kasper et al., 1999; Kroon, 2001; Argiropoulos and Humphries, 2007). The Nup98 component of these chimeras recruits histone acetylases and deacetylases via its FG-repeat domain (L H Kasper et al., 1999; Bai et al., 2006; Wang et al., 2007). This multitude of mechanisms through which Nup98 exerts control over transcription makes identifying how Nup98 restricts ORF50 transcription difficult to pinpoint although it is likely acting through a repressive binding partner. Attempts were made to transduce a Lentiviral GFP-Nup98 overexpression construct into TREx cells in order to test whether this restricted the progress of KSHV lytic infection (Figure 3.10). However, poor levels of GFP-Nup98 were detected suggesting either a low transduction efficiency or loss of the expression cassette. Attempts were made to use confocal microscopy to identify whether GFP-Nup98 positive cells exhibited an alternate phenotype to GFP-Nup98 negative cells on induction of lytic replication, however no phenotype was observed (Figure 3.11). These experiments were performed by reactivating cells with sodium butyrate, an alternative to induction via the doxycycline-

inducible mycRTA system, due to concerns this overexpressed mycRTA would induce the degradation of Nup98 sufficiently to override any effect of GFP-Nup98. However, previously described Nup98 binding partners that could be responsible for repressing ORF50 expression including histone deacetylases that could also be inactivated by sodium butyrate treatment (Davie, 2003). Overall, the poor level of GFP-Nup98 expression and potentially confounding reactivation treatments of sodium butyrate and mycRTA make drawing conclusions from these experiments difficult.

Whilst the above describes a potential role of nucleoplasmic Nup98 in acting a viral restriction factor further experiments depleting Nup98 from TREx cells showed a significant loss of Nup98 was detrimental to viral replication. Whilst Nup98-depletion had no impact on the expression of immediate-early KSHV lytic genes it did lead to reduce infectivity of virions produced at 72 h after the induction of lytic replication (Figure 4.5b). Whilst Nup98-depletion did not reduce viral DNA levels produced at this late stage it did lead to an apparent accumulation of viral capsid proteins at the cell periphery (Figure 4.6). KSHV virions assemble within the nucleus and have a multi-step egress mechanism that includes budding through the nuclear membrane (Mettenleiter et al., 2009). This posed an interesting question of how a nucleoporin was able to inhibit the final stage of egress at the plasma membrane. Serendipitously, work in 2016 highlighted the role of KSHV ORF10, a delayed early lytic protein, that selectively sequesters certain cellular mRNAs in the nucleus during lytic infection through interacting with RNA export adaptor Rae1 (Gong et al., 2016). One cellular transcript that was specifically retained encoded the cellular protein CHMP7, a member of the ESCRT-III family (Horii et al., 2006). ESCRT-III or endosomal sorting complexes

203

required for transport is a cellular protein complex involved in a variety of membrane remodelling processes within cells including the sorting of multivesicular bodies (MVB), membrane abscission during necroptosis, cytokinesis and formation of the nuclear pore complex (Guizetti, Schermelleh, Jana, et al., 2011; Webster et al., 2014; Gong et al., 2017). The nuclear retention of CHMP7 mRNA was confirmed by qRT-PCR of subcellular fractions and analysis of existing whole cell quantitative proteomic data showed a 100-fold reduction in CHMP7 protein levels at 24 h after the induction of KSHV lytic replication (Figure 4.7a and Figure 4.8a). This retention during lytic replication was shown to be ablated by Nup98 depletion by siRNA treatment and furthermore, led to increased levels of CHMP7 protein in Nup98-depleted TREx cells (Figure 4.8a). Overexpression of CHMP7 also produced a reduction in virion infectivity and led to an observable increase in viral capsid accumulation at the cell periphery (Figure 4.11b and Figure 4.12b). However, the transduction efficiency of these overexpression constructs was low (~20 %) and CHMP7 overexpression could not be confirmed in cells with viral capsid accumulation due to antibody cross-reactivity. Whilst the ESCRT-III complex acts in a variety of roles within the cell attempts to determine how CHMP7 was able to induce viral capsid accumulation at the cell periphery focused on the role of ESCRT-III in plasma membrane repair. Necroptosis is a caspase-independent form of cell death that relies on receptor-interacting serine/threonine kinase 1 (RIPK1) as its primary regulator. RIPK1 mediates necroptosis in the absence of caspase 8 activity leading to the autophosphorylation activation of the RIPK1 binding partner, RIPK3, to form the necrosome. This includes mixed-lineage kinase domain-like protein (MLKL) which is recruited by RIPK3 and phosphorylated.

MLKL then, by a poorly understood mechanism, localises to and destabilises the plasma membrane (Reviewed in (Weinlich et al., 2017)). It has been shown that ESCRT-III plays a role downstream of MLKL in shedding damaged sections of the plasma membrane. This helps maintain plasma membrane integrity so that dying cells are able to secrete cytokines and other signalling molecules into their microenvironment (Gong et al., 2017). It has been proposed that KSHV may indirectly induce necroptosis within infected cells through reduced caspase-8 activity (Feoktistova et al., 2012). Therefore, CHMP7 could be sequestered by KSHV ORF10 to prevent it recruiting ESCRT-III to the plasma membrane during late lytic replication so as not to disrupt normal viral egress. However, this specific ESCRT-III mechanism may not be the key disrupting factor for viral infectivity. Some components of the ESCRT-III complex have been shown to be critical for successful herpesvirus egress (Crump et al., 2007; Pawliczek and Crump, 2009). Furthermore, the nuclear budding step of herpesviruses also appears to require ESCRT-III components (Lee et al., 2012; Arii et al., 2018). Therefore, the finding that KSHV specifically downregulates an ESCRT-III protein is intriguing and could relate to a more specialised role of CHMP7 such as in plasma membrane repair described above or in nuclear envelope reformation (Olmos et al., 2016). Overall, Nup98 depletion appears to disrupt KSHV lytic sequestering of a viral restriction factor CHMP7 mRNA. However, during KSHV lytic replication the targeted depletion of Nup98 does not achieve as significant a reduction in Nup98 as achieved by siRNA treatment. This suggests that KSHV specifically targets the non-pore bound fraction of Nup98 to aid with early lytic replication but does not deplete Nup98 at the NPC.

Overall, Nup98 targeting by KSHV appears to be dynamic and responsive to the alternate subcellular fractions of Nup98 within the cell (Figure 6.1). KSHV appears to require Nup98 presence at a certain level at the NPC during lytic replication in order to ensure the function of KSHV ORF10 protein and its interaction with Rae1. If Nup98 levels are depleted sufficiently, the ORF10-Rae1 interaction fails to sequester cellular mRNAs in the nucleus allowing for their continued transcription at a level greater than when Nup98 is present at the NPC. This allows for CHMP7 expression to be maintained and remain functional later during KSHV lytic replication, which may then play a role disrupting viral egress. Nevertheless, KSHV actively targets the a non-pore fraction of Nup98 through the E3 ligase activity of immediate-early protein RTA. This appears to prevent the inhibitory effect of Nup98 on transcription at the ORF50 promoter and may involve Nup98 recruiting a nucleoplasmic binding partner that represses transcription.
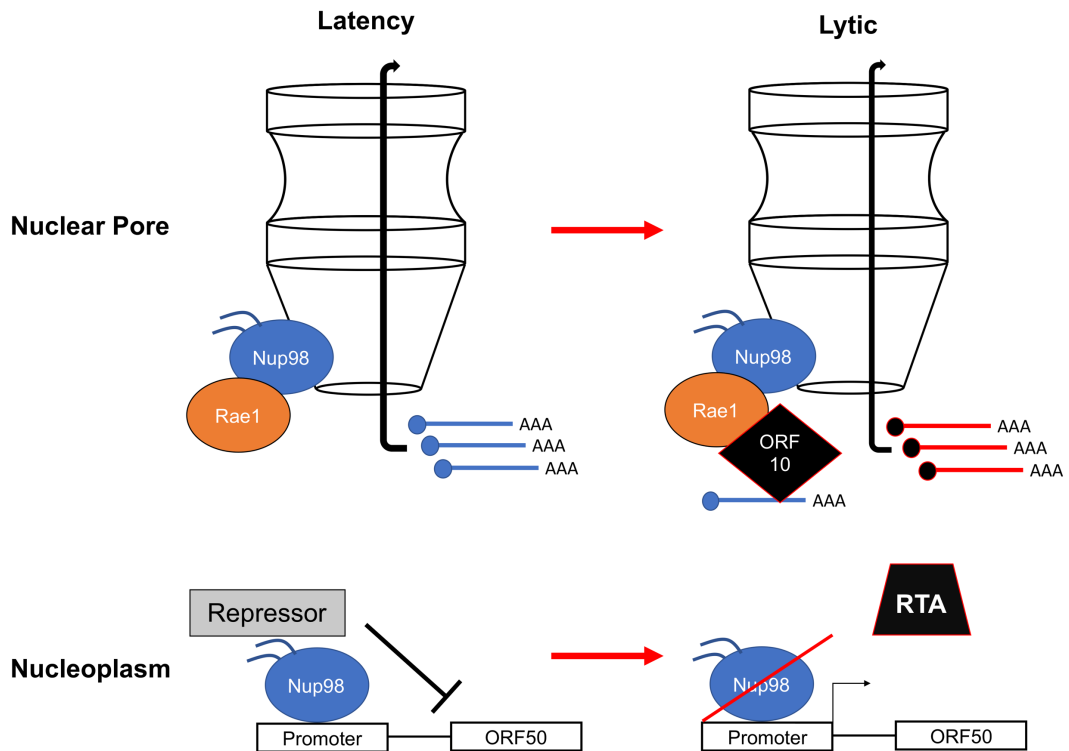
Figure 6.1 Schematic of the proposed role of Nup98 during KSHV infection. During latency Nup98 is present at the nuclear pore assisting Rae1 with mRNA export and in the nucleoplasm bound to the KSHV ORF50 promoter where it recruits repressor proteins to inhibit ORF50 transcription. On the lytic switch (red arrows) Nup98 is targeted in both pools by the virus, at the nuclear pore Nup98 is required by KSHV to anchor Rae1 to the NPC in order for KSHV ORF10 protein to sequester specific cellular mRNAs in the nucleus. In the nucleoplasm, RTA targets Nup98 for degradation helping remove repressor proteins allowing for RTA to trigger a feedback loop of ORF50 expression.

Future work should look to build on these observations through three key questions: does Nup98 bind at the ORF50 promoter, can Nup98 be overexpressed in the nucleoplasm and prevent the latent-lytic switch of KSHV, and finally do histone modifications at the ORF50 promoter depend on Nup98. The first question can be answered by continuing to use chromatin immunoprecipitation (ChIP) experiments in unreactivated and reactivated TREx cells. Initial work using a previously published Nup98 ChIP antibody were unsuccessful but future work should look to utilising the well-published 2H10 rat

207

monoclonal that was used for other Nup98 experiments in this thesis. Identification of Nup98 binding at the ORF50 promoter during KSHV latency is the first crucial step in confirming the potential negative regulatory role of Nup98 on the virus. The second question, using Nup98 overexpression constructs to repress the induction of KSHV lytic replication is more complex. As shown in previous chapters, there was no observed effect on KSHV lytic replication in TREx overexpressing GFP-Nup98 when induced to lytic replication with sodium butyrate. The difficulty of successfully inducing lytic replication without overexpressing the viral transactivator protein RTA or inducing global histone remodelling via HDACi means experiments to test for the protective effect of Nup98 should utilise alternate reactivation mechanisms. Previous work shows that KSHV lytic replication can be induced by increasing oxidative stress, hypoxia and treatment with virus-like vesicles (Davis et al., 2001; Horii et al., 2006; Li et al., 2011). Future experiments should attempt to induce KSHV lytic replication through these alternate stimuli in GFP-Nup98 overexpressing cells to characterise its potential protective effect. Finally, the question of confirming Nup98-dependent histone modifications at the ORF50 promoter will require work using ChIP for specific histone markers, with previous studies showing that during latency ORF50 exhibits H3K4me3 and H3K27me3 modifications (Günther and Grundhoff, 2010; Toth et al., 2013).

In chapter 5, the novel interactomic technique BioID was combined with TMT to create a quantitative profile of changes at the NPC during KSHV lytic infection. This built on previously established usage of BioID-nucleoporin fusion proteins that were shown to provide good coverage of the NPC (Kim et al., 2014). After difficulties establishing a good transfection efficiency and subcellular targeting of

these constructs it was decided to perform the experiments using transient transfections of TREx cells (Figure 5.3). BioID-nucleoporins were transfected into cells that were either maintained in the latent state or induced to lytic replication. The results of these experiments were by and large disappointing with minimal purification of other components of the NPC (Figure 5.4). This can be attributed to the low transfection efficiency which in conjunction with a stringent purification procedure made it difficult to harvest a high concentration of proteins. Nevertheless, the combination of BioID and TMT provide a small level of insight in changes around the nuclear envelope microenvironment during KSHV lytic infection. During lytic infection there was an observed increase in the level of proteins associated with the ribonucleoprotein complex, including preribosomal components, in the vicinity of the nuclear envelope. This potentially points to increased transport of ribosomal components during KSHV lytic infection which could relate to the concept of virally induced specialised ribosomes, which has been proposed to occur during KSHV lytic infection (Bussey et al., 2018).

Future efforts to utilise BioID to characterise changes at the NPC during viral infection should focus on developing stably expressing inducible BioID-nucleoporins. Through communication with the Roux laboratory it was highlighted that their stably expressing HEK293T cell lines were selected for low BioID-nucleoporin expression levels (Personal communication). This was due to common mistargeting of the BioID-nucleoporins into the cytoplasm, typically in the annulate laemella region. Transient transfections into latently infected B cells, exhibited good nuclear envelope staining with no mistargeting however attempts to select for stably expressing cells produced strong mistargeting effects. To alleviate these problems future attempts could look to use inducible expression

209

systems to regulate BioID-nucleoporin expression to ensure the prevention of major mistargeting effects (Firat-Karalar et al., 2014). Furthermore, recent advances in developing a lentiviral BioID toolkit mean that overcoming the problem of transfection efficiency in the traditionally difficult to transfect B cell line may also be possible (Samavarchi-Tehrani et al., 2018). Finally, the use of a smaller, more efficient biotin ligase, BioID2, should also be considered. This smaller ligase requires less biotin supplementation but achieves enhanced labelling activity (Kim et al., 2016).

Overall, the work within this thesis expands our understanding of KSHV interactions with key cellular processes during lytic infection. This work provides enticing observations into how KSHV specifically remodels the NPC to aid its replication and highlights the importance of one specific nucleoporin, Nup98. The importance of targeting Nup98 early during KSHV lytic infection may provide a new avenue for developing therapeutics that prevent the transition to lytic infection which is a key stage in the development of KSHV-related malignancy. Furthermore, this work has highlighted how the dualistic nature of Nup98 is exploited by the virus, both by targeting its nucleoplasmic role and by requiring Nup98 at the NPC. Finally, this thesis lays out an initial attempt at using interactomic techniques to produce a more comprehensive map of viral interactions and induced changes at the nuclear pore complex and provides a guide on how to develop this approach further.

References

Abelson, H.T. and Smith, G.H. 1970. Nuclear pores: the pore-annulus relationship in thin section. *Journal of Ultrasructure Research*. **30**(5–6), pp.558–588.

Akula, S.M., Pramod, N.P., Wang, F.Z. and Chandran, B. 2002. Integrin α3β1 (CD 49c/29) is a cellular receptor for Kaposi's sarcoma-associated herpesvirus (KSHV/HHV-8) entry into the target cells. *Cell*. **108**(3), pp.407–419.

Allen, N.P.C., Huang, L., Burlingame, A. and Rexach, M. 2001. Proteomic Analysis of Nucleoporin Interacting Proteins. *Journal of Biological Chemistry*. **276**(31), pp.29268–29274.

Alonso Y Adell, M. and Teis, D. 2011. Assembly and disassembly of the ESCRT-III membrane scission complex. *FEBS Letters*. **585**(20), pp.3191–3196.

Andersen, K.R., Onischenko, E., Tang, J.H., Kumar, P., Chen, J.Z., Ulrich, A., Liphardt, J.T., Weis, K. and Schwartz, T.U. 2013. Scaffold nucleoporins Nup188 and Nup192 share structural and functional properties with nuclear transport receptors. *eLife*. **2013**(2), pp.1–20.

Anderson, N.G. and Anderson, L. 1982. The Human Protein Index. *Clinical chemistry*. [Online]. **28**(4 Pt 2), pp.739–48. Available from: http://www.ncbi.nlm.nih.gov/pubmed/7074867.

Anderson, N.L. and Anderson, N.G. 1998. Proteome and proteomics: new technologies, new concepts, and new words. *Electrophoresis*. [Online]. **19**(11), pp.1853–1861. Available from: http://www.ncbi.nlm.nih.gov/pubmed/9740045.

von Appen, A. and Beck, M. 2015. Structure Determination of the Nuclear Pore Complex with Three-Dimensional Cryo electron Microscopy. *Journal of Molecular Biology*. [Online]. (2015), pp.1–10. Available from: http://dx.doi.org/10.1016/j.jmb.2016.01.004.

Von Appen, A., Kosinski, J., Sparks, L., Ori, A., DiGuilio, A.L., Vollmer, B., Mackmull, M.T., Banterle, N., Parca, L., Kastritis, P., Buczak, K., Mosalaganti, S., Hagen, W., Andres-Pons, A., Lemke, E.A., Bork, P., Antonin, W., Glavy, J.S., Bui, K.H. and Beck, M. 2015. In situ structural analysis of the human nuclear pore complex. *Nature*. **526**(7571), pp.140–143.

Argiropoulos, B. and Humphries, R.K. 2007. Hox genes in hematopoiesis and leukemogenesis. *Oncogene*. **26**(47), pp.6766–6776.

Arias, C., Weisburd, B., Stern-Ginossar, N., Mercier, A., Madrid, A.S., Bellare, P., Holdorf, M., Weissman, J.S. and Ganem, D. 2014. KSHV 2.0: a comprehensive annotation of the Kaposi's sarcoma-associated herpesvirus genome using next-generation sequencing reveals novel genomic and functional features. *PLoS pathogens*. [Online]. **10**(1), p.e1003847. [Accessed 17 June 2014]. Available from: http://www.pubmedcentral.nih.gov/articlerender.fcgi?artid=3894221&tool=pmcentrez&rendertype=abstract.

Arii, J., Watanabe, M., Maeda, F., Tokai-Nishizumi, N., Chihara, T., Miura, M., Maruzuru, Y., Koyanagi, N., Kato, A. and Kawaguchi, Y. 2018. ESCRT-III mediates budding across the inner nuclear membrane and regulates its integrity. *Nature Communications*. [Online]. **9**(1). Available from: http://dx.doi.org/10.1038/s41467-018-05889-9.

Arora, P.S., Yamagiwa, H., Srivastava, A., Bolander, M.E. and Sarkar, G. 2005. Comparative evaluation of two two-dimensional gel electrophoresis image analysis software applications using synovial fluids from patients with joint disease. *Journal of Orthopaedic Science*. **10**(2), pp.160–166.

Asally, M., Yasuda, Y., Oka, M., Otsuka, S., Yoshimura, S.H., Takeyasu, K. and Yoneda, Y. 2011. Nup358, a nucleoporin, functions as a key determinant of the nuclear pore complex structure remodeling during skeletal myogenesis. *FEBS Journal*. **278**(4), pp.610–621.

Bachi, A., Braun, I.C., Rodrigues, J.P., Panté, N., Ribbeck, K., von Kobbe, C., Kutay, U., Wilm, M., Görlich, D., Carmo-Fonseca, M. and Izaurralde, E. 2000. The C-terminal domain of TAP interacts with the nuclear pore complex and promotes export of specific CTE-bearing RNA substrates. *RNA (New York, N.Y.)*. [Online]. **6**(1), pp.136–58. [Accessed 10 October 2014]. Available from: http://www.pubmedcentral.nih.gov/articlerender.fcgi?artid=1369901&tool=pmcentrez&rendertype=abstract.

Baer, R., Bankier, A.T., Biggin, M.D., Deininger, P.L., Farrell, P.J., Gibson, T.J., Hatfull, G., Hudson, G.S., Satchwell, S.C., Séguin, C., Tuffnell, P.S. and Barrell, B.G. 1984. DNA sequence and expression of the B95-8 Epstein—Barr virus genome. *Nature*. [Online]. **310**(5974), pp.207–211. Available from: http://www.nature.com/nature/journal/v310/n5974/abs/310207a0.html%5Cn http://www.ncbi.nlm.nih.gov/pubmed/6087149.

Bai, X.T., Gu, B.W., Yin, T., Niu, C., Xi, X.D., Zhang, J., Chen, Z. and Chen, S.J. 2006. Trans-repressive effect of NUP98-PMX1 on PMX1-regulated c-FOS gene through recruitment of histone deacetylase 1 by FG repeats. *Cancer Research*. **66**(9), pp.4584–4590.

Balistreri, G., Viiliäinen, J., Turunen, M., Diaz, R., Lyly, L., Pekkonen, P., Rantala, J., Ojala, K., Sarek, G., Teesalu, M., Denisova, O., Peltonen, K., Julkunen, I., Varjosalo, M., Kainov, D., Kallioniemi, O., Laiho, M., Taipale, J., Hautaniemi, S. and Ojala, P.M. 2016. Oncogenic Herpesvirus Utilizes Stress-Induced Cell Cycle Checkpoints for Efficient Lytic Replication. *PLoS Pathogens*. **12**(2), pp.1–26.

Ballestas, M.E., Chatis, P.A. and Kaye, K.M. 1999. Efficient persistence of extrachromosomal KSHV DNA mediated by latency-associated nuclear antigen. *Science*. [Online]. **284**(5414), pp.641–644. Available from: http://www.ncbi.nlm.nih.gov/pubmed/10213686.

Bardina, M. V., Lidsky, P. V., Sheval, E. V., Fominykh, K. V., van Kuppeveld, F.J.M., Polyakov, V.Y. and Agol, V.I. 2009. Mengovirus-Induced Rearrangement of the Nuclear Pore Complex: Hijacking Cellular Phosphorylation Machinery. *Journal of Virology*. [Online]. **83**(7), pp.3150–3161. Available from: http://jvi.asm.org/cgi/doi/10.1128/JVI.01456-08.

Basel-Vanagaite, L., Muncher, L., Straussberg, R., Pasmanik-Chor, M., Yahav, M., Rainshtein, L., Walsh, C.A., Magal, N., Taub, E., Drasinover, V., Shalev,

H., Attia, R., Rechavi, G., Simon, A.J. and Shohat, M. 2006. Mutated nup62 causes autosomal recessive infantile bilateral striatal necrosis. *Annals of Neurology.* **60**(2), pp.214–222.

Bastos, R., Ribas de Pouplana, L., Enarson, M., Bodoor, K. and Burke, B. 1997. Nup84, a novel nucleoporin that is associated with CAN/Nup214 on the cytoplasmic face of the nuclear pore complex. *The Journal of cell biology.* [Online]. **137**(5), pp.989–1000. Available from: http://www.pubmedcentral.nih.gov/articlerender.fcgi?artid=2136229&tool=pmcentrez&rendertype=abstract.

Bayliss, R., Littlewood, T. and Stewart, M. 2000. Structural basis for the interaction between FxFG nucleoporin repeats and importin-β in nuclear trafficking. *Cell.* **102**(1), pp.99–108.

Beck, M., Förster, F., Ecke, M., Plitzko, J.M., Melchior, F., Gerisch, G., Baumeister, W. and Medalia, O. 2004a. Nuclear pore complex structure and dynamics revealed by cryoelectron tomography. *Science (New York, N.Y.).* [Online]. **306**(5700), pp.1387–90. [Accessed 10 January 2015]. Available from: http://www.ncbi.nlm.nih.gov/pubmed/15514115.

Beck, M., Förster, F., Ecke, M., Plitzko, J.M., Melchior, F., Gerisch, G., Baumeister, W. and Medalia, O. 2004b. Nuclear pore complex structure and dynamics revealed by cryoelectron tomography. *Science (New York, N.Y.).* [Online]. **306**(5700), pp.1387–90. Available from: http://www.ncbi.nlm.nih.gov/pubmed/15514115.

Belov, G.A., Lidsky, P. V, Mikitas, O. V, Egger, D., Lukyanov, K.A., Bienz, K. and Agol, V.I. 2004. Bidirectional increase in permeability of nuclear envelope upon poliovirus infection and accompanying alterations of nuclear pores. *Journal of virology.* [Online]. **78**(18), pp.10166–77. [Accessed 1 February 2014]. Available from: http://www.pubmedcentral.nih.gov/articlerender.fcgi?artid=514989&tool=pmcentrez&rendertype=abstract.

Beral, V., Peterman, T.A., Berkelman, R.L. and Jaffe, H.W. 1990. Kaposi's sarcoma among persons with AIDS: a sexually transmitted infection? *The Lancet.* [Online]. **335**(8682), pp.123–128. Available from: http://linkinghub.elsevier.com/retrieve/pii/014067369090001L.

Blevins, M.B., Smith, A.M., Phillips, E.M. and Powers, M. a. 2003. Complex formation among the RNA export proteins Nup98, Rae1/Gle2, and TAP. *Journal of Biological Chemistry.* **278**(23), pp.20979–20988.

Borah, S., Darricarrère, N., Darnell, A., Myoung, J. and Steitz, J.A. 2011. A viral nuclear noncoding RNA binds re-localized poly(A) binding protein and is required for late KSHV gene expression. *PLoS Pathogens.* **7**(10).

Boutell, Sadis and Everett 2002. Herpes simplex virus type 1 immediate-early protein ICP0 and is isolated RING finger domain act as ubiquitin E3 ligases in vitro. *Journal of virology.* [Online]. **76**(2), pp.841–850. Available from: http://www.ncbi.nlm.nih.gov/entrez/query.fcgi?db=pubmed&cmd=Retrieve&dopt=AbstractPlus&list_uids=11752173%5Cnpapers://9ab86218-1562-4840-bbbd-f8da4bd40616/Paper/p233.

Bower, M., Nelson, M., Young, A.M., Thirlwell, C., Newsom-Davis, T., Mandalia, S., Dhillon, T., Holmes, P., Gazzard, B.G. and Stebbing, J. 2005. Immune Reconstitution Inflammatory Syndrome Associated With Kaposi's Sarcoma.

Journal of Clinical Oncology. [Online]. **23**(22), pp.5224–5228. Available from: http://ascopubs.org/doi/10.1200/JCO.2005.14.597.

Brack, A.R., Klupp, B.G., Granzow, H., Tirabassi, R., Enquist, L.W. and Mettenleiter, T.C. 2000. Role of the cytoplasmic tail of pseudorabies virus glycoprotein E in virion formation. *Journal of virology*. [Online]. **74**(9), pp.4004–16. Available from: http://www.ncbi.nlm.nih.gov/pubmed/10756012%5Cnhttp://www.pubmedce ntral.nih.gov/articlerender.fcgi?artid=PMC111914.

Brandt, S.J., Bodine, D.M., Dunbar, C.E. and Nienhuis, A.W. 1990. Dysregulated Interleukin 6 Expression Produces Resembling Castleman ' s Disease in Mice Syndrome IL-6 Coding Sequence. *Journal of clinical investigation*. **86**(August), pp.592–599.

Brennan, C.M., Gallouzi, I.E. and Steitz, J.A. 2000. Protein ligands to HuR modulate its interaction with target mRNAs in vivo. *Journal of Cell Biology*. **151**(1), pp.1–13.

Buchwalter, A.L., Liang, Y. and Hetzer, M.W. 2014. Nup50 is required for cell differentiation and exhibits transcription-dependent dynamics. *Molecular Biology of the Cell*. [Online]. **25**(16), pp.2472–2484. Available from: http://www.molbiolcell.org/cgi/doi/10.1091/mbc.E14-04-0865.

Bui, K.H., von Appen, A., DiGuilio, A.L., Ori, A., Sparks, L., Mackmull, M.-T., Bock, T., Hagen, W., Andrés-Pons, A., Glavy, J.S. and Beck, M. 2013. Integrated Structural Analysis of the Human Nuclear Pore Complex Scaffold. *Cell*. [Online]. **155**(6), pp.1233–1243. [Accessed 5 December 2013]. Available from: http://linkinghub.elsevier.com/retrieve/pii/S0092867413014165.

Burke, B. and Roux, K.J. 2009. Nuclei Take a Position: Managing Nuclear Location. *Developmental Cell*. [Online]. **17**(5), pp.587–597. Available from: http://dx.doi.org/10.1016/j.devcel.2009.10.018.

Burýsek, L. and Pitha, P.M. 2001. Latently expressed human herpesvirus 8-encoded interferon regulatory factor 2 inhibits double-stranded RNA-activated protein kinase. *Journal of virology*. [Online]. **75**(5), pp.2345–52. Available from: http://www.pubmedcentral.nih.gov/articlerender.fcgi?artid=114818&tool=pm centrez&rendertype=abstract.

Bussey, K.A., Lau, U., Schumann, S., Gallo, A., Osbelt, L., Stempel, M., Arnold, C., Wissing, J., Gad, H.H., Hartmann, R., Brune, W., Jänsch, L., Whitehouse, A. and Brinkmann, M.M. 2018. *The interferon-stimulated gene product oligoadenylate synthetase-like protein enhances replication of Kaposi's sarcoma-associated herpesvirus (KSHV) and interacts with the KSHV ORF20 protein*.

Cai, X., Lu, S., Zhang, Z., Gonzalez, C.M., Damania, B. and Cullen, B.R. 2005. Kaposi's sarcoma-associated herpesvirus expresses an array of viral microRNAs in latently infected cells. *Proc Natl Acad Sci U S A*. [Online]. **102**(15), pp.5570–5575. Available from: http://www.ncbi.nlm.nih.gov/pubmed/15800047.

Callan, H.G. and Tomlin, S.G. 1950. Experimental studies on amphibian oocyte nuclei. I. Investigation of the structure of the nuclear membrane by means of the electron microscope. *Proceedings of the Royal Society of London. Series*

B, Biological sciences. [Online]. **137**(888), pp.367–78. Available from: http://www.ncbi.nlm.nih.gov/pubmed/14786306.

Cannon, M. 2007. The KSHV and Other Human Herpesviral G Protein-Coupled Receptors *In*: C. Boshoff and R. Weiss, eds. *Kaposi Sarcoma Herpesvirus: New Perspectives SE - 5* [Online]. Current Topics in Microbiology and Immunology. Springer Berlin Heidelberg, pp.137–156. Available from: http://dx.doi.org/10.1007/978-3-540-34344-8_5.

Capelson, M., Liang, Y., Schulte, R., Mair, W., Wagner, U. and Hetzer, M.W. 2010. Chromatin-bound nuclear pore components regulate gene expression in higher eukaryotes. *Cell*. [Online]. **140**(3), pp.372–83. [Accessed 15 December 2013]. Available from: http://www.pubmedcentral.nih.gov/articlerender.fcgi?artid=2821818&tool=pmcentrez&rendertype=abstract.

Capitanio, J.S., Montpetit, B. and Wozniak, R.W. 2017. Human Nup98 regulates the localization and activity of DExH / D-box helicase. *eLife*. **98**, pp.1–39.

Casola, S., Otipoby, K.L., Alimzhanov, M., Humme, S., Uyttersprot, N., Kutok, J.L., Carroll, M.C. and Rajewsky, K. 2004. B cell receptor signal strength determines B cell fate. *Nature Immunology*. **5**(3), pp.317–327.

Cautain, B., Hill, R., de Pedro, N. and Link, W. 2014. Components and regulation of nuclear transport processes. *The FEBS journal*. [Online]. [Accessed 3 December 2014]. Available from: http://www.ncbi.nlm.nih.gov/pubmed/25429850.

Cerveny, K.L., Cavodeassi, F., Turner, K.J., de Jong-Curtain, T.A., Heath, J.K. and Wilson, S.W. 2010. The zebrafish flotte lotte mutant reveals that the local retinal environment promotes the differentiation of proliferating precursors emerging from their stem cell niche. *Development*. [Online]. **137**(13), pp.2107–2115. Available from: http://dev.biologists.org/cgi/doi/10.1242/dev.047753.

Cesarman, E., Chang, Y., Moore, P.S., Said, J.W. and Knowles, D.M. 1995. Kaposi's sarcoma-associated herpesvirus-like DNA sequences in AIDS-related body-cavity-based lymphomas. *The New England journal of medicine*. [Online]. **332**(18), pp.1186–91. Available from: http://www.ncbi.nlm.nih.gov/pubmed/7700311.

Cesarman, E. and Knowles, D.M. 1999. The role of Kaposi's sarcoma-associated herpesvirus (KSHV/HHV-8) in lymphoproliferative diseases. *Seminars in cancer biology*. [Online]. **9**(3), pp.165–74. Available from: http://www.ncbi.nlm.nih.gov/pubmed/10343068.

Chakraborty, S., Veettil, M.V. and Chandran, B. 2012. Kaposi's Sarcoma Associated Herpesvirus Entry into Target Cells. *Frontiers in microbiology*. [Online]. **3**(January), p.6. [Accessed 5 January 2015]. Available from: http://www.pubmedcentral.nih.gov/articlerender.fcgi?artid=3262161&tool=pmcentrez&rendertype=abstract.

Chang, C.-W., Lee, C.-P., Huang, Y.-H., Yang, P.-W., Wang, J.-T. and Chen, M.-R. 2012. Epstein-Barr virus protein kinase BGLF4 targets the nucleus through interaction with nucleoporins. *Journal of virology*. [Online]. **86**(15), pp.8072–85. [Accessed 5 October 2014]. Available from: http://www.pubmedcentral.nih.gov/articlerender.fcgi?artid=3421656&tool=pmcentrez&rendertype=abstract.

Chang, C.-W., Lee, C.-P., Su, M.-T., Tsai, C.-H. and Chen, M.-R. 2015. BGLF4 Kinase Modulates the Structure and Transport Preference of the Nuclear Pore Complex To Facilitate Nuclear Import of Epstein-Barr Virus Lytic Proteins L. Hutt-Fletcher, ed. *Journal of Virology*. [Online]. **89**(3), pp.1703–1718. Available from: http://www.pubmedcentral.nih.gov/articlerender.fcgi?artid=4300756&tool=pmcentrez&rendertype=abstract.

Chang, J.T., Schmid, M.F., Rixon, F.J. and Chiu, W. 2007. Electron Cryotomography Reveals the Portal in the Herpesvirus Capsid. *Journal of Virology*. [Online]. **81**(4), pp.2065–2068. Available from: http://jvi.asm.org/cgi/doi/10.1128/JVI.02053-06.

Chang, P., Shedd, D., Gradoville, L., Chen, L., Chang, J., Miller, G. and Cho, M. 2002. Open Reading Frame 50 Protein of Kaposi ' s Sarcoma-Associated Herpesvirus Directly Activates the Viral PAN and K12 Genes by Binding to Related Response Elements Open Reading Frame 50 Protein of Kaposi ' s Sarcoma-Associated Herpesvirus Directly Activates. . **76**(7), pp.3168–3178.

Chang, P.J., Shedd, D. and Miller, G. 2005. Two subclasses of Kaposi's sarcoma-associated herpesvirus lytic cycle promoters distinguished by open reading frame 50 mutant proteins that are deficient in binding to DNA. *J Virol*. [Online]. **79**(14), pp.8750–8763. Available from: http://www.ncbi.nlm.nih.gov/pubmed/15994769.

Chang, Y., Cesarman, E., Pessin, M.S., Lee, F., Culpepper, J., Knowles, D.M. and Moore, P.S. 1994. Identification of herpesvirus-like DNA sequences in AIDS-associated Kaposi's sarcoma. *Science (New York, N.Y.)*. [Online]. **266**(5192), pp.1865–9. [Accessed 31 December 2014]. Available from: http://www.ncbi.nlm.nih.gov/pubmed/7997879.

Chapman-Smith, A. and Cronan, J.E. 1999. The enzymatic biotinylation of proteins: A post-translational modification of exceptional specificity. *Trends in Biochemical Sciences*. **24**(9), pp.359–363.

Chen, J., Huang, S. and Chen, Z. 2010. Human cellular protein nucleoporin hNup98 interacts with influenza A virus NS2/nuclear export protein and overexpression of its GLFG repeat domain can inhibit virus propagation. *Journal of General Virology*. **91**(10), pp.2474–2484.

Chen, Y.-B., Rahemtullah, A. and Hochberg, E. 2007. Primary Effusion Lymphoma. *The Oncologist*. [Online]. **12**(5), pp.569–576. Available from: http://theoncologist.alphamedpress.org/cgi/doi/10.1634/theoncologist.12-5-569.

Chiou, C.-J., Poole, L.J., Kim, P.S., Ciufo, D.M., Cannon, J.S., ap Rhys, C.M., Alcendor, D.J., Zong, J.-C., Ambinder, R.F. and Hayward, G.S. 2002. Patterns of gene expression and a transactivation function exhibited by the vGCR (ORF74) chemokine receptor protein of Kaposi's sarcoma-associated herpesvirus. *Journal of virology*. [Online]. **76**(7), pp.3421–39. Available from: http://www.pubmedcentral.nih.gov/articlerender.fcgi?artid=136009&tool=pmcentrez&rendertype=abstract.

Cho, A.R., Yang, K.J., Bae, Y., Young, Y.B., Kim, E., Lee, H., Jeong, K.K., Park, W., Rhim, H., Soo, Y.C., Imanaka, T., Moon, S., Yoon, J. and Sungjoo, K.Y. 2009. Tissue-specific expression and subcellular localization of ALADIN, the absence of which causes human triple A syndrome. *Experimental and*

Molecular Medicine. **41**(6), pp.381–386.

Choe, L., D'Ascenzo, M., Relkin, N.R., Pappin, D., Ross, P., Williamson, B., Guertin, S., Pribil, P. and Lee, K.H. 2007. 8-Plex quantitation of changes in cerebrospinal fluid protein expression in subjects undergoing intravenous immunoglobulin treatment for Alzheimer's disease. *Proteomics*. **7**(20), pp.3651–3660.

Choi-Rhee, E., Schulman, H. and Cronan, J.E. 2004. Promiscuous protein biotinylation by Escherichia coli biotin protein ligase. *Protein science : a publication of the Protein Society*. [Online]. **13**(11), pp.3043–50. Available from: http://www.ncbi.nlm.nih.gov/pubmed/15459338%5Cnhttp://www.pubmedce ntral.nih.gov/articlerender.fcgi?artid=PMC2286582.

Chook, Y.M. and Blobel, G. 1999. Structure of the nuclear transport complex karyopherin-beta2-Ran x GppNHp. *Nature*. [Online]. **399**(6733), pp.230–7. Available from: http://www.ncbi.nlm.nih.gov/pubmed/10353245.

Cingolani, G., Petosa, C., Weis, K. and Müller, C.W. 1999. Structure of importin-beta bound to the IBB domain of importin-alpha. *Nature*. **399**, pp.221–229.

Cohen, A., Brodie, C. and Sarid, R. 2006. An essential role of ERK signalling in TPA-induced reactivation of Kaposi's sarcoma-associated herpesvirus. *Journal of General Virology*. **87**(4), pp.795–802.

Conn, K.L. and Schang, L.M. 2013. Chromatin dynamics during lytic infection with herpes simplex virus 1. *Viruses*. **5**(7), pp.1758–1786.

Connolly, S.A., Jackson, J.O., Jardetzky, T.S. and Longnecker, R. 2011. Fusing structure and function: A structural view of the herpesvirus entry machinery. *Nature Reviews Microbiology*. [Online]. **9**(5), pp.369–381. Available from: http://dx.doi.org/10.1038/nrmicro2548.

Conti, E., Müller, C.W. and Stewart, M. 2006. Karyopherin flexibility in nucleocytoplasmic transport. *Current Opinion in Structural Biology*. **16**(2), pp.237–244.

Copeland, A.M., Newcomb, W.W. and Brown, J.C. 2009. Herpes Simplex Virus Replication: Roles of Viral Proteins and Nucleoporins in Capsid-Nucleus Attachment. *Journal of Virology*. [Online]. **83**(4), pp.1660–1668. Available from: http://jvi.asm.org/cgi/doi/10.1128/JVI.01139-08.

Cordes, V.C., Reidenbach, S., Rackwitz, H.R. and Franke, W.W. 1997. Identification of protein p270/Tpr as a constitutive component of the nuclear pore complex-attached intranuclear filaments. *Journal of Cell Biology*. **136**(3), pp.515–529.

Coscoy, L. 2007. Immune evasion by Kaposi's sarcoma-associated herpesvirus. *Nature Reviews Immunology*. **7**(5), pp.391–401.

Coyle, J.H., Bor, Y.C., Rekosh, D. and Hammarskjold, M.L. 2011. The Tpr protein regulates export of mRNAs with retained introns that traffic through the Nxf1 pathway. *Rna*. **17**(7), pp.1344–1356.

Crisp, M., Liu, Q., Roux, K., Rattner, J.B., Shanahan, C., Burke, B., Stahl, P.D. and Hodzic, D. 2006. Coupling of the nucleus and cytoplasm: role of the LINC complex. *The Journal of cell biology*. **172**(1), pp.41–53.

Cronshaw, J.M., Krutchinsky, A.N., Zhang, W., Chait, B.T. and Matunis, M.J. 2002. Proteomic analysis of the mammalian nuclear pore complex. *The*

Journal of cell biology. [Online]. **158**(5), pp.915–27. [Accessed 31 January 2014]. Available from: http://www.pubmedcentral.nih.gov/articlerender.fcgi?artid=2173148&tool=pmcentrez&rendertype=abstract.

Crump, C.M., Yates, C. and Minson, T. 2007. Herpes Simplex Virus Type 1 Cytoplasmic Envelopment Requires Functional Vps4. *Journal of Virology*. [Online]. **81**(14), pp.7380–7387. Available from: http://jvi.asm.org/cgi/doi/10.1128/JVI.00222-07.

Culjkovic, B., Topisirovic, I., Skrabanek, L., Ruiz-Gutierrez, M. and Borden, K.L.B. 2006. eIF4E is a central node of an RNA regulon that governs cellular proliferation. *Journal of Cell Biology*. **175**(3), pp.415–426.

Cullen, B.R. 2003. Nuclear mRNA export: insights from virology. *Trends in biochemical sciences*. [Online]. **28**(8), pp.419–24. [Accessed 19 November 2014]. Available from: http://www.ncbi.nlm.nih.gov/pubmed/12932730.

Cushman, I., Palzkill, T. and Moore, M.S. 2006. Using peptide arrays to define nuclear carrier binding sites on nucleoporins. *Methods*. **39**(4), pp.329–341.

D'Angelo, M. a, Gomez-Cavazos, J.S., Mei, A., Lackner, D.H. and Hetzer, M.W. 2012. A change in nuclear pore complex composition regulates cell differentiation. *Developmental cell*. [Online]. **22**(2), pp.446–58. [Accessed 15 January 2014]. Available from: http://www.pubmedcentral.nih.gov/articlerender.fcgi?artid=3288503&tool=pmcentrez&rendertype=abstract.

Dasso, M. and Pu, R.T. 1998. Nuclear transport: run by Ran? *American journal of human genetics*. [Online]. **63**(2), pp.311–6. [Accessed 21 January 2014]. Available from: http://www.pubmedcentral.nih.gov/articlerender.fcgi?artid=1377330&tool=pmcentrez&rendertype=abstract.

Davie, J.R. 2003. Inhibition of histone deacetylase activity by butyrate. *The Journal of nutrition*. [Online]. **133**(7 Suppl), p.2485S–2493S. Available from: http://www.ncbi.nlm.nih.gov/pubmed/12840228.

Davis, D.A., Rinderknecht, A.S., Zoeteweij, J.P., Aoki, Y., Read-Connole, E.L., Tosato, G., Blauvelt, A. and Yarchoan, R. 2001. Hypoxia induces lytic replication of Kaposi sarcoma-associated herpesvirus. *Blood*. [Online]. **97**(10), pp.3244–50. [Accessed 31 December 2014]. Available from: http://www.ncbi.nlm.nih.gov/pubmed/11342455.

Davis, L.I. and Blobel, G. 1986. Identification and characterization of a nuclear pore complex protein. *Cell*. [Online]. **45**(5), pp.699–709. Available from: http://www.ncbi.nlm.nih.gov/pubmed/3518946.

Davison, A.J. 2002. Evolution of the herpesviruses. *Veterinary Microbiology*. **86**(1–2), pp.69–88.

Davison, A.J. 2010. Herpesvirus systematics. *Veterinary Microbiology*. [Online]. **143**(1), pp.52–69. Available from: http://dx.doi.org/10.1016/j.vetmic.2010.02.014.

DeGrasse, J.A., DuBois, K.N., Devos, D., Siegel, T.N., Sali, A., Field, M.C., Rout, M.P. and Chait, B.T. 2009. Evidence for a shared nuclear pore complex architecture that is conserved from the last common eukaryotic ancestor. *Molecular & cellular proteomics : MCP*. [Online]. **8**(9), pp.2119–30.

[Accessed 21 December 2014]. Available from: http://www.ncbi.nlm.nih.gov/pubmed/10.

Delphin, C., Guan, T., Melchior, F. and Gerace, L. 1997. RanGTP targets p97 to RanBP2, a filamentous protein localized at the cytoplasmic periphery of the nuclear pore complex. *Molecular biology of the cell*. [Online]. **8**(12), pp.2379–90. Available from: http://www.pubmedcentral.nih.gov/articlerender.fcgi?artid=25714&tool=pmc entrez&rendertype=abstract.

Deng, B., O'Connor, C.M., Kedes, D.H. and Zhou, Z.H. 2007. Direct Visualization of the Putative Portal in the Kaposi's Sarcoma-Associated Herpesvirus Capsid by Cryoelectron Tomography. *Journal of Virology*. [Online]. **81**(7), pp.3640–3644. Available from: http://jvi.asm.org/cgi/doi/10.1128/JVI.02254-06.

Deng, H., Song, M.J., Chu, J.T. and Sun, R. 2002. Transcriptional regulation of the interleukin-6 gene of human herpesvirus 8 (Kaposi's sarcoma-associated herpesvirus). *J Virol*. [Online]. **76**(16), p.8252–64. Available from: http://www.ncbi.nlm.nih.gov/htbin-post/Entrez/query?db=m&form=6&dopt=r&uid=12134031.

Denning, D.P. and Rexach, M.F. 2007. Rapid Evolution Exposes the Boundaries of Domain Structure and Function in Natively Unfolded FG Nucleoporins. *Molecular & Cellular Proteomics*. [Online]. **6**(2), pp.272–282. Available from: http://www.mcponline.org/lookup/doi/10.1074/mcp.M600309-MCP200.

Dephoure, N. and Gygi, S.P. 2012. Hyperplexing: A method for higher-order multiplexed quantitative proteomics provides a map of the dynamic response to rapamycin in yeast. *Science Signaling*. **5**(217), pp.1–9.

Deshmane, S.L. and Fraser, N.W. 1989. During latency, herpes simplex virus type 1 DNA is associated with nucleosomes in a chromatin structure. *Journal of virology*. [Online]. **63**(2), pp.943–7. Available from: http://www.ncbi.nlm.nih.gov/pubmed/2536115.

van Deursen, J., Boer, J., Kasper, L. and Grosveld, G. 1996. G2 arrest and impaired nucleocytoplasmic transport in mouse embryos lacking the proto-oncogene CAN/Nup214. *The EMBO journal*. [Online]. **15**(20), pp.5574–83. Available from: http://www.pubmedcentral.nih.gov/articlerender.fcgi?artid=452302&tool=pm centrez&rendertype=abstract.

Dezube, B.J. 1996. Clinical presentation and natural history of AIDS--related Kaposi's sarcoma. *Hematology/oncology clinics of North America*. [Online]. **10**(5), pp.1023–9. Available from: http://www.ncbi.nlm.nih.gov/pubmed/8880194.

Dijkstra, M., Vonk, R.J. and Jansen, R.C. 2007. SELDI-TOF mass spectra: A view on sources of variation. *Journal of Chromatography B: Analytical Technologies in the Biomedical and Life Sciences*. **847**(1), pp.12–23.

Dingar, D., Kalkat, M., Chan, P.K., Srikumar, T., Bailey, S.D., Tu, W.B., Coyaud, E., Ponzielli, R., Kolyar, M., Jurisica, I., Huang, A., Lupien, M., Penn, L.Z. and Raught, B. 2015. BioID identifies novel c-MYC interacting partners in cultured cells and xenograft tumors. *Journal of Proteomics*. [Online]. **118**, pp.95–111. Available from: http://dx.doi.org/10.1016/j.jprot.2014.09.029.

Dittmer, D., Lagunoff, M., Renne, R., Staskus, K., Haase, A. and Ganem, D.

1998. A cluster of latently expressed genes in Kaposi's sarcoma-associated herpesvirus. *J Virol.* [Online]. **72**(10), pp.8309–8315. Available from: http://www.ncbi.nlm.nih.gov/pubmed/9733875.

Eberle, R., Hayward, G.S. and Roizman, B. 2013. The Order Herpesvirales. *Archives of Virology.* **154**(1), pp.171–177.

Eisenhardt, N., Redolfi, J. and Antonin, W. 2014. Interaction of Nup53 with Ndc1 and Nup155 is required for nuclear pore complex assembly. *Journal of Cell Science.* [Online]. **127**(4), pp.908–921. Available from: http://jcs.biologists.org/lookup/doi/10.1242/jcs.141739.

El-Aneed, A., Cohen, A. and Banoub, J. 2009. Mass spectrometry, review of the basics: Electrospray, MALDI, and commonly used mass analyzers. *Applied Spectroscopy Reviews.* **44**(3), pp.210–230.

El-Fattah, M.A. 2017. Clinical characteristics and survival outcome of primary effusion lymphoma: A review of 105 patients. *Hematological Oncology.* **35**(4), pp.878–883.

Enninga, J., Levy, D.E., Blobel, G. and Fontoura, B.M. a 2002. Role of nucleoporin induction in releasing an mRNA nuclear export block. *Science (New York, N.Y.).* [Online]. **295**(5559), pp.1523–5. [Accessed 1 February 2014]. Available from: http://www.ncbi.nlm.nih.gov/pubmed/11809937.

Epstein, M.., Achong, B.. and Barr, Y.. 1964. Virus Particles in Cultured Lymphoblasts From Burkitt'S Lymphoma. *The Lancet.* [Online]. **283**(7335), pp.702–703. Available from: http://linkinghub.elsevier.com/retrieve/pii/S0140673664915247.

Epstein, M.A., Henle, G., Achong, B.G. and Barr, Y.M. 1965. Morphological and Biological studies on a virus in cultured lymphoblasts from Burkitt's lymphoma. *The Journal of experimental medicine.* [Online]. **121**(5), pp.761–70. Available from: http://www.pubmedcentral.nih.gov/articlerender.fcgi?artid=2138004&tool=pmcentrez&rendertype=abstract%5Cnhttp://www.jem.org/cgi/doi/10.1084/jem.121.5.761.

Farge, D., Lebbé, C., Marjanovic, Z., Tuppin, P., Mouquet, C., Peraldi, M.N., Lang, P., Hiesse, C., Antoine, C., Legendre, C., Bedrossian, J., Gagnadoux, M.F., Loirat, C., Pellet, C., Sheldon, J., Golmard, J.L., Agbalika, F. and Schulz, T.F. 1999. Human herpes virus-8 and other risk factors for Kaposi's sarcoma in kidney transplant recipients. Groupe Cooperatif de Transplantation d' Ile de France (GCIF). *Transplantation.* [Online]. **67**(9), pp.1236–42. Available from: http://www.ncbi.nlm.nih.gov/pubmed/10342315.

Farnsworth, A., Goldsmith, K. and Johnson, D.C.D.C.D.C. 2003. Herpes simplex virus glycoproteins gD and gE/gI serve essential but redundant functions during acquisition of the virion envelope in the cytoplasm. *Journal of virology.* **77**(15), pp.8481–8494.

Farnsworth, A., Wisner, T.W., Webb, M., Roller, R., Cohen, G., Eisenberg, R. and Johnson, D.C. 2007. Herpes simplex virus glycoproteins gB and gH function in fusion between the virion envelope and the outer nuclear membrane. *Proceedings of the National Academy of Sciences.* [Online]. **104**(24), pp.10187–10192. Available from: http://www.pnas.org/cgi/doi/10.1073/pnas.0703790104.

Feoktistova, M., Geserick, P., Panayotova-Dimitrova, D. and Leverkus, M. 2012. Pick your poison: the Ripoptosome, a cell death platform regulating apoptosis and necroptosis. *Cell cycle (Georgetown, Tex.)*. [Online]. **11**(3), pp.460–7. Available from: http://www.ncbi.nlm.nih.gov/pubmed/22274400.

Firat-Karalar, E.N., Rauniyar, N., Yates, J.R. and Stearns, T. 2014. Proximity interactions among centrosome components identify regulators of centriole duplication. *Current Biology*. [Online]. **24**(6), pp.664–670. Available from: http://dx.doi.org/10.1016/j.cub.2014.01.067.

Fornerod, M., van Deursen, J., van Baal, S., Reynolds, a, Davis, D., Murti, K.G., Fransen, J. and Grosveld, G. 1997. The human homologue of yeast CRM1 is in a dynamic subcomplex with CAN/Nup214 and a novel nuclear pore component Nup88. *The EMBO journal*. [Online]. **16**(4), pp.807–16. Available from: http://www.pubmedcentral.nih.gov/articlerender.fcgi?artid=1169681&tool=pmcentrez&rendertype=abstract.

Fornerod, M., Ohno, M., Yoshida, M. and Mattaj, I.W. 1997. CRM1 is an export receptor for leucine-rich nuclear export signals. *Cell*. [Online]. **90**(6), pp.1051–60. [Accessed 26 December 2014]. Available from: http://linkinghub.elsevier.com/retrieve/pii/S0092867400803712.

Forwood, J.K., Lange, A., Zachariae, U., Marfori, M., Preast, C., Grubmüller, H., Stewart, M., Corbett, A.H. and Kobe, B. 2010. Quantitative structural analysis of importin-β flexibility: Paradigm for solenoid protein structures. *Structure*. **18**(9), pp.1171–1183.

Frankel, E.B., Shankar, R., Moresco, J.J., Yates, J.R., Volkmann, N. and Audhya, A. 2017. Ist1 regulates ESCRT-III assembly and function during multivesicular endosome biogenesis in Caenorhabditis elegans embryos. *Nature Communications*. [Online]. **8**(1), pp.1–13. Available from: http://dx.doi.org/10.1038/s41467-017-01636-8.

Franks, T.M., McCloskey, A., Shokirev, M., Benner, C., Rathore, A. and Hetzer, M.W. 2017. Nup98 recruits the Wdr82-Set1A/COMPASS complex to promoters to regulate H3K4 trimethylation in hematopoietic progenitor cells. *Genes and Development*. **31**(22), pp.2222–2234.

French, M.A., Price, P. and Stone, S.F. 2004. Immune restoration disease after antiretroviral therapy. *Aids*. **18**(12), pp.1615–1627.

Frey, S. and Görlich, D. 2007. A Saturated FG-Repeat Hydrogel Can Reproduce the Permeability Properties of Nuclear Pore Complexes. *Cell*. **130**(3), pp.512–523.

Frey, S. and Görlich, D. 2009. FG/FxFG as well as GLFG repeats form a selective permeability barrier with self-healing properties. *The EMBO Journal*. [Online]. **28**(17), pp.2554–2567. [Accessed 12 January 2014]. Available from: http://www.pubmedcentral.nih.gov/articlerender.fcgi?artid=2728434&tool=pmcentrez&rendertype=abstract.

Frosst, P., Guan, T., Subauste, C., Hahn, K. and Gerace, L. 2002. Tpr is localized within the nuclear basket of the pore complex and has a role in nuclear protein export. *The Journal of Cell Biology*. [Online]. **156**(4), pp.617–630. Available from: http://www.jcb.org/lookup/doi/10.1083/jcb.200106046.

Fruehling, S. and Longnecker, R. 1997. The immunoreceptor tyrosine-based

activation motif of Epstein-Barr virus LMP2A is essential for blocking BCR-mediated signal transduction. *Virology*. **235**(2), pp.241–251.

Gallucci, L. and Kann, M. 2017. Nuclear import of hepatitis B virus capsids and genome. *Viruses*. **9**(1).

Garber, D.A., Beverley, S.M. and Coen, D.M. 1993. Demonstration of circularization of herpes simplex virus DNA following infection using pulsed field gel electrophoresis. *Virology*. **197**(1), pp.459–462.

Glaunsinger, B., Chavez, L. and Ganem, D. 2005. The Exonuclease and Host Shutoff Functions of the SOX Protein of Kaposi ' s Sarcoma-Associated Herpesvirus Are Genetically Separable The Exonuclease and Host Shutoff Functions of the SOX Protein of Kaposi ' s Sarcoma-Associated Herpesvirus Are Genetically. *Journal of virology*. **79**(12), pp.7396–7401.

Glaunsinger, B. and Ganem, D. 2004. Lytic KSHV infection inhibits host gene expression by accelerating global mRNA turnover. *Molecular Cell*. **13**(5), pp.713–723.

Godden-Kent, D., Talbot, S.J., Boshoff, C., Chang, Y., Moore, P., Weiss, R.A. and Mittnacht, S. 1997. The cyclin encoded by Kaposi's sarcoma-associated herpesvirus stimulates cdk6 to phosphorylate the retinoblastoma protein and histone H1. *J Virol*. [Online]. **71**(6), pp.4193–4198. Available from: http://www.ncbi.nlm.nih.gov/pubmed/9151805.

Goedert, J.J. 2000. The epidemiology of acquired immunodeficiency syndrome malignancies. *Seminars in oncology*. [Online]. **27**(4), pp.390–401. Available from: http://www.ncbi.nlm.nih.gov/pubmed/10950365.

Goldberg, M.W. and Allen, T.D. 1992. High resolution scanning electron microscopy of the nuclear envelope: Demonstration of a new, regular, fibrous lattice attached to the baskets of the nucleoplasmic face of the nuclear pores. *Journal of Cell Biology*. **119**(6), pp.1429–1440.

Gong, D., Kim, Y.H., Xiao, Y., Du, Y., Xie, Y., Lee, K.K., Feng, J., Farhat, N., Zhao, D., Shu, S., Dai, X., Chanda, S.K., Rana, T.M., Krogan, N.J., Sun, R. and Wu, T.T. 2016. A Herpesvirus Protein Selectively Inhibits Cellular mRNA Nuclear Export. *Cell Host and Microbe*. **20**(5), pp.642–653.

Gong, Y.N., Guy, C., Olauson, H., Becker, J.U., Yang, M., Fitzgerald, P., Linkermann, A. and Green, D.R. 2017. ESCRT-III Acts Downstream of MLKL to Regulate Necroptotic Cell Death and Its Consequences. *Cell*. [Online]. **169**(2), p.286–300.e16. Available from: http://dx.doi.org/10.1016/j.cell.2017.03.020.

Gould, F., Harrison, S.M., Hewitt, E.W. and Whitehouse, A. 2009. Kaposi's sarcoma-associated herpesvirus RTA promotes degradation of the Hey1 repressor protein through the ubiquitin proteasome pathway. *Journal of virology*. [Online]. **83**(13), pp.6727–38. Available from: http://jvi.asm.org/content/83/13/6727.long.

Griffis, E.R., Altan, N., Lippincott-Schwartz, J. and Powers, M.A. 2002. Nup98 is a mobile nucleoporin with transcription-dependent dynamics. *Molecular biology of the cell*. **13**(4), pp.1282–1297.

Griffis, E.R., Craige, B., Dimaano, C., Ullman, K.S. and Powers, M.A. 2004. Distinct functional domains within nucleoporins Nup153 and Nup98 mediate transcription-dependent mobility. *Molecular biology of the cell*. [Online].

15(4), pp.1991–2002. Available from: http://www.molbiolcell.org/content/15/4/1991.short.

Gruenbaum, Y. and Aebi, U. 2014. Intermediate filaments: a dynamic network that controls cell mechanics. *F1000Prime Reports*. [Online]. **6**(July), pp.1–7. Available from: http://f1000.com/prime/reports/b/6/54.

Gruenbaum, Y., Goldman, R.D., Meyuhas, R., Mills, E., Margalit, A., Fridkin, A., Dayani, Y., Prokocimer, M. and Enosh, A. 2003. The nuclear lamina and its functions in the nucleus. *International Review of Cytology*. **226**, pp.1–62.

Gu, H. and Roizman, B. 2003. The degradation of promyelocytic leukemia and Sp100 proteins by herpes simplex virus 1 is mediated by the ubiquitin-conjugating enzyme UbcH5a. *Proc Natl Acad Sci U S A*. **100**(15), pp.8963–8968.

Guan, T., Kehlenbach, R.H., Schirmer, E.C., Kehlenbach, A., Fan, F., Clurman, B.E., Arnheim, N. and Gerace, L. 2000. Nup50, a Nucleoplasmically Oriented Nucleoporin with a Role in Nuclear Protein Export. *Molecular and Cellular Biology*. [Online]. **20**(15), pp.5619–5630. Available from: http://mcb.asm.org/cgi/doi/10.1128/MCB.20.15.5619-5630.2000.

Guizetti, J., Schermelleh, L., Jana, M., Maar, S. and Poser, I. 2011. Abscission Involves Helices of ESCRT-lll-Dependent Filaments. . **331**(March).

Guizetti, J., Schermelleh, L., Mäntler, J., Maar, S., Poser, I., Leonhardt, H., Müller-Reichert, T. and Gerlich, D.W. 2011. Cortical constriction during abscission involves helices of ESCRT-III-dependent filaments. *Science (New York, N.Y.)*. [Online]. **331**(6024), pp.1616–20. Available from: http://www.ncbi.nlm.nih.gov/pubmed/21310966.

Günther, T. and Grundhoff, A. 2010. The epigenetic landscape of latent kaposi sarcoma-associated herpesvirus genomes. *PLoS Pathogens*. **6**(6).

Gustin, K.E. and Sarnow, P. 2001. Effects of poliovirus infection on nucleo-cytoplasmic trafficking and nuclear pore complex composition. *The EMBO journal*. [Online]. **20**(1–2), pp.240–9. [Accessed 1 February 2014]. Available from: http://www.pubmedcentral.nih.gov/articlerender.fcgi?artid=140206&tool=pmcentrez&rendertype=abstract.

Gustin, K.E. and Sarnow, P. 2002. Inhibition of Nuclear Import and Alteration of Nuclear Pore Complex Composition by Rhinovirus. *Journal of Virology*. [Online]. **76**(17), pp.8787–8796. [Accessed 10 February 2014]. Available from: http://jvi.asm.org/cgi/doi/10.1128/JVI.76.17.8787-8796.2002.

Gwack, Y., Byun, H., Hwang, S., Lim, C. and Choe, J. 2001. CREB-binding protein and histone deacetylase regulate the transcriptional activity of Kaposi's sarcoma-associated herpesvirus open reading frame 50. *Journal of virology*. [Online]. **75**(4), pp.1909–17. Available from: http://www.pubmedcentral.nih.gov/articlerender.fcgi?artid=115137&tool=pmcentrez&rendertype=abstract.

Gygi, S.P., Rist, B., Gerber, S.A., Turecek, F., Gelb, M.H. and Aebersold, R. 1999. Quantitative analysis of complex protein mixtures using isotope-coded affinity tags. *Nature biotechnology*. [Online]. **17**(10), pp.994–9. Available from: http://dx.doi.org/10.1038/13690.

Hamirally, S., Kamil, J.P., Ndassa-Colday, Y.M., Lin, A.J., Jahng, W.J., Baek,

M.C., Noton, S., Silva, L.A., Simpson-Holley, M., Knipe, D.M., Golan, D.E., Marto, J.A. and Coen, D.M. 2009. Viral mimicry of Cdc2/cyclin-dependent kinase 1 mediates disruption of nuclear lamina during human cytomegalovirus nuclear egress. *PLoS Pathogens*. **5**(1).

Han, X., Aslanian, A. and Yates, J. 2008. Mass Spectrometry for Proteomics. *Curr Opin Chem Biol.* **12**(5), pp.483–490.

Harel, A., Orjalo, A. V, Vincent, T., Lachish-Zalait, A., Vasu, S., Shah, S., Zimmerman, E., Elbaum, M. and Forbes, D.J. 2003. Removal of a single pore subcomplex results in vertebrate nuclei devoid of nuclear pores. *Molecular cell*. [Online]. **11**(4), pp.853–64. [Accessed 19 January 2014]. Available from: http://www.ncbi.nlm.nih.gov/pubmed/12718872.

Hawryluk-Gara, L.A., Shibuya, E.K. and Wozniak, R.W. 2005. Vertebrate Nup53 Interacts with the Nuclear Lamina and Is Required for the Assembly of a Nup93-containing Complex. *Molecular Biology of the Cell*. [Online]. **16**(5), pp.2382–2394. Available from: http://www.molbiolcell.org/doi/10.1091/mbc.e04-10-0857.

Hengge, U.R., Ruzicka, T., Tyring, S.K., Stuschke, M., Roggendorf, M., Schwartz, R.A. and Seeber, S. 2002. Update on Kaposi's sarcoma and other HHV8 associated diseases. Part 1: epidemiology, environmental predispositions, clinical manifestations, and therapy. *The Lancet. Infectious diseases*. [Online]. **2**(5), pp.281–92. Available from: http://www.ncbi.nlm.nih.gov/pubmed/12062994.

Henle, G., Henle, W. and Diehl, V. 1968. Relation of Burkitt'S Tumor-Associated Herpes-Ytpe Virus To Infectious Mononucleosis*. *University of Pennsylvania*. [Online]. **59**(1), pp.94–101. Available from: http://www.pnas.org/content/59/1/94.short.

Herold, A., Suyama, M., Rodrigues, J.P., Braun, I.C., Kutay, U., Carmo-Fonseca, M., Bork, P. and Izaurralde, E. 2000. TAP (NXF1) belongs to a multigene family of putative RNA export factors with a conserved modular architecture. *Molecular and cellular biology*. [Online]. **20**(23), pp.8996–9008. Available from: http://www.pubmedcentral.nih.gov/articlerender.fcgi?artid=86553&tool=pmcentrez&rendertype=abstract.

Hodzic, D.M., Yeater, D.B., Bengtsson, L., Otto, H. and Stahl, P.D. 2004. Sun2 is a novel mammalian inner nuclear membrane protein. *Journal of Biological Chemistry*. **279**(24), pp.25805–25812.

Hoelz, A., Debler, E.W. and Blobel, G. 2011. The structure of the nuclear pore complex. *Annual review of biochemistry*. [Online]. **80**, pp.613–643. [Accessed 9 November 2013]. Available from: http://www.ncbi.nlm.nih.gov/pubmed/21495847.

Horii, M., Shibata, H., Kobayashi, R., Katoh, K., Yorikawa, C., Yasuda, J. and Maki, M. 2006. CHMP7, a novel ESCRT-III-related protein, associates with CHMP4b and functions in the endosomal sorting pathway. *Biochemical Journal*. [Online]. **400**(1), pp.23–32. Available from: http://biochemj.org/lookup/doi/10.1042/BJ20060897.

Hsieh, J.J. and Hayward, S.D. 1995. Masking of the CBF1/RBPJ kappa transcriptional repression domain by Epstein-Barr virus EBNA2. *Science (New York, N.Y.)*. [Online]. **268**(5210), pp.560–3. Available from:

224

http://www.ncbi.nlm.nih.gov/pubmed/7725102.

Hsu, J.L., Huang, S.Y., Chow, N.H. and Chen, S.H. 2003. Stable-Isotope Dimethyl Labeling for Quantitative Proteomics. *Analytical Chemistry*. **75**(24), pp.6843–6852.

Hu, T. and Gerace, L. 1998. cDNA cloning and analysis of the expression of nucleoporin p45. *Gene*. [Online]. **221**(2), pp.245–53. Available from: http://www.ncbi.nlm.nih.gov/pubmed/9795236.

Hülsmann, B.B., Labokha, A. a and Görlich, D. 2012. The permeability of reconstituted nuclear pores provides direct evidence for the selective phase model. *Cell*. [Online]. **150**(4), pp.738–51. Available from: http://www.ncbi.nlm.nih.gov/pubmed/22901806.

Hung, V., Udeshi, N.D., Lam, S.S., Loh, K.H., Cox, K.J., Pedram, K., Carr, S.A. and Ting, A.Y. 2016. Spatially resolved proteomic mapping in living cells with the engineered peroxidase APEX2. *Nature Protocols*. **11**(3), pp.456–475.

Hwang, J. and Espenshade, P.J. 2016. Proximity-dependent biotin labelling in yeast using the engineered ascorbate peroxidase APEX2. *Biochemical Journal*. [Online]. **473**(16), pp.2463–2469. Available from: http://biochemj.org/cgi/doi/10.1042/BCJ20160106.

Hwang, S., Gwack, Y., Byun, H., Lim, C. and Choe, J. 2001. The Kaposi's sarcoma-associated herpesvirus K8 protein interacts with CREB-binding protein (CBP) and represses CBP-mediated transcription. *Journal of virology*. [Online]. **75**(19), pp.9509–16. Available from: http://jvi.asm.org/content/75/19/9509.short.

Imbeault, M., Ouellet, M. and Tremblay, M.J. 2009. Microarray study reveals that HIV-1 induces rapid type-I interferon-dependent p53 mRNA up-regulation in human primary CD4+ T cells. *Retrovirology*. **6**, pp.1–14.

Jarnik, M. and Aebi, U. 1991. Toward a more complete 3-D structure of the nuclear pore complex. *Journal of Structural Biology*. **107**(3), pp.291–308.

Jayappa, K.D., Ao, Z. and Yao, X. 2012. The HIV-1 passage from cytoplasm to nucleus: The process involving a complex exchange between the components of HIV-1 and cellular machinery to access nucleus and successful integration. *International Journal of Biochemistry and Molecular Biology*. **3**(1), pp.70–85.

de Jesus, O., Smith, P.R., Spender, L.C., Karstegl, C.E., Niller, H.H., Huang, D. and Farrell, P.J. 2003. Updated Epstein-Barr virus (EBV) DNA sequence and analysis of a promoter for the BART (CST, BARF0) RNAs of EBV. *Journal of General Virology*. **84**(6), pp.1443–1450.

Kalverda, B., Pickersgill, H., Shloma, V. V. and Fornerod, M. 2010. Nucleoporins Directly Stimulate Expression of Developmental and Cell-Cycle Genes Inside the Nucleoplasm. *Cell*. [Online]. **140**(3), pp.360–371. [Accessed 13 December 2013]. Available from: http://www.ncbi.nlm.nih.gov/pubmed/20144760.

Kampmann, M. and Blobel, G. 2009. Three-dimensional structure and flexibility of a membrane-coating module of the nuclear pore complex. *Nature Structural and Molecular Biology*. **16**(7), pp.782–788.

Kang, M.-S., Hung, S.C. and Kieff, E. 2001. Epstein–Barr virus nuclear antigen 1 activates transcription from episomal but not integrated DNA and does not

alter lymphocyte growth. *Proceedings of the National Academy of Sciences* . [Online]. **98**(26), pp.15233–15238. Available from: http://www.pnas.org/content/98/26/15233.abstract.

Kaposi, M. 1872. Idiopathisches multiples Pigmentsarkom der Haut. *Archiv für Dermatologie und Syphilis*. [Online]. **4**(2), pp.265–273. Available from: http://link.springer.com/10.1007/BF01830024.

Kasper, L.H., Brindle, P.K., Schnabel, C.A., Pritchard, C.E., Cleary, M.L. and van Deursen, J.M. 1999. CREB binding protein interacts with nucleoporin-specific FG repeats that activate transcription and mediate NUP98-HOXA9 oncogenicity. *Molecular and cellular biology*. [Online]. **19**(1), pp.764–76. Available from: http://www.pubmedcentral.nih.gov/articlerender.fcgi?artid=83933&tool=pmc entrez&rendertype=abstract.

Kasper, L.H., Brindle, P.K., Schnabel, C.A., Pritchard, C.E.J., Cleary, M.L. and van Deursen, J.M.A. 1999. CREB Binding Protein Interacts with Nucleoporin-Specific FG Repeats That Activate Transcription and Mediate NUP98-HOXA9 Oncogenicity. *Molecular and Cellular Biology*. [Online]. **19**(1), pp.764–776. Available from: http://mcb.asm.org/lookup/doi/10.1128/MCB.19.1.764.

Kedes, D.H., Lagunoff, M., Renne, R. and Ganem, D. 1997. Identification of the gene encoding the major latency-associated nuclear antigen of the Kaposi's sarcoma-associated herpesvirus. *J Clin Invest*. [Online]. **100**(10), pp.2606–2610. Available from: http://www.ncbi.nlm.nih.gov/pubmed/9366576.

Kelley, K., Knockenhauer, K.E., Kabachinski, G. and Schwartz, T.U. 2015. Atomic structure of the Y complex of the nuclear pore. *Nature Structural & Molecular Biology*. [Online]. (March). Available from: http://www.nature.com/doifinder/10.1038/nsmb.2998.

Kelly, B.J., Fraefel, C., Cunningham, A.L. and Diefenbach, R.J. 2009. Functional roles of the tegument proteins of herpes simplex virus type 1. *Virus Research*. **145**(2), pp.173–186.

Kennedy, G., Komano, J. and Sugden, B. 2003. Epstein – Barr virus provides a survival factor to Burkitt ' s lymphomas. *Pnas*. **100**(24), pp.14269–14274.

Khan, G., Hashim, M., Parkin, D., Martel, C. De, Ferlay, J., Franceschi, S., Vignat, J., Bray, F., Forman, D., Plummer, M., Longnecker, R., Kieff, E., Cohen, J., Epstein, M., Achong, B., Barr, Y., Khan, G., Miyashita, E., Yang, B., Babcock, G., Thorley-Lawson, D., Babcock, G., Decker, L., Volk, M., Thorley-Lawson, D., Tierney, R., Steven, N., Young, L., Rickinson, A., Pope, J., Horne, M., Scott, W., Marquitz, A., Mathur, A., Chugh, P., Dittmer, D., Raab-Traub, N., Thorley-Lawson, D., Miyashita, E., Khan, G., Rowe, M., Lear, A., Croom-Carter, D., Davies, A., Rickinson, A., Li, Q., Spriggs, M., Kovats, S., Turk, S., Comeau, M., Nepom, B., Hutt-Fletcher, L., Chêne, A., Donati, D., Guerreiro-Cacais, A., Levitsky, V., Chen, Q., Falk, K., Orem, J., Kironde, F., Wahlgren, M., Bejarano, M., Cozen, W., Timofeeva, M., Li, D., Diepstra, A., Hazelett, D., Delahaye-Sourdeix, M., Edlund, C., Franke, L., Rostgaard, K., Berg, D. Van Den, Cortessis, V., Smedby, K., Glaser, S., Westra, H.-J., Robison, L., Mack, T., Ghesquieres, H., Hwang, A., Nieters, A., Sanjose, S. de, Lightfoot, T., Becker, N., Maynadie, M., Foretova, L., Roman, E., Benavente, Y., Rand, K., Nathwani, B., Glimelius, B., Staines, A., Khan, G., Philip, P., Ashari, M.

Al, Houcinat, Y., Daoud, S., Khan, G., Coates, P., Gupta, R., Kangro, H., Slavin, G., Glaser, S., Lin, R., Stewart, S., Ambinder, R., Jarrett, R., Brousset, P., Pallesen, G., Gulley, M., Khan, G., O'Grady, J., Hummel, M., Preciado, M., Knecht, H., Chan, J., Claviez, A., Murray, C., Ezzati, M., Flaxman, A., Lim, S., Lozano, R., Michaud, C., Naghavi, M., Salomon, J., Shibuya, K., Vos, T., Lopez, A., Das, P., Samarasekera, U., Bouvard, V., Baan, R., Straif, K., Grosse, Y., Secretan, B., Ghissassi, F., Benbrahim-Tallaa, L., Guha, N., Freeman, C., Galichet, L., Cogliano, V., Thorley-Lawson, D., Gross, A., Murphy, G., Pfeiffer, R., Camargo, M., Rabkin, C., Lee, J.-H., Kim, S.-H., Han, S.-H., An, J.-S., Lee, E.-S., Kim, Y.-S., Jarrett, R., Armstrong, A., Alexander, E., Murray, P., Billingham, L., Hassan, H., Flavell, J., Nelson, P., Scott, K., Reynolds, G., Constandinou, C., Kerr, D., Devey, E., Crocker, J., Young, L., Stark, G., Wood, K., Jack, F., Angus, B., Proctor, S., Taylor, P., Herling, M., Rassidakis, G., Medeiros, L., Vassilakopoulos, T., Kliche, K.-O., Nadali, G., Viviani, S., Bonfante, V., Giardini, R., Chilosi, M., Kittas, C., Gianni, A., Bonadonna, G., Pizzolo, G., Pangalis, G., Cabanillas, F., Sarris, A., Jarrett, R., Stark, G., White, J., Angus, B., Alexander, F., Krajewski, A., Freeland, J., Taylor, G., Taylor, P., Glaser, S., Gulley, M., Clarke, C., Keegan, T., Chang, E., Shema, S., Craig, F., Digiuseppe, J., Dorfman, R., Mann, R., Anton-Culver, H., Ambinder, R., Jain, A., Nalesnik, M., Reyes, J., Pokharna, R., Mazariegos, G., Green, M., Eghtesad, B., Marsh, W., Cacciarelli, T., Fontes, P., Abu-Elmagd, K., Sindhi, R., Demetris, J., Fung, J., Chapman, J., Webster, A., Wong, G., Sousa, H., Pinto-Correia, A., Medeiros, R., Dinis-Ribeiro, M., Tokunaga, M., Land, C., Uemura, Y., Tokudome, T., Tanaka, S., Sato, E., Li, S., Du, H., Wang, Z., Zhou, L., Zhao, X., Zeng, Y., Murray, C., Vos, T., Lozano, R., Naghavi, M., Flaxman, A., Michaud, C., Ezzati, M., Shibuya, K., Salomon, J., Abdalla, S., Aboyans, V., Abraham, J., Ackerman, I., Aggarwal, R., Ahn, S., Ali, M., Alvarado, M., Anderson, H., Anderson, L., Andrews, K., Atkinson, C., Baddour, L., Bahalim, A., Barker-Collo, S., Barrero, L., Bartels, D., Basáñez, M.-G., Baxter, A., Bell, M., Benjamin, E., Wang, H., Dwyer-Lindgren, L., Lofgren, K., Rajaratnam, J., Marcus, J., Levin-Rector, A., Levitz, C., Lopez, A., Murray, C., Lozano, R., Naghavi, M., Foreman, K., Lim, S., Shibuya, K., Aboyans, V., Abraham, J., Adair, T., Aggarwal, R., Ahn, S., Alvarado, M., Anderson, H., Anderson, L., Andrews, K., Atkinson, C., Baddour, L., Barker-Collo, S., Bartels, D., Bell, M., Benjamin, E., Bennett, D., Bhalla, K., Bikbov, B., Abdulhak, A. Bin, Birbeck, G., Blyth, F., Bolliger, I., Boufous, S., Bucello, C., Burch, M., Spina, M., Tirelli, U., Zagonel, V., Gloghini, A., Volpe, R., Babare, R., Abbruzzese, L., Talamini, R., Vaccher, E., Carbone, A., Magrath, I., Philip, T., Hsu, J., Glaser, S., Queiroga, E., Gualco, G., Weiss, L., Dittmer, D., Araujo, I., Klumb, C., Harrington, W., Bacchi, C., Boerma, E., Imhoff, G. van, Appel, I., Veeger, N., Kluin, P., Kluin-Nelemans, J., Stefan, D., Lutchman, R., Mucha, K., Foroncewicz, B., Ziarkiewicz-Wróblewska, B., Krawczyk, M., Lerut, J., Pączek, L., Opelz, G., Döhler, B., Flavell, K., Billingham, L., Biddulph, J., Gray, L., Flavell, J., Constandinou, C., Young, L., Murray, P., Claviez, A., Tiemann, M., Lüders, H., Krams, M., Parwaresch, R., Schellong, G., Dörffel, W., Huang, X., Nolte, I., Gao, Z., Vos, H., Hepkema, B., Poppema, S., Berg, A. van den, Diepstra, A., Chang, E., Adami, H.-O., Jia, W.-H., Huang, Q.-H., Liao, J., Ye, W., Shugart, Y., Liu, Q., Chen, L.-Z., Li, Y.-H., Lin, X., Wen, F.-L., Adami, H.-O., Zeng, Y., Zeng, Y.-

227

X., Pisani, P., Parkin, D., Muñoz, N., Ferlay, J., Imai, S., Koizumi, S., Sugiura, M., Tokunaga, M., Uemura, Y., Yamamoto, N., Tanaka, S., Sato, E., Osato, T., Lee, H., Chang, M., Yang, H.-K., Lee, B., Kim, W., Jemal, A., Bray, F., Center, M., Ferlay, J., Ward, E., Forman, D., Guggenheim, D., Shah, M., Fukayama, M., Hino, R., Uozaki, H., Uemura, N., Okamoto, S., Yamamoto, S., Matsumura, N., Yamaguchi, S., Yamakido, M., Taniyama, K., Sasaki, N., Schlemper, R., Kamangar, F., Dawsey, S., Blaser, M., Perez-Perez, G., Pietinen, P., Newschaffer, C., Abnet, C., Albanes, D., Virtamo, J., Taylor, P., Kelley, J., Duggan, J., Joossens, J., Hill, M., Elliott, P., Stamler, R., Lesaffre, E., Dyer, A., Nichols, R., Kesteloot, H., Thorley-Lawson, D., Allday, M., Young, L., Alfieri, C., Hennessy, K., Evans, H., O'Hara, C., Anderson, K., Ritz, J., Shapiro, R., Rickinson, A., Kieff, E., Rea, D., Delecluse, H., Hamilton-Dutoit, S., Marelle, L., Joab, I., Edelman, L., Finet, J., Raphael, M., Wang, D., Liebowitz, D., Kieff, E., Starzl, T., Nalesnik, M., Porter, K., Ho, M., Iwatsuki, S., Griffith, B., Rosenthal, J., Hakala, T., Shaw, B., Hardesty, R., Heslop, H., Slobod, K., Pule, M., Hale, G., Rousseau, A., Smith, C., Bollard, C., Liu, H., Wu, M.-F., Rochester, R., Amrolia, P., Hurwitz, J., Brenner, M., Rooney, C., Young, L., Deacon, E., Rowe, M., Crocker, J., Herbst, H., Niedobitek, G., Hamilton-Dutoit, S., Pallesen, G., Khan, G., Izadi, M., Taheri, S., Camargo, M., Kim, W.-H., Chiaravalli, A., Kim, K.-M., Corvalan, A., Matsuo, K., Yu, J., Sung, J., Herrera-Goepfert, R., Meneses-Gonzalez, F., Kijima, Y., Natsugoe, S., Liao, L., Lissowska, J., Kim, S., Hu, N., Gonzalez, C., Yatabe, Y., Koriyama, C., Hewitt, S., Akiba, S., Gulley, M., Taylor, P., Rabkin, C., Shankland, K., Armitage, J., Hancock, B., Hamilton-Dutoit, S., Raphael, M., Audouin, J., Diebold, J., Lisse, I., Pedersen, C., Oksenhendler, E., Marelle, L., Pallesen, G., Cohen, J., Fauci, A., Varmus, H. and Nabel, G. 2014. Global burden of deaths from Epstein-Barr virus attributable malignancies 1990-2010. *Infectious Agents and Cancer*. [Online]. **9**(1), p.38. Available from: http://infectagentscancer.biomedcentral.com/articles/10.1186/1750-9378-9-38.

Kim, D.I., Jensen, S.C., Noble, K.A., KC, B., Roux, K.H., Motamedchaboki, K. and Roux, K.J. 2016. An improved smaller biotin ligase for BioID proximity labeling. *Molecular Biology of the Cell*. [Online]. **27**(8), pp.1188–1196. Available from: http://www.molbiolcell.org/cgi/doi/10.1091/mbc.E15-12-0844.

Kim, D.I., Kc, B., Zhu, W., Motamedchaboki, K., Doye, V. and Roux, K.J. 2014. Probing nuclear pore complex architecture with proximity-dependent biotinylation. *Proceedings of the National Academy of Sciences of the United States of America*. [Online]. **111**(24), pp.E2453-61. [Accessed 16 July 2014]. Available from: http://www.ncbi.nlm.nih.gov/pubmed/24927568.

Klupp, B.G., Granzow, H., Fuchs, W., Keil, G.M., Finke, S. and Mettenleiter, T.C. 2007. Vesicle formation from the nuclear membrane is induced by coexpression of two conserved herpesvirus proteins. *Proceedings of the National Academy of Sciences*. [Online]. **104**(17), pp.7241–7246. Available from: http://www.pubmedcentral.nih.gov/articlerender.fcgi?artid=1855391&tool=pmcentrez&rendertype=abstract%5Cnhttp://www.pnas.org/cgi/doi/10.1073/pnas.0701757104.

Knipe, D.M. and Cliffe, A. 2008. Chromatin control of herpes simplex virus lytic and latent infection. *Nature Reviews Microbiology*. **6**(3), pp.211–221.

von Kobbe C, van Deursen JM, Rodrigues, J.P., Sitterlin, D., Bachi, a, Wu, X., Wilm, M., Carmo-Fonseca, M. and Izaurralde, E. 2000. Vesicular stomatitis virus matrix protein inhibits host cell gene expression by targeting the nucleoporin Nup98. *Molecular cell*. [Online]. **6**(5), pp.1243–52. Available from: http://www.ncbi.nlm.nih.gov/pubmed/11106761.

König, R., Zhou, Y., Elleder, D., Diamond, T.L., Bonamy, G.M.C., Irelan, J.T., Chiang, C. yuan, Tu, B.P., De Jesus, P.D., Lilley, C.E., Seidel, S., Opaluch, A.M., Caldwell, J.S., Weitzman, M.D., Kuhen, K.L., Bandyopadhyay, S., Ideker, T., Orth, A.P., Miraglia, L.J., Bushman, F.D., Young, J.A. and Chanda, S.K. 2008. Global Analysis of Host-Pathogen Interactions that Regulate Early-Stage HIV-1 Replication. *Cell*. **135**(1), pp.49–60.

Koonin, E. V, Senkevich, T.G. and Dolja, V. V 2006. The ancient Virus World and evolution of cells. *Biology direct*. [Online]. **1**, p.29. Available from: http://www.ncbi.nlm.nih.gov/pubmed/16984643%5Cnhttp://www.pubmedce ntral.nih.gov/articlerender.fcgi?artid=PMC1594570.

Kraemer, D., Wozniak, R.W., Blobel, G. and Radu, a 1994. The human CAN protein, a putative oncogene product associated with myeloid leukemogenesis, is a nuclear pore complex protein that faces the cytoplasm. *Proceedings of the National Academy of Sciences of the United States of America*. [Online]. **91**(4), pp.1519–23. Available from: http://www.pubmedcentral.nih.gov/articlerender.fcgi?artid=43191&tool=pmc entrez&rendertype=abstract.

Krishnan, H.H., Naranatt, P.P., Smith, M.S., Zeng, L., Bloomer, C. and Chandran, B. 2004. Concurrent expression of latent and a limited number of lytic genes with immune modulation and antiapoptotic function by Kaposi's sarcoma-associated herpesvirus early during infection of primary endothelial and fibroblast cells and subsequent decline of l. *Journal of virology*. [Online]. **78**(7), pp.3601–20. Available from: http://www.pubmedcentral.nih.gov/articlerender.fcgi?artid=371072&tool=pm centrez&rendertype=abstract.

Kroon, E. 2001. NUP98-HOXA9 expression in hemopoietic stem cells induces chronic and acute myeloid leukemias in mice. *The EMBO Journal*. [Online]. **20**(3), pp.350–361. Available from: http://emboj.embopress.org/cgi/doi/10.1093/emboj/20.3.350.

Krull, S., Thyberg, J., Björkroth, B., Rackwitz, H.-R. and Cordes, V.C. 2004. Nucleoporins as Components of the Nuclear Pore Complex Core Structure and Tpr as the Architectural Element of the Nuclear Basket. *Molecular Biology of the Cell*. [Online]. **15**(9), pp.4261–4277. Available from: http://www.molbiolcell.org/doi/10.1091/mbc.e04-03-0165.

Kutay, U., Ralf Bischoff, F., Kostka, S., Kraft, R. and Görlich, D. 1997. Export of importin α from the nucleus is mediated by a specific nuclear transport factor. *Cell*. **90**(6), pp.1061–1071.

Kutok, J.L. and Wang, F. 2006. Spectrum of Epstein-Barr Virus–Associated Diseases. *Annual Review of Pathology: Mechanisms of Disease*. [Online]. **1**(1), pp.375–404. Available from: http://www.annualreviews.org/doi/10.1146/annurev.pathol.1.110304.10020

9.

Kwon, K. and Beckett, D. 2000. Function of a conserved sequence motif in biotin holoenzyme synthetases. *Protein science : a publication of the Protein Society*. **9**(8), pp.1530–1539.

Lam, D.H. and Aplan, P.D. 2001. NUP98 gene fusions in hematologic malignancies. *Leukemia*. **15**(11), pp.1689–1695.

Lambert, J.P., Tucholska, M., Go, C., Knight, J.D.R. and Gingras, A.C. 2015. Proximity biotinylation and affinity purification are complementary approaches for the interactome mapping of chromatin-associated protein complexes. *Journal of Proteomics*. [Online]. **118**, pp.81–94. Available from: http://dx.doi.org/10.1016/j.jprot.2014.09.011.

Lan, K., Kuppers, D.A., Verma, S.C., Sharma, N., Murakami, M. and Robertson, E.S. 2005. Induction of Kaposi's Sarcoma-Associated Herpesvirus Latency-Associated Nuclear Antigen by the Lytic Transactivator RTA: a Novel Mechanism for Establishment of Latency. *Journal of Virology*. [Online]. **79**(12), pp.7453–7465. Available from: http://jvi.asm.org/cgi/doi/10.1128/JVI.79.12.7453-7465.2005.

Lane, B.R., Liu, J., Bock, P.J., Schols, D., Coffey, M.J., Strieter, R.M., Polverini, P.J. and Markovitz, D.M. 2002. Interleukin-8 and growth-regulated oncogene alpha mediate angiogenesis in Kaposi's sarcoma. *Journal of Virology*. [Online]. **76**(22), pp.11570–11583. Available from: http://www.pubmedcentral.nih.gov/articlerender.fcgi?artid=136744&tool=pmcentrez&rendertype=abstract.

Lane, M.D., Rominger, K.L., Young, D.L. and Lynen, F. 1964. The Enzymatic Synthesis of Holotranscarboxylase from Apotranscarboxylase and (+)-Biotin. *The Journal of biological chemistry*. **239**(9), pp.2865–2871.

Lee, C.-P., Huang, Y.-H., Lin, S.-F., Chang, Y., Chang, Y.-H., Takada, K. and Chen, M.-R. 2008. Epstein-Barr virus BGLF4 kinase induces disassembly of the nuclear lamina to facilitate virion production. *Journal of virology*. [Online]. **82**(23), pp.11913–26. Available from: http://www.pubmedcentral.nih.gov/articlerender.fcgi?artid=2583647&tool=pmcentrez&rendertype=abstract.

Lee, C.P., Liu, P.T., Kung, H.N., Su, M.T., Chua, H.H., Chang, Y.H., Chang, C.W., Tsai, C.H., Liu, F.T. and Chen, M.R. 2012. The ESCRT Machinery Is Recruited by the Viral BFRF1 Protein to the Nucleus-Associated Membrane for the Maturation of Epstein-Barr Virus. *PLoS Pathogens*. **8**(9).

Lee, J.S., Raja, P. and Knipe, D.M. 2016. Herpesviral ICP0 Protein Promotes Two Waves of Heterochromatin Removal on an Early Viral Promoter during Lytic Infection. *mBio*. [Online]. **7**(1), pp.924–938. Available from: http://mbio.asm.org/lookup/doi/10.1128/mBio.02007-15.

Leuzinger, H., Ziegler, U., Schraner, E.M., Fraefel, C., Glauser, D.L., Heid, I., Ackermann, M., Mueller, M. and Wild, P. 2005. Herpes simplex virus 1 envelopment follows two diverse pathways. *Journal of virology*. [Online]. **79**(20), pp.13047–59. Available from: http://www.pubmedcentral.nih.gov/articlerender.fcgi?artid=1235821&tool=pmcentrez&rendertype=abstract.

Li, M., Lee, H., Guo, J., Neipel, F., Fleckenstein, B., Ozato, K. and Jung, J.U. 1998. Kaposi's sarcoma-associated herpesvirus viral interferon regulatory

factor. *Journal of virology*. [Online]. **72**(7), pp.5433–40. Available from: http://www.ncbi.nlm.nih.gov/pubmed/9620998.

Li, M., Lee, H., Yoon, D.W., Albrecht, J.C., Fleckenstein, B., Neipel, F. and Jung, J.U. 1997. Kaposi's sarcoma-associated herpesvirus encodes a functional cyclin. *J Virol*. [Online]. **71**(3), pp.1984–1991. Available from: http://www.ncbi.nlm.nih.gov/pubmed/9032330.

Li, X., Feng, J. and Sun, R. 2011. Oxidative Stress Induces Reactivation of Kaposi's Sarcoma-Associated Herpesvirus and Death of Primary Effusion Lymphoma Cells. *Journal of Virology*. [Online]. **85**(2), pp.715–724. Available from: http://jvi.asm.org/cgi/doi/10.1128/JVI.01742-10.

Li, X. and Zhu, F. 2009. Identification of the nuclear export and adjacent nuclear localization signals for ORF45 of Kaposi's sarcoma-associated herpesvirus. *Journal of virology*. [Online]. **83**(6), pp.2531–9. [Accessed 25 June 2015]. Available from: http://www.pubmedcentral.nih.gov/articlerender.fcgi?artid=2648283&tool=pmcentrez&rendertype=abstract.

Li, X.W., Rees, J.S., Xue, P., Zhang, H., Hamaia, S.W., Sanderson, B., Funk, P.E., Farndale, R.W., Lilley, K.S., Perrett, S. and Jackson, A.P. 2014. New insights into the DT40 B cell receptor cluster using a proteomic proximity labeling assay. *Journal of Biological Chemistry*. **289**(21), pp.14434–14447.

Liang, Y., Chang, J., Lynch, S., Lukac, D.M. and Ganem, D. 2002. The lytic switch protein of KSHV activates gene expression via functional interaction with RBP-Jk, the target of the Notch signaling pathway. *Genes Dev*. **16**, pp.1977–1989.

Liang, Y., Franks, T.M., Marchetto, M.C., Gage, F.H. and Hetzer, M.W. 2013. Dynamic Association of NUP98 with the Human Genome. *PLoS Genetics*. **9**(2).

Liang, Y. and Ganem, D. 2004. RBP-J (CSL) is essential for activation of the K14/vGPCR promoter of Kaposi's sarcoma-associated herpesvirus by the lytic switch protein RTA. *Journal of virology*. [Online]. **78**(13), pp.6818–26. Available from: http://www.pubmedcentral.nih.gov/articlerender.fcgi?artid=421686&tool=pmcentrez&rendertype=abstract.

Liashkovich, I., Hafezi, W., Kühn, J.M., Oberleithner, H. and Shahin, V. 2011. Nuclear delivery mechanism of herpes simplex virus type 1 genome. *Journal of molecular recognition : JMR*. [Online]. **24**(3), pp.414–21. [Accessed 30 December 2014]. Available from: http://www.ncbi.nlm.nih.gov/pubmed/21504018.

Lieberman, P.M. 2013. Keeping it quiet: Chromatin control of gammaherpesvirus latency. *Nature Reviews Microbiology*. [Online]. **11**(12), pp.863–875. Available from: http://dx.doi.org/10.1038/nrmicro3135.

Light, W.H., Freaney, J., Sood, V., Thompson, A., D'Urso, A., Horvath, C.M. and Brickner, J.H. 2013. A Conserved Role for Human Nup98 in Altering Chromatin Structure and Promoting Epigenetic Transcriptional Memory. *PLoS Biology*. **11**(3).

Lim, R.Y.H., Huang, N.-P., Köser, J., Deng, J., Lau, K.H.A., Schwarz-Herion, K., Fahrenkrog, B. and Aebi, U. 2006. Flexible phenylalanine-glycine nucleoporins as entropic barriers to nucleocytoplasmic transport.

Proceedings of the National Academy of Sciences of the United States of America. [Online]. **103**(25), pp.9512–7. Available from: http://www.pubmedcentral.nih.gov/articlerender.fcgi?artid=1480438&tool=p mcentrez&rendertype=abstract.

Lim, R.Y.H. and Kapinos, L.E. 2015. How to operate a nuclear pore complex by kap-centric control. *Nucleus*. **6**(5), pp.366–372.

Lin, S.-F., Sun, R., Heston, L., Gradoville, L., Shedd, D., Haglund, K., Rigsby, M. and Miller, G. 1997. Identification, Expression, and Immunogenicity of Kaposi's Sarcoma-Associated Herpesvirus-Encoded Small Viral Capsid Antigen. *Journal of Virology*. **71**(4), pp.3069–3076.

Lindsay, M.E., Plafker, K., Smith, A.E., Clurman, B.E. and Macara, I.G. 2002. Npap60/Nup50 is a tri-stable switch that stimulates importin-alpha:beta-mediated nuclear protein import. *Cell*. **110**(3), pp.349–360.

Liu, S.M. and Stewart, M. 2005. Structural basis for the high-affinity binding of nucleoporin Nup1p to the Saccharomyces cerevisiae importin-β homologue, Kap95p. *Journal of Molecular Biology*. **349**(3), pp.515–525.

Loomis, J.S., Courtney, R.J. and Wills, J.W. 2006. Packaging Determinants in the UL11 Tegument Protein of Herpes Simplex Virus Type 1. *Journal of Virology*. [Online]. **80**(21), pp.10534–10541. Available from: http://jvi.asm.org/cgi/doi/10.1128/JVI.01172-06.

Lu, F., Day, L., Gao, S.-J. and Lieberman, P.M. 2006. Acetylation of the latency-associated nuclear antigen regulates repression of Kaposi's sarcoma-associated herpesvirus lytic transcription. *Journal of virology*. [Online]. **80**(11), pp.5273–82. Available from: http://www.pubmedcentral.nih.gov/articlerender.fcgi?artid=1472144&tool=p mcentrez&rendertype=abstract.

Lu, F., Zhou, J., Wiedmer, A., Madden, K., Lieberman, P.M. and Yuan, Y. 2003. Chromatin Remodeling of the Kaposi ' s Promoter Correlates with Reactivation from Latency Chromatin Remodeling of the Kaposi ' s Sarcoma-Associated Herpesvirus ORF50 Promoter Correlates with Reactivation from Latency. *Journal of virology*. **77**(21), pp.11425–11435.

Lukac, D.M., Garibyan, L., Kirshner, J.R., Palmeri, D. and Ganem, D. 2001a. DNA binding by Kaposi's sarcoma-associated herpesvirus lytic switch protein is necessary for transcriptional activation of two viral delayed early promoters. *Journal of virology*. [Online]. **75**(15), pp.6786–99. Available from: http://www.pubmedcentral.nih.gov/articlerender.fcgi?artid=114405&tool=pm centrez&rendertype=abstract.

Lukac, D.M., Garibyan, L., Kirshner, J.R., Palmeri, D. and Ganem, D. 2001b. DNA Binding by Kaposi's Sarcoma-Associated Herpesvirus Lytic Switch Protein Is Necessary for Transcriptional Activation of Two Viral Delayed Early Promoters. *Journal of Virology*. [Online]. **75**(15), pp.6786–6799. Available from: http://www.pubmedcentral.nih.gov/articlerender.fcgi?artid=114405&tool=pm centrez&rendertype=abstract.

Lukac, D.M., Renne, R., Kirshner, J.R. and Ganem, D. 1998. Reactivation of Kaposi's sarcoma-associated herpesvirus infection from latency by expression of the ORF 50 transactivator, a homolog of the EBV R protein. *Virology*. [Online]. **252**(2), pp.304–12. Available from:

http://www.sciencedirect.com/science/article/pii/S0042682298994867.

Luna, R.E., Zhou, F., Baghian, A., Chouljenko, V., Forghani, B., Gao, S., Kousoulas, K.G. and Irol, J. V 2004. Kaposi ' s Sarcoma-Associated Herpesvirus Glycoprotein K8 . 1 Is Dispensable for Virus Entry. *Society*. **78**(12), pp.6389–6398.

Lupu, F., Alves, A., Anderson, K., Doye, V. and Lacy, E. 2008. Nuclear pore composition regulates neural stem/progenitor cell differentiation in the mouse embryo. *Developmental cell*. [Online]. **14**(6), pp.831–42. [Accessed 11 June 2015]. Available from: http://www.pubmedcentral.nih.gov/articlerender.fcgi?artid=2495767&tool=p mcentrez&rendertype=abstract.

Lutzmann, M., Kunze, R., Buerer, A., Aebi, U. and Hurt, E. 2002. Modular self-assembly of a Y-shaped multiprotein complex from seven nucleoporins. *EMBO Journal*. **21**(3), pp.387–397.

Luxton, G.W., Lee, J.I., Haverlock-Moyns, S., Schober, J.M. and Smith, G.A. 2006. The Pseudorabies Virus VP1/2 Tegument Protein Is Required for Intracellular Capsid Transport. *J Virol*. [Online]. **80**(1), pp.201–209. Available from: http://www.ncbi.nlm.nih.gov/entrez/query.fcgi?cmd=Retrieve&db=PubMed& dopt=Citation&list_uids=16352544.

Lynch, D.T., Zimmerman, J.S. and Rowe, D.T. 2002. Epstein-Barr virus latent membrane protein 2B (LMP2B) co-localizes with LMP2A in perinuclear regions in transiently transfected cells. *Journal of General Virology*. **83**(5), pp.1025–1035.

Ma, Z., Hopcraft, S.E., Yang, F., Petrucelli, A., Guo, H., Ting, J.P.Y., Dittmer, D.P. and Damania, B. 2017. NLRX1 negatively modulates type I IFN to facilitate KSHV reactivation from latency. *PLoS Pathogens*. **13**(5), pp.1–20.

Ma, Z., Jacobs, S.R., West, J.A., Stopford, C., Zhang, Z., Davis, Z., Barber, G.N., Glaunsinger, B.A., Dittmer, D.P. and Damania, B. 2015. Modulation of the cGAS-STING DNA sensing pathway by gammaherpesviruses. *Proceedings of the National Academy of Sciences*. [Online]. **112**(31), pp.E4306–E4315. Available from: http://www.pnas.org/lookup/doi/10.1073/pnas.1503831112.

Majerciak, V. and Zheng, Z.-M. 2009. Kaposi's sarcoma-associated herpesvirus ORF57 in viral RNA processing. *Frontiers in bioscience (Landmark edition)*. [Online]. **14**(5), pp.1516–28. Available from: http://www.pubmedcentral.nih.gov/articlerender.fcgi?artid=2654597&tool=p mcentrez&rendertype=abstract.

Makise, M., Mackay, D.R., Elgort, S., Shankaran, S.S., Adam, S.A. and Ullman, K.S. 2012. The Nup153-Nup50 protein interface and its role in nuclear import. *Journal of Biological Chemistry*. **287**(46), pp.38515–38522.

Malik, P., Tabarraei, A., Kehlenbach, R.H., Korfali, N., Iwasawa, R., Graham, S. V and Schirmer, E.C. 2012. Herpes simplex virus ICP27 protein directly interacts with the nuclear pore complex through Nup62, inhibiting host nucleocytoplasmic transport pathways. *The Journal of biological chemistry*. [Online]. **287**(15), pp.12277–92. [Accessed 5 October 2014]. Available from: http://www.pubmedcentral.nih.gov/articlerender.fcgi?artid=3320978&tool=p mcentrez&rendertype=abstract.

Mansfeld, J., Güttinger, S., Hawryluk-Gara, L.A., Panté, N., Mall, M., Galy, V.,

Haselmann, U., Mühlhäusser, P., Wozniak, R.W., Mattaj, I.W., Kutay, U. and Antonin, W. 2006. The Conserved Transmembrane Nucleoporin NDC1 Is Required for Nuclear Pore Complex Assembly in Vertebrate Cells. *Molecular Cell*. **22**(1), pp.93–103.

Martin, J., Laker, M., Kambugu, A., Janka, D., Orem, J., Mwaka, A., Maurer, T. and Mbidde, E. 2009. Kaposi's sarcoma-associated immune reconstitution inflammatory syndrome (KS-IRIS) in Africa: initial findings from a prospective evaluation. *Infectious Agents and Cancer*. [Online]. **4**(Suppl 2), p.O17. Available from: http://infectagentscancer.biomedcentral.com/articles/10.1186/1750-9378-4-S2-O17.

Martin, J.N., Ganem, D.E., Osmond, D.H., Page-Schafer, K.A., Macrae, D. and Kedes, D.H. 1998. Sexual Transmission and the Natural History of Human. *The New England journal of medicine*. **338**(14), pp.948–954.

Matta, H. and Chaudhary, P.M. 2004. Activation of alternative NF-kappa B pathway by human herpes virus 8-encoded Fas-associated death domain-like IL-1 beta-converting enzyme inhibitory protein (vFLIP). *Proc Natl Acad Sci U S A*. [Online]. **101**(25), pp.9399–9404. Available from: http://www.ncbi.nlm.nih.gov/pubmed/15190178.

Matthews, R.E. 1979. The classification and nomenclature of viruses. Summary of results of meetings of the International Committee on Taxonomy of Viruses in The Hague, September 1978. *Intervirology*. [Online]. **11**(3), pp.133–5. Available from: http://www.ncbi.nlm.nih.gov/pubmed/429146.

Maul, G.G., Negorev, D., Bell, P. and Ishov, A.M. 2000. Review: Properties and assembly mechanisms of ND10, PML2 bodies, or PODs. *Journal of Structural Biology*. **129**(2–3), pp.278–287.

McAlister, G.C., Huttlin, E.L., Haas, W., Ting, L., Jedrychowski, M.P., Rogers, J.C., Kuhn, K., Pike, I., Grothe, R.A., Blethrow, J.D. and Gygi, S.P. 2012. Increasing the multiplexing capacity of TMTs using reporter ion isotopologues with isobaric masses. *Analytical Chemistry*. **84**(17), pp.7469–7478.

McDowell, M.E., Purushothaman, P., Rossetto, C.C., Pari, G.S. and Verma, S.C. 2013. Phosphorylation of Kaposi's sarcoma-associated herpesvirus processivity factor ORF59 by a viral kinase modulates its ability to associate with RTA and oriLyt. *Journal of virology*. [Online]. **87**(14), pp.8038–52. Available from: http://www.pubmedcentral.nih.gov/articlerender.fcgi?artid=3700218&tool=pmcentrez&rendertype=abstract.

McGeoch, D.J., Cook, S., Dolan, A., Jamieson, F.E. and Telford, E.A. 1995. Molecular phylogeny and evolutionary timescale for the family of mammalian herpesviruses. *Journal of molecular biology*. [Online]. **247**(3), pp.443–58. Available from: http://www.ncbi.nlm.nih.gov/pubmed/7714900.

McGeoch, D.J., Davison, A.J., Dolan, A., Gatherer, D. and Sevilla-Reyes, E.E. 2008a. Molecular Evolution of the Herpesvirales *In*: *Origin and Evolution of Viruses* [Online]. Elsevier, pp.447–475. Available from: http://linkinghub.elsevier.com/retrieve/pii/B9780123741530000205.

McGeoch, D.J., Davison, A.J., Dolan, A., Gatherer, D. and Sevilla-Reyes, E.E. 2008b. Molecular Evolution of the Herpesvirales *In*: *Origin and Evolution of*

Viruses [Online]. Elsevier, pp.447–475. Available from: http://linkinghub.elsevier.com/retrieve/pii/B9780123741530000205.

McVoy, M.A. and Adler, S.P. 1994. Human Cytomegalovirus DNA Replicates after Early Circularization by Concatemer Formation, and Inversion Occurs within the Concatemer. *J. of Virology*. [Online]. **68**(2), pp.1040–1051. Available from: http://jvi.asm.org/content/68/2/1040.full.pdf.

Merat, R., Amara, A., Lebbe, C., de The, H., Morel, P. and Saib, A. 2002. HIV-1 infection of primary effusion lymphoma cell line triggers Kaposi's sarcoma-associated herpesvirus (KSHV) reactivation. *International journal of cancer. Journal international du cancer*. **97**, pp.791–795.

Mercader, M., Taddeo, B., Panella, J.R., Chandran, B., Nickoloff, B.J. and Foreman, K.E. 2000. Induction of HHV-8 lytic cycle replication by inflammatory cytokines produced by HIV-1-infected T cells. *American Journal of Pathology*. **156**(6), pp.1961–1971.

Merrill, S.A. and Hanson, P.I. 2010. Activation of human VPS4A by ESCRT-III proteins reveals ability of substrates to relieve enzyme autoinhibition. *Journal of Biological Chemistry*. **285**(46), pp.35428–35438.

Mesri, E.A., Cesarman, E. and Boshoff, C. 2010. Kaposi's sarcoma and its associated herpesvirus. *Nat Rev Cancer*. [Online]. **10**(10), pp.707–719. Available from: http://www.ncbi.nlm.nih.gov/pubmed/20865011.

Mettenleiter, T.C. 2002. Herpesvirus Assembly and Egress. *Journal of Virology*. [Online]. **76**(4), pp.1537–1547. Available from: http://jvi.asm.org/cgi/doi/10.1128/JVI.76.4.1537-1547.2002.

Mettenleiter, T.C., Klupp, B.G. and Granzow, H. 2009. Herpesvirus assembly: An update. *Virus Research*. **143**(2), pp.222–234.

Mettenleiter, T.C., Müller, F., Granzow, H. and Klupp, B.G. 2013. The way out: What we know and do not know about herpesvirus nuclear egress. *Cellular Microbiology*. **15**(2), pp.170–178.

Mierzwa, B.E., Chiaruttini, N., Redondo-Morata, L., Moser von Filseck, J., König, J., Larios, J., Poser, I., Müller-Reichert, T., Scheuring, S., Roux, A. and Gerlich, D.W. 2017. Dynamic subunit turnover in ESCRT-III assemblies is regulated by Vps4 to mediate membrane remodelling during cytokinesis. *Nature cell biology*. [Online]. **19**(June). Available from: http://www.nature.com/doifinder/10.1038/ncb3559%5Cnhttp://www.ncbi.nlm.nih.gov/pubmed/28604678.

Monette, A., Ajamian, L., López-Lastra, M. and Mouland, A.J. 2009. Human immunodeficiency virus type 1 (HIV-1) induces the cytoplasmic retention of heterogeneous nuclear ribonucleoprotein A1 by disrupting nuclear import: implications for HIV-1 gene expression. *The Journal of biological chemistry*. [Online]. **284**(45), pp.31350–62. [Accessed 1 February 2014]. Available from: http://www.pubmedcentral.nih.gov/articlerender.fcgi?artid=2781532&tool=pmcentrez&rendertype=abstract.

Monette, A., Panté, N. and Mouland, A.J. 2011a. HIV-1 remodels the nuclear pore complex. *The Journal of cell biology*. [Online]. **193**(4), pp.619–31. [Accessed 25 September 2013]. Available from: http://www.pubmedcentral.nih.gov/articlerender.fcgi?artid=3166874&tool=pmcentrez&rendertype=abstract.

Monette, A., Panté, N. and Mouland, A.J. 2011b. HIV-1 remodels the nuclear pore complex. *The Journal of Cell Biology*. [Online]. **193**(4), pp.619–31. [Accessed 15 November 2013]. Available from: http://www.pubmedcentral.nih.gov/articlerender.fcgi?artid=3166874&tool=pmcentrez&rendertype=abstract.

Moore, M.S. 1998. Ran and Nuclear Transport. *Journal of Biological Chemistry*. [Online]. **273**(36), pp.22857–22860. [Accessed 19 January 2014]. Available from: http://www.jbc.org/cgi/doi/10.1074/jbc.273.36.22857.

Moore, M.S. and Blobel, G. 1993. The GTP-binding protein Ran/TC4 is required for protein import into the nucleus. *Nature*. [Online]. **365**(6447), pp.661–3. [Accessed 21 January 2014]. Available from: http://www.ncbi.nlm.nih.gov/pubmed/8413630.

Moore, P.S., Kingsley, L.A., Holmberg, S.D., Spira, T., Gupta, P., Hoover, D.R., Parry, J.P., Conley, L.J., Jaffe, H.W. and Chang, Y. 1996. Kaposi's sarcoma-associated herpesvirus infection prior to onset of Kaposi's sarcoma. *AIDS (London, England)*. [Online]. **10**(2), pp.175–80. Available from: https://www.researchgate.net/profile/John_Parry4/publication/14366110_KSHV_infection_prior_to_onset_of_Kaposi's_sarcoma/links/542d53360cf277d58e8cbf26.pdf.

Morita, E., Sandrin, V., McCullough, J., Katsuyama, A., Baci Hamilton, I. and Sundquist, W.I. 2011. ESCRT-III Protein Requirements for HIV-1 Budding. *Cell Host & Microbe*. [Online]. **9**(3), pp.235–242. Available from: http://linkinghub.elsevier.com/retrieve/pii/S1931312811000382.

Nakajima, T., Uchida, C., Anderson, S.F., Chee-Gun, L., Hurwitz, J., Parvin, J.D. and Montminy, M. 1997. RNA helicase A mediates association of CBP with RNA polymerase II. *Cell*. [Online]. **90**(6), pp.1107–1112. Available from: https://www.scopus.com/inward/record.uri?eid=2-s2.0-0030967951&partnerID=40&md5=f13a8d9077890c48a639f0afafe33d3c.

Nakamura, H., Lu, M., Gwack, Y., Souvlis, J., Zeichner, S.L. and Jung, J.U. 2003. Global Changes in Kaposi's Sarcoma-Associated Virus Gene Expression Patterns following Expression of a Tetracycline-Inducible Rta Transactivator. *Journal of Virology*. [Online]. **77**(7), pp.4205–4220. Available from: http://jvi.asm.org/cgi/doi/10.1128/JVI.77.7.4205-4220.2003.

Nakielny, S., Shaikh, S., Burke, B. and Dreyfuss, G. 1999. Nup153 is an M9-containing mobile nucleoporin with a novel Ran-binding domain. *The EMBO journal*. [Online]. **18**(7), pp.1982–95. Available from: http://www.pubmedcentral.nih.gov/articlerender.fcgi?artid=1171283&tool=pmcentrez&rendertype=abstract.

Naranatt, P.P., Krishnan, H.H., Smith, M.S. and Chandran, B. 2005. Kaposi's sarcoma-associated herpesvirus modulates microtubule dynamics via RhoA-GTP-diaphanous 2 signaling and utilizes the dynein motors to deliver its DNA to the nucleus. *Journal of virology*. [Online]. **79**(2), pp.1191–206. Available from: http://www.ncbi.nlm.nih.gov/pubmed/15613346%5Cnhttp://www.pubmedcentral.nih.gov/articlerender.fcgi?artid=PMC538527.

Nigg, E.A., Kitten, G.T. and Vorburger, K. 1992. Targeting lamin proteins to the nuclear envelope: the role of CaaX box modifications. *Biochemical Society Transactions*. [Online]. **20**(2), pp.500–504. Available from:

http://biochemsoctrans.org/lookup/doi/10.1042/bst0200500.

Di Nunzio, F., Danckaert, A., Fricke, T., Perez, P., Fernandez, J., Perret, E., Roux, P., Shorte, S., Charneau, P., Diaz-Griffero, F. and Arhel, N.J. 2012. Human nucleoporins promote HIV-1 docking at the nuclear pore, nuclear import and integration. *PloS one*. [Online]. **7**(9), p.e46037. [Accessed 11 November 2013]. Available from: http://www.pubmedcentral.nih.gov/articlerender.fcgi?artid=3457934&tool=pmcentrez&rendertype=abstract.

O'Farrell, P.H. 1975. High resolution two-dimensional electrophoresis of proteins. *J Biol Chem*. [Online]. **250**(10), pp.4007–4021. Available from: http://www.ncbi.nlm.nih.gov/pubmed/236308.

O'Reilly, A.J., Dacks, J.B. and Field, M.C. 2011. Evolution of the karyopherin-β family of nucleocytoplasmic transport factors; ancient origins and continued specialization. *PLoS ONE*. **6**(4).

Ocwieja, K.E., Brady, T.L., Ronen, K., Huegel, A., Roth, S.L., Schaller, T., James, L.C., Towers, G.J., Young, J.A.T., Chanda, S.K., König, R., Malani, N., Berry, C.C. and Bushman, F.D. 2011. HIV integration targeting: A pathway involving transportin-3 and the nuclear pore protein RanBP2. *PLoS Pathogens*. **7**(3), pp.19–21.

Oda, Y., Huang, K., Cross, F.R., Cowburn, D. and Chait, B.T. 1999. Accurate quantitation of protein expression and site-specific phosphorylation. *Proceedings of the National Academy of Sciences of the United States of America*. [Online]. **96**(12), pp.6591–6596. Available from: http://www.pnas.org/content/96/12/6591.long.

Oka, M., Asally, M., Yasuda, Y., Ogawa, Y., Tachibana, T. and Yoneda, Y. 2010. The Mobile FG Nucleoporin Nup98 Is a Cofactor for Crm1-dependent Protein Export K. Weis, ed. *Molecular Biology of the Cell*. [Online]. **21**(11), pp.1885–1896. Available from: http://www.molbiolcell.org/doi/10.1091/mbc.e09-12-1041.

Olmos, Y., Perdrix-Rosell, A. and Carlton, J.G. 2016. Membrane Binding by CHMP7 Coordinates ESCRT-III-Dependent Nuclear Envelope Reformation. *Current Biology*. [Online]. **26**(19), pp.2635–2641. Available from: http://dx.doi.org/10.1016/j.cub.2016.07.039.

Olsson, M., Schéele, S. and Ekblom, P. 2004. Limited expression of nuclear pore membrane glycoprotein 210 in cell lines and tissues suggests cell-type specific nuclear pores in metazoans. *Experimental Cell Research*. **292**(2), pp.359–370.

Ong, S.-E., Blagoev, B., Kratchmarova, I., Kristensen, D.B., Steen, H., Pandey, A. and Mann, M. 2002. Stable Isotope Labeling by Amino Acids in Cell Culture, SILAC, as a Simple and Accurate Approach to Expression Proteomics. *Molecular & Cellular Proteomics*. [Online]. **1**(5), pp.376–386. Available from: http://www.mcponline.org/lookup/doi/10.1074/mcp.M200025-MCP200.

Ori, A., Banterle, N., Iskar, M., Andrés-Pons, A., Escher, C., Khanh Bui, H., Sparks, L., Solis-Mezarino, V., Rinner, O., Bork, P., Lemke, E. a and Beck, M. 2013. Cell type-specific nuclear pores: a case in point for context-dependent stoichiometry of molecular machines. *Molecular systems biology*. [Online]. **9**(648), p.648. [Accessed 24 August 2014]. Available from:

http://www.pubmedcentral.nih.gov/articlerender.fcgi?artid=3619942&tool=p mcentrez&rendertype=abstract.

Otsuka, S., Iwasaka, S., Yoneda, Y., Takeyasu, K. and Yoshimura, S.H. 2008. Individual binding pockets of importin-beta for FG-nucleoporins have different binding properties and different sensitivities to RanGTP. *Proc Natl Acad Sci U S A*. [Online]. **105**(42), pp.16101–16106. Available from: http://www.ncbi.nlm.nih.gov/pubmed/18845677%5Cnhttp://www.pnas.org/content/105/42/16101.full.pdf.

Owen, C.B., Hughes, D.J., Baquero-Perez, B., Berndt, A., Schumann, S., Jackson, B.R. and Whitehouse, A. 2014. Utilising proteomic approaches to understand oncogenic human herpesviruses (Review). *Molecular and clinical oncology*. [Online]. **2**(6), pp.891–903. [Accessed 4 October 2014]. Available from: http://www.ncbi.nlm.nih.gov/pubmed/25279171.

Padmakumar, V.C., Libotte, T., Lu, W., Zaim, H., Abraham, S., Noegel, A. a, Gotzmann, J., Foisner, R. and Karakesisoglou, I. 2005. The inner nuclear membrane protein Sun1 mediates the anchorage of Nesprin-2 to the nuclear envelope. *Journal of cell science*. [Online]. **118**(Pt 15), pp.3419–30. [Accessed 8 June 2015]. Available from: http://www.ncbi.nlm.nih.gov/pubmed/16079285.

Panda, D., Gold, B., Tartell, M.A., Rausch, K., Casas-Tinto, S. and Cherry, S. 2015. The transcription factor FoxK participates with Nup98 to regulate antiviral gene expression. *mBio*. **6**(2), pp.1–10.

Panda, D., Pascual-Garcia, P., Dunagin, M., Tudor, M., Hopkins, K.C., Xu, J., Gold, B., Raj, A., Capelson, M. and Cherry, S. 2014. Nup98 promotes antiviral gene expression to restrict RNA viral infection in Drosophila. *Proceedings of the National Academy of Sciences of the United States of America*. [Online]. **111**(37), pp.E3890-9. [Accessed 29 June 2015]. Available from: http://www.pubmedcentral.nih.gov/articlerender.fcgi?artid=4169978&tool=p mcentrez&rendertype=abstract.

Panté, N., Bastos, R., McMorrow, I., Burke, B. and Aebi, U. 1994. Interactions and three-dimensional localization of a group of nuclear pore complex proteins. *The Journal of cell biology*. [Online]. **126**(3), pp.603–17. Available from: http://www.pubmedcentral.nih.gov/articlerender.fcgi?artid=2120134&tool=p mcentrez&rendertype=abstract.

Panté, N. and Kann, M. 2002. Nuclear pore complex is able to transport macromolecules with diameters of about 39 nm. *Molecular biology of the cell*. [Online]. **13**(2), pp.425–34. [Accessed 22 December 2014]. Available from: http://www.ncbi.nlm.nih.gov/pubmed/65638.

Park, N., Katikaneni, P., Skern, T. and Gustin, K.E. 2008. Differential targeting of nuclear pore complex proteins in poliovirus-infected cells. *Journal of virology*. [Online]. **82**(4), pp.1647–55. [Accessed 11 November 2013]. Available from: http://www.pubmedcentral.nih.gov/articlerender.fcgi?artid=2258732&tool=p mcentrez&rendertype=abstract.

Pasdeloup, D., Blondel, D., Isidro, A.L. and Rixon, F.J. 2009. Herpesvirus capsid association with the nuclear pore complex and viral DNA release involve the nucleoporin CAN/Nup214 and the capsid protein pUL25. *Journal of virology*.

[Online]. **83**(13), pp.6610–23. [Accessed 3 October 2014]. Available from: http://www.pubmedcentral.nih.gov/articlerender.fcgi?artid=2698519&tool=p mcentrez&rendertype=abstract.

Paulose-Murphy, M., Ha, N., Xiang, C., Chen, Y., Gillim, L., Yarchoan, R., Meltzer, P., Bittner, M., Trent, J. and Zeichner, S. 2001. Transcription program of human herpesvirus 8 (Kaposi's sarcoma-associated herpesvirus). *Journal of Virology*. **75**(10), pp.4843–4853.

Pawliczek, T. and Crump, C.M. 2009. Herpes Simplex Virus Type 1 Production Requires a Functional ESCRT-III Complex but Is Independent of TSG101 and ALIX Expression. *Journal of Virology*. [Online]. **83**(21), pp.11254–11264. Available from: http://jvi.asm.org/cgi/doi/10.1128/JVI.00574-09.

Penkert, R.R. and Kalejta, R.F. 2011. Tegument protein control of latent herpesvirus establishment and animation. *Herpesviridae*. [Online]. **2**(1), p.3. Available from: http://herpesviridae.biomedcentral.com/articles/10.1186/2042-4280-2-3.

Peric-Hupkes, D., Meuleman, W., Pagie, L., Bruggeman, S.W.M., Solovei, I., Brugman, W., Gräf, S., Flicek, P., Kerkhoven, R.M., van Lohuizen, M., Reinders, M., Wessels, L. and van Steensel, B. 2010. Molecular Maps of the Reorganization of Genome-Nuclear Lamina Interactions during Differentiation. *Molecular Cell*. **38**(4), pp.603–613.

Pertel, P.E. 2002. Human herpesvirus 8 glycoprotein B (gB), gH, and gL can mediate cell fusion. *Journal of virology*. [Online]. **76**(9), pp.4390–400. Available from: http://www.pubmedcentral.nih.gov/articlerender.fcgi?artid=155071&tool=pm centrez&rendertype=abstract.

Pertel, P.E., Spear, P.G. and Longnecker, R. 1998. Human herpesvirus-8 glycoprotein B interacts with Epstein-Barr virus (EBV) glycoprotein 110 but fails to complement the infectivity of EBV mutants. *Virology*. **251**(2), pp.402–413.

Peters, R. 2009. Translocation through the nuclear pore: Kaps pave the way. *BioEssays: news and reviews in molecular, cellular and developmental biology*. [Online]. **31**(4), pp.466–77. [Accessed 15 January 2014]. Available from: http://www.ncbi.nlm.nih.gov/pubmed/19274657.

Peters, R. 2005. Translocation through the nuclear pore complex: selectivity and speed by reduction-of-dimensionality. *Traffic*. [Online]. **6**(5), pp.421–7. [Accessed 18 January 2014]. Available from: http://www.ncbi.nlm.nih.gov/pubmed/15813752.

Phillips, R., Kondev, J. and Theriot, J. 2009. *Physical biology of the cell*. New York: Garland Science.

Pierce, N.W., Kleiger, G., Shan, S.O. and Deshaies, R.J. 2009. Detection of sequential polyubiquitylation on a millisecond timescale. *Nature*. [Online]. **462**(7273), pp.615–619. Available from: http://dx.doi.org/10.1038/nature08595.

Poffenberger, K.L. and Roizman, B. 1985. A Noninverting Genome of a Viable Herpes Simplex Virus 1: Presence of Head-to-Tail Linkages in Packaged Genomes and Requirements for Circularization After Infection. *Journal of Virology*. [Online]. **53**(2), pp.587–595. Available from: https://www.ncbi.nlm.nih.gov/pmc/articles/PMC254674/pdf/jvirol00125-

239

0253.pdf.

Polizzotto, M.N., Uldrick, T.S., Hu, D. and Yarchoan, R. 2012. Clinical Manifestations of Kaposi Sarcoma Herpesvirus Lytic Activation: Multicentric Castleman Disease (KSHV-MCD) and the KSHV Inflammatory Cytokine Syndrome. *Front Microbiol*. [Online]. **3**, p.73. Available from: http://www.ncbi.nlm.nih.gov/pubmed/22403576.

Porter, F.W., Brown, B. and Palmenberg, A.C. 2010. Nucleoporin Phosphorylation Triggered by the Encephalomyocarditis Virus Leader Protein Is Mediated by Mitogen-Activated Protein Kinases. *Journal of Virology*. [Online]. **84**(24), pp.12538–12548. Available from: http://www.ncbi.nlm.nih.gov/pmc/articles/PMC3004318/.

Porter, F.W. and Palmenberg, A.C. 2009. Leader-induced phosphorylation of nucleoporins correlates with nuclear trafficking inhibition by cardioviruses. *Journal of virology*. [Online]. **83**(4), pp.1941–51. [Accessed 21 January 2014]. Available from: http://www.pubmedcentral.nih.gov/articlerender.fcgi?artid=2643766&tool=pmcentrez&rendertype=abstract.

Powers, M.A., Forbes, D.J., Dahlberg, J.E. and Lund, E. 1997. The vertebrate GLFG nucleoporin, Nup98, is an essential component of multiple RNA export pathways. *The Journal of cell biology*. [Online]. **136**(2), pp.241–50. [Accessed 1 February 2014]. Available from: http://www.pubmedcentral.nih.gov/articlerender.fcgi?artid=2134807&tool=pmcentrez&rendertype=abstract.

Pratt, Z.L., Zhang, J. and Sugden, B. 2012. The Latent Membrane Protein 1 (LMP1) Oncogene of Epstein-Barr Virus Can Simultaneously Induce and Inhibit Apoptosis in B Cells. *Journal of Virology*. [Online]. **86**(8), pp.4380–4393. Available from: http://jvi.asm.org/lookup/doi/10.1128/JVI.06966-11.

Pritchard, C.E., Fornerod, M., Kasper, L.H. and van Deursen, J.M. 1999. RAE1 is a shuttling mRNA export factor that binds to a GLEBS-like NUP98 motif at the nuclear pore complex through multiple domains. *The Journal of cell biology*. [Online]. **145**(2), pp.237–54. Available from: http://www.pubmedcentral.nih.gov/articlerender.fcgi?artid=2133102&tool=pmcentrez&rendertype=abstract.

Prokocimer, M., Davidovich, M., Nissim-rafinia, M., Wiesel-motiuk, N., Bar, D.Z., Barkan, R., Meshorer, E. and Gruenbaum, Y. 2009. Nuclear lamins : key regulators of nuclear structure and activities. . **13**(6), pp.1059–1085.

Rabut, G., Doye, V. and Ellenberg, J. 2004. Mapping the dynamic organization of the nuclear pore complex inside single living cells. *Nature cell biology*. [Online]. **6**(11), pp.1114–21. [Accessed 23 February 2015]. Available from: http://www.ncbi.nlm.nih.gov/pubmed/15502822.

Raices, M. and D'Angelo, M. a 2012. Nuclear pore complex composition: a new regulator of tissue-specific and developmental functions. *Nature reviews. Molecular cell biology*. [Online]. **13**(11), pp.687–99. [Accessed 13 September 2014]. Available from: http://www.ncbi.nlm.nih.gov/pubmed/23090414.

Rainbow, L., Platt, G.M., Simpson, G.R., Sarid, R., Gao, S.J., Stoiber, H., Herrington, C.S., Moore, P.S. and Schulz, T.F. 1997. The 222- to 234-kilodalton latent nuclear protein (LNA) of Kaposi's sarcoma-associated

herpesvirus (human herpesvirus 8) is encoded by orf73 and is a component of the latency-associated nuclear antigen. *J Virol*. [Online]. **71**(8), pp.5915–5921. Available from: http://www.ncbi.nlm.nih.gov/pubmed/9223481.

Rajani, K.R., Pettit Kneller, E.L., McKenzie, M.O., Horita, D. a, Chou, J.W. and Lyles, D.S. 2012. Complexes of vesicular stomatitis virus matrix protein with host Rae1 and Nup98 involved in inhibition of host transcription. *PLoS pathogens*. [Online]. **8**(9), p.e1002929. [Accessed 1 February 2014]. Available from: http://www.pubmedcentral.nih.gov/articlerender.fcgi?artid=3460625&tool=pmcentrez&rendertype=abstract.

Ray, N. and Enquist, L.W. 2004. Transcriptional Response of a Common Permissive Cell Type to Infection by Two Diverse Alphaherpesviruses. *Journal of Virology*. [Online]. **78**(7), pp.3489–3501. Available from: http://jvi.asm.org/cgi/doi/10.1128/JVI.78.7.3489-3501.2004.

Reddy, K.L., Zullo, J.M., Bertolino, E. and Singh, H. 2008. Transcriptional repression mediated by repositioning of genes to the nuclear lamina. *Nature*. [Online]. **452**(7184), pp.243–7. [Accessed 1 October 2013]. Available from: http://www.ncbi.nlm.nih.gov/pubmed/18272965.

Rees, J.S., Li, X.-W., Perrett, S., Lilley, K.S. and Jackson, A.P. 2015. Protein Neighbors and Proximity Proteomics. *Molecular & Cellular Proteomics*. [Online]. **14**(11), pp.2848–2856. Available from: http://www.mcponline.org/lookup/doi/10.1074/mcp.R115.052902.

Rees, J.S., Li, X.W., Perrett, S., Lilley, K.S. and Jackson, A.P. 2015. Selective proteomic proximity labeling assay using tyramide (SPPLAT): A quantitative method for the proteomic analysis of localized membrane-bound protein clusters. *Current Protocols in Protein Science*. **2015**(April), 19.27.1-19.27.18.

Van Regenmortel, M.H., Maniloff, J. and Calisher, C. 1991. The concept of virus species. *Archives of virology*. [Online]. **120**(3–4), pp.313–4. Available from: http://www.ncbi.nlm.nih.gov/pubmed/1958131.

Ren, Y., Seo, H.-S., Blobel, G. and Hoelz, A. 2010. Structural and functional analysis of the interaction between the nucleoporin Nup98 and the mRNA export factor Rae1. *Proceedings of the National Academy of Sciences*. [Online]. **107**(23), pp.10406–10411. Available from: http://www.pnas.org/cgi/doi/10.1073/pnas.1005389107.

Rhee, H., Zou, P., Udeshi, N.D., Martell, J.D., Mootha, V.K., Carr, S.A. and Ting, A.Y. 2013. Proteomic mapping of mitochondria in living cells via spatially restricted enzymatic tagging. *Science (New York, N.Y.)*. [Online]. **339**(6125), pp.1328–1331. Available from: http://www.ncbi.nlm.nih.gov/pubmed/23371551.

Ribbeck, K. and Görlich, D. 2001. Kinetic analysis of translocation through nuclear pore complexes. *The EMBO journal*. [Online]. **20**(6), pp.1320–1330. Available from: http://www.pubmedcentral.nih.gov/articlerender.fcgi?artid=145537&tool=pmcentrez&rendertype=abstract.

Ribbeck, K. and Görlich, D. 2002. The permeability barrier of nuclear pore complexes appears to operate via hydrophobic exclusion. *EMBO Journal*. **21**(11), pp.2664–2671.

Rock, K.L., Gramm, C., Rothstein, L., Clark, K., Stein, R., Dick, L., Hwang, D. and Goldberg, A.L. 1994. Inhibitors of the proteasome block the degradation of most cell proteins and the generation of peptides presented on MHC class I molecules. *Cell*. **78**(5), pp.761–771.

Ross, P.L., Huang, Y.N., Marchese, J.N., Williamson, B., Parker, K., Hattan, S., Khainovski, N., Pillai, S., Dey, S., Daniels, S., Purkayastha, S., Juhasz, P., Martin, S., Bartlet-Jones, M., He, F., Jacobson, A. and Pappin, D.J. 2004. Multiplexed Protein Quantitation in *Saccharomyces cerevisiae* Using Amine-reactive Isobaric Tagging Reagents. *Molecular & Cellular Proteomics*. [Online]. **3**(12), pp.1154–1169. Available from: http://www.mcponline.org/lookup/doi/10.1074/mcp.M400129-MCP200.

Rout, M.P., Aitchison, J.D., Magnasco, M.O. and Chait, B.T. 2003. Virtual gating and nuclear transport: The hole picture. *Trends in Cell Biology*. **13**(12), pp.622–628.

Roux, K.J., Kim, D.I., Raida, M. and Burke, B. 2012. A promiscuous biotin ligase fusion protein identifies proximal and interacting proteins in mammalian cells. *The Journal of cell biology*. [Online]. **196**(6), pp.801–10. [Accessed 11 July 2014]. Available from: http://www.pubmedcentral.nih.gov/articlerender.fcgi?artid=3308701&tool=pmcentrez&rendertype=abstract.

Rowe, M., Rowe, D.T., Gregory, C.D., Young, L.S., Farrell, P.J., Rupani, H. and Rickinson, A.B. 1987. Differences in B cell growth phenotype reflect novel patterns of Epstein-Barr virus latent gene expression in Burkitt's lymphoma cells. *The EMBO journal*. [Online]. **6**(9), pp.2743–51. Available from: http://www.ncbi.nlm.nih.gov/pubmed/2824192.

Russo, J.J., Bohenzky, R. a, Chien, M.C., Chen, J., Yan, M., Maddalena, D., Parry, J.P., Peruzzi, D., Edelman, I.S., Chang, Y. and Moore, P.S. 1996. Nucleotide sequence of the Kaposi sarcoma-associated herpesvirus (HHV8). *Proceedings of the National Academy of Sciences of the United States of America*. **93**(December), pp.14862–14867.

Sadler, R., Wu, L., Forghani, B., Renne, R., Zhong, W., Herndier, B. and Ganem, D. 1999. A complex translational program generates multiple novel proteins from the latently expressed kaposin (K12) locus of Kaposi's sarcoma-associated herpesvirus. *J Virol*. [Online]. **73**(7), pp.5722–5730. Available from: http://www.ncbi.nlm.nih.gov/pubmed/10364323.

Safai, B. and Good, R.A. 1981. Kaposi's Sarcoma: A Review and Recent Developments. *CA: A Cancer Journal for Clinicians*. [Online]. **31**(1), pp.2–12. Available from: http://doi.wiley.com/10.3322/canjclin.31.1.2.

Sam, M.D., Evans, B.T., Coen, D.M. and Hogle, J.M. 2009. Biochemical, Biophysical, and Mutational Analyses of Subunit Interactions of the Human Cytomegalovirus Nuclear Egress Complex. *Journal of Virology*. [Online]. **83**(7), pp.2996–3006. Available from: http://jvi.asm.org/cgi/doi/10.1128/JVI.02441-08.

Samavarchi-Tehrani, P., Abdouni, H., Samson, R. and Gingras, A.-C. 2018. A versatile lentiviral delivery toolkit for proximity-dependent biotinylation in diverse cell types. *Molecular & Cellular Proteomics*. [Online], mcp.TIR118.000902. Available from: http://www.ncbi.nlm.nih.gov/pubmed/29991506%0Ahttp://www.mcponline.o

rg/lookup/doi/10.1074/mcp.TIR118.000902.

Sanchez, C., Lachaize, C., Janody, F., Bellon, B., Röder, L., Euzenat, J., Rechenmann, F. and Jacq, B. 1999. Grasping at molecular interactions and genetic networks in Drosophila melanogaster using FlyNets, an internet database. *Nucleic Acids Research*. **27**(1), pp.89–94.

Santarelli, R., Farina, A., Granato, M., Gonnella, R., Raffa, S., Leone, L., Bei, R., Modesti, A., Frati, L., Torrisi, M.R. and Faggioni, A. 2008. Identification and characterization of the product encoded by ORF69 of Kaposi's sarcoma-associated herpesvirus. *Journal of Virology*. **82**(9), pp.4562–4572.

Sathish, N., Zhu, F.X. and Yuan, Y. 2009. Kaposi's sarcoma-associated herpesvirus ORF45 interacts with kinesin-2 transporting viral capsid-tegument complexes along microtubules. *PLoS pathogens*. [Online]. **5**(3), p.e1000332. [Accessed 25 June 2015]. Available from: http://www.pubmedcentral.nih.gov/articlerender.fcgi?artid=2647735&tool=pmcentrez&rendertype=abstract.

Satterly, N., Tsai, P.-L., van Deursen, J., Nussenzveig, D.R., Wang, Y., Faria, P. a, Levay, A., Levy, D.E. and Fontoura, B.M. a 2007. Influenza virus targets the mRNA export machinery and the nuclear pore complex. *Proceedings of the National Academy of Sciences of the United States of America*. [Online]. **104**(6), pp.1853–8. Available from: http://www.pubmedcentral.nih.gov/articlerender.fcgi?artid=1794296&tool=pmcentrez&rendertype=abstract.

Schindelin, J., Arganda-Carreras, I., Frise, E., Kaynig, V., Longair, M., Pietzsch, T., Preibisch, S., Rueden, C., Saalfeld, S., Schmid, B., Tinevez, J.-Y., White, D.J., Hartenstein, V., Eliceiri, K., Tomancak, P. and Cardona, A. 2012. Fiji: an open-source platform for biological-image analysis. *Nature methods*. [Online]. **9**(7), pp.676–82. Available from: http://www.ncbi.nlm.nih.gov/pubmed/22743772.

Schleicher, K.D., Dettmer, S.L., Kapinos, L.E., Pagliara, S., Keyser, U.F., Jeney, S. and Lim, R.Y.H. 2014. Selective transport control on molecular velcro made from intrinsically disordered proteins. *Nature Nanotechnology*. [Online]. **9**(7), pp.525–530. Available from: http://dx.doi.org/10.1038/nnano.2014.103.

Schmidt, H.B. and Görlich, D. 2016. Transport Selectivity of Nuclear Pores, Phase Separation, and Membraneless Organelles. *Trends in Biochemical Sciences*. [Online]. **41**(1), pp.46–61. Available from: http://dx.doi.org/10.1016/j.tibs.2015.11.001.

Schumann, S., Jackson, B.R., Baquero-Perez, B. and Whitehouse, A. 2013. Kaposi's sarcoma-associated herpesvirus ORF57 protein: exploiting all stages of viral mRNA processing. *Viruses*. [Online]. **5**(8), pp.1901–1923. [Accessed 11 February 2014]. Available from: http://www.pubmedcentral.nih.gov/articlerender.fcgi?artid=3761232&tool=pmcentrez&rendertype=abstract.

Segref, A., Sharma, K., Doye, V., Hellwig, A., Huber, J., Lührmann, R. and Hurt, E. 1997. Mex67p, a novel factor for nuclear mRNA export. Binds to both poly(A)+RNA and nuclear pores. *EMBO Journal*. **16**(11), pp.3256–3271.

Sharma-Walia, N., Naranatt, P., Krishnan, H., Zeng, L. and Chandran, B. 2004. Kaposi's sarcoma-associated herpesvirus/human herpesvirus 8 envelope

glycoprotein gB induces the integrin-dependent focal adhesion kinase-Src-phosphatidylinositol 3-kinase-rho GTPase signal pathways and cytoskeletal rearrangements. *Journal of virology*. [Online]. **78**(8), pp.4207–4223. Available from: http://www.ncbi.nlm.nih.gov/entrez/query.fcgi?cmd=Retrieve&db=PubMed&dopt=Citation&list_uids=15047836%0Apapers2://publication/uuid/18C3E287-78E7-49CF-A9A8-80FD2178EC2F.

Sharma, A., Solmaz, S.R., Blobel, G. and Melčák, I. 2015. Ordered regions of channel nucleoporins Nup62, Nup54, and Nup58 form dynamic complexes in solution. *Journal of Biological Chemistry*. **290**(30), pp.18370–18378.

Shimi, T., Kittisopikul, M., Tran, J., Goldman, A.E., Adam, S.A., Zheng, Y., Jaqaman, K. and Goldman, R.D. 2015. Structural organization of nuclear lamins A, C, B1, and B2 revealed by superresolution microscopy. *Molecular Biology of the Cell*. [Online]. **26**(22), pp.4075–4086. Available from: http://www.molbiolcell.org/cgi/doi/10.1091/mbc.E15-07-0461.

Shukla, D. and Spear, P.G. 2001. Herpesviruses and heparan sulfate: An intimate relationship in aid of viral entry. *Journal of Clinical Investigation*. **108**(4), pp.503–510.

Simmonds, P., Adams, M.J., Benkő, M., Breitbart, M., Brister, J.R., Carstens, E.B., Davison, A.J., Delwart, E., Gorbalenya, A.E., Harrach, B., Hull, R., King, A.M.Q., Koonin, E. V., Krupovic, M., Kuhn, J.H., Lefkowitz, E.J., Nibert, M.L., Orton, R., Roossinck, M.J., Sabanadzovic, S., Sullivan, M.B., Suttle, C.A., Tesh, R.B., van der Vlugt, R.A., Varsani, A. and Zerbini, F.M. 2017. Consensus statement: Virus taxonomy in the age of metagenomics. *Nature Reviews Microbiology*. [Online]. **15**(3), pp.161–168. Available from: http://www.nature.com/doifinder/10.1038/nrmicro.2016.177.

Singh, V. V., Dutta, D., Ansari, M.A., Dutta, S., Chandran, B. and Longnecker, R. 2014. Kaposi's Sarcoma-Associated Herpesvirus Induces the ATM and H2AX DNA Damage Response Early during De Novo Infection of Primary Endothelial Cells, Which Play Roles in Latency Establishment. *Journal of Virology*. [Online]. **88**(5), pp.2821–2834. Available from: http://jvi.asm.org/cgi/doi/10.1128/JVI.03126-13.

Smit, M.J., Verzijl, D., Casarosa, P., Navis, M., Timmerman, H. and Leurs, R. 2002. Kaposi's sarcoma-associated herpesvirus-encoded G protein-coupled receptor ORF74 constitutively activates p44/p42 MAPK and Akt via G(i) and phospholipase C-dependent signaling pathways. *J Virol*. [Online]. **76**(4), p.1744–52. Available from: http://www.ncbi.nlm.nih.gov/cgi-bin/Entrez/referer?http://jvi.asm.org/cgi/content/full/76/4/1744.

Sodeik, B., Ebersold, M.W. and Helenius, A. 1997. Microtubule-mediated transport of incoming herpes simplex virus 1 capsids to the nucleus. *The Journal of cell biology*. [Online]. **136**(5), pp.1007–21. Available from: http://www.ncbi.nlm.nih.gov/pubmed/9060466.

Song, M.J., Brown, H.J., Wu, T. and Sun, R.E.N. 2001. Transcription Activation of Polyadenylated Nuclear RNA by Rta in Human Herpesvirus 8 / Kaposi ' s Sarcoma-Associated Herpesvirus. *Society*. **75**(7), pp.3129–3140.

Song, M.J., Hwang, S., Wong, W., Round, J., Martinez-Guzman, D., Turpaz, Y., Liang, J., Wong, B., Johnson, R.C., Carey, M. and Sun, R. 2004. The DNA architectural protein HMGB1 facilitates RTA-mediated viral gene expression

in gamma-2 herpesviruses. *Journal of virology*. **78**(23), pp.12940–12950.

Soulier, J., Grollet, L., Oksenhendler, E., Cacoub, P., Cazals-Hatem, D., Babinet, P., d'Agay, M.F., Clauvel, J.P., Raphael, M., Degos, L. and et al. 1995. Kaposi's sarcoma-associated herpesvirus-like DNA sequences in multicentric Castleman's disease. *Blood*. [Online]. **86**(4), pp.1276–1280. Available from: http://www.ncbi.nlm.nih.gov/pubmed/7632932.

Spear, P.G. and Longnecker, R. 2003. Herpesvirus Entry: an Update. *Journal of Virology*. [Online]. **77**(19), pp.10179–10185. Available from: http://jvi.asm.org/cgi/doi/10.1128/JVI.77.19.10179-10185.2003.

Stevens, J.G., Wagner, E.K., Devi-Rao, G.B., Cook, M.L. and Feldman, L.T. 1987. RNA complementary to a herpesvirus alpha gene mRNA is prominent in latently infected neurons. *Science*. **235**(1979), pp.1056–1059.

Stoffler, D., Feja, B., Fahrenkrog, B., Walz, J., Typke, D. and Aebi, U. 2003. Cryo-electron Tomography Provides Novel Insights into Nuclear Pore Architecture: Implications for Nucleocytoplasmic Transport. *Journal of Molecular Biology*. [Online]. **328**(1), pp.119–130. [Accessed 22 December 2014]. Available from: http://linkinghub.elsevier.com/retrieve/pii/S0022283603002663.

Strunze, S., Engelke, M.F., Wang, I.-H., Puntener, D., Boucke, K., Schleich, S., Way, M., Schoenenberger, P., Burckhardt, C.J. and Greber, U.F. 2011. Kinesin-1-mediated capsid disassembly and disruption of the nuclear pore complex promote virus infection. *Cell host & microbe*. [Online]. **10**(3), pp.210–23. [Accessed 15 November 2013]. Available from: http://www.ncbi.nlm.nih.gov/pubmed/21925109.

Sukegawa, J. and Blobel, G. 1993. A nuclear pore complex protein that contains zinc finger motifs, binds DNA, and faces the nucleoplasm. *Cell*. [Online]. **72**(1), pp.29–38. [Accessed 10 October 2014]. Available from: http://linkinghub.elsevier.com/retrieve/pii/009286749390047T.

Sun, Q., Zachariah, S. and Chaudhary, P.M. 2003. The human herpes virus 8-encoded viral FLICE-inhibitory protein induces cellular transformation via NF-kappaB activation. *J Biol Chem*. [Online]. **278**(52), pp.52437–52445. Available from: http://www.ncbi.nlm.nih.gov/pubmed/14563855.

Sun, R., Lin, S.-F., Gradoville, L., Yuan, Y., Zhu, F. and Miller, G. 1998. A viral gene that activates lytic cycle expression of Kaposi's sarcoma-associated herpesvirus. *Medical Sciences*. **95**(September), pp.10866–10871.

Sun, R., Lin, S.F., Gradoville, L. and Miller, G. 1996. Polyadenylylated nuclear RNA encoded by Kaposi sarcoma-associated herpesvirus. *Proceedings of the National Academy of Sciences of the United States of America*. [Online]. **93**(21), pp.11883–8. [Accessed 5 January 2015]. Available from: http://www.pubmedcentral.nih.gov/articlerender.fcgi?artid=38153&tool=pmc entrez&rendertype=abstract.

Sun, R., Lin, S.F., Staskus, K., Gradoville, L., Grogan, E., Haase, A. and Miller, G. 1999. Kinetics of Kaposi's sarcoma-associated herpesvirus gene expression. *J Virol*. [Online]. **73**(3), p.2232–42. Available from: http://www.ncbi.nlm.nih.gov/htbin-post/Entrez/query?db=m&form=6&dopt=r&uid=9971806%5Cnhttp://jvi.asm.org/cgi/content/full/73/3/2232.

Swaminathan, S. 2005. Post-transcriptional gene regulation by gamma

herpesviruses. *Journal of Cellular Biochemistry*. **95**(4), pp.698–711.

Szklarczyk, D., Morris, J.H., Cook, H., Kuhn, M., Wyder, S., Simonovic, M., Santos, A., Doncheva, N.T., Roth, A., Bork, P., Jensen, L.J. and Von Mering, C. 2017. The STRING database in 2017: Quality-controlled protein-protein association networks, made broadly accessible. *Nucleic Acids Research*. **45**(D1), pp.D362–D368.

Tabtieng, T., Degterev, A. and Gaglia, M.M. 2018. Caspase-Dependent Suppression of Type I Interferon Signaling Promotes Kaposi's Sarcoma-Associated Herpesvirus Lytic Replication J. U. Jung, ed. *Journal of Virology*. [Online]. **92**(10), pp.e00078-18. Available from: http://jvi.asm.org/lookup/doi/10.1128/JVI.00078-18.

Takahashi, Y., He, H., Tang, Z., Hattori, T., Liu, Y., Young, M.M., Serfass, J.M., Chen, L., Gebru, M., Chen, C., Wills, C.A., Atkinson, J.M., Chen, H., Abraham, T. and Wang, H.G. 2018. An autophagy assay reveals the ESCRT-III component CHMP2A as a regulator of phagophore closure. *Nature Communications*. [Online]. **9**(1). Available from: http://dx.doi.org/10.1038/s41467-018-05254-w.

Terry, L.J. and Wente, S.R. 2007. Nuclear mRNA export requires specific FG nucleoporins for translocation through the nuclear pore complex. *Journal of Cell Biology*. **178**(7), pp.1121–1132.

Thome, M., Schneider, P., Hofmann, K., Fickenscher, H., Meinl, E., Neipel, F., Mattmann, C., Burns, K., Bodmer, J.-L., Schröter, M., Scaffidi, C., Krammer, P.H., Peter, M.E. and Tschopp, J. 1997. Viral FLICE-inhibitory proteins (FLIPs) prevent apoptosis induced by death receptors. *Nature*. [Online]. **386**(6624), pp.517–521. Available from: http://www.nature.com/doifinder/10.1038/386517a0.

Thompson, A., Schäfer, J., Kuhn, K., Kienle, S., Schwarz, J., Schmidt, G., Neumann, T. and Hamon, C. 2003. Tandem Mass Tags: A Novel Quantification Strategy for Comparative Analysis of Complex Protein Mixtures by MS/MS. *Analytical Chemistry*. [Online]. **75**(8), pp.1895–1904. Available from: http://pubs.acs.org/doi/abs/10.1021/ac0262560.

Thorley-Lawson, D.A. 2001. Epstein-Barr virus: exploiting the immune system. *Nature Reviews Immunology*. [Online]. **1**(1), pp.75–82. Available from: http://www.nature.com/doifinder/10.1038/35095584.

Timney, B.L., Tetenbaum-Novatt, J., Agate, D.S., Williams, R., Zhang, W., Chait, B.T. and Rout, M.P. 2006. Simple kinetic relationships and nonspecific competition govern nuclear import rates in vivo. *Journal of Cell Biology*. **175**(4), pp.579–593.

Tomkinson, B., Robertson, E. and Kieff, E. 1993. Epstein-Barr virus nuclear proteins EBNA-3A and EBNA-3C are essential for B-lymphocyte growth transformation. *Journal of virology*. [Online]. **67**(4), pp.2014–25. Available from: http://www.pubmedcentral.nih.gov/articlerender.fcgi?artid=240270&tool=pmcentrez&rendertype=abstract.

Toth, Z., Brulois, K. and Jung, J.U. 2013. The chromatin landscape of Kaposi's sarcoma-associated herpesvirus. *Viruses*. **5**(5), pp.1346–1373.

Toyama, B.H., Savas, J.N., Park, S.K., Harris, M.S., Ingolia, N.T., Yates, J.R. and Hetzer, M.W. 2013. Identification of Long-Lived Proteins Reveals

Exceptional Stability of Essential Cellular Structures. *Cell*. [Online]. **154**(5), pp.971–982. [Accessed 29 August 2013]. Available from: http://linkinghub.elsevier.com/retrieve/pii/S0092867413009458.

Trotman, L.C., Mosberger, N., Fornerod, M., Stidwill, R.P. and Greber, U.F. 2001. Import of adenovirus DNA involves the nuclear pore complex receptor CAN/Nup214 and histone H1. *Nature Cell Biology*. [Online]. **3**, pp.1092–100. Available from: http://www.ncbi.nlm.nih.gov/pubmed/11781571.

Tsai, W.H., Wang, P.W., Lin, S.Y., Wu, I.L., Ko, Y.C., Chen, Y.L., Li, M. and Lin, S.F. 2012. Ser-634 and Ser-636 of Kaposi's sarcoma-associated herpesvirus RTA are involved in transactivation and are potential CDK9 phosphorylation sites. *Frontiers in Microbiology*. **3**(FEB), pp.1–14.

Ullman, K.S., Shah, S., Powers, M. a and Forbes, D.J. 1999. The nucleoporin nup153 plays a critical role in multiple types of nuclear export. *Molecular biology of the cell*. [Online]. **10**(3), pp.649–64. Available from: http://www.pubmedcentral.nih.gov/articlerender.fcgi?artid=25193&tool=pmc entrez&rendertype=abstract.

Unwin, P.N.T. and Milligan, R.A. 1982. A large particle associated with the perimeter of the nuclear pore complex. *Journal of Cell Biology*. **93**(1), pp.63–75.

Uv, A.E., Roth, P., Xylourgidis, N., Wickberg, A., Cantera, R. and Samakovlis, C. 2000. Members only encodes a Drosophila nucleoporin required for Rel protein import and immune response activation. *Genes and Development*. **14**(15), pp.1945–1957.

Uzer, G., Thompson, W.R., Sen, B., Xie, Z., Yen, S.S., Miller, S., Bas, G., Styner, M., Rubin, C.T., Judex, S. and Burridge, K. 2015. Enabled by a LINCed Nucleus. . **33**(6), pp.2063–2076.

Vaquerizas, J.M., Suyama, R., Kind, J., Miura, K., Luscombe, N.M. and Akhtar, A. 2010. Nuclear pore proteins Nup153 and megator define transcriptionally active regions in the Drosophila genome. *PLoS Genetics*. **6**(2).

Varnaitė, R. and MacNeill, S.A. 2016. Meet the neighbors: Mapping local protein interactomes by proximity-dependent labeling with BioID. *Proteomics*. [Online]. **16**(19), pp.2503–2518. Available from: http://www.ncbi.nlm.nih.gov/pubmed/27329485.

Veetti, M.V., Sadagopan, S., Kerur, N., Chakraborty, S. and Chandran, B. 2010. Interaction of c-Cbl with myosin IIA regulates bleb associated macropinocytosis of Kaposi's sarcoma-associated herpesvirus. *PLoS Pathogens*. **6**(12).

Verschuren, E.W., Jones, N. and Evan, G.I. 2004. The cell cycle and how it is steered by Kaposi's sarcoma-associated herpesvirus cyclin. *Journal of General Virology*. **85**(6), pp.1347–1361.

Visa, N., Izaurralde, E., Ferreira, J., Daneholt, B. and Mattaj, I.W. 1996. A nuclear cap-binding complex binds Balbiani ring pre-mRNA cotranscriptionally and accompanies the ribonucleoprotein particle during nuclear export. *Journal of Cell Biology*. **133**(1), pp.5–14.

Vita, D.J. and Broadie, K. 2017. ESCRT-III Membrane Trafficking Misregulation Contributes To Fragile X Syndrome Synaptic Defects. *Scientific Reports*. [Online]. **7**(1), p.8683. Available from:

http://www.nature.com/articles/s41598-017-09103-6.

Vogel, J., Hinrichs, S.H., Reynolds, R.K., Luciw, P.A. and Jay, G. 1988. The HIV tat gene induces dermal lesions resembling Kaposi's sarcoma in transgenic mice. *Nature*. [Online]. **335**(6191), pp.606–611. Available from: http://www.nature.com/doifinder/10.1038/335606a0.

Vollmer, B., Lorenz, M., Moreno-Andrés, D., Bodenhöfer, M., De Magistris, P., Astrinidis, S.A., Schooley, A., Flötenmeyer, M., Leptihn, S. and Antonin, W. 2015. Nup153 Recruits the Nup107-160 Complex to the Inner Nuclear Membrane for Interphasic Nuclear Pore Complex Assembly. *Developmental Cell*. [Online], pp.717–728. Available from: http://linkinghub.elsevier.com/retrieve/pii/S1534580715003159.

Wabinga, H.R., Parkin, D.M., Wabwire-Mangen, F. and Mugerwa, J.W. 1993. Cancer in Kampala, Uganda, in 1989-91: changes in incidence in the era of AIDS. *International journal of cancer*. [Online]. **54**(1), pp.26–36. Available from: http://www.ncbi.nlm.nih.gov/pubmed/8478145.

Wagner, R.S., Kapinos, L.E., Marshall, N.J., Stewart, M. and Lim, R.Y.H. 2015. Promiscuous Binding of Karyopherinβ1 Modulates FG Nucleoporin Barrier Function and Expedites NTF2 Transport Kinetics. *Biophysical journal*. [Online]. **108**(4), pp.918–27. [Accessed 20 February 2015]. Available from: http://www.ncbi.nlm.nih.gov/pubmed/25692596.

Walther, T.C., Alves, A., Pickersgill, H., Loïodice, I., Hetzer, M., Galy, V., Hülsmann, B.B., Köcher, T., Wilm, M., Allen, T., Mattaj, I.W. and Doye, V. 2003. The conserved Nup107-160 complex is critical for nuclear pore complex assembly. *Cell*. **113**(2), pp.195–206.

Wang, G.G., Cai, L., Pasillas, M.P. and Kamps, M.P. 2007. NUP98-NSD1 links H3K36 methylation to Hox-A gene activation and leukaemogenesis. *Nature Cell Biology*. **9**(7), pp.804–812.

Wang, S.E., Wu, F.Y., Chen, H., Shamay, M., Zheng, Q. and Hayward, G.S. 2004. Early activation of the Kaposi's sarcoma-associated herpesvirus RTA, RAP, and MTA promoters by the tetradecanoyl phorbol acetate-induced AP1 pathway. *Journal of virology*. [Online]. **78**(8), pp.4248–67. Available from: http://www.pubmedcentral.nih.gov/articlerender.fcgi?artid=374264&tool=pmcentrez&rendertype=abstract.

Wang, S.E., Wu, F.Y., Fujimuro, M., Zong, J., Hayward, S.D. and Hayward, G.S. 2003. Role of CCAAT / Enhancer-Binding Protein Alpha (C / EBP α) in Activation of the Kaposi ' s Sarcoma-Associated Herpesvirus Protein (RAP) Promoter in Cooperation with the KSHV Replication and Transcription Activator (RTA) and RAP Role of CCAAT / Enhan. *Journal of virology*. **77**(1), pp.600–623.

Wang, X., Zhu, N., Li, W., Zhu, F., Wang, Y. and Yuan, Y. 2015. Mono-ubiquitylated ORF45 Mediates Association of KSHV Particles with Internal Lipid Rafts for Viral Assembly and Egress. *PLoS Pathogens*. **11**(12), pp.1–26.

Washburn, M.P., Wolters, D. and Yates 3rd, J.R. 2001. Large-scale analysis of the yeast proteome by multidimensional protein identification technology. *Nat Biotechnol*. [Online]. **19**(3), pp.242–247. Available from: http://www.ncbi.nlm.nih.gov/pubmed/11231557.

Wasinger, V.C., Cordwell, S.J., Cerpa-Poljak, A., Yan, J.X., Gooley, A.A., Wilkins,

M.R., Duncan, M.W., Harris, R., Williams, K.L. and Humphery-Smith, I. 1995. Progress with gene-product mapping of the Mollicutes:Mycoplasma genitalium. *Electrophoresis*. [Online]. **16**(1), pp.1090–1094. Available from: http://doi.wiley.com/10.1002/elps.11501601185.

Watanabe, Y. and Kanai, A. 2011. Systems biology reveals microRNA-mediated gene regulation. *Frontiers in Genetics*. **2**(JUNE), pp.1–13.

Watson, M.L. 1959. Further observations on the nuclear envelope of the animal cell. *The Journal of biophysical and biochemical cytology*. **6**(2), pp.147–156.

Webster, B.M., Colombi, P., Jäger, J. and Lusk, C.P. 2014. Surveillance of Nuclear Pore Complex Assembly by ESCRT-III/Vps4. *Cell*. [Online]. **159**(2), pp.388–401. [Accessed 9 October 2014]. Available from: http://linkinghub.elsevier.com/retrieve/pii/S0092867414011611.

Weinlich, R., Oberst, A., Beere, H.M. and Green, D.R. 2017. Necroptosis in development, inflammation and disease. *Nature Reviews Molecular Cell Biology*. [Online]. **18**(2), pp.127–136. Available from: http://dx.doi.org/10.1038/nrm.2016.149.

Weller, S.K. and Coen, D.M. 2012. Herpes Simplex Viruses: Mechanisms of DNA Replication. *Cold Spring Harbor Perspectives in Biology*. **4**(9), pp.a013011–a013011.

Werner, T., Becher, I., Sweetman, G., Doce, C., Savitski, M.M. and Bantscheff, M. 2012. High-resolution enabled TMT 8-plexing. *Analytical Chemistry*. **84**(16), pp.7188–7194.

Whitley, R. 1996. *Medical Microbiology* 4th ed. (S. Baron, ed.). Galveston: University of Texas Medical Branch at Galveston.

Wild, P., Senn, C., Manera, C.L., Sutter, E., Schraner, E.M., Tobler, K., Ackermann, M., Ziegler, U., Lucas, M.S. and Kaech, A. 2009. Exploring the nuclear envelope of herpes simplex virus 1-infected cells by high-resolution microscopy. *Journal of virology*. [Online]. **83**(1), pp.408–19. [Accessed 30 December 2014]. Available from: http://www.pubmedcentral.nih.gov/articlerender.fcgi?artid=2612326&tool=pmcentrez&rendertype=abstract.

Wischnitzer, S. 1973. The Submicroscopic Morphology of the Interphase Nucleus. *International Review of Cytology*. **34**(C), pp.1–48.

Wisner, T.W. and Johnson, D.C. 2004. Redistribution of cellular and herpes simplex virus proteins from the trans-Golgi network to cell junctions without enveloped capsids. *Journal Of Virology*. **78**(21), pp.11519–11535.

Woodward, C.L., Prakobwanakit, S., Mosessian, S. and Chow, S. a 2009. Integrase interacts with nucleoporin NUP153 to mediate the nuclear import of human immunodeficiency virus type 1. *Journal of Virology*. [Online]. **83**, pp.6522–6533. [Accessed 3 February 2014]. Available from: http://www.pubmedcentral.nih.gov/articlerender.fcgi?artid=2698555&tool=pmcentrez&rendertype=abstract.

Woźniakowski, G. and Samorek-Salamonowicz, E. 2015. Animal herpesviruses and their zoonotic potential for cross-species infection. *Annals of Agricultural and Environmental Medicine*. **22**(2), pp.191–194.

Wu, J., Matunis, M. and Kraemer, D. 1995. Nup358, a cytoplasmically exposed nucleoporin with peptide repeats, Ran-GTP binding sites, zinc fingers, a

cyclophilin A homologous domain, and a leucine-rich. *Journal of Biological ….* [Online]. **270**, pp.14209–14213. [Accessed 16 November 2013]. Available from: http://www.jbc.org/content/270/23/14209.short.

Xie, W., Chojnowski, A., Boudier, T., Lim, J.S.Y., Ahmed, S., Ser, Z., Stewart, C. and Burke, B. 2016. A-type Lamins Form Distinct Filamentous Networks with Differential Nuclear Pore Complex Associations. *Current Biology*. [Online]. **26**(19), pp.2651–2658. Available from: http://dx.doi.org/10.1016/j.cub.2016.07.049.

Xu, D., Farmer, A. and Chook, Y.M. 2010. Recognition of nuclear targeting signals by Karyopherin-β proteins. *Current Opinion in Structural Biology*. [Online]. **20**(6), pp.782–790. Available from: http://dx.doi.org/10.1016/j.sbi.2010.09.008.

Yajima, M., Kanda, T. and Takada, K. 2005. Critical role of Epstein-Barr Virus (EBV)-encoded RNA in efficient EBV-induced B-lymphocyte growth transformation. *J Virol.* [Online]. **79**(7), pp.4298–4307. Available from: http://dx.doi.org/10.1128/JVI.79.7.4298-4307.2005.

Yamashita, M. and Emerman, M. 2004. Capsid Is a Dominant Determinant of Retrovirus Infectivity in Nondividing Cells. *Journal of Virology*. [Online]. **78**(11), pp.5670–5678. Available from: http://jvi.asm.org/cgi/doi/10.1128/JVI.78.11.5670-5678.2004.

Yang, W. and Musser, S.M. 2006. Nuclear import time and transport efficiency depend on importin β concentration. *Journal of Cell Biology*. **174**(7), pp.951–961.

Yang, Z., Yan, Z. and Wood, C. 2008. Kaposi's sarcoma-associated herpesvirus transactivator RTA promotes degradation of the repressors to regulate viral lytic replication. *Journal of virology*. [Online]. **82**(7), pp.3590–603. Available from: http://jvi.asm.org/content/82/7/3590.full.

Yaseen, N.R. and Blobel, G. 1999. Two distinct classes of Ran-binding sites on the nucleoporin Nup-358. *Proceedings of the National Academy of Sciences of the United States of America*. **96**(10), pp.5516–5521.

Yates, J.R., Eng, J.K., McCormack, A.L. and Schieltz, D. 1995. Method to Correlate Tandem Mass Spectra of Modified Peptides to Amino Acid Sequences in the Protein Database. *Analytical Chemistry*. **67**(8), pp.1426–1436.

Ye, F., Zhou, F., Bedolla, R.G., Jones, T., Lei, X., Kang, T., Guadalupe, M. and Gao, S.J. 2011. Reactive oxygen species hydrogen peroxide mediates Kaposi's sarcoma-associated herpesvirus reactivation from latency. *PLoS Pathogens*. **7**(5).

Yokoyama, N., Hayashi, N., Seki, T., Pante, N., Ohba, T., Nishil, K., Kuma, K., Hayashida, T., Miyata, T., Aebi, U., Fukui, M. and Nishimoto, T. 1995. A giant nucleopore protein that binds Ran/TC4. *Nature*. [Online]. **376**, pp.184–188. [Accessed 16 November 2013]. Available from: http://www.nature.com/nature/journal/v376/n6536/abs/376184a0.html.

Yoshimura, S.H., Kumeta, M. and Takeyasu, K. 2014. Structural Mechanism of Nuclear Transport Mediated by Importin β and Flexible Amphiphilic Proteins. *Structure (London, England : 1993)*. [Online]. **22**(12), pp.1699–1710. [Accessed 2 December 2014]. Available from: http://www.ncbi.nlm.nih.gov/pubmed/25435324.

Young, L.S. and Rickinson, A.B. 2004. Epstein-Barr virus: 40 Years on. *Nature Reviews Cancer*. **4**(10), pp.757–768.

Yu, Y., Wang, S.E. and Hayward, G.S. 2005. The KSHV immediate-early transcription factor RTA encodes ubiquitin E3 ligase activity that targets IRF7 for proteosome-mediated degradation. *Immunity*. **22**(1), pp.59–70.

Zhang, T. and Wang, L. 2017. Epidemiology of Kaposi's sarcoma-associated herpesvirus in Asia: Challenges and opportunities. *Journal of medical virology*. [Online]. **89**(4), pp.563–570. Available from: http://www.ncbi.nlm.nih.gov/pubmed/27531516.

Zhang, X., Chen, S., Yoo, S., Chakrabarti, S., Zhang, T., Ke, T., Oberti, C., Yong, S.L., Fang, F., Li, L., de la Fuente, R., Wang, L., Chen, Q. and Wang, Q.K. 2008. Mutation in Nuclear Pore Component NUP155 Leads to Atrial Fibrillation and Early Sudden Cardiac Death. *Cell*. [Online]. **135**(6), pp.1017–1027. Available from: http://dx.doi.org/10.1016/j.cell.2008.10.022.

Zhang, X., Yang, H., Corydon, M.J., Zhang, X., Pedersen, S., Korenberg, J.R., Chen, X.N., Laporte, J., Gregersen, N., Niebuhr, E., Liu, G. and Bolund, L. 1999. Localization of a human nucleoporin 155 gene (NUP155) to the 5p13 region and cloning of its cDNA. *Genomics*. **57**(1), pp.144–151.

Zhou, H., Xu, M., Huang, Q., Gates, A.T., Zhang, X.D., Castle, J.C., Stec, E., Ferrer, M., Strulovici, B., Hazuda, D.J. and Espeseth, A.S. 2008. Genome-Scale RNAi Screen for Host Factors Required for HIV Replication. *Cell Host and Microbe*. [Online]. **4**(5), pp.495–504. Available from: http://dx.doi.org/10.1016/j.chom.2008.10.004.

Zhu, F.X., Cusano, T. and Yuan, Y. 1999. Identification of the immediate-early transcripts of Kaposi's sarcoma-associated herpesvirus. *Journal of virology*. [Online]. **73**(7), pp.5556–67. Available from: http://jvi.asm.org/cgi/doi/10.1128/JVI.75.19.9509-9516.2001.

Ziegler, J.L., Templeton, A.C. and Vogel, C.L. 1984. Kaposi's sarcoma: a comparison of classical, endemic, and epidemic forms. *Seminars in oncology*. [Online]. **11**(1), pp.47–52. Available from: http://www.ncbi.nlm.nih.gov/pubmed/6538992.

Zieske, L.R. 2006. A perspective on the use of iTRAQ^{TM} reagent technology for protein complex and profiling studies. *Journal of Experimental Botany*. **57**(7), pp.1501–1508.